Investigation of the functional roles of calcium channels, inflammatory cytokines and tumour micro-environmental factors in a human *in vitro* model of breast cancer calcification

Shane O'Grady

Department of Molecular & Cellular Therapeutics, RCSI

A thesis submitted to the School of Postgraduate Studies, Faculty of Medicine and Health Sciences, Royal College of Surgeons in Ireland, in fulfilment of the degree of Doctor of Philosophy

Principal investigator: Dr. Maria Morgan

May 2018

Candidate Thesis Declaration

I declare that this thesis, which I submit to RCSI for examination in consideration of the award of a higher degree is my own personal effort. Where any of the content presented is the result of input or data from a related collaborative research programme this is duly acknowledged in the text such that it is possible to ascertain how much of the work is my own. I have not already obtained a degree in RCSI or elsewhere on the basis of this work. Furthermore, I took reasonable care to ensure that the work is original, and, to the best of my knowledge, does not breach copyright law, and has not been taken from other sources except where such work has been cited and acknowledged within the text.

Signed _____

Student Number _____

Date _____

Table of contents

Abbreviations 6

Figures 9

Tables 12

Summary 13

Chapter 1.0 General introduction 15

1.1 Breast cancer 16
1.1.1 Breast Cancer in Ireland 16
1.1.2 Breast cancer aetiology 16
1.1.3 Types of breast cancer 18
1.1.4 Treatment 22
1.1.5 Mammographic screening 24

1.2 Breast cancer and microcalcifications 26
1.2.1 Mammary microcalcifications: An introduction 26
1.2.2 Mammographic characterisation of microcalcifications 27
1.2.3 Chemical composition of microcalcifications 30
1.2.4 Microcalcifications and patient prognosis 31
1.2.5 Biological effects of microcalcifications 36

1.3 *In vivo* mineralisation 38
1.3.1 Physiological mineralisation 38
1.3.2 Phosphate-phosphate balance 39
1.3.3 Regulators of *in vivo* mineralisation 40
1.3.4 Pathological calcification 41

1.4 Formation of breast microcalcifications 43
1.4.1 Osteomimicry of breast cancer cells 43
1.4.2 Osteomimicry of breast cancer cells and microcalcifications 44
1.4.3 *In vitro* models of mineralisation 46
1.4.4 Development of an *in vitro* model of microcalcification 47
1.4.5 Key findings from our *in vitro* model of microcalcification 48
1.4.6 Other *in vitro* studies of mammary calcification 49
1.4.7 Remaining questions surrounding the formation of microcalcifications 51

1.5 Thesis overview 53

Chapter 2.0 Materials and methods 54

2.1 Cell culture materials and methods 55
2.1.1 Equipment 55
2.1.2 Cell culture reagents 55

2.1.3 Subculture 55
2.1.4 Long term storage and recovery of cell lines 56

2.2 Assessment of breast cancer mineralisation 57
2.2.1 Reagent preparation 57
2.2.2 Experimental set-up 57
2.2.3 Alamar Blue 57
2.2.4 Alizarin Red S Staining 58
2.2.5 von Kossa Staining 58
2.2.6 o-cresolphthalein complexone (OCP) calcium assay 59
2.2.7 BCA Protein Assay 59
2.2.8 Alkaline phosphatase assay 59

2.3 Gene expression analysis 60
2.3.1 mRNA Isolation 60
2.3.2 Nucleic acid quantification 61
2.3.3 cDNA synthesis & qPCR analysis 61
2.3.4 Semi-quantitative PCR 62
2.3.5 Agarose gel electrophoresis 63
2.3.6 siRNA knockdown 63
2.3.7 Plasmid preparation and purification 64
2.3.8 Plasmid transfection 65

2.4 Hydroxyapatite stimulation experiments 65
2.4.1 Experimental set up 65
2.4.2 THP-1 macrophage differentiation 65
2.4.3 IL-6 ELISA 66

2.5 SDS-PAGE and western blotting 66
2.5.1 Sample preparation 66
2.5.2 SDS-PAGE gel preparation 67
2.5.3 SDS-PAGE gel electrophoresis and transfer 67
2.5.4 Western blotting 68

2.6 Tumoursphere assays 68

2.7 *In vivo* work 69

2.8 Raman spectroscopy 69
2.8.1 Sample preparation 69
2.8.2 Raman spectroscopy analysis 70

2.9 Statistics 70

Chapter 3.0 Establishment of an *in vitro* model of mammary calcification in human breast cancer cells 71

3.1 Introduction 72
3.1.1 *In vitro* mineralisation models 72
3.1.2 Human breast cancer cell lines and microcalcifications 73

3.1.3 Aims of this chapter 74

3.2 Results 75

3.2.1 Establishment of standard mineralisation and staining procedure for murine 4T1 cell line 75

3.2.2 Assessing mineralisation potential of MCF-7 cells 76

3.2.3 Assessing mineralisation potential of HER2 overexpressing MCF-7 cells 78

3.2.4 Assessing mineralisation potential of ZR-75-1 cells 79

3.2.5 Assessing mineralisation potential of SKBR3 cells 80

3.2.6 Assessing mineralisation potential of HCC1954 cells 82

3.2.7 Assessing mineralisation of MDA-MB-231 cells 83

3.2.8 Summary of characterisation study for mineralisation-capable human breast cancer cell lines 84

3.2.8 Investigating the specific mineralisation requirements of the MDA-MB-231 cell line 84

3.2.9 Alkaline phosphatase and microcalcifications 87

3.2.10 Exogenous ALP promotes *in vitro* mineralisation in breast cancer cell lines 91

3.2.11 Bioinformatic analysis of ALP expression 93

3.2.12 Inorganic Pi and breast cancer cell mineralisation 94

3.3 Discussion 98

3.4 Summary and conclusions 108

Chapter 4.0 Microcalcifications as a result of loss of endogenous mineralisation inhibitors and alteration of Ca^{2+} transport pathways 110

4.1 Introduction 111

4.1.1 Mineralisation associated proteins and breast cancer 111

4.1.2 Calcium/Magnesium balance 112

4.1.3 Aims of this chapter 114

4.2 Results 115

4.2.1 BMP-2 expression in mineralising MDA-MB-231 cells 115

4.2.2 Loss of ENPP1 expression in mineralising MDA-MB-231 cultures 118

4.2.3 Decreased MGP expression in mineralising MDA-MB-231 cells 121

4.2.4 RUNX2 and MDA-MB-231 mineralisation 121

4.2.5 Role of intracellular Ca^{2+} accumulation and TRPM7 channel activity in microcalcification formation 125

4.2.6 Breast calcifications and magnesium 133

4.2.7 PMCA channels and MDA-MB-231 mineralisation 138

4.3 Discussion 142

4.4 Summary and conclusions 154

Chapter 5.0 Inflammation and cancer stemness: Investigating potential tumour promoting effects of microcalcifications 155

5.1 Introduction 156
5.1.1 Tumour promoting effects of microcalcifications 156
5.1.2 Aims of this chapter 157

5.2 Results 158
5.2.1 Inflammatory effect of hydroxyapatite on breast cancer cells 158
5.2.2 THP-1 monocytes and HA stimulation 162
5.2.3 Inflammatory cytokines and formation of microcalcifications 164
5.2.4 Microcalcifications and cancer stem cells 172
5.2.5 In vivo mineralisation of MDA-MB-231 cells 184
5.2.6 Raman analysis of *in vitro* microcalcification samples 185

5.3 Discussion 190

5.4 Summary and conclusions 204

Chapter 6.0 Concluding discussion 205

6.1 Summary of key findings 206

6.2 Future recommendations 208

6.3 Conclusion 210

Chapter 7.0 References 211

Chapter 8.0 Appendix 241
8.1 Supporting information 242
8.2 Presentations 250
8.3 Students supervised 251
8.4 Publications 251
8.5 Science promotion and other academic activities 251

Abbreviations

IC_{50}	Half maximal inhibitory concentration
2-APB	2-Aminoethoxydiphenyl borate
AA	Ascorbic acid
ADCC	Antibody-dependent cellular cytotoxicity
Akp2	Alkaline phosphatase 2
ALP	Alkaline phosphatase
AM	Acetoxymethyl
AMP	2-Amino-2-methyl-1-propanol
Ank	Progressive ankylosis protein
ANKH	Ankylosis protein homolog
ANOVA	Analysis of variance
APS	Ammonium persulfate
ATP	Adenosine triphosphate
BAPTA-AM	BAPTA acetoxymethyl ester.
BCA	Bicinchoninic acid assay
Bcl-2	B-cell lymphoma 2
BI-RADS	Breast Imaging Reporting and Data System
βG	β-glycerophosphate
BMP2	Bone morphogenetic protein 2
BSA	Bovine serum albumin
BSP	Bone sialoprotein
CDK7	Cyclin-dependent kinase 7
CA1	Carbonic anhydrase I
CaSR	Calcium sensing receptor
CDH1	Cadherin-1/Epithelial cadherin
cDNA	Complementary DNA
ChIP-seq	Chromatin immunoprecipitation with sequencing
CK	Cytokeratin
CM	Conditioned media
CMV	Cytomegalovirus
CNA	Copy number alteration
COX-2	Cyclooxygenase-2
CSCs	Cancer stem cells
DCIS	Ductal carcinoma *in situ*
DDT	Dichlorodiphenyltrichloroethane
Dex	Dexamethasone
DMEM	Dulbecco's modified eagle's medium
DMSO	Dimethyl sulfoxide
ECL	Enhanced chemiluminescence
ECM	Extracellular matrix
EDTA	Ethylenediaminetetraacetic acid
EGF	Epidermal growth factor
EGFR	Epidermal growth factor receptor ()
ELISA	Enzyme-linked immunosorbent assay
EMT	Epithelial-mesenchymal transition
ENPP1	Ectonucleotide pyrophosphatase/phosphodiesterase
ER	Estrogen receptor
FBS	Foetal bovine serum
GFP	Green fluorescent protein

gp130	Glycoprotein 130
GR	Glucocorticoid receptor
H&E	Hematoxylin and eosin
HA	Hydroxyapatite
HDAC	Histone deacetylase
HEPES	Hydroxyethyl piperazineethanesulfonic acid
HER2	Human epidermal growth factor receptor 2
HMEC	Human mammary epithelial cells
IL	Interleukin
IL-6R	IL-6 receptor
JAK	Janus kinases
JNK	c-Jun N-terminal kinase
kDa	Kilo Dalton
LB	Luria-Bertani
LCIS	Lobular carcinoma *in situ*
MAPK	Mitogen-activated protein kinase
miR	Micro RNA
M-CSF	Macrophage colony-stimulating factor
M-CSF	Macrophage colony-stimulating factor
MEK2	Dual specificity mitogen-activated protein kinase kinase 2
METABRIC	Molecular Taxonomy of Breast Cancer International Consortium
MGP	Matrix gla protein
MMP	Matrix metalloproteinase
mRNA	Messenger ribonucleic acid
n.s	Not significant
NF-κB	Nuclear factor kappa-light-chain-enhancer of activated B cells
NPM-ALK	Nucleophosmin-anaplastic lymphoma kinase
OC	Osteogenic cocktail
OCN	Osteocalcin
OCP	O-cresolphthalein complexone
OPN	Osteopontin
OS	Overall survival
PAGE	Polyacrylamide gel electrophoresis
PBS	Phosphate buffered saline
PCA	Principal component analysis
pCR	Pathological complete response
PCR	Polymerase chain reaction
PGE2	Prostaglandin E2
pHEMA	Poly2-hydroxyethyl methacrylate
PHOSPHO1	Phosphoethanolamine/phosphocholine phosphatase
Pi	Phosphate
PI3K	Phosphatidylinositol-4,5-bisphosphate 3-kinase
PLC	Phospholipase C
PMA	Phorbol 12-myristate 13-acetate
PMCA	Plasma membrane Ca^{2+}-ATPase
pNPP	p-nitrophenyl phosphate
PPARγ	Peroxisome proliferator-activated receptor γ
PPi	Pyrophosphate
PR	Progesterone receptor
PTEN	Phosphatase and tensin homolog
PVDF	Polyvinylidene fluoride

qPCR	Quantitative polymerase chain reaction
Rb	Retinoblastoma
RFS	Recurrence free survival
RIPA	Radioimmunoprecipitation assay
RNA	Ribonucleic acid
ROR2	Receptor tyrosine kinase-like orphan receptor 2
RPM	Revolutions per minute
RPMI	Roswell Park Memorial Institute
RUNX2	Runt-related transcription factor 2
SD	Standard deviation
SDS	Sodium dodecyl sulphate
SERD	Selective estrogen receptor degrader
SERM	Selective estrogen receptor modulator
shRNA	Short hairpin RNA
sIL-6R	Soluble IL-6 receptor
siRNA	Short interfering RNA
SOC	Super optimal broth with catabolite repression
SPCA	Secretory pathway Ca^{2+}-ATPases
STAT3	Signal transducer and activator of transcription factor 3
Syk	Spleen tyrosine kinase
TAE	Tris-acetate-EDTA
TAM	Tumour associated macrophages
TBS	Tris buffered saline
TE	Tris-EDTA
TEMED	Tetramethylethylenediamine
TFE	Tumoursphere forming efficiency
TGF-β	Transforming growth factor beta
TNAP	Tissue non-specific alkaline phosphatase
TNF-α	Tumour necrosis factor
TNM	Tumour node metastasis
TP53	Tumour protein p53
TRP	Transient receptor potential
TRPM7	Transient receptor potential cation channel, subfamily M, member 7
VEGF	Vascular endothelial growth factor
VSMCs	Vascular smooth muscle cells
Wnt	Wingless-related integration site
YAP	Yes-associated protein

Figures

Chapter 1.0

Figure 1.1 Invasive breast cancer incidence trend:1994-2013
Figure 1.2 Potential relationship between differentiation hierarchy of luminal and myoepithelial cell lineages and the molecular subtypes of breast cancer
Figure 1.3 Changes in age adjusted breast cancer incidence rate of different stages in women aged 50 or more in the Netherlands, 1989 to 2012
Figure 1.4 Mammographic and histological appearance and distribution patterns of microcalcification
Figure 1.5 Vascular calcification as an imbalance between calcification promoters and inhibitors
Figure 1.6 Proposed mechanism of mammary cell mineralisation

Chapter 2.0

Figure 2.1 Assembly order of transfer sandwich for western blotting

Chapter 3.0

Figure 3.1 Positive mineralisation in 4T1 cells
Figure 3.2 MCF-7 cells do not undergo *in vitro* microcalcification formation
Figure 3.3 HER2 overexpressing MCF-7 cells do not undergo *in vitro* microcalcification formation
Figure 3.4 ZR-75-1 cells do not undergo *in vitro* microcalcification formation
Figure 3.5 SKBR3 cells undergo *in vitro* microcalcification formation
Figure 3.6 HCC1954 cells do not undergo *in vitro* microcalcification formation
Figure 3.7 MDA-MB-231 cells undergo *in vitro* microcalcification formation
Figure 3.8 Assessing the mineralisation requirements of MDA-MB-231 cells
Figure 3.9 Investigating the effect of collagen coating on MDA-MB-231 mineralisation
Figure 3.10 Activity and expression of ALP enzyme in mineralising MDA-MB-231 cells
Figure 3.11 Comparison of ALP activity in mineralising and non-mineralising breast cancer cells
Figure 3.12 Exogenous ALP promotes mineralisation in non-mineralising MCF-7 cells
Figure 3.13 Exogenous ALP promotes mineralisation increases MDA-MB-231 mineralisation
Figure 3.14 Effect of the ALP inhibitor levamisole on MDA-MB-231 mineralisation
Figure 3.15 Bioinformatic analysis of ALP expression
Figure 3.16 Inorganic phosphate induced mineralisation of MDA-MB-231 cells
Figure 3.17 ALP activity of MDA-MB-231 cells under inorganic phosphate conditions
Figure 3.18 ALP activity of SKBR3 cells under inorganic phosphate conditions
Figure 3.19 Inorganic phosphate induced mineralisation of MCF-7 cells

Chapter 4.0

Figure 4.1 Expression of BMP2 in mineralising MDA-MB-231 cells
Figure 4.2 BMP2 promotes MDA-MB-231 calcification
Figure 4.3 BMP2 stimulates MDA-MB-231 alkaline phosphatase activity
Figure 4.4 BMP2 does not alter mineralisation capability of luminal MCF-7 cells
Figure 4.5 Onset of MDA-MB-231 mineralisation is accompanied by downregulation on ENPP1
Figure 4.6 Anti-mineralisation effect of pyrophosphate in MDA-MB-231 cells
Figure 4.7 OC+Dex decreases MGP expression in MDA-MB-231 cells
Figure 4.8 Elevated RUNX2 expression in MDA-MB-231 cells
Figure 4.9 OC+Dex increases RUNX2 expression in MDA-MB-231 cells
Figure 4.10 siRNA knockdown of RUNX2 decreases MDA-MB-231 mineralisation
Figure 4.11 Overexpression of RUNX2 does not alter MDA-MB-231 mineralisation
Figure 4.12 Effect of increased calcium levels on MDA-MB-231 mineralisation
Figure 4.13 MDA-MB-231 mineralisation is inhibited by intracellular calcium chelation
Figure 4.14 Upregulation of TRPM7 and TRPC1 channels during MDA-MB-231 mineralisation
Figure 4.15 Inhibition of MDA-MB-231 mineralisation by the TRP channel modulator 2-APB
Figure 4.16 Inhibition of MDA-MB-231 mineralisation by the TRPM7 channel inhibitor NS8593
Figure 4.17 Inhibition of MDA-MB-231 ALP activity by the 2-APB and NS8593
Figure 4.18 siRNA knockdown of TRPM7 reduces MDA-MB-231 mineralisation
Figure 4.19 Magnesium potently inhibits development of MDA-MB-231 calcifications
Figure 4.20 Magnesium does not affect MDA-MB-231 cultured in non-calcifying media
Figure 4.21 Magnesium alters ALP activity in MDA-MB-231 cells
Figure 4.22 Inhibition of TRPM7 channel does not attenuate anti-mineralisation effect of magnesium
Figure 4.23 MDA-MB-231 proliferation is not affected by magnesium or inhibition of the TRPM7 channel
Figure 4.24 PMCA1/2 and MDA-MB-231 mineralisation
Figure 4.25 Expression of PMCA1/2 in mineralising MDA-MB-231 cells

Chapter 5.0

Figure 5.1 Hydroxyapatite upregulates COX2 in MDA-MB-231 cells
Figure 5.2 Hydroxyapatite upregulates IL-6 in MDA-MB-231 cells
Figure 5.3 Upregulation of IL-6 in hydroxyapatite stimulated cells is inhabited by intracellular calcium chelation.

Figure 5.4 Increased expression of inflammatory markers in THP-1 macrophages following stimulation with HA or MDA-MB-231 conditioned media

Figure 5.5 Hydroxyapatite nanoparticles induce an inflammatory response in MDA-MB-231 cells

Figure 5.6 sIL-6R promotes MDA-MB-231 mineralisation

Figure 5.7 Activation of IL-6 trans-signalling pathway promotes MDA-MB-231 mineralisation

Figure 5.8 MDA-MB-231 cells are unresponsive to IL-6 without sIL-6R co-stimulation

Figure 5.9 OC+Dex promotes STAT3 phosphorylation in SKBR3 cells

Figure 5.10 JSI-124 and MDA-MB-231 mineralisation

Figure 5.11 Suppression of MDA-MB-231 mineralisation by inflammatory cytokines IL-1β and TNF-α

Figure 5.12 Suppression of MDA-MB-231 ALP activity by inflammatory cytokines IL-1β and TNF-α
Figure 5.13 Tumoursphere formation in MDA-MB-231 cells
Figure 5.14 Tumoursphere formation in SKBR3 cells
Figure 5.15 MDA-MB-231 do not mineralise as tumoursphere cultures
Figure 5.16 Effect of OC+Dex on expression of EMT and cancer stemness markers in MDA-MB-231 cells
Figure 5.17 Effect of OC+Dex on expression of EMT and cancer stemness markers in SKBR3 cells
Figure 5.18 Effect of TRPM7 channel inhibition on MDA-MB-231 tumoursphere formation
Figure 5.19 Effect of TRPM7 siRNA knockdown on formation of MDA-MB-231 tumourspheres
Figure 5.20 Effect of TRPM7 siRNA knockdown on expression of a panel of EMT and cancer stemness markers
Figure 5.21 *In vivo* mineralisation of the MDA-MB-231 cell line
Figure 5.22 Mineralisation of MDA-MB-231 cells grown on CaF_2 windows
Figure 5.23 Raman analysis of mineralising MDA-MB-231 cells
Figure 5.24 PCA of Raman spectra of mineralising MDA-MB-231 cells

Tables

Chapter 1

Table 1.1 Breast imaging and reporting data system (BI-RADS) categories for mammography and its association with microcalcification appearance

Table 1.2 Key studies demonstrating association between mammographic calcifications and key prognostic factors in breast cancer patients

Chapter 2

Table 2.1 Growth media requirements, seeding density and original source of all cell lines used

Table 2.2 Primer sequences utilised for qPCR

Table 2.3 Pre-designed siRNA (Sigma) utilised in this study

Table 2.4 SDS-PAGE gel formulation

Table 2.5 Primary and secondary Western blotting antibodies

Chapter 3

Table 3.1 Summary of a characterisation study of the mineralisation potential of a panel of human breast cancer cell lines

Chapter 8

Table 8.1 Key studies demonstrating association between mammographic calcifications and prognostic factors in breast cancer patients

Table 8.2 Formulation of buffers used

Table 8.3 Oral and poster conference presentations

Summary

Microcalcifications are frequently the sole mammographic indicator of breast cancer with several studies suggesting that their presence may also be indicative of increased tumour grade, HER2 overexpression and poor prognosis. Despite their widespread diagnostic usage, the mechanism by which microcalcifications form and their contribution to tumour progression remain poorly understood. Previously, our lab established an *in vitro* model using a murine cell line. In order to advance our understanding of these vital diagnostic markers, we have expanded these findings and developed a human *in vitro* model of microcalcification formation.

Following extensive testing of a panel of human breast cancer cell lines, the MDA-MB-231 and SKBR3 cell lines were identified as suitable for our studies. Positive mineralisation was observed in one out of three tested HER2+ cell lines, indicating HER2 overexpression by itself is insufficient to induce *in vivo* mineralisation. Formation of calcifications was accompanied by increased expression of the osteogenic markers RUNX2, BMP2, and ALP. Inhibition of the cation channel TRPM7 resulted in a dose-dependent decrease in calcium deposition, implicating a functional role for the channel. Calcification was also inhibited by the intracellular Ca^{2+} chelator BAPTA-AM and by Mg^{2+}. The role of other calcium handling proteins including PMCA1 and PMCA2 was also investigated. Finally, we investigated possible links between microcalcification and pro-tumourigenic effects. Culturing breast cancer cells in mineralisation media increased formation of tumourspheres, indicating an increase in cancer stem-cell properties. We also observed an increased IL-1β, IL-6 and COX2 in both breast cancer cells and associated macrophages following stimulation with hydroxyapatite. Inflammatory cytokines were also observed to modulate *in vitro* mineralisation, suggesting a complex interplay between the formation and release of calcified particles and their subsequent interaction with surrounding tumour cells.

The results of this thesis reaffirms and expands on our labs previous findings, that breast cancer cell lines can be utilised as effective *in vitro* model for tumour calcification and that formation of these calcifications is the result of an active, cell-mediated process, involving interaction between mineralisation associated proteins including BMP2 and ALP, as well as Ca^{2+} channels and tumour associated cytokines.

Chapter 1.0

General introduction

1.1 Breast cancer

1.1.1 Breast Cancer in Ireland

Despite many advances in both detection and treatment, breast cancer remains a significant concern for the health of women worldwide. With an estimated 1.67 million new cases diagnosed in 2012, breast cancer is the second most common cancer in the world and the fifth cause of death from cancer overall (WHO, 2017). Statistics on the Irish population match those seen worldwide. With an average of 3,168 new cases of invasive breast cancer reported per year in Ireland between 2015 to 2017 (NCRI, 2017), breast cancer is the most common form of cancer diagnosis in women, with the exception of non-melanoma skin cancer, representing almost a third of new female cancer cases. Breast cancer incidence amongst Irish women currently stands at 122.4 per 100,000. This compares poorly with the rest of Europe, with an average rate of 106.6 per 100,000. Ireland currently ranks 6th in Europe for breast cancer incidence (EUCAN, 2017).

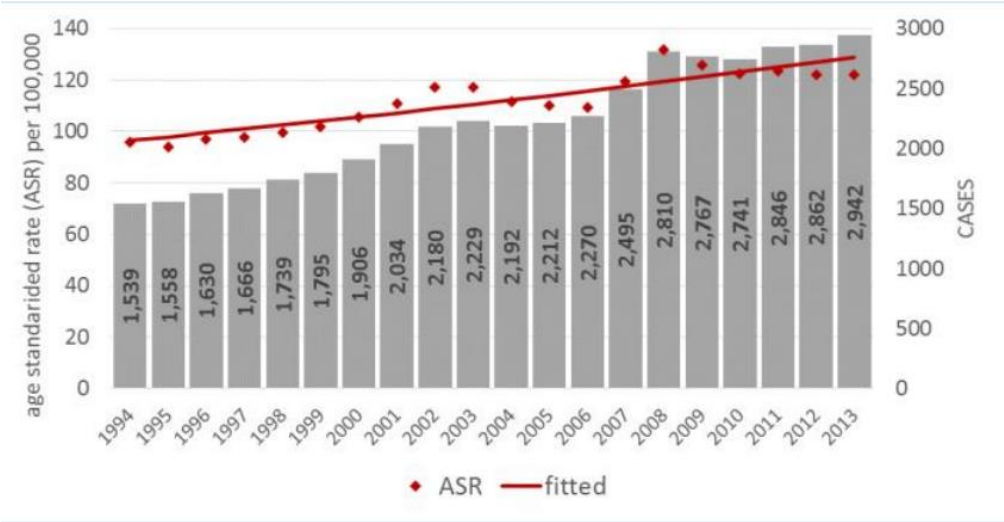

Figure 1.1 Female invasive breast cancer incidence trend:1994-2013. Incidence rate of invasive breast in Irish women displays an annual percentage change of +1.5% (95% CI 1.1-1.9%) in the period of 1994 to 2013. Reproduced from "Cancer Trends No 29. Breast cancer" (NCRI, 2016).

1.1.2 Breast cancer aetiology

As with all forms of cancer, the conversion of normal breast tissue to a cancerous lesion is a complex, multi-step process involving loss of proliferative control, suppression of apoptotic pathways, activation of angiogenic and survival pathways, acquisition of a migratory, invasive phenotype and evasion of anti-tumour immune responses (Hanahan and Weinberg, 2000).

Underlying this progression is an intricate mix of somatic mutations, genetic susceptibilities, diet, environmental factors and lifestyle choices. Unsurprisingly, the greatest risk factor is gender, with women accounting for over 99% of cases (NCRI, 2017). Like most other forms of cancer, age has a significant impact on risk, with incidence peaking between 50 and 65. Incidence begins to decline after this point, primarily due to the post-menopausal status of this cohort. Early onset of menopause confers a decreased risk of breast cancer. The opposite effect is seen with early menstruation, with menarche earlier than 12 years of age conferring a significant increase in lifetime risk (Collaborative Group on Hormonal Factors in Breast, 2012). These results highlight the importance of “lifetime exposure” to reproductive hormones. The role of endogenous hormones in the development of breast cancer is also demonstrated by the increased risks observed in users of hormonal birth-control and hormone replacement therapy (Gray et al., 2017).

Approximately 10% of breast cancer cases can be attributed to an inherited, high-penetrance genetic factor, of which the best characterised are the DNA repair genes *BRCA1* and *BRCA2* (Honrado et al., 2004). Estimates of penetrance vary significantly although a meta-analysis found cumulative breast cancer risks by age 70 years of 57% and 47% for *BRCA1* and *BRCA2* carriers, respectively (Chen and Parmigiani, 2007). A significant increase in ovarian cancer risk is also observed (40% for *BRCA1* and 18% for *BRCA2*). Other characterised genetic risk factors include mutated *TP53*, loss of phosphatase and tensin homolog (*PTEN*) and mutations of phosphatidylinositol-4,5-bisphosphate 3-kinase (*PI3K*) (Harro and Monteiro, 2017).

As with other cancers, lifestyle and diet are important contributors to breast cancer risk. Smoking plays a relatively small role in breast cancer risk in comparison to other cancers, although smokers do have a significantly increased risk, especially women who start smoking before delivery of their first child, when breast tissue is especially vulnerable to genotoxic damage (Gaudet et al., 2013, Catsburg et al., 2015). Alcohol consumption, even in moderation is a significant contributor to breast cancer risk (Chen et al., 2011). Association between breast cancer and alcohol consumption seems particularly strong for patients with estrogen receptor positive (ER+) tumours, as ethanol stimulates proliferation and aromatase expression in ER+ breast cancer cell lines (Etique et al., 2004).

Obesity significantly increases risk of post-menopausal breast cancer although surprisingly may decrease risk in pre-menopausal women (Suzuki et al., 2009). Obesity influences breast cancer risk and prognosis in multiple ways, including increased aromatase activity, secretion of inflammatory cytokines, elevated levels of mitogenic and pro-angiogenic factors including insulin and leptin, and increased risk of surgical complications (Chan and Norat, 2015). Composition of breast tissue also exerts a significant effect on breast cancer risk as women with a high percentage of dense breast tissue have a 4-6 fold increased risk compared to those with less dense breasts (Sak et al., 2015).

Possible environmental risk factors include exposure to chemicals including dichlorodiphenyltrichloroethane (DDT), dioxins and air pollution (Rodgers et al., 2018), ionising radiation (Gilbert, 2009) and exposure to light at night, resulting in disrupted circadian rhythm (James et al., 2017).

1.1.3 Types of breast cancer

Breast cancer can be divided into many different types and subtypes, based on tissue of origin, gene expression profiles and hormone receptor status. Mammary gland epithelium consists of two cellular lineages: luminal cells (further subdivided into ductal and alveolar luminal cells) surrounding the ductal lumen and myoepithelial cells located in the basal compartment (Visvader, 2009). These two distinct cellular compartments are formed from a branching hierarchical structure of differentiation of mammary stem cells. The heterogeneity of breast cancer subtypes is now believed to reflect this hierarchy, with different molecular subtypes of breast cancer representing the original cell type from which a particular tumour is derived.

The majority of breast cancer cases (75-90%) arise in the epithelial lining of the mammary glands. These can be further divided into lobular (10-15%) and ductal carcinoma (65-75%) (NCRI, 2012, NCRI, 2016). Both forms of carcinoma can be found in a “pre-cancerous”, non-invasive *in situ* lesion, localised to the epithelial lining. Ductal carcinoma *in situ* (DCIS) was once a rare finding, but its incidence rate has increased rapidly due to the expansion of mammographic screening processes in many countries. DCIS does not usually cause a palpable lump, and the majority are detected by mammography (Carraro et al., 2014). Whilst DCIS (and the lobular equivalent, LCIS) are by themselves non-lethal, their detection is cause for concern as they are considered a precursor to invasive breast cancer.

This is evidenced by the significant increase in breast cancer risk in women with previously detected DCIS as well as genetic and histological similarities between DCIS and invasive tumours in the same patient (Carraro et al., 2014).

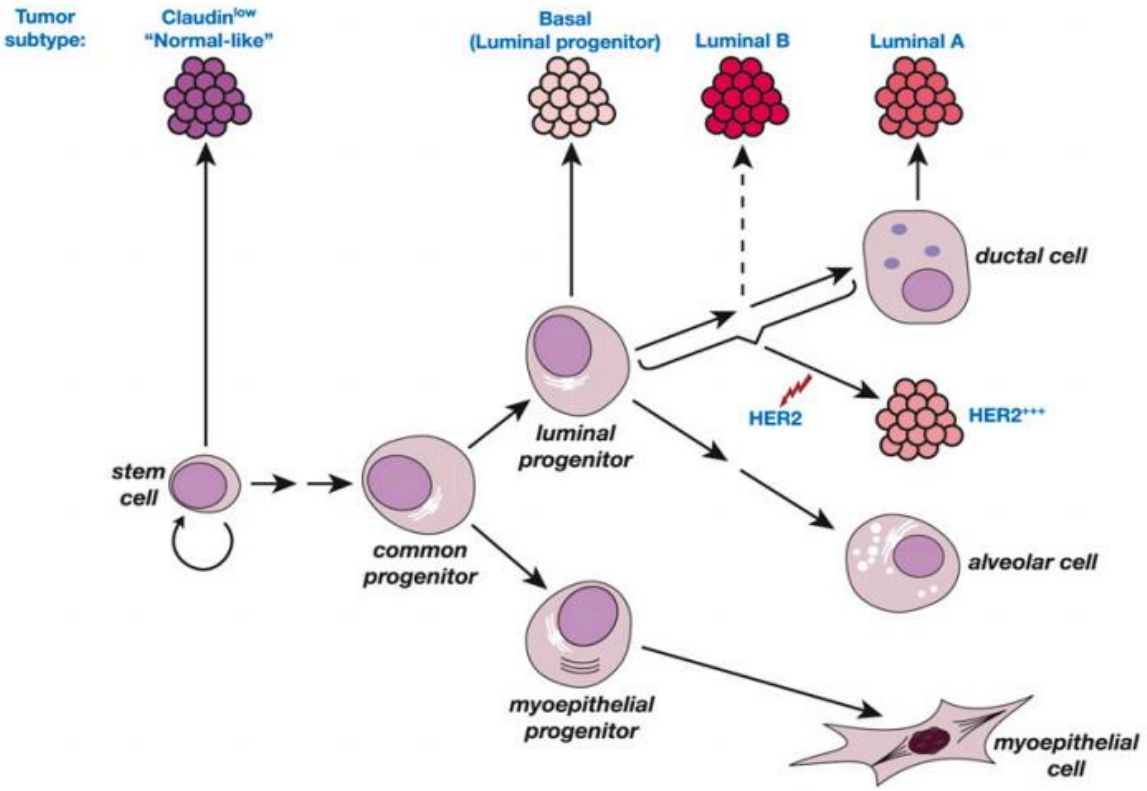

Figure 1.2 Potential relationship between differentiation hierarchy of luminal and myoepithelial cell lineages and the molecular subtypes of breast cancer. Luminal and myoepithelial cell lineages form as a result of differentiation of mammary stem cells, resulting in a branching hierarchy of cell types, which may be reflective of the high degree of heterogeneity within breast cancer. Reproduced from Visvader (2009).

Breast tumours are also characterised by expression of three receptor proteins, estrogen receptor (ER), progesterone receptor (PR) and human epidermal growth factor receptor 2 (HER2). Expression of these receptors is typically examined by immunohistochemical analysis of biopsy samples and is a critical factor in determining future treatment. In addition, the usage of microarray analysis has also greatly expanded clinical understanding of different breast cancer subtypes and may yield a more complete picture than simple immunohistochemical analysis. A ground-breaking study by Perou et al. analysed expression of a panel of 8,102 genes in 65 surgical specimens, and found that tumours could be divided into 4 distinct, molecular subtypes based on expression patterns of a set of “intrinsic genes” (Perou et al., 2000).

Subsequent analysis has further refined characterisation of these subtypes and showed links between subtype and patient prognosis (Sorlie et al., 2001). Luminal tumours constitute the largest subtype (~70%) of breast cancers and are characterised by their expression of genes associated with the ER signalling pathway (Eroles et al., 2012). Luminal tumours can be further divided into luminal-A and luminal-B. Luminal-B tumours have increased expression of a group of proliferative genes, and tend to be associated with higher histologic grade and worse prognosis than luminal-A tumours (Ades et al., 2014).

Approximately 20% of breast cancer cases fall into the category of HER2 enriched, defined by amplification of the *HER2* gene (Eroles et al., 2012). No natural ligand has been identified for HER2. Instead, the HER2 extracellular domain exists permanently in a conformational state resembling that of an active receptor. The constitutionally active HER2 functions as a dimerisation partner for other members of the epidermal growth factor receptor family. Dimerisation triggers auto-phosphorylation and activation of multiple cell signalling pathways including mitogen-activated protein kinase (MAPK), phospholipase C (PLC) and PI3-K (Koutras and Evans, 2008). HER2-positive tumours tend to be aggressive, with a high proliferative index, frequent relapse and decreased survival relative to the luminal subtype (Yersal and Barutca, 2014, Dai et al., 2015). Development of the recombinant monoclonal antibody trastuzumab (Herceptin) has significantly improved outcome for patients with HER2+ tumours (Rayson et al., 2014). Trastuzumab binds to the extracellular domain of HER2 and is believed to function through numerous mechanisms including inhibition of the PI3K pathway (Delord et al., 2005) and promoting antibody-dependent cellular cytotoxicity (ADCC) based killing of tumour cells (Arnould et al., 2006).

The basal-like subtype is named for its characteristic expression of genes usually associated with basal epithelial cells such as the cytokeratins CK-5/6, CK-14 and CK-17 (Perou et al., 2000). From an immunohistochemical view, basal-like tumour are usually characterised as triple-negative (ER-, PR-, HER2-). Although the terms “basal” and “triple-negative” are often used interchangeably, and the two characterisations do share significant overlap, the terms are not synonymous, with one study demonstrating that up to 30% of triple-negative tumours do not fit into the basal-like subtype when analysed (Bertucci et al., 2008).

This discrepancy between the histological staining usually used to identify triple-negative tumours and the gene expression based classification of the basal subtype reflects the high degree of heterogeneity of triple-negative breast cancers (Abramson and Mayer, 2014). From a clinical perspective, basal-like tumours are highly aggressive often associated with short overall survival time, higher recurrence rate and frequent metastasis (Abd El-Rehim et al., 2004, Banerjee et al., 2006, Foulkes et al., 2004).

Normal-like breast cancers are poorly characterised with very few studies available in the literature. They are usually triple-negative but differ from basal-like cancers in their lack of CK5 and epidermal growth factor receptor (EGFR) expression. They also express several genes usually found in adipose tissue including fatty-acid binding protein 4 and peroxisome proliferator-activated receptor γ (PPARγ) (Perou et al., 2000). Their prognosis lies in between that of luminal and basal-like. The existence of this particular subtype is still debatable with several studies suggesting that contamination of experimental samples with small amounts of non-cancerous cells from surrounding tissue may be responsible (Hu et al., 2006, Parker et al., 2009, Prat and Perou, 2011, Sontrop et al., 2016). The observation that when cancerous cells are harvested for analysis through highly accurate micro-dissection, no traces of the normal-like subtype remains would seem to support the hypothesis that this subtype may be nothing more than a technical artefact (Weigelt et al., 2010).

The original grouping of four subtypes was expanded upon with the discovery of the claudin low subtype in 2007 (Herschkowitz et al., 2007). This subtype is named for its low expression of claudins 3, 4, 7 as well as several other genes in tight junctions and cell-cell adhesion such as occludin, and E-cadherin. Claudin low tumours share certain characteristics with basal-like tumours such as low expression of luminal genes and triple negative status. Despite low expression of proliferation related genes, claudin-low tumours tend to have a poor prognosis (Eroles et al., 2012, Prat and Perou, 2011). In addition, the METABRIC study used a combined molecular profiling of both gene expression and copy number alterations (CNAs) in 2,000 breast cancer patients to generate 10 distinct “integrative clusters”, with significant variations in prognosis, expression profiles and genomic alterations (Curtis et al., 2012).

The different molecular subtypes may represent the differentiation stage of the cell from which they are originally derived. For instance, expression analysis of luminal progenitor cells shows a close relationship with the basal-like subtype, while claudin-low tumour most closely match the mammary stem cell population (Visvader and Stingl, 2014, Sreekumar et al., 2015).

1.1.4 Treatment

Current treatment of breast cancer will vary between patients depending on multiple factors but can involve endocrine therapy, broad cytotoxic chemotherapy, targeted molecular therapy, surgery and radiation therapy. An important early step in a patient's treatment is to determine their tumours expression level (or lack thereof) of ER, PR and HER2 as this will guide treatment options. ER expression renders luminal type tumours vulnerable to hormonal based therapy and current standard treatment involves inhibition or modulation of the estrogen signalling pathway through agents such as aromatase inhibitors or the selective estrogen receptor modulator (SERM) tamoxifen which, when used as part of a five-year adjuvant therapy, reduces recurrence and mortality by approximately 50% and 30%, respectively (Early Breast Cancer Trialists' Collaborative, 2011). Current evidence now supports a longer treatment program, with 10 years usage of tamoxifen offering significant survival benefits in comparison to 5 years (Davies et al., 2013).

Treatment of ER+ tumours will also vary depending on age of the patient and whether they are pre- or post-menopausal. Aromatase inhibitors, which function by blocking a key step in the estrogen biosynthesis pathway (aromatization of circulating androgens to estrone) are more effective than tamoxifen in post-menopausal women (Dowsett et al., 2010). ER signalling can also be targeted via selective estrogen receptor degrader (SERD) drugs, of which fulvestrant was first-in-class to be approved. Fulvestrant binds ER and creates an unstable complex, leading to increased degradation of the receptor (Nathan and Schmid, 2017).

Patients with HER2 expressing tumours will usually be treated with trastuzumab or other HER2 targeting agents. Addition of trastuzumab to chemotherapy regimens improves overall survival by almost 35% (Moja et al., 2012) and also results in improvements to response and risk of recurrence (Esteva et al., 2010). Despite its significant impact on the treatment of HER2-amplified breast tumours, resistance remains a huge barrier.

Response rates to trastuzumab as a monotherapy are low, with intrinsic resistance observed in 66% to 88% of HER2-overexpressing tumours (Nahta and Esteva, 2006, Oliveras-Ferraros et al., 2012) and even in patients that do respond to treatment, resistance typically sets in within a few months (Gajria and Chandarlapaty, 2011). Newer HER2 targeting drugs such as the tyrosine kinase inhibitor lapatinib or pertuzumab, another HER2 targeting antibody capable of blocking receptor dimerisation may improve patient response rate and outcome (Vrbic et al., 2013). Combination therapy with lapatinib and trastuzumab achieved a pathological complete response (pCR) of 51.3% compared to 29.5% for trastuzumab alone (Baselga et al., 2012). However, these new drugs are also subject to the development of resistance (Rexer and Arteaga, 2012).

Triple-negative tumours lack robust molecular targets, thus making their treatment difficult. Treatment typically involves usage of cytotoxic chemotherapy, often a combination of anthracyclines and taxanes (Shastry and Yardley, 2013, Yao et al., 2017). Response may be improved by addition of platinum drugs like carboplatin and certain forms of targeted therapy, including inhibitors of EGFR, poly(ADP-ribose) polymerase (PARP) and PI3K (Abramson et al., 2015, Mayer et al., 2014). There is now a significant drive to identify novel targets in triple-negative tumours (Kalimutho et al., 2015). Cyclin-dependent kinase 7 (CDK7) was recently shown to be highly expressed in triple-negative breast cancer and can be targeted via combination of CDK7 and BCL-2/BCL-XL inhibitors (Li et al., 2017). Basal-like tumours show higher sensitivity to a variety of chemotherapy regimens than other subtypes, although survival rates remain low (Carey et al., 2007, Shastry and Yardley, 2013, Yadav et al., 2014).

Surgical treatment of breast cancer has changed radically over the years. The total removal of the breast (known as a mastectomy) that was once the mainstay of surgical treatment for breast cancer has been shown to offer no survival benefit over less extreme, breast conserving therapy, consisting of a lumpectomy to remove just the tumour and a small amount of surrounding tissue followed by radiation therapy (Johns and Dixon, 2016). Survival rates for breast cancer have improved considerably in the last few decades (NCRI, 2017) but issues such as drug resistance and lack of effective therapies for patients with advanced breast cancer remain a challenge.

As with most other forms of cancer, patients whose breast cancer is caught in the early stage will typically respond much better to treatment. Patients with advanced metastatic breast cancer have median survival from time of first distant metastasis ranging from 2.2 years for patients with a luminal A type tumour to only half a year for those with a basal-like cancer (Kennecke et al., 2010). Early detection is therefore crucial in ensuring the best possible chance for a patient to overcome their cancer.

1.1.5 Mammographic screening

To aid in this crucial endeavour of early detection, many countries now offer free x-ray based screening programmes. Mammographic screening is offered to women in Ireland aged between 50 and 64 for free once every two years by BreastCheck. Since being established in 1998, the BreastCheck programme has provided 1.5 million mammograms to over 500,000 women resulting in the early detection of over 9,800 cases of breast cancer (BreastCheck, 2017). In 2015, 145,822 women received a mammogram through the BreastCheck programme (an uptake rate of 74.7% of the 198,986 women invited). Of these, 5,830 women were re-called for assessment, resulting in detection of 785 invasive breast tumours and 201 case of ductal carcinoma in situ (DCIS). Mammography in Ireland was implemented in a two-stage process, with approximately half of the country beginning screening in 2000, with the other half initiating in 2007. This phased-rollout provides the opportunity for a closely-matched, geographical control group. A recent analysis of the impact of BreastCheck on breast cancer mortality found a 9% lower rate in the region with earlier implementation of screening, although the authors also point out the real benefit is likely to be higher as the full benefits of screening are only realised after many years of screening (Hanley et al., 2017).

Despite a huge effort by many governments and healthcare organisations to promote screening, its routine uptake amongst the general population has long been a controversial issue. Many of the lesions detected through mammography are small, benign growths unlikely to progress to malignant breast cancer and pose little threat to the women. However, as prediction of which lesions will develop into full-blown invasive cancer is difficult, women presenting with these types of growths will usually be treated.

There is still some debate as to whether the efficacy of mammography in catching early stage tumours is enough to mitigate the harms associated with overtreatment and with exposure of large numbers of women to unnecessary radiation, not to mention the emotional impact associated with a positive cancer diagnosis. A meta-analysis of 11 large scale studies (all with a cohort size of at least 50,000) by the Independent UK Panel on Breast Cancer Screening demonstrated a reduction in relative risk of breast cancer mortality of 20% in patients who had undergone screening versus those who had not (Marmot et al., 2013). Other studies have reached similar conclusions (Nelson et al., 2009, The Canadian Task Force on Preventive Health Care, 2011, Pace and Keating, 2014, Weedon-Fekjær et al., 2014).

A meta-analysis by the Cochrane collaboration also arrived at a figure of approximately 20% but had very different conclusions. Pointing out issues with inadequate randomisation and bias associated with reporting cause of death, they concluded that several studies should be excluded from consideration. When these studies deemed inadequate were removed from analysis, the benefit of screening declined from an initial relative risk value of 0.81 to 1.02 (Gøtzsche and Jørgensen, 2013). The findings of Gotzsche & Jorgensen have been challenged by many groups [summarised in (Feig, 2014)], although some other studies have been in support. For instance, a recent study argued that in many countries (including Ireland), breast cancer mortality had already started to decline before the implementation of screening (Bleyer et al., 2016). In addition, a recent analysis of the Dutch mammography screening programme from 1989 to 2013 found a steep increase in the incidence of both *in situ* and stage 1, but not stage 2-4 breast tumours (Fig.1.3), concluding that up to 24% of breast cancers found due to screening represented overdiagnosis (Autier et al., 2017). They also estimated screening to reduce mortality by 5% at most whilst improved treatment was associated with a 28% reduction.

It is worth noting however, that although some disagreement may exist over the efficacy of mammography in population screening, its effectiveness as a diagnostic method is widely accepted. Mammographic imaging is combined with a clinical exam and analysis of a small biopsy sample (usually taken from a fine-needle aspiration or core-needle biopsy) into a “triple-assessment” , which taken together demonstrates a sensitivity and specificity approaching 100% (Kharkwal et al., 2014,

Morris et al., 2001, Chalya et al., 2013). Whether or not mammography should be utilized in screening programmes remains a difficult question to answer. Clearly, a greater understanding of the underlying molecular mechanisms of breast cancer is required to fully determine which groups of women should be screened and if any of their detected lesions are likely to progress.

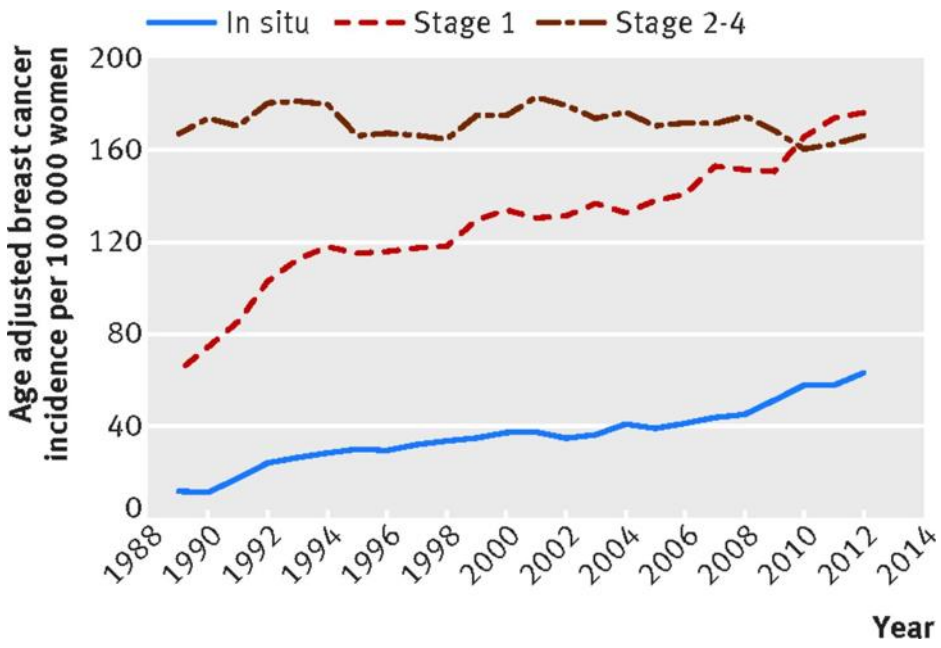

Figure 1.3 Changes in age adjusted breast cancer incidence rate of different stages in women aged 50 or more in the Netherlands, 1989 to 2012. Significant increases were observed in both *in situ* and stage 1 but not more advanced tumours (stage 2-4). Reproduced from Autier (2007).

1.2 Breast cancer and microcalcifications

1.2.1 Mammary microcalcifications: An introduction

Despite the controversy, mammographic screening remains a vital tool in early detection of breast cancer in many countries, with most utilizing the Breast Imaging Reporting and Data System (BI-RADS), a standardized system for classifying and reporting clinical findings from mammography. Mammograms are scored on a number of features including density, architectural distortions and calcifications, and placed into one of 7 BI-RADS categories, ranging from “Incomplete Assessment” (Category 0) up to “Known Biopsy-Proven Malignancy” (Category 6), each with a recommended course of action (Table 1.1) (Eberl et al., 2006).

Microcalcifications are small calcified deposits, appearing as bright white spots in mammograms. First identified in 1951 (Leborgne, 1951), they have long been a highly useful marker of breast cancer, with somewhere between 30 and 50% of non-palpable tumours found in screening identified solely due to the presence of microcalcifications (Gülsün et al., 2003, Venkatesan et al., 2009). They are also present in the majority of DCIS cases (Hofvind et al., 2011). Microcalcifications are categorized based on their size, shape, chemical composition and spatial distribution within the breast.

Structurally speaking microcalcifications can take several forms, ranging from a dispersal of fine particles classified as “powdery” up to long, branching structures called “casting-type”. In addition to their morphology, microcalcifications can also be categorized based on their chemical structure. Type I calcifications are composed of calcium oxalate [$CaC_2O_4 \cdot 2H_2O$] crystals which take the form of amber coloured pyramidal structures whilst Type II consist of calcium phosphate in the form of calcium hydroxyapatite [$Ca_{10}(PO_4)_6(OH)_2$] (Scimeca et al., 2014). Type I calcifications are generally found solely in benign tumours whilst type II calcifications are mostly seen in malignant tumours (Haka et al., 2002, Radi, 1989).The BI-RADS system includes specifications on how calcifications should be classified based on morphology and distribution (Eberl et al., 2006).

1.2.2 Mammographic characterisation of microcalcifications

Calcifications detected by mammography can be characterised based on a number of attributes, including morphology, size, distribution and number. Based on these features, radiographers will then assign calcifications to a BI-RADS category indicative of their likelihood of malignancy (Table 1.1). Calcification morphologies typically considered low-risk include “popcorn-like”, eggshell or dystrophic, whilst calcifications of a coarse heterogeneous or fine-linear morphology convey a significantly increased risk of malignancy. A clear understanding of the relationship between different calcification morphologies and their formation can help inform clinical understanding as to which are likely to indicate the presence of cancerous tissue. For example, a benign eggshell-calcification is depicted below (Fig. 1.4 A). These thin, spherical structures usually form as the result of calcium deposition on the surface of an oil cyst, and are totally unrelated to breast cancer. In contrast, the long, thin branching structure of fine-linear type (often referred to as casting)

calcification (Fig. 1.4 B) indicates spread of calcium deposition along the inner duct, and is highly suggestive of malignancy (Rao et al., 2016).

Suspicious microcalcifications can be further stratified with risk of malignancy based on morphology. A meta-analysis of 40 studies representing a total of 10,665 patients with mammographically detected calcifications demonstrated pooled malignancy rates of 13% for coarse heterogeneous, 27% for amorphous or indistinct, 50% for pleomorphic, and 78% for fine-linear (Rominger et al., 2012). Other studies have found similar results, with fine-linear calcifications regarded as extremely suspicious (Kim et al., 2015c, Bent et al., 2010).

In addition to morphology, the spatial distribution of microcalcifications within the breast tissue can also inform clinical opinion (Bent et al., 2010, Burnside et al., 2007). Calcifications grouped in a linear (representing spread of calcified deposits along a duct) or segmental pattern (calcium deposition within a duct and associated branches, following the shape of a breast lobe) are considered high risk, and are significantly more likely to represent a malignancy than calcifications in a clustered distribution (5 calcifications within an area of 1 cm^2).

Table 1.1. Breast imaging and reporting data system (BI-RADS) categories for mammography and its association with microcalcification appearance. Adapted from D'Orsi (2013).

Category	Description	Management	Likelihood of malignancy
0	Incomplete	Additional imaging required	Not applicable
1	Negative	Continue routine screening	0%
2	Benign	Continue routine screening	0%
3	Probably benign	Short interval follow up	0 – 2%
4 **A** **B** **C**	 Low suspicion Intermediate suspicion High suspicion	May require biopsy	 2 – 10% 10 – 50% 50 – 95%
5	Highly suggestive of malignancy	Biopsy required	>95%
6	Biopsy proven malignancy	Begin treatment	Not applicable

		Calcification morphology	BI-RADS category
Calcifications	Typically benign	Skin Vascular Dystrophic Eggshell Large rod-like Popcorn-like	2 or 3
	Suspicious	Amorphous Coarse heterogeneous Fine-pleomorphic Fine-linear (casting)	4B 4B 4B 4C
	Extremely suspicious	Fine-linear (casting) in a segmental distribution	5

In turn, clustered calcifications (an intermediate category) are considered more suspicious than calcifications in a diffuse (random distribution within the breast) or regional (calcifications spread in a larger volume >2 cm^2). Some calcifications (eg. vascular or thick linear) can form a linear pattern, yet still be considered likely to be benign based on their underlying morphology (Arancibia Hernández et al., 2016). This highlights the necessity to consider both morphology and distribution of calcifications when assessing likelihood of malignancy.

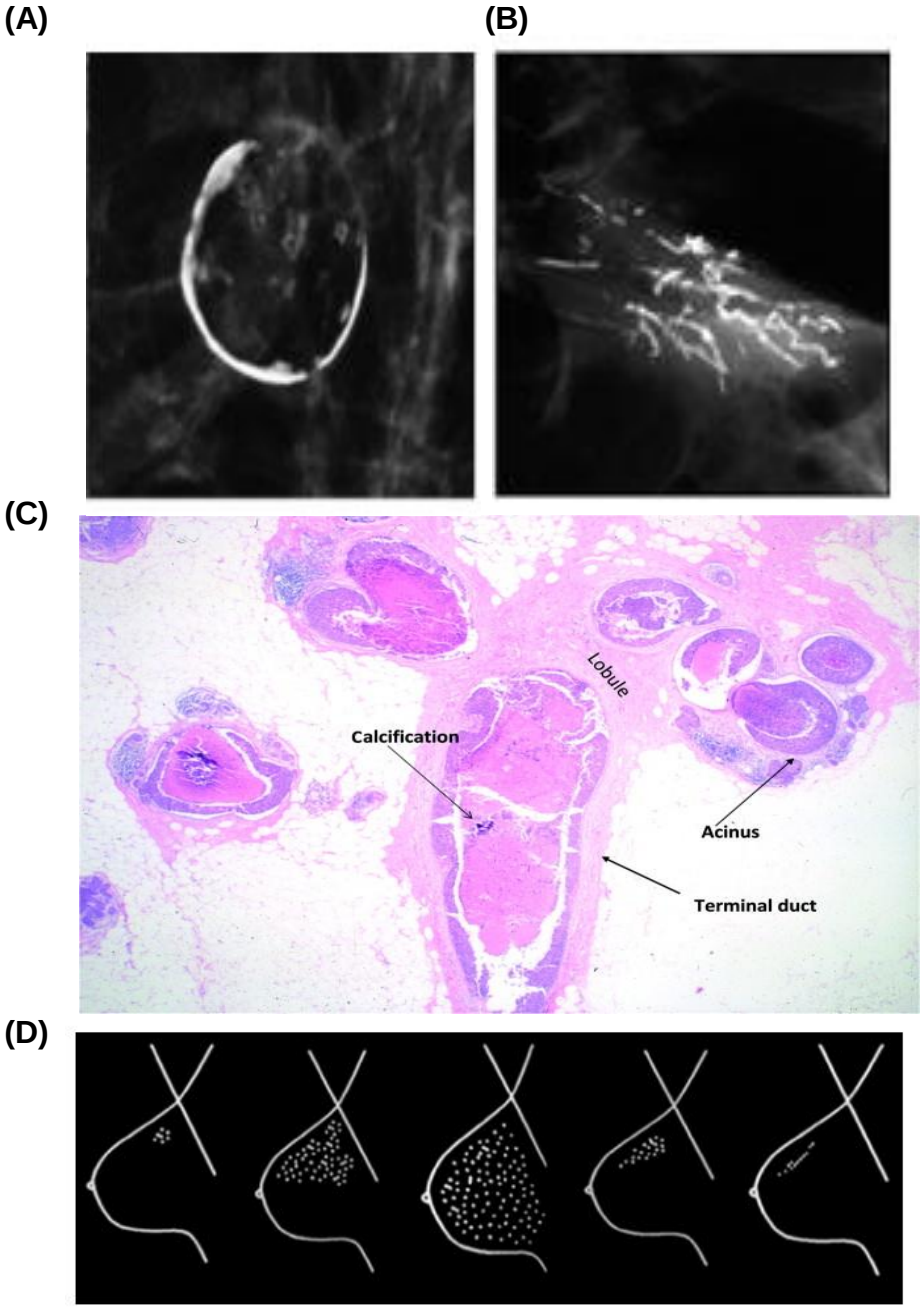

Figure 1.4 Mammographic and histological appearance and distribution patterns of microcalcification. Mammographic appearance of benign (A) and malignant (B) microcalcifications can vary significantly. H&E stained section shows presence of calcification within ductal lumen (C). Images taken from Tabar and Dean (2008), Rao (2016) and D'Orsi (2013). Possible distributions of microcalcifications (D) are represented above in the following order; clustered, regional, diffuse, segmental and linear. Adapted from Arancbia Hernàndez (2016).

1.2.3 Chemical composition of microcalcifications

In addition to their morphology and distribution pattern, microcalcifications can be categorised based on their chemical composition. Type I calcifications are composed of calcium oxalate [$CaC_2O_4 \cdot 2H_2O$] crystals whilst type II consist of calcium phosphate in the form of calcium hydroxyapatite [$(Ca_{10}(PO_4)_6(OH)_2$].

Type I calcifications are generally found solely in benign tumours whilst type II calcifications may be found in either benign or malignant tumours (Radi, 1989, Haka et al., 2002). In an analysis of microcalcifications taken from 25 patients, Frappart et al. found type II calcifications in all cases of infiltrating carcinomas and intraductal adenocarcinomas and in 50% of benign tumours whilst type I calcifications were only present in benign samples (Frappart et al., 1984). Similarly, Winston et al. examined biopsy samples from 55 women and found that in the 8 patients presenting with exclusively calcium oxalate calcifications, all had benign growths. In contrast, 40% (19/47) of patients with type II calcifications (either as the sole form of calcification present or in conjunction with type I crystals) had carcinoma (Winston et al., 1993).

Although mammography cannot distinguish type I and type II calcifications, recent studies utilising Raman spectroscopy have shown that addition of this analysis technique could be a clinically useful strategy. Raman spectroscopy measures energy shifts in inelastically scattered light to generate a molecule-specific spectrum and has been used to analyse biopsy samples, successfully distinguishing type I and type II calcifications (Saha et al., 2011, Barman et al., 2013, Haka et al., 2002, Haka et al., 2005). Loss of light through scattering typically limits Raman spectroscopy analysis to a relatively shallow depth, recent developments have allowed for analysis at a depth of up to 40 mm of tissue (Ghita et al., 2017). This raises the possibility of utilising Raman analysis as a non-invasive, clinical imaging technique to identify calcifications likely to be representative of a malignancy. A recent study even found that Raman analysis of whole blood samples could detect shifts in the Raman spectrum characteristic of calcium oxalate and calcium hydroxyapatite, which were increased in blood from breast cancer patients (Bilal et al., 2016).

Raman analysis has also been used to identify several notable differences between benign and malignant calcifications. The carbonate content of calcifications is inversely correlated to malignancy, with calcifications representative of invasive, *in situ* and benign disease possessing a mean carbonate content of 1.41, 1.83 and 2.08% respectively (Haka et al., 2002, Baker et al., 2010). Carbonate content was also significantly lower in high grade invasive cancers or DCIS tumours. When the ratio of protein matrix to mineral was analysed, the opposite pattern was observed, with increased protein content going from benign to *in situ* to invasive. Combining both these metrics yielded a linear discriminant model capable of identifying malignancy lesions with a sensitivity and specificity of 90% and 96%, respectively (Baker et al., 2010).

A recent study using energy dispersive X-ray microanalysis to probe the chemical composition of microcalcifications in a group of patients with either benign or malignant breast lesions identified significant amounts of magnesium substituted hydroxyapatite, a novel form of microcalcification which was only found in malignant lesions (Scimeca et al., 2014). A subsequent study using X-ray diffraction found small amounts of the magnesium-containing calcium phosphate crystal whitlockite in calcification samples from breast cancer patients (Scott et al., 2016). The percentage of whitlockite in samples increased significantly from benign to *in situ* lesions to invasive tumours. The biological relevance of the magnesium content of microcalcifications remains unclear but its specificity to malignant lesions may prove highly valuable alongside carbonate percentage as a guide to distinguishing benign from malignant growths.

1.2.4 Microcalcifications and patient prognosis

In addition to their utility in the detection of breast cancer, the presence of calcifications on a mammogram may also be indicative of patient prognosis. Tabar et al. analysed mammograms of 343 patients with invasive breast cancers and found that 1-9 mm sized tumours with associated casting-type calcifications behaved as if they were much larger tumours with mortality rate similar to that seen in women with much larger, higher grade tumours (Tabár et al., 2000). This was followed by a second study by Tabar et al. with a larger cohort which found huge variation in survival rates of women diagnosed with small invasive tumours (Tabar et al., 2004).

Women with 1-9 mm tumours associated with casting-type calcifications had a far higher mortality rate than would be expected for tumours of this small size (20 year survival rate of 72% compared to 95% for women with similar sized lesions but without casting-type calcifications). Results from a study by Thurfjell et al. supports the findings of Tabar, with their analysis of 96 cases of invasive breast cancer cases showing a clear link between presence of casting-type calcifications and survival (Thurfjell et al., 2001). Similarly, Peacock et al. compared 50 women diagnosed with small invasive tumours and associated casting-type calcifications with tumour size and lymph node matched controls (Peacock et al., 2004).

There were 5 deaths in the calcification group but none in the control, a difference that was found to statistically significant (Peacock et al., 2004). In a study of 498 patients diagnosed with invasive breast cancer, Tsau et al. found that the presence of casting calcifications was associated with a 3.47-fold increased hazard ratio for mortality compared to other mammographic findings (Tsau et al., 2015). Ling et al. found that women presenting with calcifications had a 2-fold increase in risk of relapse and a 2.4-fold increased risk of dying from breast cancer compared with women without calcifications (Ling et al., 2013). The most recent study identified for this literature review found patients with mammographic calcifications to have risk ratios of 2.46 for local recurrence, 2.24 for metastasis and 2.5 for mortality following breast-conserving therapy (Qi et al., 2017).

It is worth noting that not all studies are in agreement over the prognostic value of calcifications. In a study of 515 women with 1–15 mm tumours, the adjusted odds ratio for breast cancer death in patients with casting calcifications was 1.6 although this was not found to be significant (Månsson et al., 2009). James et al. found the presence of casting-type calcifications to be associated with small, high-grade tumours but not with survival (James et al., 2003). Evans et al. also did not find any association between patient survival and type calcifications (Evans et al., 2006).

Many studies have also highlighted links between microcalcifications and increased risk of recurrence, with most studies finding between a 2- to 5- fold increase in risk. In a study of 409 patients treated with breast conserving surgery, Qi et al. found a 2.46 fold increased rate of local recurrence in patients with mammographically detected calcifications (Qi et al., 2017). Patients with calcifications in a linear or segmental distribution were particularly likely to suffer a relapse.

Rauch et al. found a 5.2-fold increase in local recurrence in patients presenting with fine linear microcalcifications (Rauch et al., 2016). Increased risk of recurrence is supported by recent studies using the Oncotype assay, a diagnostic assay which uses a 21-gene expression signature to estimate likelihood of recurrence. Patients presenting with calcifications are significantly more likely to be assigned to the "high-risk" category than those without (Chae et al., 2016, Yepes et al., 2014, Woodard et al., 2017). In contrast, in a study of 937 cases of invasive carcinoma, Naseem et al. did not find any association between the presence of calcifications and recurrence (Naseem et al., 2015). A possible explanation for this may lie in the findings of Holmberg et al., which showed a 2.1-fold increase in recurrence in patients with fine linear calcifications compared to those without calcifications (Holmberg et al., 2013). Interestingly, when cases of invasive carcinoma and DCIS were analysed separately, this increase was found to mainly be confined to the DCIS sub-cohort. The fact that Naseem et al.'s cohort consisted only of invasive carcinomas may explain their inability to detect any increase in recurrence risk in patients with calcification.

Calcifications have also shown a significant association with high tumour grade. Rauch et al. found tumour grade to be significantly associated with calcification morphology, with the highest risk conveyed by fine-linear calcifications (3.4-fold increase relative to calcifications of a punctate/amorphous morphology (Rauch et al., 2016). Naseem et al. observed a borderline-significant (P=0.057) trend toward increased tumour grade in calcification associated tumours, with the rate of calcification increasing from 30.7% for grade I to 39.8% for grade II and 41.3% for grade III (Naseem et al., 2015). A recent study involving over 8,000 cases of invasive breast cancers found calcifications to be associated with 1.43-fold increased risk of high tumour grade (Nyante et al., 2017). Similar results were found in an analysis of mammography data from over 7,000 patients in China (Zheng et al., 2017).

Perhaps the most consistent finding in these studies is a strong association between the presence of calcifications and HER2 overexpression. A recent microarray analysis found the *ERBB2* gene to be amongst the most differentially expressed between patients with highly suspicious calcifications versus those without (Shin et al., 2017).

In addition, a meta-analysis encompassing a total of 17,745 breast cancers found that the presence of calcifications carried a pooled odds ratio of HER2 overexpression of 3.14, regardless of whether the detected calcification was found with or without an associated mass (Elias et al., 2014).

Calcifications may also be associated with tumour invasion into the lymphatic system, although not all studies are in agreement. Tabar et al. found the presence of casting calcifications to confer a 3.29-fold increased risk of positive lymph node status, relative to stellate lesions with no calcifications (Tabar et al., 2004). Several other studies have also found an increased rate of lymph node involvement in patients with calcifications (Ling et al., 2013, Zheng et al., 2017), although others have failed to find an association (Naseem et al., 2015, Shin et al., 2017).

Similarly, inconsistent results were found with tumour size, with studies finding calcifications to be associated with either increased (Jiang et al., 2011, Ling et al., 2013) or decreased tumours size (Nyante et al., 2017), or not associated at all (Naseem et al., 2015, Palka et al., 2007, Qi et al., 2017).

Despite some disagreement within the literature, the majority of evidence thus far does seem to indicate an important role for microcalcifications, and in particular those of a casting-type morphology, in predicting prognosis, risk of malignancy, likelihood of recurrence and numerous other clinically important attributes. Many of these discrepancies could likely be resolved through the usage of large-scale meta-analysis, which has been done for some clinical factors relevant to mammographic calcifications, but not all. For instance, the relationship between calcification morphology and risk of malignancy was analysed by a meta-analysis encompassing over 10,000 patients and provided strong evidence of a high degree of risk associated with calcifications of a pleomorphic or fine-linear morphology (Rominger et al., 2012).

A selection of some of the key studies demonstrating these associations is summarised in Table 1.2. A more comprehensive table can be found in the appendix (Table 8.1).

Table 1.2 Key studies demonstrating association between mammographic calcifications and key prognostic factors in breast cancer patients. Note, "fine-linear" and "casting" are used interchangeable depending on terminology used within each individual study.

References	Study Cohort	Key Findings
(Bennett et al., 2011)	232 screen-detected cases of invasive cancer	• 3-fold increased hazard-ratio for mortality in patients with comedo-type DCIS with associated calcification.
(Cen et al., 2017b)	419 cases of invasive ductal carcinoma with BI-RADS 3–5 calcifications	• Calcification density associated with lymph node status
(Ferranti et al., 2000)	982 screen detected carcinomas	• Presence of microcalcifications associated with increased tumour grade and size and positive node status.
(Gajdos et al., 2002)	543 mammographically detected nonpalpable malignancies	• Calcifications associated with more extensive intraductal carcinoma and HER2 positivity, invasive cancers presenting as masses with calcifications associated with lymphatic invasion
(Hofvind et al., 2011)	217 cases of pure DCIS with no microinfiltration	• 84% of DCIS cases with associated fine linear and fine linear branching calcifications were high grade lesions.
(Holmberg et al., 2013)	Case-cohort study of 198 patients with DCIS	• 16-fold increased relative risk of ipsilateral, *in situ* recurrence in patients with casting-calcifications
(Kim et al., 2008)	Analysis of ultrasound findings in 435 invasive cancers and 23 cases of DCIS	• Presence of calcifications significantly associated with high grade and HER2 positivity in DCIS
(Ling et al., 2013)	721 cases of confirmed invasive ductal carcinoma	• Significantly decreased RFS and OS in patients with calcifications • Increased tumour size and lymph node involvement, lower ER/PR expression and higher HER2 expression
(Naseem et al., 2015)	937 cases of breast cancer	• Calcifications more common in patients with HER2 over-expression, heterogeneous density and multifocal breast disease. Borderline significant ($p = 0.057$) with increased grade. • No significant association between calcifications and node status, tumour size or rate of recurrence.
(Rauch et al., 2016)	1657 patients with DCIS and calcifications	• Casting calcifications associated with high tumour grade, increased risk of recurrence and comedonecrosis
(Tabár et al., 2000)	343 screen detected invasive cancers, 1-14 mm size	• 20 year survival of 55% for patients with casting calcifications versus 87% for patients without • Greater likelihood of high-grade tumours in patients with casting calcifications
(Tabar et al., 2004)	714 screen detected invasive cancers, 1-14 mm size	• Presence of casting calcifications associated with higher histological grade, positive lymph node status and decreased survival
(Tsau et al., 2015)	498 patients diagnosed with invasive breast cancer	• Casting calcifications associated with 3.47-fold increased hazard ratio for mortality
(Wang et al., 2008)	Retrospective study of preoperative mammograms in 152 breast carcinoma patients	• Higher rate of HER2 over-expression, TNM III stage and axillary lymph node metastasis in patients with calcifications.
(Qi et al., 2017)	409 patients with breast carcinoma treated with breast conserving surgery	• Calcifications associated with risk ratios of 2.46 for local recurrence, 2.24 for metastasis and 2.5 for mortality.

1.2.5 Biological effects of microcalcifications

With a significant body of evidence to demonstrate a link between calcifications and a range of prognostic factors, it is interesting to speculate how the presence of calcifications could potentially be directly influencing tumour behaviour. The first studies to investigate the potential biological significance of calcifications on breast cancer found that stimulation of MCF-7 and Hs578T breast cancer cell lines with synthetic, hydroxyapatite (HA) particles (representative of malignancy associated, type II microcalcifications) lead to increased mitogenesis (Morgan et al., 2001). Pathi et al. also observed increased proliferation in both MDA-MB-231 and MCF-7 cells grown on HA-mineralised scaffolds as compared to non-mineralised scaffolds (Pathi et al., 2010).

Although the precise mechanism of HA stimulation in breast cancer cells has not been fully elucidated, direct cell-crystal contact and intracellular dissolution of the crystals appears to be essential as separation of cells and the crystals by transwell membranes results in an elimination of HA induced mitogenic response (Cooke et al., 2003). Similar effects were seen when cells were treated with the vacuolar type proton pump ATPase inhibitor bafilomycin A1 to inhibit lysosomal dissolution of the HA crystals, indicating the importance of both endocytosis and intracellular crystal dissolution in cellular response to HA. HA crystals exert a stimulatory effect on other cell types by a bi-phasic mechanism, involving a rapid but transient spike in intracellular Ca^{2+} followed by a second, slower but longer acting rise in Ca^{2+} over time (Halverson et al., 1998). HA stimulation of cells cultured in a Ca^{2+} free media abolished the first peak but not the second. In contrast, the second phase could be blocked by the addition of ammonium chloride which alkalises phagolysosomes and inhibits intracellular dissolution of calcium containing crystals. These results indicate that HA crystals stimulate an initial influx of Ca^{2+} from the extracellular media by direct cell-crystal interactions before phagocytosis and dissolution yields a second, gradual rise in intracellular Ca^{2+}.

In addition to stimulating proliferation, HA crystals also exert a potent inflammatory effect in breast cancer cells. HA stimulated MCF-7 cells display increased levels of prostaglandin E2 (PGE2) (Morgan et al., 2001). This increase was likely mediated by increased expression of cyclooxygenase-2 (COX2), as HA crystals upregulate COX2 expression (Cooke et al., 2003), and blocking COX2 activity with aspirin lead to a decrease of PGE2 in HA stimulated cells (Morgan et al., 2001).

COX2 is a significant promoter of breast tumour development. COX-2 is upregulated in breast cancer, with one study even finding a link between increased immunohistochemical staining for COX-2 and the presence of mammographic calcifications (Qiu et al., 2017). Long term aspirin use decreases risk of developing breast cancer (Luo et al., 2012) and may improve patient survival (Fraser et al., 2014). In addition, COX-2 expression is associated with tumour size and grade (Miglietta et al., 2010) and promotes epithelial-mesenchymal transition (EMT) and invasion (Bocca et al., 2014). Considering the multiple tumour-promoting effects associated with COX-2 expression in breast tissue, the link between microcalcifications and COX-2 may play a role in the unusually aggressive nature of calcification-associated tumours observed in some studies (Tabár et al., 2000, Tabar et al., 2004).

HA was also found to upregulate production of matrix metalloproteinases (MMPs) in both normal and cancerous breast cells (Cooke et al., 2003, Morgan et al., 2001). MMPs are known promoters of metastasis and tumour growth due to their role in degradation of the extracellular matrix (ECM) surrounding the tumour. Multiple studies have shown HA has also been shown to upregulate MMP expression in other cell types (Cheung et al., 1997, McCarthy et al., 1992, McCarthy et al., 2001, Reuben et al., 2001). MMPs are multi-functional promoters of breast tumour progression. In addition to their well-known activity in promoting invasion via ECM degradation, MMPs can also activate and release precursor growth factors from surrounding tissue, decrease apoptotic signalling through cleavage of Fas ligands, promote EMT and modulate tumour-immune surveillance via proteolytic activation of TGF-β (Gialeli et al., 2011, Kessenbrock et al., 2010). Many of the biological effects of HA stimulation demonstrated in both breast cancer and other cell types are known promoters of tumour progression and invasion. It seems likely that the presence of calcifications within the tumour microenvironment could be directly stimulating both tumour other associated cells, and potentially play a role in the tumours spread.

A detailed understanding of the formation process of microcalcifications could therefore help inform clinical understanding of the early events of breast tumourigenesis.

1.3 *In vivo* mineralisation

1.3.1 Physiological mineralisation

In addition to forming type II microcalcifications, hydroxyapatite is also present under normal physiological conditions, forming the primary inorganic component of bone, teeth and other calcified structures. Formation of HA microcalcifications in breast tumours is likely to follow a similar process. Physiological mineralisation is regulated primarily by a mesenchymal cell known as an osteoblast. These cells lay down a network of ECM proteins, primarily collagen I which is subsequently mineralised with hydroxyapatite (Tomoaia and Pasca, 2015). Multiple methods of mineralisation have been proposed in the literature.

Matrix vesicles are small (20-200 nm) spherical particles that bud off from the outer membrane of chondrocytes, osteoblasts, and odontoblasts. Their membranes are enriched in several factors crucial to mineralisation including tissue non-specific alkaline phosphatase (TNAP), ectonucleotide pyrophosphatase/phosphodiesterase (ENPP1), annexins and phosphatidyl serine (Golub, 2009). Matrix vesicles may facilitate mineralisation by concentrating Ca^{2+} and phosphate (Pi), regulating the ratio of Pi to its inhibitory counterpart pyrophosphate (PPi) and providing nucleation sites. Vesicles are then released from mineralising cells where they can deposit calcium phosphate onto nearby collagen (Anderson, 2003). Mineralisation-competent vesicles have been shown to be released from vascular smooth muscle cells in *in vitro* models of vascular calcification and to be important mediators of pathological calcification (Kapustin et al., 2011). The release of exosomes, which share many similarities to matrix vesicles (Shapiro et al., 2015), has been demonstrated in breast cancer cells and appears to stimulate a range of tumour promoting effects, including drug-resistance, invasion and immune modulation (Lowry et al., 2015, Wu et al., 2016).

Collagen may also directly promote its own mineralisation. The 3D arrangement of collagen results in a staggered arrangement and a series of “holes” that can act to nucleate Ca^{2+} and Pi ions (Xu et al., 2015b). Mineral deposition can occur both inside (intrafibrillar) and outside (interfibrillar) collagen polypeptide (Landis and Jacquet, 2013). Recent evidence also suggests that mineralisation may begin with deposition of an amorphous calcium-phosphate product within the collagen fibrils, before subsequent crystallisation to hydroxyapatite (Boonrungsiman et al., 2012, Mahamid et al., 2011).

Apoptosis also seems to play a role in biomineralisation. Terminally differentiated, hypertrophic chondrocytes in the growth plate of long bones are observed to undergo a carefully coordinated program of apoptotic death leaving behind a scaffold for osteoblast mediated mineralisation (Kronenberg, 2003). They also leave behind small membrane enclosed vesicles containing fragments of the former cells contents called apoptotic bodies. Due to the non vascularised nature of articular cartilage and absence of phagocytes that would normally remove remains of apoptotic cells, chondrocytes apoptotic bodies are believed to remain within the ECM of developing bones and precipitate calcium in a similar manner to matrix vesicles (Hashimoto et al., 1998). Apoptotic bodies have been shown to be an important contributor to pathological vascular calcification (Proudfoot et al., 2000, Reynolds et al., 2004).

1.3.2 Phosphate-phosphate balance

Regardless of the precise mechanism by which mineralisation occurs, a crucial factor in regulating this process is the balance between phosphate (Pi) and pyrophosphate (PPi), and the enzymes responsible for their production. PPi, which consists of two molecules of Pi joined by an ester bond, acts as a vital endogenous inhibitor of mineralisation, primarily through adsorption to the forming HA crystals and interfering with nucleation (Golub, 2009). PPi is produced extracellularly by the transmembrane enzyme ectonucleotide pyrophosphatase/phosphodiesterase 1 (ENPP1), which degrades extracellular ATP to PPi and AMP, as well as intracellularly as a by-product of several metabolic pathways and exported out of the cell by ankylosis protein (ANK) (Terkeltaub, 2001). Interestingly, ENPP1 can also positively regulate mineralisation in certain contexts. Osteoblast specific deletion of ENPP1 results in improperly differentiated and inactive osteoblasts (Nam et al., 2011).

Mice with *Enpp1* knockdown display extensive calcification of the cardiovascular system, highlighting its importance in preventing aberrant mineralisation (Li et al., 2014b). The inhibitory effect of ENPP1 and its PPi product are counteracted by the activity of the alkaline phosphatase (ALP) enzyme which hydrolyses PPi to Pi, simultaneously removing a source of inhibition and producing free Pi for HA formation (Millán, 2013). This double-action makes ALP activity a powerful driver of both physiological and pathological mineralisation.

Mice with a knockout mutation in the alkaline phosphatase 2 (*Akp2*) gene exhibit significant mineralisation defects (Yamamoto et al., 2011). The primary role of ALP in promoting mineralisation may lie in its ability to remove the inhibitory effect of PPi, rather than generation of free Pi (O'Neill, 2006).

A second phosphatase has now been identified with an important role in regulating Pi levels in matrix vesicles. The phosphatase PHOSPHO1 is highly specific for phosphoethanolamine and phosphocholine, two membrane phospholipids that are enriched in the membrane of matrix vesicles (Roberts et al., 2004) and its expression in mineralised tissue is over 100 times greater than in soft tissue (Roberts et al., 2007). PHOSPHO1 is present within matrix vesicles and its inhibition significantly reduces the mineralising capability of these vesicles (Roberts et al., 2007). *Phospho1*$^{-/-}$ mice display severe skeletal defects including decreased bone density, spontaneous fractures and scoliosis (Yadav et al., 2011). This phenotype is not reversed by ALP overexpression and knockout of both PHOSPHO1 and ALP resulted in the almost total absence of skeletal mineralisation, indicating that the two proteins have complimentary but non-redundant roles in mineralisation.

1.3.3 Regulators of *in vivo* mineralisation

In addition to the Pi-PPi balance previously discussed, a range of other inhibitors have been described that tightly regulate calcium deposition to specific locations in the body. The vitamin K-dependent calcification inhibitor matrix gla protein (MGP) inhibits mineralisation through a variety of mechanisms including binding Ca^{2+}ions, direct inhibition of crystal growth and modulation of osteogenic signalling pathways (Proudfoot and Shanahan, 2006). *Mgp*$^{-/-}$ mice develop extensive vascular calcification and typically die after 2 months (Luo et al., 1997, El-Maadawy et al., 2003). The inhibitory effect of MGP on minimisation is dependent on γ-carboxylation of five glutamate residues to create Ca^{2+}binding sites (Schurgers et al., 2013).

Fetuin-A is a liver produced, plasma protein that acts as a mineralisation inhibitor by binding $Ca^{2+}$and Pi ions, resulting in formation of large protein-mineral aggregates, stabilising the minerals as colloids and facilitating their transport and clearing (Jahnen-Dechent et al., 2011). Osteopontin (OPN) is a highly-phosphorylated protein, ubiquitously expressed but found in high concentrations in areas of mineralised tissues including ectopic calcifications (Hunter, 2013). Removal of phosphorylation from OPN significantly reduces its inhibitory effect on HA formation (Hunter et al., 1994).

OPN also appears to have a highly disorganised structure, with this flexible structure allowing for multiple binding interactions between the protein and HA crystals (Azzopardi et al., 2010).

In addition to inhibitor proteins, mineralisation is also regulated by the levels of particular ions. Unsurprisingly, the levels of both $Ca^{2+}$and Pi ions significantly promote development of mineralisations (Villa-Bellosta et al., 2011, Lau et al., 2010). Increased Pi levels can cause formation of HA nanocrystals, which trigger osteogenic changes in vascular smooth muscle cells (Sage et al., 2011). In contrast, Mg^{2+} ions are potent inhibitors of HA crystal nucleation. Mg^{2+} inhibits formation of HA crystals by numerous mechanisms including blocking attachment sites for $Ca^{2+}$and Pi ions, disrupting the crystal structure and by stabilising the precursor amorphous calcium-phosphate stage, preventing its conversion to mature HA (Ding et al., 2014). Other ions have also shown mineralisation regulatory function, including NaCl, KCl and bicarbonate (Villa-Bellosta et al., 2011).

1.3.4 Pathological calcification

Together, these various mineralisation inhibitors tightly regulate deposition of calcium and prevent the pathological mineralisation of soft tissue. However, this careful balance is perturbed in a number of diseases, resulting in formation of ectopic calcifications. A well-studied example is vascular calcification. Vascular calcification is caused by disruption of the various inhibitory processes previously described, resulting in deposition of calcium within the collagenous matrix of the intimal or medial layers of the arterial wall. This causes a stiffening of the arterial wall, and a substantial increase in risk of atherosclerosis and other forms of cardiovascular disease (Towler and Demer, 2011). Vascular calcification may be triggered by a variety of conditions including inflammation and oxidative stress (Byon et al., 2008), kidney dysfunction and elevated serum Pi (Hruska et al., 2007) aging and diabetes (O'Neill, 2006). Studies have implicated an active, cell regulated process in the formation of calcium deposits within the vasculature. Vascular smooth muscle cells (VSMCs) grown under mineralisation promoting conditions undergo phenotypic conversion to an osteogenic state, upregulating mineralisation associated genes including ALP, bone morphogenetic protein 2 (BMP2) and the osteogenic transcription factor runt-related transcription factor 2 (RUNX2) (Chen et al., 2006b).

Ectopic expression of bone associated genes in conjunction with loss of typical VSMC markers like smooth muscle specific α-actin results in a mineralisation promoting phenotype and subsequent deposition of calcium. Differentiation to this osteogenic phenotype seems to be crucial to mineralisation as mice with smooth muscle specific *Runx2* knockout do not undergo vascular calcification (Sun et al., 2012).

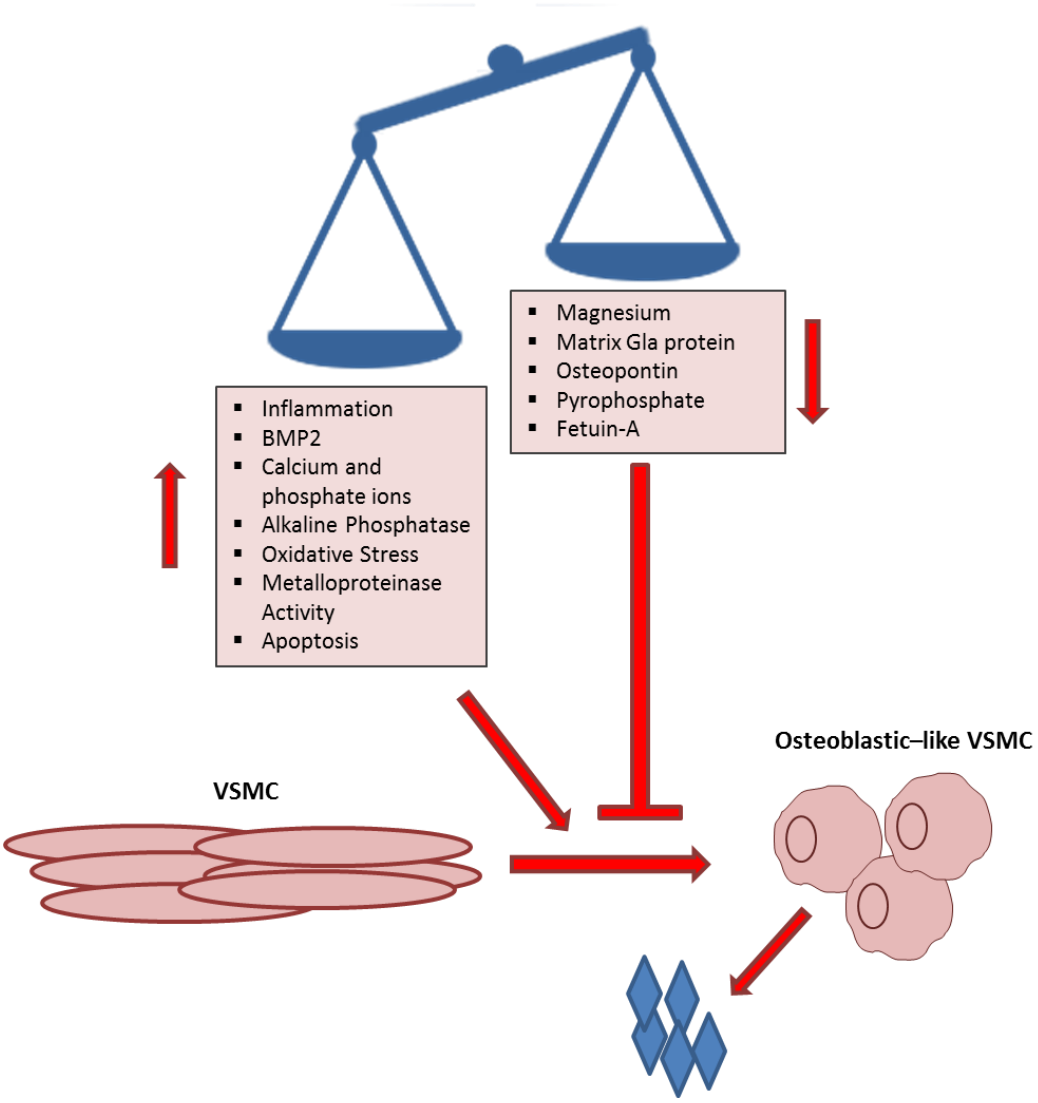

Figure 1.5 Vascular calcification as an imbalance between calcification promoters and inhibitors. Under normal physiological conditions, soft tissue mineralisation is prevented through a careful balance of mineralisation promoting factors (e.g. Ca^{2+}/Pi concentrations, inflammatory cytokines, apoptosis) and mineralisation inhibitors (e.g. Mg^{2+}, osteopontin). This balance can be knocked out of place by various causes including injury to the vessel wall, diabetes, cardiovascular disease or impaired kidney function, resulting in transdifferentiation of vascular smooth muscle cells (VSMCs) to an osteoblastic-like phenotype, capable of promoting mineralisation of the local extracellular matrix.

1.4 Formation of breast microcalcifications

1.4.1 Osteomimicry of breast cancer cells

As a well-established form of pathological calcification, it is possible that results from studies of vascular calcification may provide clues to the origin of breast microcalcifications. In particular, the finding of a cell-driven process of formation coupled with phenotypic conversion to an osteoblast-like state are highly interesting as expression of bone associated proteins in breast tumours is well established. Ectopic expression of mineralisation associated genes in breast tissue may also be a significant promoter of tumourigenesis, with many studies highlighting tumour prompting effects for these genes. BMP2 is expressed in both primary breast tumours and many breast cancer cell lines (Alarmo and Kallioniemi, 2010), and seems to contribute to EMT and development of cell-stemness via the Rb and CD44 signalling (Huang et al., 2017). RUNX2 is highly expressed in triple-negative breast tumours and appears to act as marker within this subtype (McDonald et al., 2014, Das et al., 2009).

It is also speculated that acquisition of this osteomimetic phenotype may underlie the high frequency of bone-metastases in breast cancer (Awolaran et al., 2016). Overexpression of the bone-matrix protein bone sialoprotein (BSP) in MDA-231BR, a sub-clone of the MDA-MB-231 cell line that metastasises exclusively to the brain, resulted in acquisition of a bone-seeking metastatic phenotype (Zhang et al., 2004). ENPP1 is upregulated in cell lines capable of metastasising to the bone models (MDA-MB-231) compared to those incapable (MCF-7/SKBR3), and its overexpression results in a significant increase in the number of bone metastases formed (Lau et al., 2013). A recent study found that co-stimulation of breast cancer cells with fibroblast conditioned media and BMP2 resulted in an EMT effect and generation of osteoblast-like breast cancer cells. Acquisition of an osteoblast-like phenotype was accompanied by ectopic expression of a host of bone associated genes, as well as an increase in proliferation, drug resistance and migration towards osteoblast cells, indicating a propensity towards bone metastasis (Tan et al., 2016). Acquisition of this phenotype involved signalling through RUNX2, already established as a vital contributor to pathological calcification (Sun et al., 2012).

1.4.2 Osteomimicry of breast cancer cells and microcalcifications

In addition to contributing to tumour growth and development, several groups have noted an association between expression of mineralisation associated genes and the presence of microcalcifications and hypothesised that osteomimicry of breast tumours could be involved in the formation of microcalcifications. Bellahcene & Castronovo found increased immunostaining for osteonectin and osteopontin in *in situ* and invasive breast carcinomas when compared with normal breast tissue (Bellahcène and Castronovo, 1995). They also noted that microcalcifications, when present, were usually found in areas with high immunoreactivity.

Osteopontin is an important inhibitor of calcium deposition in soft tissue (Steitz et al., 2002) and is believed to act as an inducible inhibitor (Speer et al., 2002). Therefore, the increased expression observed in calcification associated tumours may reflect a protective response and an attempt to limit further calcification. In a study of 141 cases of invasive carcinoma, Wang et al. found that microcalcifications were significantly more common in osteopontin positive tumours (54.3% vs 30.6% for osteopontin negative tumours) and were particularly frequent when calcifications were found in combination with a mass (72.7% for osteopontin positive tumours vs 18.2% for osteopontin negative tumours) (Wang et al., 2010b). The majority of calcifications found in osteopontin positive tumours were of a pleomorphic morphology, a form of calcification significantly associated with malignancy (Kim et al., 2015c). Scimeca et al. also found significantly increased osteopontin in infiltrating carcinomas with microcalcifications compared to those without, and also observed a focal staining pattern with high osteopontin signal around calcifications (Scimeca et al., 2014). Similar levels of upregulation were also observed for BMP2 and the mesenchymal marker vimentin, leading to the authors conclusion that formation of microcalcifications results from an EMT process and acquisition of an osteogenic phenotype.

Bellahcène et al. also demonstrated increased expression of BSP in breast carcinomas, with particularly high staining in samples with associated microcalcifications (Bellahcène et al., 1994, Castronovo and Bellahcène, 1998). DAPI staining also revealed the presence of DNA within microcalcifications, leading to the hypothesis that microcalcifications may represent the “fossils” of cancer cells, formed from mineralisation of secreted proteins around individual or clusters of breast cancer cells.

Bone sialoprotein (BSP) is a non-collagenous glycosylated phosphoprotein. Multiple lines of evidence implicate BSP as a potent inducer of mineralisation. (Gordon et al., 2007). Significant amounts of BSP are found in matrix vesicles (Nahar et al., 2008) where it is believed to play an important role in HA nucleation. BSP also plays an important role in development of breast tumours. BSP transfected breast cancer cells tend to metastasise to bone at a greater rate than their wild type counterparts (Zhang et al., 2004) and increased serum BSP levels is associated with bone metastases (Klevesath et al., 2013).

Breast carcinomas with associated calcifications have also recently been shown to display high levels of the transient receptor potential (TRP) ion channels TRPC1 and TRPM7 (Mandavilli et al., 2013). The functional relationship between these channels and microcalcifications has not been explored, although both channels have previously been shown to be significantly upregulated in breast carcinomas and to play a role in migration, invasion and proliferation (Guilbert et al., 2009, Ouadid-Ahidouch et al., 2012, Middelbeek et al., 2012).

Although many of these studies have been simply correlative, some have shown clear mechanistic links between mineralisation genes and the generation of microcalcifications. Most of these studies have focused on BMP2. R3230 rat tumour cells transfected with human-BMP2 form tumours with extensive areas of calcification following implantation into the mammary fat pad of a Fischer 344 rat (Liu et al., 2008). Observations of increased serum BMP2 in rats implanted with BMP2 overexpressing cells lead the authors to then test for humoral effects of BMP2 in formation of microcalcifications. Subsequent analysis demonstrated that rats with bilateral implantation (one fat pad with transfected cells, the other with untransfected) formed calcifications in both transfected and untransfected sides, indicating that BMP signalling can act humorally to induce microcalcification formation.

A second study by the same group demonstrated that transfection wasn't necessary: a single intraperitoneal injection of BMP2 into Fischer 344 rats bearing syngeneic R3230 breast tumours was sufficient to induce microcalcification formation in a dose and time dependent manner (Liu et al., 2010). This model has since been used to develop novel HA-specific fluorescent probes for *in vivo* imaging of microcalcifications (Bhushan et al., 2008, Inoue et al., 2011).

Formation of calcifications has also been observed in xenograft studies of BMP2 overexpressing MCF-7 cells (Clement et al., 2005). BMP2 overexpression may not be necessary for *in vivo* formation of microcalcifications as several studies have demonstrated positive mineralisation of breast tumours in mouse models using untransfected cell lines. Evidence from our group showed that implantation of the murine 4T1.2 cell line into the mammary fat pads of female BALB/c mice results in development of microcalcifications in 5/6 tumours (Cox et al., 2012a). The human triple-negative MDA-MB-231 cell line has also been shown to form calcified tumours following subcutaneous injection (Felix et al., 2015, Wilson et al., 2014).

1.4.3 *In vitro* models of mineralisation

Understanding the mechanisms of mineralisation in both physiological and pathological contexts has necessitated the development of reliable *in vitro* models. Mineralisation assays are most commonly used to explore physiological mineralisation by osteoblasts and mesenchymal stem cells, but have also been adapted to studies of vascular calcification and other forms of pathological calcium deposition. Mineralisation can be induced by culturing suitable cells for relatively long periods (often up to 4 weeks) with a combination of reagents designed to support calcification. Multiple formulations have been described within the literature, but almost all contain a source of Pi. Although this can be achieved by direct addition of inorganic sodium phosphate (Schäck et al., 2013), more common is the usage of β-glycerophosphate, an ester compound of phosphoric acid and glycerol, which acts as an organic Pi donor via cleavage by the alkaline phosphatase enzyme. β-glycerophosphate is rapidly hydrolysed to free Pi in osteoblast cultures (Boskey et al., 1996).

Ascorbic acid (usually in the form of ascorbic acid 2-phosphate, a stable, long-acting derivative) is also frequently added to osteogenic medias. Ascorbic acid is an essential co-factor for the enzyme prolyl hydroxylase, which hydroxylates proline residues in collagen. This post-translational modification is essential for formation of collagens distinctive helical structure (Langenbach and Handschel, 2013). Collagen provides a structural framework for deposition of calcium phosphate and formation of larger mineralised structures (Veis and Dorvee, 2013). A typical formulation of osteogenic media is 10 mM β-glycerophosphate and 50 µg/mL ascorbic acid.

Additional Ca^{2+} can also be added (Yang et al., 2004) although this is generally not necessary as the level of Ca^{2+} already present in standard tissue culture media is sufficient for mineralisation without supplementation. Finally, the synthetic glucocorticoid dexamethasone acts as a potent stimulator of osteogenic differentiation in certain cell types. Dexamethasone is typically used at a concentration of 10 or 100 nM and has been shown to exert a species specific effect, increasing mineralisations in cultures of cells derived from both human and rat sources whilst inhibiting osteogenic differentiation of murine cells (Taylor et al., 2014).

Mineralising cells often display a lag-phase before calcium deposition first becomes apparent. This is characterised by a phase of proliferation, increase in ALP activity, upregulation of various mineralisation associated genes and assembly of a collagenous matrix, suitable for mineralisation (Hoemann et al., 2009). Mineralisation can be assessed in a variety of ways but perhaps the most common is by histological staining and visual inspection. Two commonly used stains in the study of mineralising cells are Alizarin Red S and von Kossa, which test for the presence of Ca^{2+} and Pi, respectively. Other metrics such as changes in expression of mineralisation associated genes, measurement of ALP activity by enzymatic assay and quantification of deposited calcium are also routinely performed.

A more detailed inspection of the chemical and morphological characteristics of deposited minerals can be performed using a variety of techniques, including x-ray diffraction, Raman spectroscopy or electron microscopy. These techniques allow for confirmation that any mineralisations formed in *in vitro* cultures are representative of physiological mineralisations (Boskey and Roy, 2008).

1.4.4 Development of an *in vitro* model of microcalcification

Using the same reagents and protocols from established osteoblast studies (Langenbach and Handschel, 2013), our group developed the first *in vitro* model of microcalcification. A combination of 10 mM β-glycerophosphate and 50 µg/mL ascorbic acid (termed osteogenic cocktail or OC) was found to effectively induce mineralisation in several breast cancer cell lines. The majority of this previous work was done using the murine 4T1 cell line, a highly tumourigenic and invasive cell line originally derived from a spontaneously arising mammary tumour of a $MMTV^{+}$ BALB/c mouse (Pulaski and Ostrand-Rosenberg, 2001).

Positive mineralisation was observed in both 4T1 and a highly-metastatic sub-clone, 4T1.2 (Cox et al., 2012a, Cox et al., 2012b). Mineralisation was also observed in the triple-negative, human cell line Hs578Ts(i)8, an invasive Hs578T sub-clone (Hughes et al., 2008), derived through sequential passaging Hs578T cells through a Matrigel invasion chamber. Interestingly, mineralisation was not observed in the parental Hs578T cell line, indicating that at some point in their transition to a more aggressive phenotype, the cells acquired mineralisation capability. This finding may be relevant to the findings of an unusually aggressive nature demonstrated for small tumours with associated calcifications (Tabár et al., 2000, Tabar et al., 2004). Analysis of deposited mineralisations in all cell lines by Raman spectroscopy confirmed the presence of hydroxyapatite, representative of malignancy associated type II microcalcifications (Frappart et al., 1984). No calcium oxalate (typically associated with benign breast lesions) was detected in any mineralising cell line, confirming the clinical relevance of the calcifications formed by this model. 4T1 and 4T1.2 cells mineralised in both the presence and absence of dexamethasone, although to a significantly greater extent when dexamethasone was excluded, whilst Hs578Ts(i)8 cells required the presence of dexamethasone in order to undergo mineralisation. This is in agreement with previous findings of dexamethasone's species-specific effect (Langenbach and Handschel, 2013). No mineralisation was observed in the non-tumourigenic MCF10a cell line.

1.4.5 Key findings from our *in vitro* model of microcalcification

Findings from our previous work have contributed significantly to understanding of the formation of microcalcifications. Perhaps the key outcome of these studies was the demonstration of an active, regulated process of mineral deposition with many similarities to physiological mineralisation (Cox et al., 2012a, Cox et al., 2012b).

Mineralisation was found to be highly dependent on activity of ALP. All cell lines found capable of mineralisation had significant levels of ALP activity, whilst the non-mineralising MCF10a cell line had no detectable ALP activity. Addition of the ALP inhibitor levamisole completely blocked mineralisation of cells cultured with β-glycerophosphate, although it had no effect on cells mineralised with inorganic Pi, as free Pi was readily available without requiring hydrolysis of β-glycerophosphate by ALP.

Mineralisation was also blocked by addition of phosphonoformic acid, an inhibitor of Na(+)-dependent Pi transporters. Unlike ALP inhibition, targeting Pi transport was effective in experiments with both organic β-glycerophosphate and inorganic sodium phosphate. Mineralisation was also highly increased when exogenous ALP was included in culture media, further highlighting the central role of this enzyme in formation of mineralisations. Addition of exogenous BMP2 resulted in a 30-fold increase in calcium deposition. In a qPCR analysis, upregulation of BSP and collagen I was observed in mineralising 4T1 cells.

Expression of the mineralisation inhibitor protein osteopontin was also increased after 21 days under mineralisation promoting conditions, although direct addition of exogenous osteopontin did not decrease mineral formation, likely due to the high levels of ALP present in mineralising cell lines. Phosphorylation of certain amino acid residues is known to be critical to osteopontins role as a mineralisation regulator and removal of these phosphorylations by ALP inhibits the function of osteopontin (Jono et al., 2000). The 4T1 cell line represents a robust model for mammary calcifications, as positive mineralisation was also observed in cells cultured in a 3D collagen scaffold as well as following implantation in a mouse xenograft model. Some of the key findings of our previous studies are highlighted in Fig. 1.6, below.

1.4.6 Other *in vitro* studies of mammary calcification

Since its development, other groups have also utilised our model to probe the molecular mechanisms underlying formation of mammary calcifications. Zheng et al. examined the role of carbonic anhydrase I (CA1) in mineralising 4T1 cells (Zheng et al., 2015). CA1 belongs to a family of enzymes that catalyse the interconversion of carbon dioxide and water to bicarbonate. CA1 has previously been shown to promote the formation of calcium carbonate which may facilitate formation of microcalcifications by acting as a seed for subsequent hydroxyapatite formation (Adeva-Andany et al., 2015). CA1 expression was significantly increased in cases of breast cancer compared with benign fibroadenomas and was increased further by incubation with OC media. Inhibition of CA1 activity by the small molecule inhibitor acetazolamide resulted in decreased CA1 expression and calcium deposition. CA1 has not been studied much in relation to breast cancer, but other carbonic anhydrase enzymes have been shown to be important regulators of tumourigenesis.

Most notably CAIX, a hypoxia-inducible protein, is crucial in allowing breast cancer cells to survive in a harsh, hypoxic microenvironments (Span et al., 2003). CAIX is highly expressed in breast cancer cells (detected in 25/39 malignant tumours versus no detection in 3 normal breast tissue samples) and is associated with HER2 expression (Bartosova et al., 2002).

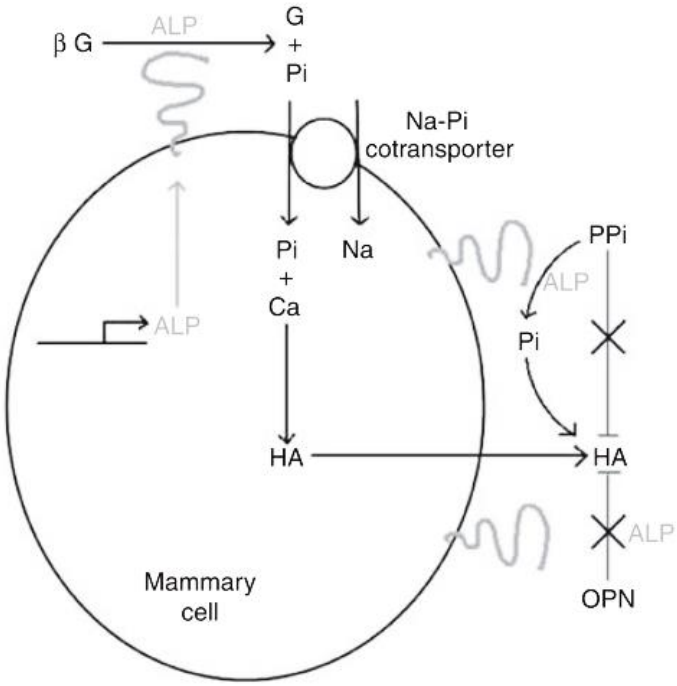

Figure 1.6 Proposed mechanism of mammary cell mineralisation. Hydrolysis of β-glycerophosphate (βG) by extracellular alkaline phosphatase (ALP) results in release of free phosphate (Pi) and glycerol (G). Pi is transported inside the cell by type II family of Na-Pi cotransporters, where it combines with calcium (Ca) to form hydroxyapatite (HA). ALP also mediates the degradation of pyrophosphate (PPi), thus removing its inhibitory effect on mineralisation. ALP also dephosphorylates osteopontin (OPN). Adapted from (Cox et al., 2012a).

More recently, Dang et al. used inorganic Pi to induce mineralisation in the human MCF-7 cell line and highlighted a role for secretory pathway Ca^{2+}-ATPases SPCA1 and SPCA2 in development of microcalcifications (Dang et al., 2017). Expression of SPCA1 and SPCA2 was elevated by the presence of OC media and transfection with a SPCA2 containing plasmid resulted in significant increases in calcium deposition. Transfection with a catalytically inactive SPCA2 mutant failed to increase calcification, highlighting the importance of an active pumping process. In a bioinformatic analysis, they also observed expression of SPCA2 to be highest in HER2 overexpressing cells, the subtype of breast cancer most commonly associated with the presence of microcalcifications.

SPCA2 expression is significantly increased in breast cancer where it induces constitutive Ca^{2+}influx and signalling via an unconventional activation of the store-operated Ca^{2+} channel Orai1 (Feng et al., 2010). Expression of SPCA1/2 is also significantly increased during lactation and appears to act as important mediators of transcellular migration of Ca^{2+}(Cross et al., 2013). Ca^{2+}entering at the basolateral side of ductal epithelial cells is pumped into vesicles by SPCA1/2, before packaging into micelles and exocytosis into the lumen. Calcifications can also sometimes be found during lactation although these are usually considered to display a benign morphology (Joshi et al., 2013).

The involvement of SPCA proteins in both breast cancer and lactation is interesting as although other studies have pointed out potential links between the physiological role of breast tissue in concentrating Ca^{2+} during lactation and a possible dysregulation of these Ca^{2+} handling pathways in the development of microcalcifications (Cross et al., 2014), this represents the first piece of *in vitro* evidence in support of such a link. Ca^{2+} levels in breast epithelial cells are controlled by a wide variety of pumps, channels and buffer proteins. It seems highly likely that SPCA1 and SPCA2 are not the only Ca^{2+} transport proteins to be involved in formation of microcalcifications. Transepithelial transport of Ca^{2+}during lactation is handled by two sets of ATPase pumps. In addition to the SPCA proteins previously discussed, the plasma membrane Ca^{2+-} ATPase (PMCA) family of Ca^{2+}transporters also play a significant role in both physiological Ca^{2+} transport and breast tumour progression (Peters et al., 2016). Furthermore, Mandavilli et al. showed high expression of the Ca^{2+} channels TRPC1 and TRPM7 in carcinomas with associated calcifications (Mandavilli et al., 2012). Both of these Ca^{2+} transporters may potentially contribute to the formation of microcalcifications but have never been examined in an *in vitro* setting.

1.4.7 Remaining questions surrounding the formation of microcalcifications

Although the development of an *in vitro* model of microcalcification has significantly enhanced our understanding of the *in vivo* generation of microcalcifications, many questions still remain regarding their formation. The majority of previous work has focused on the murine 4T1 cell line.

Although studies from both our lab and others has shown successful mineralisation in some human breast cancer cell lines, the number of cell lines tested to date for mineralisation potential is low and not representative of the diverse range of molecular subtypes of breast cancer. Although microcalcifications show a strong association with the HER2 subtype in patient studies (Killelea et al., 2013b, Wang et al., 2008), it is not currently known if any particular subtypes of breast cancer cell lines are more likely to mineralise under *in vitro* conditions.

Using the inhibitor compound phosphonoformic acid, a vital role was previously established for active Pi transport. However, microcalcifications are composed of both Ca^{2+} and Pi. Results from other studies have demonstrated a role for SPCA proteins in formation of microcalcifications (Dang et al., 2017) and other groups have suggested the involvement of other Ca^{2+} transporters (Mandavilli et al., 2012, Cross et al., 2014). It is not currently known if calcifications will occur more readily under increased Ca^{2+} conditions, and if so, what transport mechanisms are involved. Is influx of Ca^{2+} into mineralising cells required or is a simple increase in extracellular Ca^{2+} sufficient to induce mineralisation? The balance between various promoters and inhibitors is known to be central to the development of other forms of pathological calcification but remains an unexplored possibility in the context of mammary calcifications. Which of the previously identified regulators of physiological and pathological calcification also play a role in controlling breast calcification and how do they relate to tumour phenotype and behaviour?

Finally, although several studies have found associations between the presence of microcalcifications and tumour aggressiveness, direct *in vitro* evidence of a mechanistic link between these two features is relatively sparse. Stimulation of breast cancer cells has been shown to upregulate various inflammatory markers and metalloproteinase activity, as well as increase proliferation (Cooke et al., 2003, Morgan et al., 2001, Morgan et al., 2004).

However, the number of inflammatory markers studied to date is low. In addition, links between calcifications and other potentially tumour promoting effects such as generation of cancer stem cells remains unexplored.

1.5 Thesis overview

This thesis aims to expand on previous findings on the *in vitro* formation of breast microcalcifications. The involvement of an active regulated process in the formation of breast calcifications has been demonstrated (primarily in mouse derived cell lines) although many questions remain regarding both the mechanism of formation and potential consequences on cell behaviour. The primary hypothesis of this thesis is that human breast cancer cell lines can be utilised as an effective model of microcalcification formation and that calcification may be linked to cell phenotype and the development of tumour promoting effects. Each chapter is summarised below. Each results chapter (3, 4 and 5) contains a brief introduction of information relevant to that chapter, results and a discussion and conclusion section.

- Chapter 1 is a comprehensive literature review of relevant information regarding breast cancer, the clinical relevance of breast microcalcifications, mechanisms of *in vivo* mineralisation and *in vitro* methods for their study, previous findings on the *in vitro* formation of microcalcifications and significant areas warranting further research.
- Chapter 2 describes the materials and methods used in this thesis.
- Chapter 3 aims to form a comprehensive survey of the mineralisation potential of a panel of breast cancer cell lines representative of all major molecular subtypes.
- Chapter 4 explores if an imbalance between pro- and anti-mineralisation regulators could mediate formation of microcalcifications. In addition, several Ca^{2+} handling proteins will be investigated.
- Chapter 5 investigates potential links between the presence of calcifications and several known tumour promoting effects such as inflammation and generation of cancer stem cells.
- Chapter 6 contains an overall discussion of this thesis and conclusion.
- Chapter 7 contains reference details for all studies cited in this thesis.
- Chapter 8 is an appendix and contains supplementary experimental information as well as details of presentations, conferences attended, outreach work and other significant activities carried out during the course of this thesis.

Chapter 2.0

Materials and methods

2.1 Cell culture materials and methods

2.1.1 Equipment

All cell lines were cultured in a cell culture incubator (Panasonic IncuSafe), maintained at 37°C and 5% CO_2. All cell culture procedures were carried out inside a laminar flow biosafety cabinet (Haier) to maintain sterility. Sterile technique was utilised at all times with standard practice including spraying all items to enter the hood with 70% ethanol, allowing 15 minutes of airflow through the cell culture hood before starting any procedure, addition of bactericidal agents to water baths, and routine cleaning of all cell culture equipment. All liquid reagents not certified sterile by the manufacturer were sterilised by passing through a 0.2 µm syringe filter. Cells were maintained in T75 or T175 tissue culture flasks (Sarstedt). All cell culture plastics were either provided in individually wrapped, sterile packages or were sterilised by autoclave (15 minutes, 121°C). All images of cells were captured using a ZEISS Axiocam ERc 5s camera module (5 megapixels) connected to a Nikon Eclipse TS100 inverted microscope. Cells were routinely checked for *Mycoplasma* contamination with the MycoAlert kit (Lonza). No contamination was detected at any point in our investigations.

2.1.2 Cell culture reagents

All cell culture reagents were purchased from Labtech International. All breast cancer cell lines were maintained in DMEM or RPMI media, supplemented with 10% heat-inactivated foetal bovine serum (FBS), 1% penicillin/streptomycin and 2 mM L-glutamine. The monocytic THP-1 cell line was maintained in RPMI supplemented with 10% heat-inactivated foetal bovine serum (FBS), 1% penicillin/streptomycin, 2 mM L-glutamine, 10 mM HEPES and 0.05 mM β-mercaptoethanol. Media requirements for each cell line are detailed below (Table 2.1).

2.1.3 Subculture

All breast cancer cell lines were adherent, requiring trypsination in order to be subcultured or used for experiments. Growth media was removed before cells were gently washed with pre-warmed Ca^{2+}/Mg^{2+} free PBS. After addition of pre-warmed trypsin solution (0.25% trypsin, 0.02% EDTA in Ca^{2+}/Mg^{2+} free PBS), flasks were returned to a 37°C incubator until cells could be dislodged by gentle tapping (usually 2-8 minutes).

Pre-warmed media was added (twice the original volume of trypsin) and the suspended cells were transferred to centrifuge tubes and spun for 5 minutes at 350 x g. Supernatant was removed and the cell pellet was gently resuspended in fresh media.

Cells were counted by mixing 40 µL of cell suspension with 40 µL of a 0.4% trypan blue/PBS solution and 120 µL of culture media to create a 1:5 dilution. 10 µL of this dilution was loaded into a haemocytometer and analysed under 40X magnification. Dead cells were distinguished from live cells through uptake of the trypan blue dye. Cell counts were performed in all 4 corner squares. The average of these 4 counts was corrected for dilution factor (5X) and multiplied by 10^4 to calculate the total number of cells in 1 mL.

Table 2.1 Growth media requirements, seeding density and original source of all cell lines used. For cells cultured in DMEM, a high-glucose formulation (4,500 mg/L) was used for routine growth, while a low-glucose format (1,000 mg/L) was used for mineralisation assays.

Cell Line	Molecular Subtype	Growth Media	Seeding Density (6 well plate)
MCF-7	Luminal	DMEM + 10ug/mL insulin	0.15 x10^6
HER2-MCF-7	Luminal (HER2 Positive)	DMEM + 10ug/mL insulin	0.15 x10^6
SKBR3	HER2	DMEM	0.2x10^6
ZR-75-1	Luminal	DMEM	0.4 x10^6
MDA-MB-231	Basal	DMEM	0.2 x10^6
HCC1954	Basal (HER2 Positive)	RPMI	0.25 x10^6
THP-1	Monocytic cell line	RPMI + 10 mM HEPES + 0.05 mM β-mercaptoethanol.	2 x10^6

2.1.4 Long term storage and recovery of cell lines

Cells to be stored were trypsinised as described above, and resuspended in Recovery™ freezing medium (ThermoFisher). Cells were transferred to sterile cryovials and stored overnight at -80°C in a CoolCell (Sigma) to provide a consistent 1°C/minute freezing rate. Cells were then transferred to a liquid nitrogen dewar for long term storage. Cells were recovered from storage by removal from the dewar, rapid thawing in a 37°C waterbath, dilution with pre-warmed media, centrifugation at 350 x g for 5 minutes, resuspension in fresh media and addition to a cell culture flask at an appropriate concentration.

2.2 Assessment of breast cancer mineralisation

2.2.1 Reagent preparation

The individual components of the osteogenic cocktail (OC) were prepared by dissolving β- glycerophosphate (Sigma) to a concentration of 1 M and ascorbic acid (Sigma) as a 5mg/mL solution in sterile, cell-culture grade water. Dexamethasone (Sigma) was dissolved in DMSO to a concentration of 100 µM. All reagents were sterilised by passing through a 0.22 µm rated syringe filter and subsequently frozen in single use aliquots. Mineralisation media was prepared by diluting β-glycerophosphate and ascorbic acid 100-fold in the appropriate culture media for the cell line to be tested, for a final concentration of 10 mM and 50 µg/mL respectively. Dexamethasone was diluted 1,000-fold for a final concentration of 100 nM. All other compounds used in the course of this study were dissolved in PBS or DMSO (according to manufacturer's instructions) at an appropriate concentration, aliquoted into single-use tubes and stored at -20°C.

2.2.2 Experimental set-up

Cells to be tested for mineralisation capability were seeded into 6 well tissue culture plates in regular growth media and grown to 70 – 80% confluence (See Table 2.1 for typical seeding densities). Media was removed and either replaced with fresh growth media (Control), media supplemented with an osteogenic cocktail (10 mM β-glycerophosphate and 50 µg/mL ascorbic acid) or media supplemented with osteogenic cocktail and 100 nM dexamethasone. Cells were grown under these conditions for up to 28 days, with half the media in each well changed twice a week. Mineralisation was assessed on a weekly basis, using Alizarin Red S and von Kossa staining, as well as the o-cresolphthalein complexone (OCP) calcium assay. Viability was monitored using the Alamar Blue assay. Protocols for all techniques are detailed below.

2.2.3 Alamar Blue

In order to ensure that none of our experimental treatments were having an adverse effect on cell lines during testing, cell viability was monitored using the resazurin based Alamar Blue assay (Invitrogen). Media was removed from wells to be tested, followed by a rinse with pre-warmed PBS. Alamar Blue reagent was diluted 1:10 in the appropriate growth media for the cell line being tested and added to the cells (2mL per well). All samples were incubated at 37ºC for 2 hours.

100 µL was transferred in triplicate to a 96 well plate and fluorescence was measured using a Wallac plate-reader (excitation at 530 nm, emission at 590 nm). Data was standardised by assigning a value of 1 to readings from “day 7 Control” and expressing all subsequent readings as a factor of this value.

2.2.4 Alizarin Red S Staining

Wells to be stained were fixed by removal of culture media, followed by rinsing with warm PBS and fixation in 10% formaldehyde-PBS solution for 30 minutes. Once fixation was complete, the formaldehyde solution was removed and all wells were allowed to air dry. Alizarin Red S (Sigma, 122777) was prepared as a 2% solution in distilled water, adjusted to pH 4.4 with ammonium hydroxide and filtered through a 0.22 µm rated syringe filter to remove any undissolved particulate. Wells were rinsed once with water then incubated with 1.5 mL of the Alizarin solution for 4 minutes at room temperature. The staining solution was subsequently removed and each well was washed 4 times with distilled water to reduce nonspecific binding. Wells were allowed to air dry then analysed by light microscopy. Bright red staining indicates a positive result for calcium. The specific formulation of Alizarin used in our studies (2%, pH 4.4) has previously been optimised for hydroxyapatite staining (Shoji, 1993), the same calcium phosphate crystals found in type II calcifications often associated with malignant disease. In contrast, calcium oxalate (the principal component of benign type calcifications) will only stain with Alizarin at a pH of 7 (Proia and Brinn, 1985).

2.2.5 von Kossa Staining

von Kossa staining was carried out on separate wells, to verify results from Alizarin staining. All wells were fixed following the same procedure used for Alizarin stained wells. 1.5 mL of a 5% silver nitrate solution (Sigma) was added to each well and plates were incubated for 1 hour under a desktop lamp. Silver nitrates solution was then removed and all wells were washed 3 times with distilled water. Wells were incubated with 1.5 mL of a 5% sodium thiosulphate solution (Sigma, 72049) for 2 minutes to remove any unreacted silver. After removal of the sodium thiosulphate and 3 washes with distilled water, plates were allowed to air dry before examination by light microscopy. Dark brown/black staining indicates a positive result for calcium phosphate. von Kossa is an indirect method of detecting calcium deposits, which relies on substitution of associated Pi with silver ions (Rungby et al., 1993). Subsequent reduction to metallic silver results in dark brown to black staining.

Both Alizarin Red S and von Kossa have previously been used to successfully identify breast microcalcifications, both *in vitro* (Cox et al., 2012a) and *in vivo* (Wilson et al., 2014).

2.2.6 o-cresolphthalein complexone (OCP) calcium assay

Samples for the OCP assay were created by removal of medium from each well, rinsing once with PBS and incubating with 500 µL of 1 M nitric acid for 1 hour to dissolve any calcium deposits. Samples were stored at -20 ºC until analysis. Samples were diluted in 1 M nitric acid to within range of the assays standard curve (typically a 1:2 – 1:100 dilution). 70 µL of each dilution was added to a 96 well plate in triplicate followed by 70 µL OCP solution (Sigma) and 175 µL of amino-2-methyl-1-propanol (AMP; Sigma). Ca^{2+} and OCP form a bright purple complex which is stabilised by AMP. A standard curve was generated by diluting a Ca^{2+} solution (Sigma) in nitric acid to a range of 0–10 ppm. A representative standard curve is shown in the appendix (Fig. 8.1). Absorbance was read at 572 nm on a Wallac plate reader.

2.2.7 BCA Protein Assay

Following extraction of Ca^{2+} by nitric acid, protein samples were generated by rinsing wells twice with ddH_2O before adding 500 µL of a 0.1 N NaOH, 0.1% SDS solution to each well and incubating at room temperature until the cell monolayer was observed to have dissolved. Supernatants were transferred to fresh Eppendorf tubes, centrifuged at 14,000 x g for 10 minutes to pellet any cell debris and stored at -20 ºC. Protein quantitation was carried out using a QuantiPro BCA Assay Kit (Sigma, QPBCA) following manufacturer's instructions. Briefly, samples were diluted in PBS to within range of the kits standard curve (typically a 1:200 – 1:500 dilution) and incubated for 1 hour at 37ºC with 200 µL the prepared BCA reagent. Absorbance was read at 562 nm using a Wallac plate reader. A representative standard curve is shown in the appendix (Fig. 8.2) The total protein amount of each well was calculated by comparison to a BSA standard curve and used to standardise results from the OCP calcium assay.

2.2.8 Alkaline phosphatase assay

To measure alkaline phosphatase (ALP) activity, cells were washed once with cold PBS, scraped into 1 mL PBS, pelleted by 5 minutes centrifugation at 400 x g and resuspension in 100 µL ALP buffer (100 mM Tris-HCL pH 9.5, 100 mM NaCl, 5 mM MgCl, 1% Triton X-100).

Samples were placed on ice for 1 hour with occasional vortexing, before storage at -20ºC. For analysis, ALP samples were thawed and diluted with ALP buffer (typically between 1:3 to 1:50). 50 µL of each samples was added to a flat bottom, clear plastic 96-well plate along with 50 µL of p-nitrophenyl phosphate (pNPP) chromogenic substrate (Sigma).

A standard curve of purified bovine ALP (Sigma) was prepared in the range of 0 – 100 mU/mL using the batch information sheet to calculate units of enzymatic activity. Samples were incubated at 37ºC for 30 minutes. A representative standard curve is shown in the appendix (Fig. 8.3). ALP activity results in conversion of the colourless pNPP substrate to a yellow-coloured product. Absorbance was measured by Wallac plate reader at 405 nm. All results were normalised to protein content as determined by BCA assay (As described in 2.2.9).

2.3 Gene expression analysis

2.3.1 mRNA Isolation

To analyse changes in gene expression, cells were drained of culture media and rinsed once with PBS. 1 mL of Trizol (Invitrogen) was added to each well. Cell monolayers were dispersed by repeated pipetting of the Trizol across the surface of each well. Samples were transferred to sterile, nuclease free Eppendorf tubes and incubated at room temperature for 5 minutes. 200 µL of chloroform was added to each sample followed by vigorous shaking for 15 seconds. Samples were incubated at room temperature for 2 minutes then centrifuged at 14,000 x g for 20 minutes at 4 ºC. The RNA containing, upper aqueous layer was carefully removed, taking care not to disturb the DNA containing interphase and transferred to a fresh Eppendorf tube. RNA was precipitated by addition of molecular biology grade isopropanol (500 µL per tube) followed by incubation at room temperature for 10 minutes and centrifugation at 14,000 x g for 20 minutes at 4ºC.

Supernatants were removed and the RNA pellet was washed by addition of 1 mL molecular biology grade ethanol (70%, prepared with nuclease free water), vortexing of each sample and centrifugation at 14,000 x g for 10 minutes at 4ºC. Supernatants were removed and the RNA pellet was air-dried in a laminar flow PCR-workstation for 10 minutes. RNA was dissolved in 20 µL of nuclease free water and heated to 55 ºC for 10 minutes.

RNA was quantified by absorbance at 260 nm and purity by the ratio of absorbance at 260/230 nm and 260/280 using a NanoDrop 2000 spectrophotometer. Samples were stored at -80ºC.

2.3.2 Nucleic acid quantification

RNA and DNA were quantified using a NanoDrop 1000 spectrophotometer. To initialise the instrument, the pedestal was first wiped with a lint-free tissue before 1 µL nuclease free water was loaded. The instrument arm was gently lowered into place and the NanoDrop software was allowed to run through the initialisation program. A blank reading was then taken using the same solvent as the sample to be tested (either nuclease free water or TE buffer). Samples were then loaded and analysed using the "Nucleic acids" option (selecting either DNA or RNA as appropriate). Upper and lower pedestals were wiped clean with a lint-free tissue in between samples. Purity was determined by 260/280 and 260/230 ratios. Pure RNA generally displays a 260/280 ratio of ~2.0 while DNA should be between 1.8-2. Significant differences from these ratios may indicate contamination by salts, proteins or ethanol.

2.3.3 cDNA synthesis & qPCR analysis

1µg of RNA was transcribed to cDNA using Applied Biosystems High Capacity cDNA Reverse Transcription Kit, following manufacturer's recommendations. Primer sequences were either taken from pre-existing studies or designed using NCBI Primer Blast (Available at http://www.ncbi.nlm.nih.gov/tools/primer-blast/). All primers sequences are listed below (Table 2.2). Primers were resuspended in nuclease free water to a concentration of 100 µM to create a master-stock. Working-stock aliquots were made by diluting master-stock 1:10 in nuclease free water to a concentration of 10 µM.

cDNA was diluted 1:10 in nuclease free water and 4 µL cDNA was used in each qPCR reaction. Changes in gene expression were analysed using the SensiFAST SYBR Lo-ROX qPCR kit (Bioline). Each reaction contained 4 µL cDNA, 10 µL SensiFAST, 0.8 µL forward primer, 0.8 µL reverse primer and 4.4 µL nuclease free water. Primer specificity was confirmed after each run by melt curve analysis. A representative graph is included in the appendix (Fig. 8.5 B). Reactions were carried out in an AB7500 qPCR system using the following temperature profile: 95 ºC for 2 minutes followed by 40 cycles of 95ºC for 15 seconds (denaturation), 60ºC for 15 seconds (annealing) and 72ºC for 30 seconds (elongation).

Fluorescence data was acquired during the elongation stage. A representative graph is included in the appendix (Fig. 8.5 A).

Purified primers were purchased from Sigma while qPCR microplates and seals were purchased from FisherScientific. Results were normalised to a housekeeping gene (18S) and analysed using the delta-delta-Ct (ddCt) method.

Table 2.2 Primer sequences utilised for qPCR

Target	Forward primer	Reverse primer
18S	AACCCGTTGAACCCCATT	CCATCCAATCGGTAGTAGCG
ALP	CCACGTCTTCACATTTGGTG	ATGGCAGTGAAGGGCTTCTT
BMP2	TCAAGCCAAACACAAACAGC	ACGTCTGAACAATGGCATGA
COX2	AAGTCCCTGAGCATCTACGG	ACTGCTCATCACCCCATTCA
E-cadherin	TGCCCAGAAAATGAAAAAGG	GTGTATGTGGCAATGCGTTC
ENPP1	CAAAGGTCGCTGTTTCGAGAG	TGCACGTCTCCTGGTAATCTAAA
gp130	CGGACAGCTTGAACAGAATGT	ACCATCCCACTCACACCTCA
IL-1β	ATGATGGCTTATTACAGTGGCAA	GTCGGAGATTCGTAGCTGGA
IL-6	AGTTCCTGCAGAAAAAGGCA	AAAGCTGCGCAGAATGAGAT
MGP	TCCGAGAACGCTCTAAGCCT	GCAAAGTCTGTAGTCATCACAGG
mIL-6R	CATTGCCATTGTTCTGAGGTTC	GTGCCACCCAGCCAGCTATC
Nanog	GGTGTGACGCAGAAGGCCTCA	CCCAGTCGGGTTCACCAGGCA
Oct4	GGCTCGAGAAGGATGTGGTCCG	GGGCTCCCATAGCCTGGGGT
PMCA1	ACCCACTGAGTCTCTCTTGC	TCTGAAGGAGGAGCATGCAA
PMCA2	CCAGTACAAACGCCACCAAA	CTGGCTCCGAATGAACATGG
RUNX2	CCTGAACTCTGCACCAAGTC	GAGGTGGCAGTGTCATCATC
sIL-6R	GCGACAAGCCTCCCAGGTTC	GTGCCACCCAGCCAGCTATC
Snail	TAGCGAGTGGTTCTTCTGCG	AGGGCTGCTGGAAGGTAAAC
Sox2	GGGGAAAGTAGTTTGCTGCC	CGCCGCCGATGATTGTTATT
TRPC1	ATCAAAAGGCAAGGTCAAACGG	ACAGATCTTGGCGCAGTTCGT
TRPM7	CAGAAACCAAGCGCTTTCCT	AATTCAACGGCCAACTGACC
Twist	GGACAAGCTGAGCAAGATTCA	CGGAGAAGGCGTAGCTGAG
Vimentin	GAGAACTTTGCCGTTGAAGC	GCTTCCTGTAGGTGGCAATC

2.3.4 Semi-quantitative PCR

In some cases, gene expression was assessed by semi-quantitative PCR rather than qPCR. Each PCR reaction was set up the same as for qPCR, but substituting MyTaq Red (Bioline) for SensiFAST qPCR reagent. Reactions were carried out in an Applied Biosystems ProFlex PCR

System using the following temperature profile: 95ºC for 2 minutes followed by 15-35 cycles (depending on target expression level) of 95ºC for 15 seconds (denaturation), 60ºC for 15 seconds (annealing) and 72ºC for 30 seconds (elongation). A final elongation step of 72ºC for 7 minutes was followed by an indefinite hold at 4ºC.

2.3.5 Agarose gel electrophoresis

Agarose gels were prepared by microwaving a 1.2% solution of agarose (Sigma) in TAE buffer. Solution was allowed to cool slightly before adding SYBR Safe DNA stain (ThermoFisher) at a 1:30,000 dilution. The solution was poured into a gel casting chamber, with a comb inserted to form wells. The gel was allowed to solidify at room temperature for 40 minutes before submersion in TAE buffer. DNA samples were then carefully loaded into the wells. MyTaq Red contains a red dye and glycerol, eliminating the need for addition of a loading dye. A 100-1,0000 bp ladder (Medical Supply Company) was included to allow for assessment of band size. Gels were run at a constant voltage of 100V for 45-60 minutes, until dye had migrated most of the way down the gel. Bands were imaged using an Amersham 600 imaging system, using blue light excitation (460 nm). Densitometry analysis of bands was performed using ImageJ.

2.3.6 siRNA knockdown

siRNA knockdown was performed using Lipofectamine RNAiMAX transfection reagent (Biosciences) and pre-designed siRNA (Sigma). Details of all siRNA used are detailed below (Table 2.2). siRNA was suspended in nuclease free water to a concentration of 100 µM. Single use aliquots of 10 µM were then prepared in nuclease free water from the master stock. Transfection was performed on actively dividing cells at approximately 60-80% confluency. Briefly, 250 µL serum free OptiMEM media (Gibco) was added to two separate Eppendorf tubes. 6 µL Lipofectamine was added to one tube, and 2µL of 10 µM siRNA was added to the second tube.

The two tubes were then combined and mixed by gentle pipetting before incubation at room temperature for 15-20 minutes. Finally, 500 µL of the transfection mix was added dropwise to cells in a 6 well plate, containing 1.5 mL DMEM. Plates were gently rocked to ensure even distribution of transfection complexes, and returned to the incubator. Changes in gene expression was assessed 72 hours post transfection by qPCR.

Table 2.3 Pre-designed siRNA (Sigma) utilised in this study.

siRNA	Product code
Universal negative control	SIC001
TRPM7	SASI_Hs01_00120022
Runx2	SASI_Hs01_00222686
PMCA1	SASI_Hs01_00039081
PMCA2	SASI_Hs01_00155229

2.3.7 Plasmid preparation and purification

pCMV-Runx2 plasmid was kindly supplied by Prof. G. Karsenty (Columbia University, New York). This plasmid contains a full-length copy of the mouse Runx2 cDNA, which shares 93% homology with the human mRNA (Zhang et al., 2000). pCMV-Runx plasmid was supplied absorbed onto filter paper. Plasmid was first extracted by incubation in 100 µL TE buffer at room temperature for 20 minutes. 3µL (~100ng) was used to transform a 30 µL aliquot of DH5α competent *E.coli* cells (ThermoFisher).

Cells were incubated on ice for 30 minutes, heat-shocked for 30 seconds at 42°C, then returned to ice for 2 minutes. 950 µL pre-warmed SOC media was added and cells were incubated in a 37°C shaking incubator for 1 hour. 100 µL was spread onto Luria-Bertani (LB) agar plates with 100 µg/mL ampicillin and incubated overnight at 37°C. The following morning, a single colony was inoculated into 5 mL LB with 100 µg/mL ampicillin. After 12-18 hr incubation in a 37°C shaking incubator, bacterial cells were pelleted by centrifugation at 15,000 x g for 2 minutes. Bacterial pellets were then used to isolate and purify plasmid using Monarch plasmid miniprep kit (New England BioLabs), following the manufacturer's instructions.

pCMV-GFP plasmid to be used as a control was provided by Addgene. This plasmid was provided in the form of an "agar-stab" culture. A sterile inoculating loop was used to streak an LB agar + 100 µg/mL ampicillin plate directly from the agar culture. From that point on, plasmids were isolated following the procedure previously described. Stocks of plasmid containing *E.coli* were prepared by mixing 500 µL of an overnight bacterial culture with 500 µL 50% sterile glycerol. This stock was stored at -80°C and used to produce further cultures for plasmid preparation.

2.3.8 Plasmid transfection

Plasmids were transfected into breast cancer cells following the same procedure used to transfect siRNA (2.3.6). 5 µg of plasmid was used to transfect a single well of a six-well plate. Increased expression was confirmed 72 hours post transfection by qPCR.

2.4 Hydroxyapatite stimulation experiments

2.4.1 Experimental set up

Cells to be stimulated were seeded into 6 well plates and grown to confluency. Cells were rendered quiescent by overnight serum starvation (0.5% FBS). Hydroxyapatite (HA) nanoparticles (Sigma) were measured into glass vials, sealed with aluminium foil and sterilised/depyrogenated by heating to 200°C for 2 hours. HA particles were suspended in culture media and dispersed by sonication immediately prior to use. HA was used at a concentration of 50, 100 or 200 µg/cm^2. HA concentration was measured in µg/cm^2 as the crystals are comprised of an insoluble precipitate which rapidly sinks to the bottom of a tissue culture plate once added. Calculating HA concentration by surface area, rather than volume allowed for a consistent exposure between different plate sizes.

Conditioned media (CM) was generated by incubating confluent, serum-starved MDA-MB-231 cultures with 1 mL DMEM (0.5% FBS) or HA particles suspended in 1 mL DMEM (0.5% FBS) for 24 hours. CM was transferred to an Eppendorf tube and centrifuged for 5 minutes at 14,000 x g in a chilled centrifuge (4°C). Conditioned media was transferred to a new Eppendorf, taking care not to disturb the pelleted HA. Conditioned media was stored at -80°C before usage. Cell monolayers were collected in 1 mL Trizol and used for mRNA purification and analysis. In some experiments, MDA-MB-231 cells were cultured with the intracellular Ca^{2+} chelator BAPTA-AM (20 µM for 4 hours) to suppress intracellular Ca^{2+} increase upon HA stimulation. Control samples were treated with a DMSO vehicle control.

2.4.2 THP-1 macrophage differentiation

The THP-1 human monocytic cell line was grown as a suspension culture and required differentiation to adherent macrophages with phorbol 12-myristate 13-acetate (PMA) before usage in experiments.

THP-1 cells were seeded into 6 well plates at a concentration of 1-3x10^6 cells/well in RPMI supplemented with 10 mM HEPES and 0.05 mM β-mercaptoethanol. PMA

(Sigma) was added at a concentration of 10 nM. Cells were incubated for 24 hours before the PMA containing media was removed. Successful differentiation was confirmed by observation under microscope. Differentiated cells adhered to the tissue culture plate. Representative images of PMA differentiated THP-1 cells showing clear morphological differences are included in the appendix (Fig. 8.6). Fresh RPMI was added and the cells were returned to the incubator for 24 hours. Finally, cells were serum starved in 0.5% FBS DMEM overnight before stimulation with HA particles or MDA-MB-231 conditioned media.

2.4.3 IL-6 ELISA

IL-6 concentration of MDA-MB-231 conditioned media was measured by ELISA (Immunotools) following manufacturer instructions. Briefly, high-binding ELISA plates (SantaCruz) were incubated with IL-6 capture antibody diluted 1:100 in PBS (100 µL/well) overnight at room temperature. Plates were washed 4x with PBST (PBS + 0.1% Tween-20) in between all subsequent steps. Wells were blocked for 2 hours at room temperature with 300 µL 2% BSA in PBS. Blocking buffer was removed before addition of samples in triplicate. A standard curve was prepared from purified rh-IL6 using serial dilution in ELISA diluent (PBST+ 1% BSA). Plates were incubated for 2 hours at room temperature. Samples were decanted and 100 µL of detection antibody diluted 1:100 in ELISA diluent. Plates were incubated for 2 hours at room temperature before removal of antibody solution and addition of HRP-streptavidin diluted 1:1000 in ELISA diluent. Plates were incubated for 30 minutes at room temperature. HRP solution was decanted and wells were incubated with 100 µL TMB solution (Biolegend) at room temperature on an orbital shaker, with colour development monitored. The reaction was stopped by addition of 50 µL 1M HCL, and absorbance was measured at 450 nm.

2.5 SDS-PAGE and western blotting

2.5.1 Sample preparation

To prepare samples for analysis by western blot, cells were washed once with ice-cold PBS. Cells were scraped into ice-cold PBS and pelleted by centrifugation at 400 x g for 5 minutes at 4°C. Supernatant was removed and pellets were solubilised in 100 µL RIPA buffer (Sigma) with proteinase and phosphatase inhibitor cocktails (Sigma) added at a concentration of 1% each. Samples were stored on ice for 30 minutes with occasional vortexing. Samples were centrifuged at 14,000 x g for 5 minutes at 4°C to pellet any insoluble material. Protein concentration was

determined by BCA assay, and samples were diluted with water to achieve equal concentrations. A 5X SDS loading buffer (250 mM Tris-HCl, pH 6.8, 10% SDS, 30% glycerol, 5% β-mercaptoethanol, 0.05% bromophenol blue) was added and samples were boiled at 95°C for 5 minutes.

2.5.2 SDS-PAGE gel preparation

Gel casting apparatus was assembled by placing a rubber seal between two glass plates and clamping in place. The seal was checked for leaks by filling the inner chamber of the glass plates with water. Resolving and stacking gel solutions were prepared as detailed below, leaving out the APS and TEMED until immediately before casting. A 10% acrylamide gel was chosen based on the molecular weights of the proteins to be analysed. The resolving gel was poured first and overlaid with water-saturated butanol to exclude oxygen. Once the lower, resolving layer was polymerised (30-40 minutes), the butanol was decanted and resolving gel was rinsed with ddH_2O. The stacking gel was then added and a gel comb inserted to create wells.

Table 2.4 SDS-PAGE gel formulation

10% Resolving gel	
Water	2.7 mL
1.5 M Tris-HCL, pH 8.8	1.75 mL
30% acrylamide	2.3 mL
10% SDS	70 µL
10% APS	70 µL
TEMED	3 µL

5% Stacking gel	
Water	1.4 mL
0.5 M Tris-HCL, pH 6.8	620 µL
30% acrylamide	425 µL
10% SDS	25 µL
10% APS	25 µL
TEMED	2.5 µL

2.5.3 SDS-PAGE gel electrophoresis and transfer

SDS-PAGE gels were placed into the electrophoresis chamber (Atto) and the inner chamber was filled with SDS running buffer (25 mM Tris, 192 mM glycine, 0.1% SDS). Samples were then carefully loaded into gel wells. Gels were run at 60 V until samples migrated to the boundary of the two gel layers, then switched to 120 V for the remainder of the run. Samples were run until the dye band migrated to the bottom of the gel. A pre-stained 10 to 245 kDa protein ladder (Assay Genie) was run alongside samples to allow for size determination. After run completion, the apparatus was disassembled, and the gels removed from their glass plates Gels were equilibrated for 10 minutes in transfer buffer (25 mM Tris, 192 mM glycine,

10% methanol). PVDF membrane was activated in methanol for 30 seconds, then incubated in transfer buffer for 10 minutes.

Transfer sandwich was assembled as detailed in Fig. 2.1. The transfer apparatus was assembled, filled with chilled transfer buffer and an icepack to prevent excess heat build-up and run at 200 mA for 90 minutes. Once the run was completed, the transfer apparatus was disassembled and the membrane rinsed in ddH_2O.

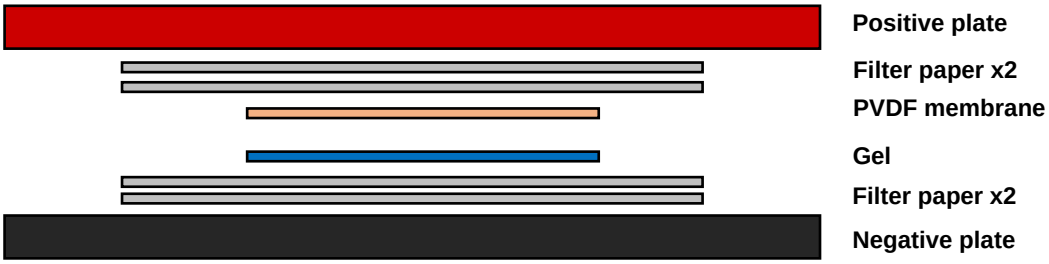

Figure 2.1 Assembly order of transfer sandwich for western blotting.

2.5.4 Western blotting

Membranes were blocked for 1 hour at room temperature with 5% BSA in TBS, then incubated overnight on a roller at 4°C with primary antibody in TBST + 5% BSA. All antibodies used are detailed below (Table 2.5). Membranes were washed for 5 minutes in TBST 3 times, then incubated for one hour at room temperature with secondary antibody in TBST + 5% BSA. Membranes were again washed 3 times for 5 minutes. Finally, ECL detection reagent (GE Healthcare) was added and the membranes were imaged using an Amersham 600 imaging system. Bands were quantified by densitometry (ImageJ) and normalised to β-actin controls.

Table 2.5 Primary and secondary Western blotting antibodies.

Target	Species	Supplier	Concentration
β-actin	Mouse, monoclonal	Santa Cruz	1:1,000
STAT3	Mouse, monoclonal	Novus Biologicals	1:1,000
pSTAT3	Mouse, monoclonal	Novus Biologicals	1:1,000
Secondary antibody, anti-mouse	Goat, anti-mouse	Santa Cruz	1:2,000

2.6 Tumoursphere assays

Poly2-hydroxyethyl methacrylate (pHEMA, Santa Cruz) was used to create non-adherent tissue culture plates. A solution of 120 mg/ml pHEMA in 95% ethanol was stirred overnight at 65°C to create a 10X solution. This stock was diluted 1:10 in

95% ethanol and used to coat a 6-well plate (1mL/well). Plates were left in a 37°C incubator for 48 hours to dry.

Cells were trypsinised as previously described, passed several times through a 25 G needle to ensure a single cell suspension and resuspended in serum-free DMEM/F12 supplemented with 2% B27 serum-free supplement (Biosciences) and 20 ng/mL epidermal growth factor (Immunotools) at a concentration of 2,500 cells/mL. 2 mL cell suspension (5,000 cells total) was added to each well of a pHEMA coated 6-well plate. Plates were gently rocked to evenly disperse the cells, then returned to the incubator for up to 7 days. Formation of tumourspheres was observed by light microscopy at 40X magnification and spheres over 50 µm were counted in each well.

In some replicates, spheres were collected by centrifugation, resuspended in 500 µL PBS and deposited onto poly-lysine coated microscope slides (Sigma) using a Cytospin 4 cytocentrifuge (ThermoFisher) and Shandon EZ Single cytofunnels (ThermoFisher), which separate cells from a liquid suspension and deposits them as a thin layer. Cells were spun for 5 minutes at 55 x g.

2.7 *In vivo* work

In vivo samples were generated and kindly provided by Dr. Will Brackenbury (University of York, U.K.). Experiments were approved by the University of York Ethical Review Process. 1×10^6 MDA-MB-231-GFP cells were suspended in Matrigel and injected into both inguinal mammary fat pads of six-week-old female *Rag2*$^{-/-}$ *Il2rg*$^{-/-}$ mice under isoflurane anaesthesia. Mice were euthanized when primary tumours reached 10% of starting body weight, or at the first sign of discomfort from metastatic burden.

Tumours were fixed in 4% paraformaldehyde and frozen. Cryosections were cut and transferred to glass slides. Sections were stained by Alizarin Red S as previously described.

2.8 Raman spectroscopy

2.8.1 Sample preparation

To prepare samples for Raman spectroscopy analysis, 20mm diameter calcium fluoride windows (Crystan) were placed in the bottom of 6-well plates and incubated with 2 mL DMEM at 37°C for 1 hour. MDA-MB-231 cells were seeded at a concentration of $0.8\text{x}10^6$ cells/well. The following day, media was removed and cells

were switched to either OC+Dex or DMEM with 10 mM sodium phosphate, 50 µg/mL ascorbic acid and 100 nM dexamethasone media to induce mineralisation. Cells grown in DMEM media alone were used as a control. Samples were taken at days 3, 7, 11 and 14. Media was removed and each window was washed once with PBS, fixed in 10% formalin-PBS for 30 minutes, rinsed with ddH_2O and air dried.

2.8.2 Raman spectroscopy analysis

All Raman analysis was carried out by Pascaline Bouzy (Department of Physics & Astronomy, University of Exeter). Raman analysis was performed using an InVia Renishaw Raman micro-spectrometer coupled to a Leica microscope with a 50X long working distance objective. The excitation beam was an 830 nm diode laser with a laser power around 100 mW. For these experiments, the instrument was configured with a 600 lines per mm diffraction grating. The maps were collected with an exposure time of 30 s and a step size of 9.9 µm using the WiRE 4.0 software (Renishaw, Gloucestershire, UK). Spectra were extracted from the maps for each condition using Matlab software (Mathworks, USA). An average of 40 spectra was analysed per sample. Each mean spectrum was reduced in the spectral region 500-1800 cm^{-1}, baseline corrected (elastic function with 9 points), vector normalised and smoothed with Savistsky-Golay algorithm (polynom order 2 and window 9) using OPUS software (Bruker Optics GmbH).

2.9 Statistics

All statistical analysis was carried out using GraphPad Prism 7 software. Student t-tests were used to compare two treatment groups. Differences between multiple treatment groups were analysed be one-way or two-way ANOVA, with post-hoc analysis to confirm significance. A P value of less than 0.05 was deemed statistically significant.

Chapter 3.0

Establishment of an *in vitro* model of mammary calcification in human breast cancer cells

3.1 Introduction

3.1.1 *In vitro* mineralisation models

Previous work from this lab resulted in the development of the first *in vitro* model of microcalcification formation. This model was based on studies of osteoblast mineralisation, which utilise a number of osteogenic reagents to initiate cell differentiation, activation of pro-mineralisation signalling pathways and the development of calcium deposits (Langenbach and Handschel, 2013).

The three main osteogenic reagents utilised in this study are β-glycerophosphate, ascorbic acid and dexamethasone. β-glycerophosphate is an ester compound of phosphoric acid and glycerol, which acts as an organic Pi donor via cleavage by the alkaline phosphatase enzyme. This release of Pi is essential to the formation of calcium-phosphate deposits. Ascorbic acid is essential for secretion and maturation of extracellular matrix components (ECM), most notably collagen. Collagen provides a structural framework for deposition of calcium phosphate and formation of larger mineralised structures (Veis and Dorvee, 2013). Finally, dexamethasone is used to increase expression of mineralisation promoting genes and drive differentiation of osteoblasts to a mineralising phenotype. Dexamethasone exerts a species specific effect, increasing mineralisations in cultures of cells derived from both human and rat sources whilst inhibiting osteogenic differentiation of murine cells (Taylor et al., 2014). Together, these three reagents create the optimum environment for *in vitro* mineralisation.

Mineralisation is routinely tested using both histological staining and direct quantification of deposited calcium. Two commonly used stains in the study of mineralising cells are Alizarin Red S and von Kossa. Alizarin Red S, when used at an acidic pH, binds to Ca^{2+} ions at the surface of hydroxyapatite crystals, staining areas of high calcium concentration a bright-red (Moriguchi et al., 2003). von Kossa is an indirect method of detecting calcium deposits, which relies on substitution of associated Pi with silver ions (Rungby et al., 1993). Subsequent reduction to metallic silver results in dark brown to black staining. Both of these stains have previously been used to successfully identify breast microcalcifications, both *in vitro* (Cox et al., 2012a) and *in vivo* (Wilson et al., 2014).

The mammary calcification model developed previously in our lab, using the same reagents and protocols from established osteoblast studies (Langenbach and Handschel, 2013), revealed an active, regulated process of mineral deposition with many similarities to physiological mineralisation. The majority of this previous work focused on the murine 4T1 cell line, which was shown to effectively mineralise when incubated with a combination of β-glycerophosphate and ascorbic acid. Mineralisation was found to be dependent on activity of alkaline phosphatase (or free Pi) and the sodium-dependent Pi cotransporter, PiT-1.

Two separate formulations of mineralisation promoting media were used, β-glycerophosphate and ascorbic acid (OC) or β-glycerophosphate, ascorbic acid and dexamethasone (OC+Dex). Testing a panel of cell lines in both the presence and absence of dexamethasone allowed for the identification of optimal mineralisation conditions for each cell line, which are likely to vary in their reaction to dexamethasone depending on their original source. For instance, in these previous studies the human derived Hs578Ts(i)8 cell line required dexamethasone for mineralisation whilst the murine 4T1 cell line exhibited significantly less calcium deposition in dexamethasone containing media.

Since development of our model of breast microcalcification formation, other groups have utilised it to investigate novel players in the process, including the secretory pathway Ca^{2+} -ATPases (SPCA) Ca^{2+} efflux channels (Dang et al., 2017) and carbonic anhydrase (Zheng et al., 2015).

3.1.2 Human breast cancer cell lines and microcalcifications

Although previous work from this lab has looked at mineralisation in human breast cancer cell lines, the number of cells examined was low and not representative of the diversity of breast cancer subtypes. Only one human breast cancer cell line was found to successfully mineralise. Hs578Ts(i)8 is a highly invasive sub-clone of the triple-negative Hs578T cell line, derived from sequential passages through a Matrigel invasion chamber (Hughes et al., 2008) and was found to develop mineralisation after 21 days when cultured with OC+Dex. Interestingly, no mineralisation was observed in the parental Hs578T cell line, indicating a possible relationship between the aggressiveness of a cell line and the ability to form microcalcifications.

This may have some clinical relevance in consideration of certain studies finding associations between mammographic detection of microcalcifications and increased tumour aggressiveness and poor prognosis (Tabár et al., 2000, Tabar et al., 2004, Qi et al., 2017, Zheng et al., 2017). Negative results were also observed in the immortalised, non-tumourigenic MCF10A cell line.

This finding that the ability to mineralise is not a universal attribute of breast cancer cell lines may signify the importance of a particular cell lines genetic background. Cell lines derived from different molecular subtypes of breast tumour vary significantly in their aggressiveness, gene expression profiles, cytokine secretion and responsiveness to therapeutic agents (Holliday and Speirs, 2011). It is not currently known if any particular subtypes of breast cancer cell lines are more likely to mineralise under *in vitro* conditions. In patient studies, microcalcifications show strong association with the HER2 overexpressing subtype of breast cancer (Killelea et al., 2013a, Cen et al., 2017a, Bae et al., 2013). However, the hypothesis that the *in vitro* mineralisation potential of cell lines follows a similar pattern remains untested. A thorough examination of the mineralisation potential of a representative selection of human breast cancer cells is thus merited.

3.1.3 Aims of this chapter

The primary aims of this chapter are as follows.

- Investigate a panel of human breast cancer cell lines for *in vitro* mineralisation potential.
- Identify any notable differences in tumour subtype between mineralising and non-mineralising cell lines.
- Examine effect of both organic and inorganic phosphate sources on cell mineralisation.
- Investigate the interactions between the alkaline phosphatase enzyme and β-glycerophosphate and the role of released Pi in initiation of mineralisation.

3.2 Results

3.2.1 Establishment of standard mineralisation and staining procedure for murine 4T1 cell line

In order to provide a positive control with which to compare our panel of human breast cancer cell lines to, we elected to begin with the murine 4T1 cell line, which has previously been shown by our lab to be an effective model of microcalcification formation (Cox et al., 2012a). 4T1 cells were cultured for up to 28 days in DMEM culture media (Control) or DMEM supplemented with 50 µg/ml ascorbic acid and 10 mM β-glycerophosphate (OC) or OC with 100 nM dexamethasone (OC + Dex). Identical plates were formalin fixed and stained at weekly intervals (7, 14, 21 and 28 days). Samples were stained with Alizarin Red S (2%, pH 4.4) and von Kossa (5% silver nitrate) to detect the presence of calcium and phosphate, respectively. Positive staining was observed in both Alizarin Red S stained (Fig. 3.1 A) and von Kossa stained samples (Fig 3.1 B), beginning at day 21 and increasing in intensity by day 28. These two positive staining results together strongly indicate the presence of calcium phosphate in the form of hydroxyapatite, which was previously confirmed by Raman spectroscopy (Cox et al., 2012a).

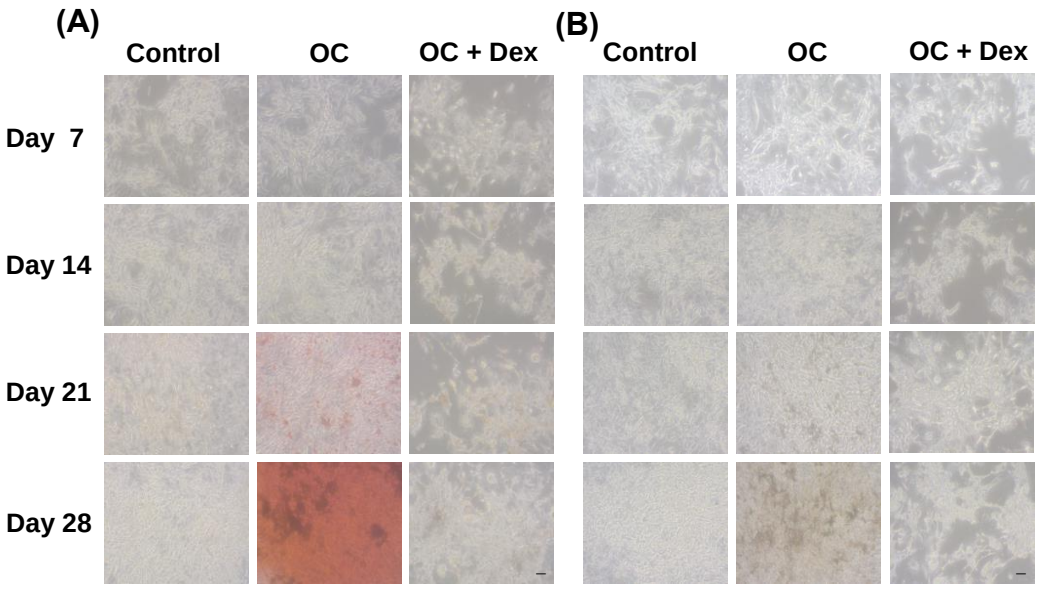

Figure 3.1 Positive mineralisation in 4T1 cells. Representative images were captured at 10X magnification of Alizarin Red S stained (A) and von Kossa stained (B) cell monolayers at the specified time points. Positive staining was observed in both Alizarin Red S (A) and von Kossa (B) stained samples, when cells were cultured in OC supplemented media. Control=regular growth media. OC (osteogenic cocktail) = 50 µg/ml ascorbic acid and 10 mM β-glycerophosphate. Dex=100 nM dexamethasone. Scale bar represents 50 µm.

3.2.2 Assessing mineralisation potential of MCF-7 cells

The ER+ luminal A cell line MCF-7 was selected as the first human cell line to test for mineralisation capability. Following the previously established protocol for the murine 4T1 cell line, MCF-7 cells were grown in 6-well plates for up to 28 days in DMEM culture media (Control) or DMEM supplemented with ascorbic acid and β-glycerophosphate (OC) or OC with dexamethasone (OC + Dex). One replicate plate was formalin fixed and stained with Alizarin Red S and von Kossa at weekly intervals. Neither stain resulted in a positive result at any time point or treatment group (Fig. 3.2 A, B).

Calcium was extracted from the cell monolayer by a 1-hour incubation with nitric acid, before quantification by the o-cresolphthalein complexone (OCP) assay. Results were normalised against protein content as measured by bicinchoninic acid (BCA) assay. Calcium content of MCF-7 cell monolayers grown in control media averaged 5.7-9.2 ppm/mg protein throughout the 28-day time course (Fig. 3.2 C). No significant increases were observed in cells cultured in OC or OC+Dex media at any time point. An alamar blue assay was also conducted to determine if any treatment group was having a detrimental effect on cell viability. Cells cultured in control media or either of the mineralisation promoting media maintained good viability throughout the experiment as evidenced by the similar viability values at all tested time points (Fig. 3.2 D).

These results demonstrate that microcalcification formation is not a universal property of human breast cancer cell lines.

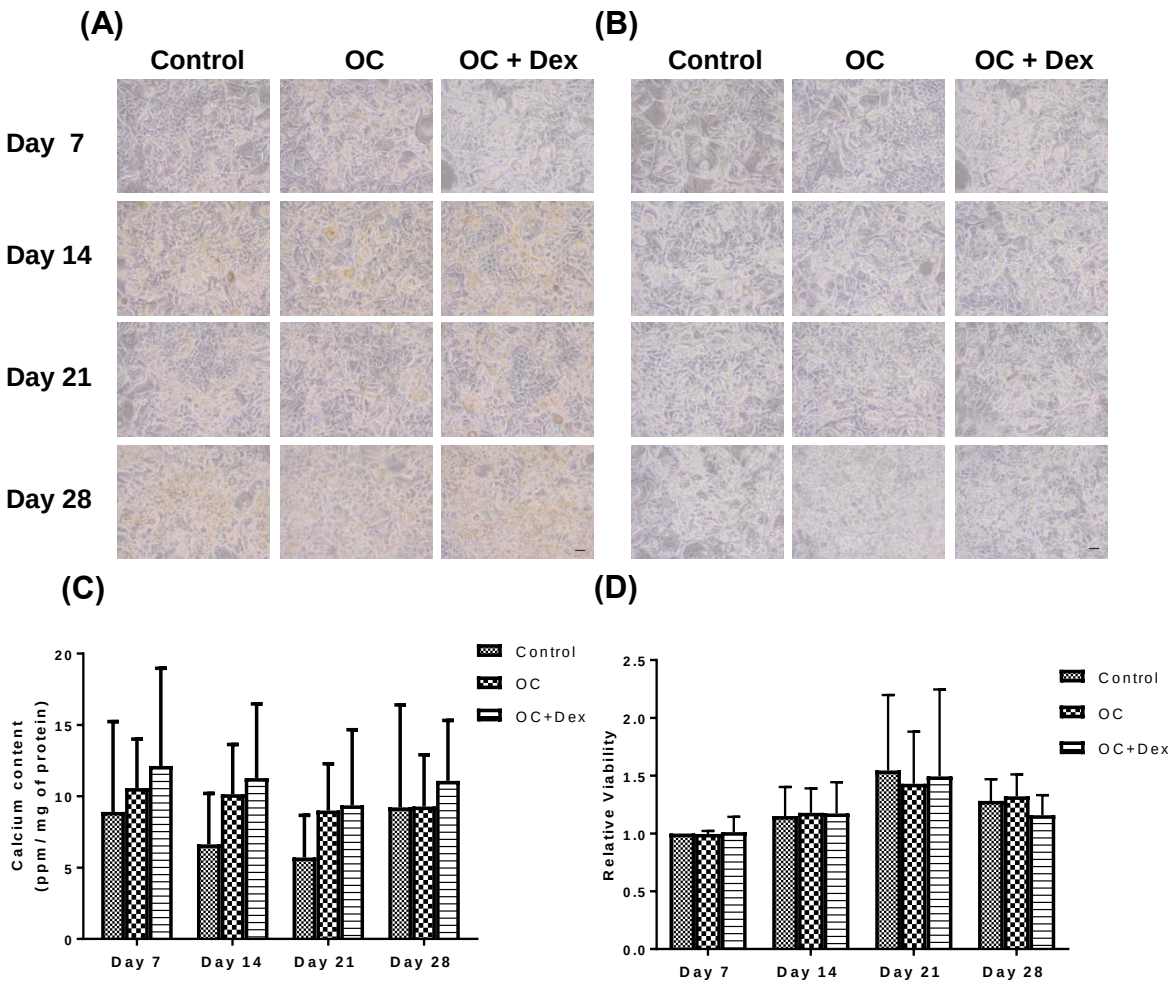

Figure 3.2 MCF-7 cells do not undergo *in vitro* microcalcification formation. Representative images were captured at 10X magnification of Alizarin Red S stained (A) and von Kossa stained (B) cell monolayers at the specified time points. No positive staining (red for Alizarin Red S, dark brown/black for von Kossa) was observed at any time point or treatment group. The calcium content of MCF-7 cell monolayers was determined by the o-cresolphthalein (OCP) assay and normalised to protein content (C). Each time point represents mean + SD (n=3). The viability of MCF-7 cells cultured in control media or media supplemented with OC or OC+Dex was determined by Alamar blue assay (D). Each time point represents mean + SD (n=3). Statistical significance was determined by two-way ANOVA. Control=regular growth media. OC (osteogenic cocktail) = 50 µg/ml ascorbic acid and 10 mM β-glycerophosphate. Dex=100 nM dexamethasone. Scale bar represents 50 µm.

3.2.3 Assessing mineralisation potential of HER2 overexpressing MCF-7 cells

Several studies have found an increased rate of HER2 overexpression in patients presenting with microcalcification associated breast tumours (Cen et al., 2017a, Elias et al., 2014, Li et al., 2014a). However, a potential role between the HER2 receptor and the *in vitro* formation of microcalcifications has never been explored. We repeated our mineralisation experiment with a HER2 overexpressing sub-clone of the luminal MCF-7 cell line (Pegram et al., 1997), to assess any difference in mineralisation capability between the parental and HER2 expressing cell lines. Similar to the parental cell line, no positive staining was detected by Alizarin Red S or von Kossa staining in HER2-MCF-7 cells in any treatment group (Fig. 3.3 A, B). Calcium content of HER2-MCF-7 cells grown in control media ranged from 10.3–14.2 ppm/mg protein, which was not statistically different from the calcium content of both HER2-MCF-7 cells grown in OC or OC+Dex supplemented media (9.5 – 16.8 and 8.9 – 18.5 ppm/mg protein, respectively) and to the parental MCF-7 cell lines, indicating that HER2 overexpression does not alter either the mineralisation potential or basal calcium content of the parental MCF-7 cell line (Fig. 3.3 C). Finally, the viability of HER2-MCF-7 cells was tested with an alamar blue assay. No significant changes were detected between groups at any time point (Fig. 3.3. D). Results of this experiment demonstrate that HER2 overexpression is not sufficient by itself to induce mineralisation.

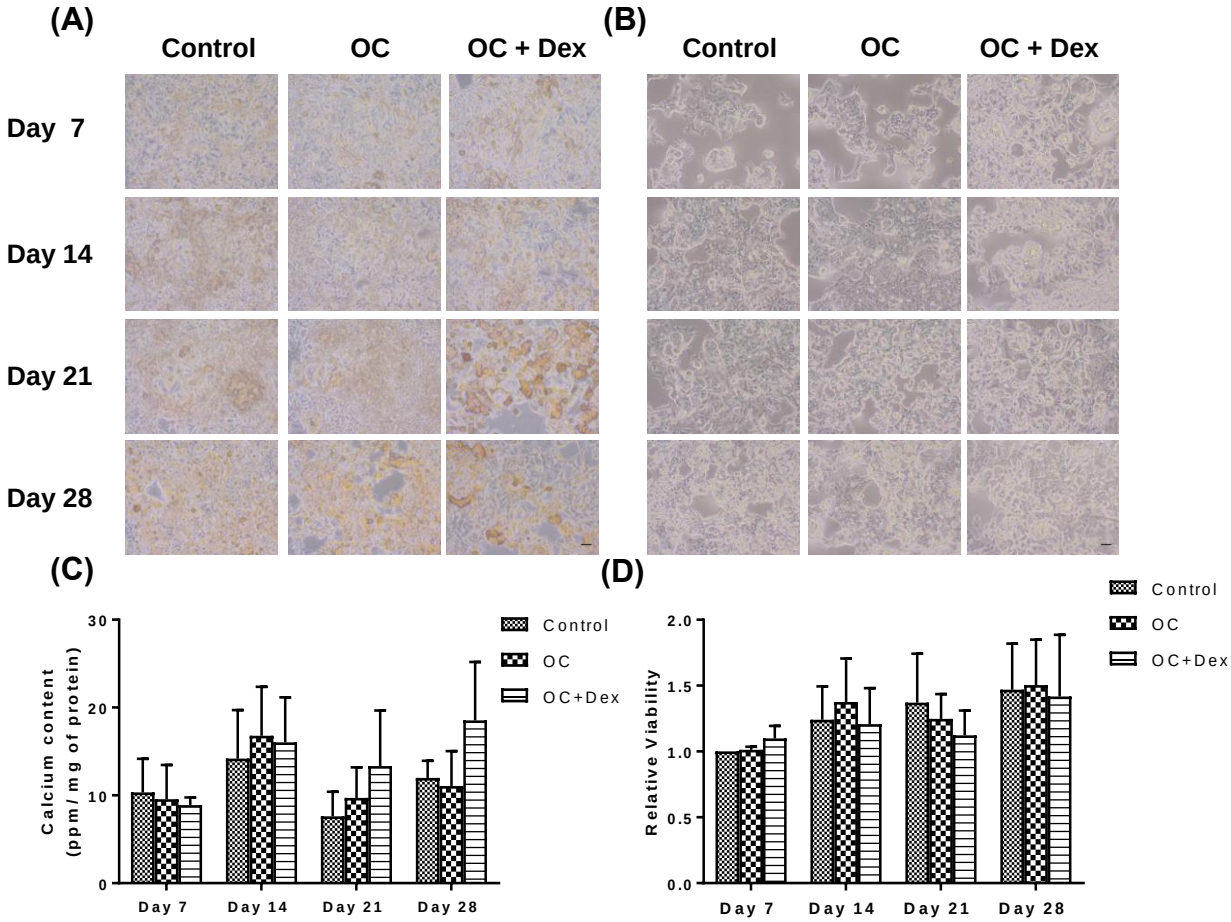

Figure 3.3 HER2 overexpressing MCF-7 cells do not undergo *in vitro* microcalcification formation. Representative images were captured at 10X magnification of Alizarin Red S stained (A) and von Kossa stained (B) cell monolayers at the specified time points. No positive staining (red for Alizarin Red S, dark brown/black for von Kossa) was observed at any time point or treatment group. The calcium content of HER2-MCF-7 cell monolayers was determined by the o-cresolphthalein (OCP) assay and normalised to protein content (C). Each time point represents mean + SD (n=3). The viability of HER2-MCF-7 cells cultured in control media or media supplemented with OC or OC+Dex was determined by Alamar blue assay (D). Each time point represents mean + SD (n=3). Statistical significance was determined by two-way ANOVA. Control=regular growth media. OC (osteogenic cocktail) = 50 µg/ ml ascorbic acid and 10 mM β-glycerophosphate. Dex=100 nM dexamethasone. Scale bar represents 50 µm.

3.2.4 Assessing mineralisation potential of ZR-75-1 cells

We next assessed the mineralisation potential of the luminal B ZR-75-1 cell line. Similar to our previous investigations into luminal cell lines, results for the ZR-75-1 cell line were also found to be negative. No positive staining was observed at any time point in either Alizarin Red S (Fig. 3.4 A) or von Kossa stained (Fig. 3.4 B) samples. Similar results were observed in the OCP assay, with not significant differences observed between any group at any time point (Fig. 3.4 C). Unlike our other tested cell lines, we did see some significant differences in viability between groups, with a slight drop in viability observed in OC samples at day 14 compared to control samples (Fig. 3.4 D, $P < 0.05$).

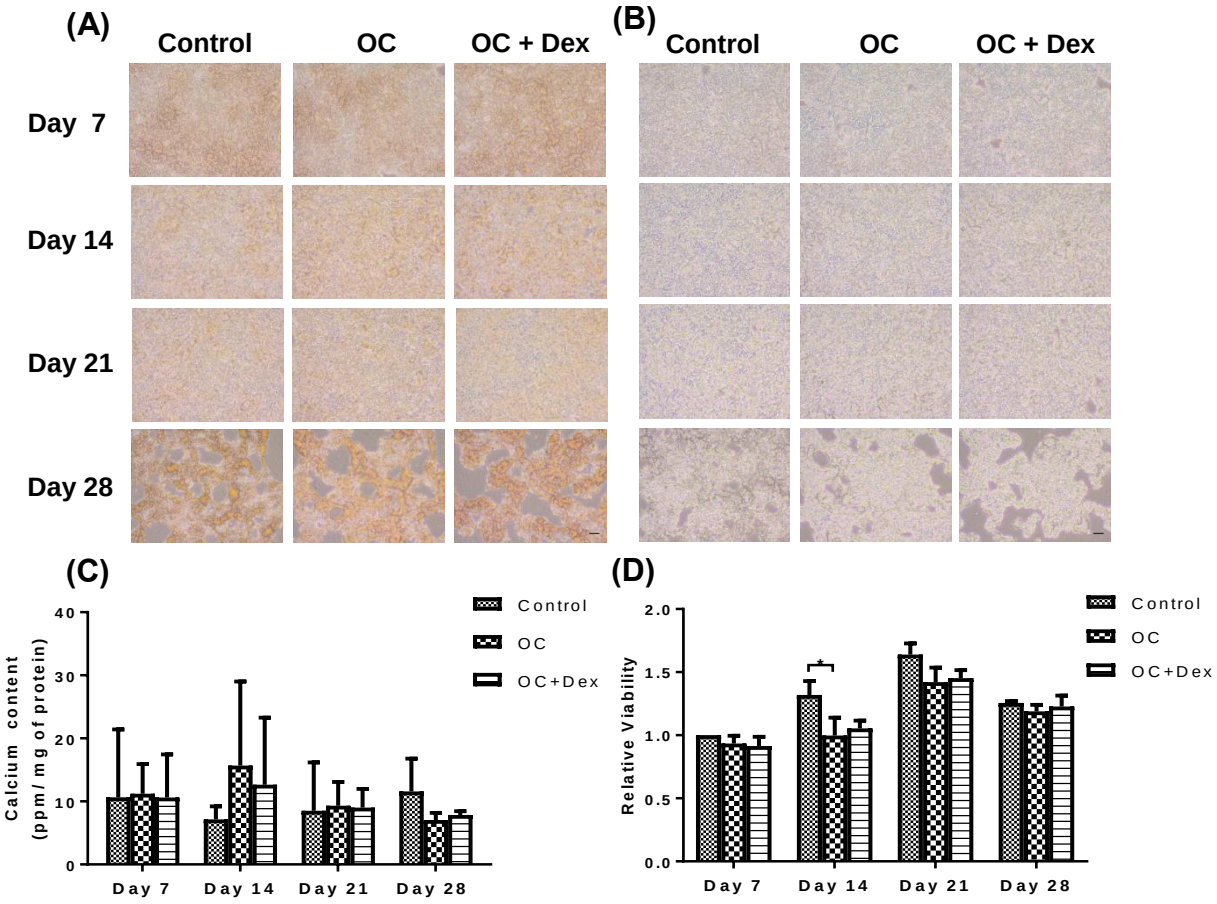

Figure 3.4 ZR-75-1 cells do not undergo *in vitro* microcalcification formation. Representative images were captured at 10X magnification of Alizarin Red S stained (A) and von Kossa stained (B) cell monolayers at the specified time points. No positive staining (red for Alizarin Red S, dark brown/black for von Kossa) was observed at any time point or treatment group. The calcium content of ZR-75-1 cell monolayers was determined by the o-cresolphthalein (OCP) assay and normalised to protein content (C). Each time point represents mean + SD (n=3). The viability of ZR-75-1 cells cultured in control media or media supplemented with OC or OC+Dex was determined by Alamar blue assay (D). Each time point represents mean + SD (n=3). Statistical significance was determined by two-way ANOVA *P<0.05. Control=regular growth media. OC (osteogenic cocktail) = 50 µg/ ml ascorbic acid and 10 mM β-glycerophosphate. Dex=100 nM dexamethasone. Scale bar represents 50 µm.

3.2.5 Assessing mineralisation potential of SKBR3 cells

We next selected the HER2 overexpressing SKBR3 cell line. Positive mineralisation results were observed in this cell as evidenced by strong staining in both Alizarin Red S (Fig. 3.5 A) and von Kossa (Fig. 3.5 B). Staining was first evident at day 14 for both stains, in cells cultured in OC+Dex media. Some staining was observed in cells grown with OC media alone, although significantly fainter. Both Alizarin Red S and von Kossa staining increased in intensity throughout the time course, with cells grown with OC+Dex displaying markedly greater staining at all time points tested than cells grown in OC alone.

Calcium content of control cells did not vary significantly throughout the course of this experiment, varying from 5.4 – 34.8 ppm/mg protein (Fig 3.5 C). In contrast, cells grown in either OC or OC+Dex media began to accumulate calcium by day 14. Calcium in cells incubated with OC rose to 130 ppm/mg protein by day 14 and stayed at approximately that level for the remainder of the experiment. Cells grown in OC+Dex media continually increased their calcium content, rising to 222.5 ppm/mg protein by day 21 ($P < 0.05$) and 271.2 ppm/mg protein by day 28 ($P < 0.01$). A small decrease in viability was observed in OC+Dex treated groups at day 28 ($P < 0.05$, Fig. 3.5 D).

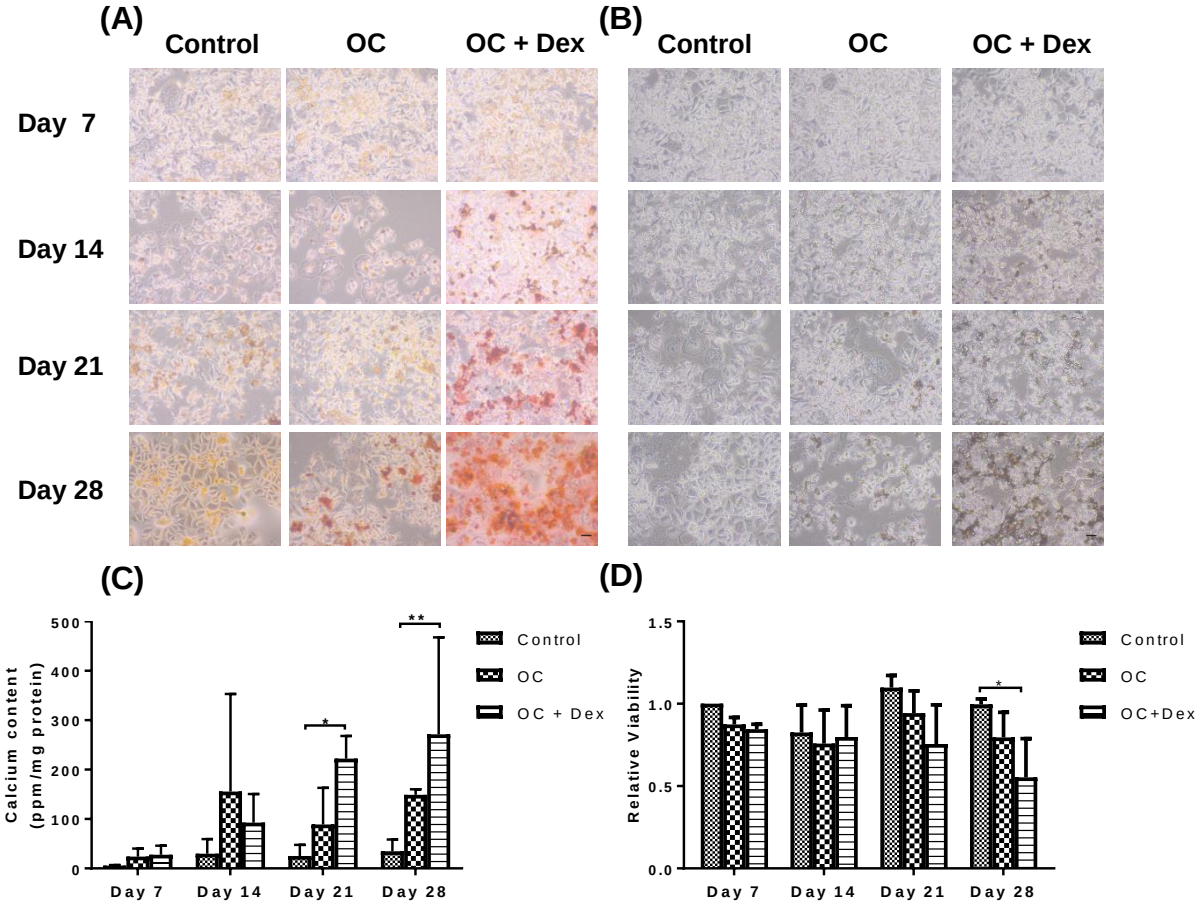

Figure 3.5 SKBR3 cells undergo *in vitro* microcalcification formation. Representative images were captured at 10X magnification of Alizarin Red S stained (A) and von Kossa stained (B) cell monolayers at the specified time points. Positive staining (red for Alizarin Red S, dark brown/black for von Kossa) was observed in OC+Dex treated cells beginning at day 14. The calcium content of SKBR3 cell monolayers was determined by the o-cresolphthalein (OCP) assay and normalised to protein content (C). Each time point represents mean + SD (n=3). The viability of SKBR3 cells cultured in control media or media supplemented with OC or OC+Dex was determined by Alamar blue assay (D). Each time point represents mean + SD (n=2). Statistical significance was determined by two-way ANOVA. *P<0.05, **P<0.01. Control=regular growth media. OC (osteogenic cocktail) = 50 µg/ ml ascorbic acid and 10 mM β-glycerophosphate. Dex=100 nM dexamethasone. Scale bar represents 50 µm.

3.2.6 Assessing mineralisation potential of HCC1954 cells

To further test a possible role for HER2 in microcalcification formation, we selected another HER2 positive cell line, HCC1954. Unlike the SKBR3 cell line, HCC1954 was not capable of mineralising *in vitro*, as evidenced by lack of either Alizarin Red S (Fig 3.6 A) or von Kossa (Fig 3.6 B) staining. Calcium content of HCC1954 as measured by OCP assay was not significantly altered in any group throughout the time course of this experiment (Fig 3.6 C). All three groups displayed a rise in calcium content at day 28, although this result was not statistically significant. As this increase occurred in only one replicate and was not accompanied by any positive Alizarin Red S or von Kossa staining, this rise in calcium levels was likely an anomaly and not the result of a mineralisation process. Viability of HCC1954 cells remained relatively unchanged throughout the 28 time course (Fig. 3.6 D).

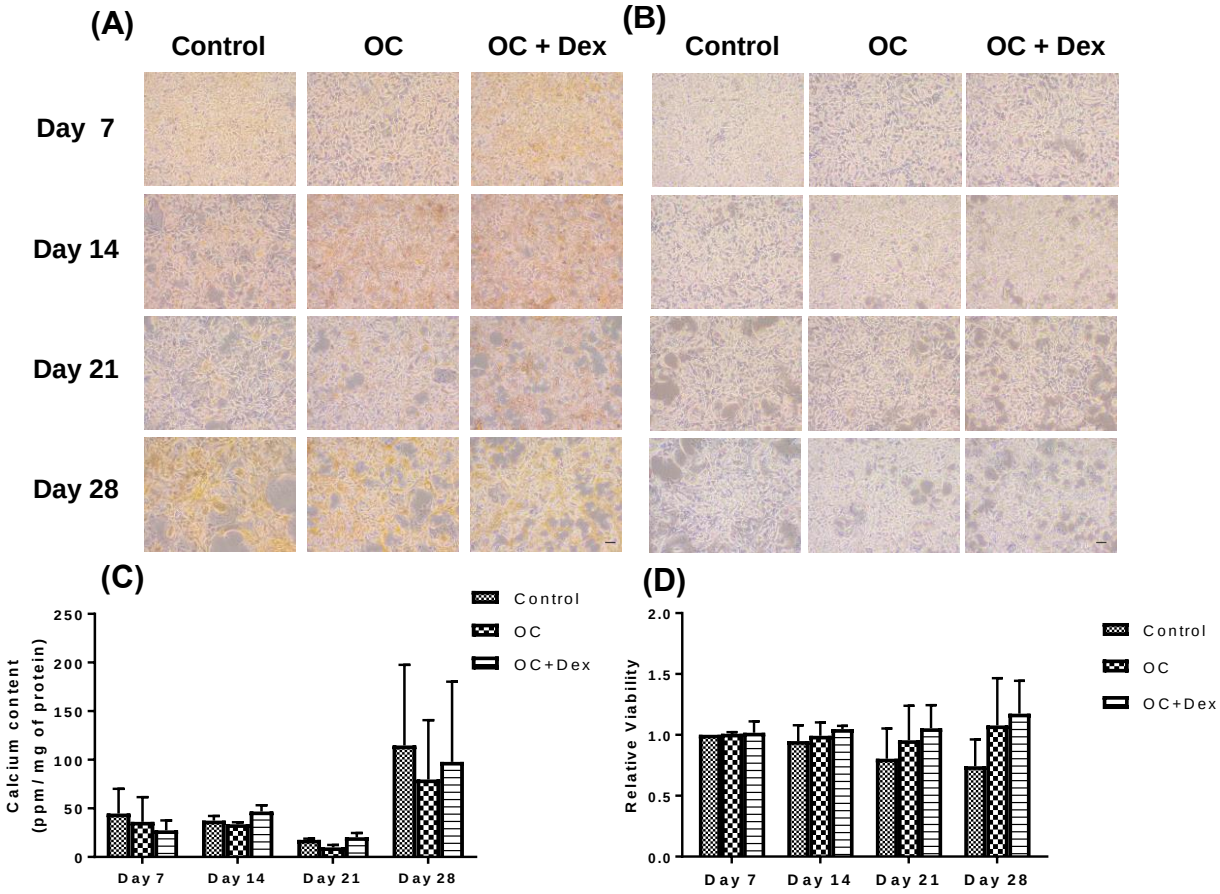

Figure 3.6 HCC1954 cells do not undergo *in vitro* microcalcification formation. Representative images were captured at 10X magnification of Alizarin Red S stained (A) and von Kossa stained (B) cell monolayers at the specified time points. No positive staining (red for Alizarin Red S, dark brown/black for von Kossa) was observed at any time point or treatment group. The calcium content of HCC1954 cell monolayers was determined by the o-cresolphthalein (OCP) assay and normalised to protein content (C). Each time point represents mean + SD (n=3). The viability of HCC1954 cells cultured in control media or media supplemented with OC or OC+Dex was determined by Alamar blue assay (D). Each time point represents mean + SD (n=2). Control=regular growth media. OC (osteogenic cocktail) = 50 µg/ ml ascorbic acid and 10 mM β-glycerophosphate. Dex=100 nM dexamethasone. Statistical significance was determined by two-way ANOVA. Scale bar represents 50 µm.

3.2.7 Assessing mineralisation of MDA-MB-231 cells

The final cell line to be tested in our panel was the triple-negative MDA-MB-231 cell line. Results for this cell line were positive, with both Alizarin Red S and von Kossa staining first appearing in cells cultured in OC+Dex media at day 14 (Fig. 3.7 A, B). Both staining modalities initially appeared faint, gradually increasing in intensity over the remainder of the time course. Analysis of calcium content revealed substantial differences between treatment groups (Fig. 3.7 C). Cells grown in control media displayed a calcium content of between 12.8 – 34.9 ppm/mg protein, with cells grown in OC media exhibiting similar levels (9.3 – 38.9 ppm/mg protein).

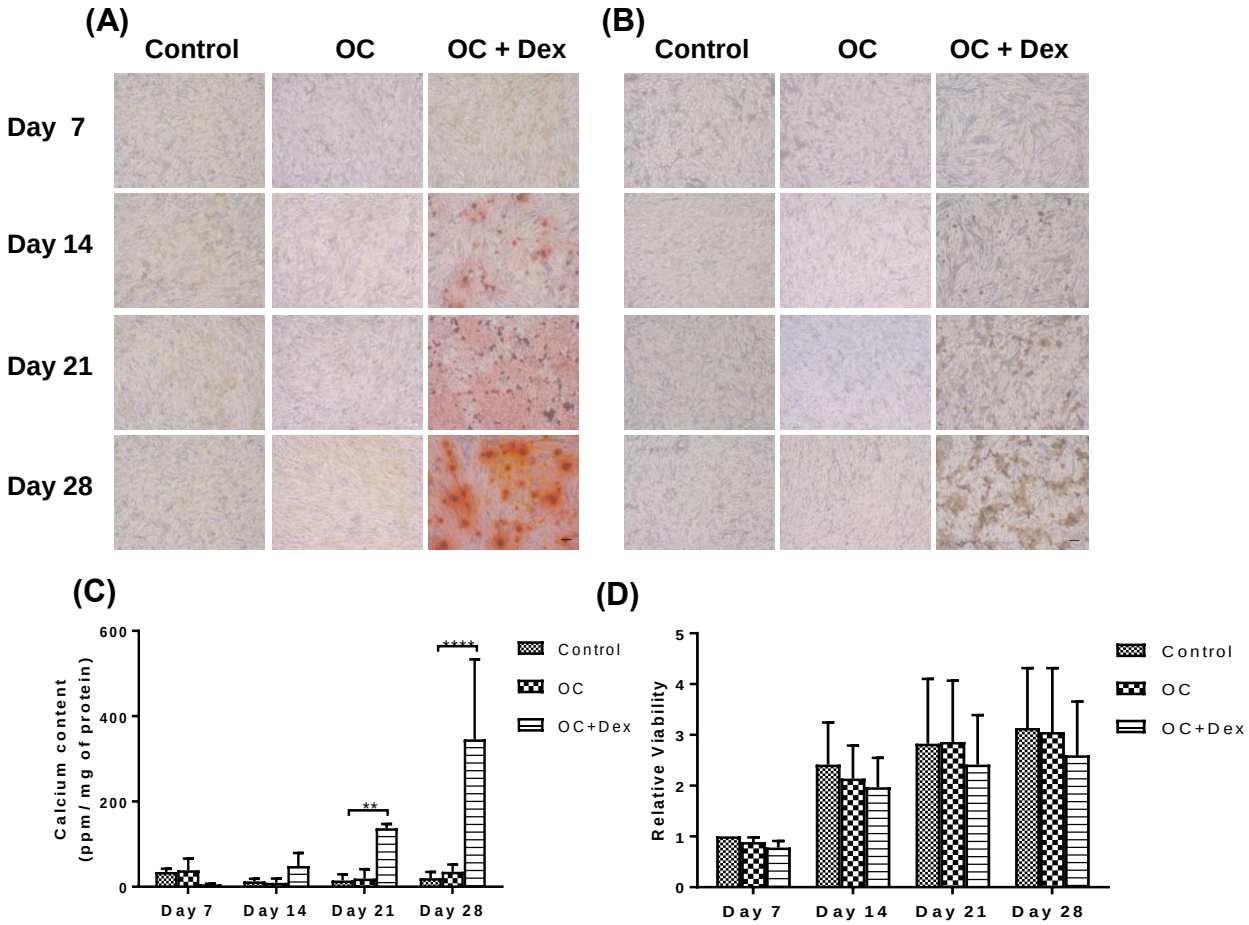

Figure 3.7 MDA-MB-231 cells undergo *in vitro* microcalcification formation. Representative images were captured at 10X magnification of Alizarin Red S stained (A) and von Kossa stained (B) cell monolayers at the specified time points. No positive staining (red for Alizarin Red S, dark brown/black for von Kossa) was observed at any time point or treatment group. The calcium content of MDA-MB-231 cell monolayers was determined by the o-cresolphthalein (OCP) assay and normalised to protein content (C). Each time point represents mean + SEM (n=3). The viability of MDA-MB-231 cells cultured in control media or media supplemented with OC or OC+Dex was determined by Alamar blue assay (D). Each time point represents mean + SD (n=3). Statistical significance was determined by two-way ANOVA. **P<0.01, ****P<0.0001. Control=regular growth media. OC (osteogenic cocktail) = 50 µg/ ml ascorbic acid and 10 mM β-glycerophosphate. Dex=100 nM dexamethasone. Scale bar represents 50 µm.

In cells grown in OC+Dex media, calcium content began to raise at day 14 (48.6 ppm/mg protein), with the increase in calcium reaching statistical significance at day 21 (137.4 ppm/mg protein, $P < 0.01$) and day 28 (345.8 ppm/mg protein, $P < 0.0001$). Alamar blue assays showed a steady increase in cellular viability in all three groups during the 28-day time course, with all three groups displaying an approximate threefold increase at day 28 compared to day 7 (Fig. 3.7 D). No significant differences were found between treatment groups at any time point.

3.2.8 Summary of characterisation study for mineralisation-capable human breast cancer cell lines

Results of our screen are illustrated in Table 3.1. In summary, the luminal breast cancer cell lines MCF-7 (as well as a HER2 overexpressing clone) and ZR-75-1 as well as the HER2 overexpressing HCC1954 did not produce calcifications under any of our tested *in vitro* conditions. Positive mineralisation was noted for the HER2 overexpressing SKBR3 and the triple negative MDA-MB-231 cell lines.

Table 3.1 Summary of a characterisation study of the mineralisation potential of a panel of human breast cancer cell lines

Cell line	Subtype	*In vitro* mineralisation capability	Initial mineralisation	Mineralisation requirements
MCF-7	Luminal A	No	-	-
HER2-MCF-7	Luminal (with HER2 overexpression)	No	-	-
ZR-75-1	Luminal B	No	-	-
SKBR3	HER2 overexpressing	Yes	Day 14	OC+Dex > OC
HCC1954	HER2 overexpressing	No	-	-
MDA-MB-231	Triple negative	Yes	Day 14	OC+Dex

3.2.8 Investigating the specific mineralisation requirements of the MDA-MB-231 cell line

Although both SKBR3 and MDA-MB-231 cells were capable of producing mineralisations, results from MDA-MB-231 cells tended to be slightly more reliable and consistent. In addition, the MDA-MB-231 cell line maintained greater viability during long-term (28 days) studies (Fig. 3.5 D, 3.7 D) and was used for the majority of this thesis, although certain studies were also conducted with both SKBR3 and MCF-7 cells.

To evaluate the specific mineralisation requirements for the MDA-MB-231 cell line and optimise our protocol, cells were next cultured in either control DMEM media or media supplemented with OC+Dex or individual components of the OC+Dex formulation (ascorbic acid, β-glycerophosphate and dexamethasone). Alizarin Red S staining at day 21 revealed a strong osteogenic response only in cells treated with the full OC+Dex supplemented media (Fig 3.8 A). No individual component was capable of inducing mineralisation by itself.

We also investigated the potential effect of different formulations of DMEM cell culture media, in particular glucose concentrations as previous studies on *in vitro* calcification models have found regulatory effects of glucose concentration on calcium deposition (Balint et al., 2001, Garcia-Hernandez et al., 2012). Our previous characterisation study on the mineralisation potential of human breast cancer cell lines utilised a low-glucose formulation of DMEM media (5.5 mM). MDA-MB-231 cells were cultured in either low or high glucose (25 mM) formulations of OC+Dex supplemented media for up to 28 days prior to fixation and staining with Alizarin Red S. Cells were observed to begin mineralising by day 14 when cultured in OC+Dex supplemented low glucose DMEM, as opposed to day 21 for high glucose (Fig. 3.8 B).

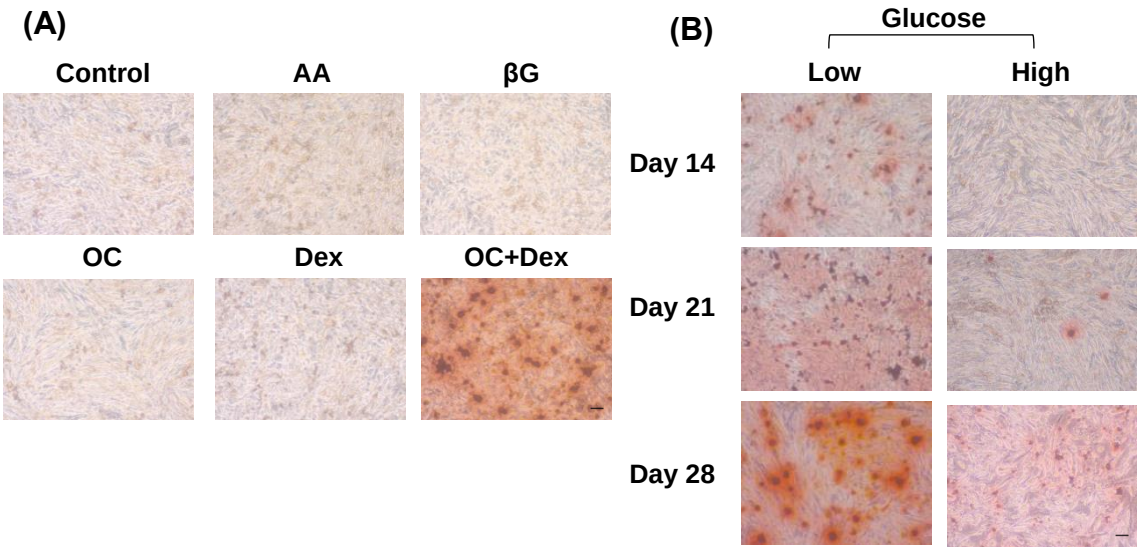

Figure 3.8 Assessing the mineralisation requirements of MDA-MB-231 cells. Representative images were captured at 10X magnification of Alizarin Red S stained MDA-MB-231 cells grown in control media, OC+Dex media or media supplemented with individual components of OC+Dex (A). Alizarin Red S staining was carried out at day 21. Control = DMEM, AA = 50 µg/ ml ascorbic acid, βG = 10 mM β-glycerophosphate, OC (osteogenic cocktail) = AA & βG, Dex=100 nM dexamethasone. The effect of glucose concentration on MDA-MB-231 mineralisation was assessed by culturing cells in low (5.5 mM) or high glucose (25 mM) OC+Dex supplemented DMEM (B). Scale bar represents 50 µm.

Alizarin Red S staining was substantially stronger at all time points for cells cultured in low glucose DMEM. These findings are in agreement with previous, unpublished results from this lab (Fig. 8.7). Low glucose DMEM was thus selected as the optimal mineralisation media for the rest of our studies.

In addition to glucose concentration, we also wanted to examine if providing cells with a collagen rich environment could enhance their osteogenic differentiation. Collagen is known to provide a structural framework for deposition of calcium phosphate (Veis and Dorvee, 2013) and some studies have shown enhanced osteogenic differentiation of mesenchymal cells when cultured on collagen coated plates (Chiu et al., 2012, Chiu et al., 2014). In order to determine if collagen could also improve our *in vitro* assay, we compared collagen coated to standard tissue culture plates, analysing both calcium deposition and ALP activity.

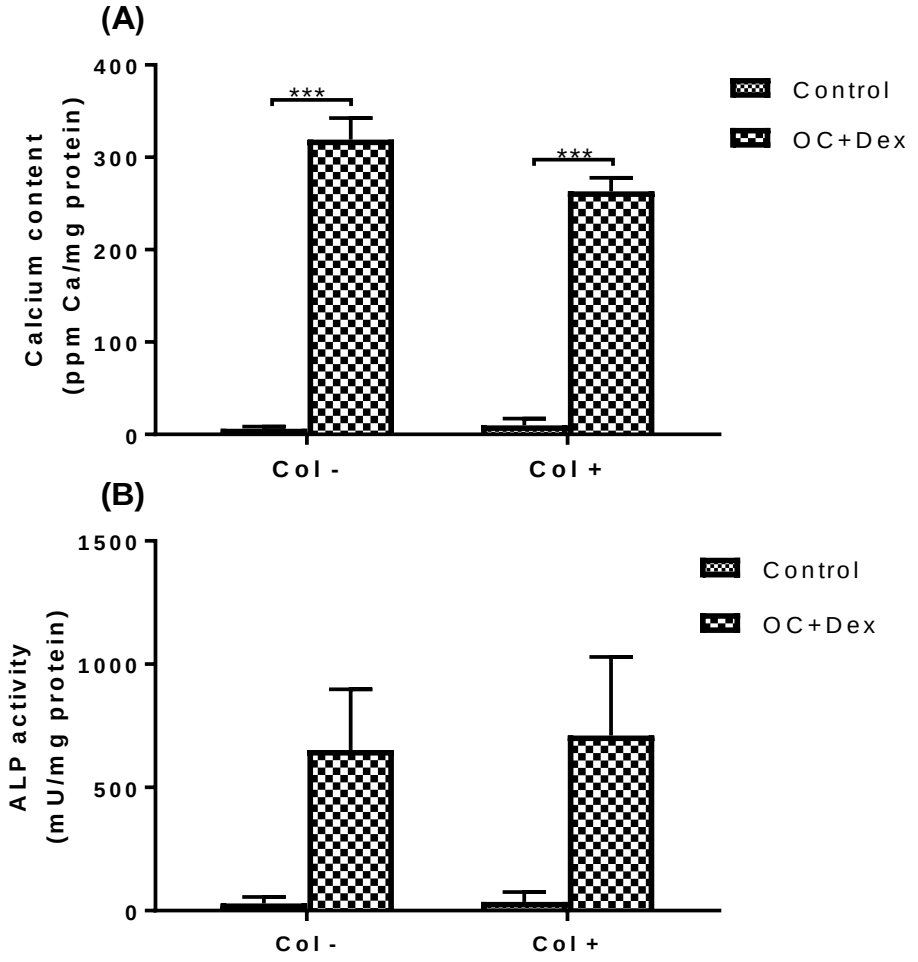

Figure 3.9 Investigating the effect of collagen coating on MDA-MB-231 mineralisation. MDA-MB-231 cells were cultured for up to 28 days in control media or OC+Dex supplemented media. Cells were cultured on either standard tissue culture plates (Col -) or plates pre-coated in collagen (Col +). Calcium content was measured at day 28 by OCP assay (A) ALP activity was measured at day 14 by chromogenic conversion of para-nitrophenyl phosphate (B). Each point represents mean + SD (N=2). Statistical significance was determined by two-way ANOVA. ***P<0.001.

We did not observe any significant alterations in either calcium deposition (Fig. 3.9 A) or ALP activity (Fig. 3.9 B) in MDA-MB-231 cells cultured on collagen coated plates. We therefore elected to use standard tissue culture plates for the duration of our studies.

3.2.9 Alkaline phosphatase and microcalcifications

Of central importance to our OC+Dex combination is the organic Pi source β-glycerophosphate, which is degraded by the alkaline phosphatase (ALP) enzyme to release free Pi, required for development of mineralisation (Beck et al., 2000). We examined ALP in mineralising MDA-MB-231 cells via enzymatic assay (monitoring chromogenic conversion of para-nitrophenylphosphate to para-nitrophenol) and quantitative polymerase chain reaction (qPCR). Endogenous levels of ALP activity in unstimulated MDA-MB-231 cells (control DMEM media) varied between 135 – 313 mU/mg protein over the 28 day time course (Fig. 3.10 A).

Addition of OC supplementation was observed to slightly depress ALP activity, dropping to a low of 68.5 mU/mg protein at day 7, although this change was not statistically significant. No significant differences were observed in either control or OC treated cells throughout the 28 days, indicating that ALP activity in the MDA-MB-231 cell line remains relatively stable without additional stimulation. In contrast, the addition of dexamethasone promoted a strong induction of ALP activity, which increased continually throughout the time course, reaching a peak of 1004 mU/mg protein at day 28 ($P < 0.0001$). Levels of ALP activity were significantly greater in OC+Dex supplemented media compared to both control and OC groups, at days 14, 21 and 28. In addition, ALP activity of OC+Dex stimulated cells increased in a continuous, time-dependent manner, with higher levels observed at days 21 ($P < 0.05$) and 28 ($P < 0.001$) as compared to the earliest time point of 7 days.

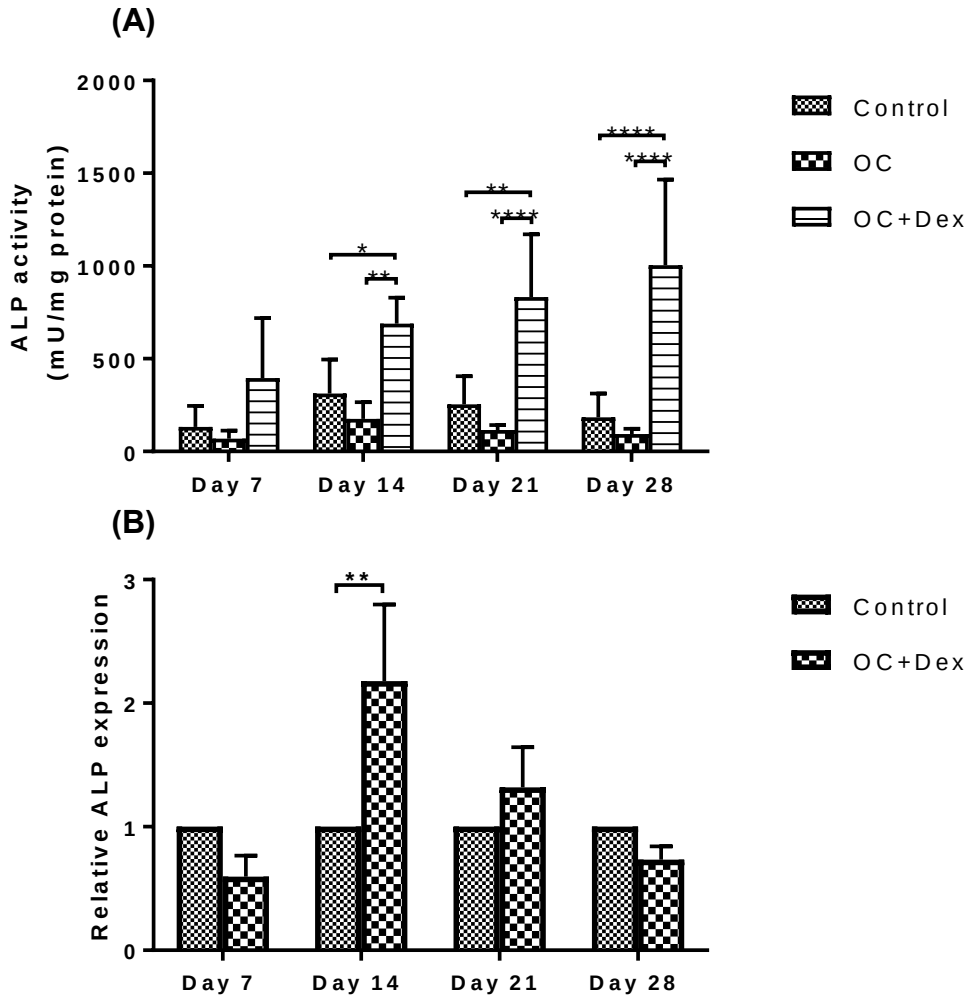

Figure 3.10 Activity and expresson of ALP enzyme in mineralising MDA-MB-231 cells. ALP activity was analysed every 7 days by incubation with the ALP substrate p-nitrophenyl phosphate (PNPP), monitoring absorbance at 405 nm (A). ALP activity was normalised to protein content. Each point represents the mean + SD (n=4). Changes in gene expression were monitored by qPCR (B). Each point represents mean + SD (N=4). Statistical significance was determined by two-way ANOVA. *P<0.05, **P<0.01, **P<0.001, ****P<0.0001.

Analysis of ALP expression by qPCR also revealed significant changes (Fig. 3.10 B), with ALP expression at day 14 increased two-fold in OC+Dex stimulated cells compared to control at the same time ($P < 0.01$). RNA samples were not taken from cells grown in OC media due to lack of positive mineralisation, preventing comparision of the effect of OC+Dex media versus OC alone on ALP expression. Taken together, these results show that dexamethasone acts as a potent ALP inducer, at both a transcriptional and activity level. In contrast, the lack of increased ALP activity in cells treated with OC alone suggests that neither β-glycerophosphate or ascorbic acid acts as an ALP inducer in the absence of dexamethasone.

We next examined ALP activity in two other breast cancer cell lines from our panel, the mineralising SKBR3 and non-mineralising MCF-7 cell lines. In the SKBR3 cell lines, ALP activity of control cells varied between 35.4 and 64.7 mU/mg, with no significant changes observed between any time points (Fig. 3.11 A). Levels were similar in cells grown in OC media (15.8 - 68.5 mU/mg). Some increases were observed in cells grown in OC+Dex media. Unlike dexamethasone stimulated MDA-MB-231 cells, which continually increased ALP activity over the entire 28-day time course, ALP levels of dexamethasone stimulated SKBR3 cells increased only temporarily at day 7 up to 210 mU/mg, which was significantly increased as compared to both control (35.4) and OC (21.4) values at the same time point ($P < 0.01$). ALP levels in OC+Dex stimulated cells was similar to both control and OC groups at all other time points. No significant increases were observed at any time point or treatment group for the non-mineralising MCF-7 cell line (Fig. 3.11 B).

By taking ALP activities of MDA-MB-231, SKBR3 and MCF-7 cells grown in control media over a 28 day time period, we were able to analyse endogenous levels of ALP activity in unstimulated cells (Fig. 3.11 C). Even without the substantial increase of ALP activity induced by OC+Dex, MDA-MB-231 cells grown in standard DMEM media demonstrated a relatively high level of ALP activity, ranging from 40 to 580 mU/mg protein and averaging at 249.7. This was significantly elevated relative to ALP levels of both SKBR3 ($P < 0.05$) and MCF-7 ($P < 0.0001$). Alhough levels of ALP activity in SKBR3 cells were lower than MDA-MB-231, they remained signicantly elevated relative to the non-mineralising MCF-7 cells line (31.98 v 1.77, $P < 0.05$).

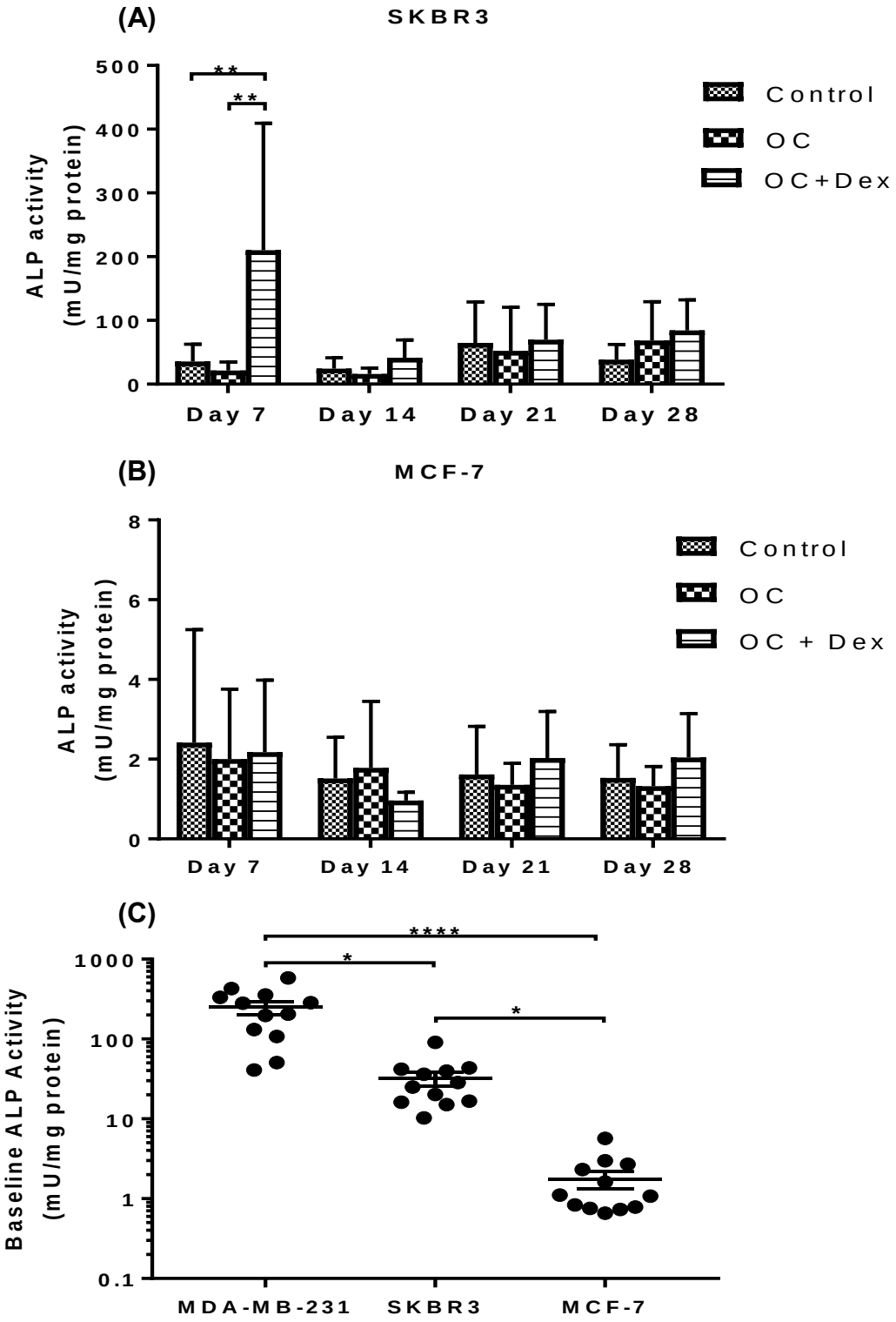

Figure 3.11 Comparison of ALP activity in mineralising and non-mineralising breast cancer cells. ALP activity was analysed in SKBR3 (A) and MCF-7 cells (B) every 7 days by incubation with the ALP substrate p-nitrophenyl phosphate (PNPP), monitoring absorbance at 405 nm. ALP activity was normalised to protein content. Statistical significance was determined by two-way ANOVA (N=3). ALP activity was compared between three cell lines (MDA-MB-231, SKBR3 & MCF-7) by taking all "Control" values througout each time point, for a total of N=12 for each cell line. *P<0.05, **P<0.001, ****P<0.0001.

3.2.10 Exogenous ALP promotes *in vitro* mineralisation in breast cancer cell lines

As the mineralisation capable MDA-MB-231 and SKBR3 cell lines displayed a significantly higher level of ALP activity than the non mineralising MCF-7 cell line, we hypothesised that increased ALP activity is a key difference between mineralising and non-mineralising cell lines. To test this, we cultured MCF-7 cells in OC or OC+Dex media in either the presence or absence of exogenous ALP. Cells were formalin fixed after 7 days and stained with Alizarin Red S. As observed previously, no positive staining was observed in OC or OC+Dex stimulated MCF-7 cells in the absence of ALP, indicating no mineralisation (Fig. 3.12). However, the addition of exogenous ALP promoted a strong mineralisation effect, as evidenced by the significant Alizarin Red S staining by day 7.

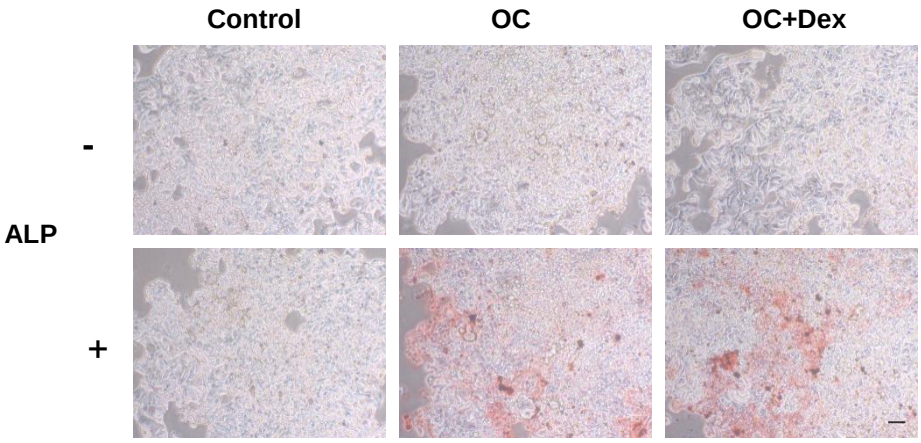

Figure 3.12 Exogenous ALP promotes mineralisation in non-mineralising MCF-7 cells. Representative images (N=2) were captured at 10X magnification of Alizarin Red S stained MCF-7 cells cultured for 7 days in control, OC or OC+Dex supplemented media in either the presence or absence of exogenous ALP (200 mU/mL). Positive Alizarin Red S staining at day 28 indicates a strong mineralisation effect. Scale bar represents 50 µm.

We next examined if addition of exogenous ALP could enhance the ability of MDA-MB-231 cells to produce microcalcifications. Cells were grown in control, OC or OC+Dex media, in either the presence or absence of exogenous ALP. Addition of ALP resulted in significantly darker staining in OC+Dex stimulated cells by day 28 (Fig. 3.13). Exogenous ALP also produced a positive Alizarin Red S staining in OC stimulated cells although this staining appeared more widespread and non-specific than the staining observed in OC+Dex induced mineralisation samples.

Interestingly, although Alizarin Red S staining in cells cultured with both OC+Dex and ALP displayed the same non-specific distribution as cells cultured with OC and ALP, localised deposits of increased intensity staining were also observed against the high background level of staining, similar to the more localised staining observed in OC+Dex induced mineralisation samples. We speculate that this different staining pattern between OC and OC+Dex samples in the presence of exogenous ALP indicates that the dexamethasone in our OC+Dex treatment groups is exerting a pro-mineralisation effect outside of its role in increasing ALP activity, possibly via an increase in expression of bone associated proteins which may act to nucleate calcium-phosphate mineralisation, resulting in the more physiologically relevant and localised staining pattern observed.

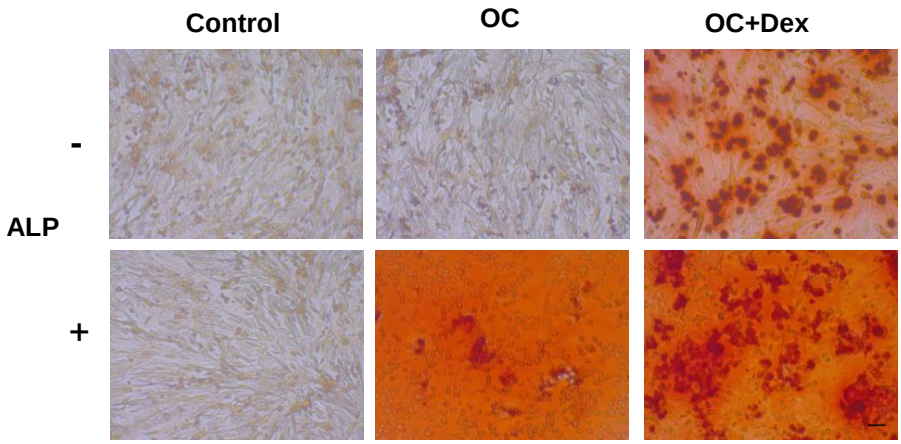

Figure 3.13 Exogenous ALP promotes mineralisation increases MDA-MB-231 mineralisation. Representative images (N=2) were captured at 10X magnification of Alizarin Red S stained MDA-MB-231 cells cultured for 28 days in control, OC or OC+Dex supplemented media in either the presence or absence of exogenous ALP (1U/mL). Positive Alizarin Red S staining at day 28 indicates a strong mineralisation effect. Scale bar represents 50 µm.

Considering the profound effect of exogenous ALP on mineralisation, we next examined whether inhibition of endogenous ALP activity would suppress MDA-MB-231 mineralisation. We found that additon of 100 µM levamisole significantly reduced Alizarin Red S staining in OC+Dex cultured MDA-MB-231 cells (Fig. 3.14). Positive red staining was observed in OC+Dex cultured MDA-MB-231 cells by day 14. However, this was markedly reduced in wells with levamisole. Levamisole did not induce any difference in Alizarin Red S staining in either control or OC cultured cells.

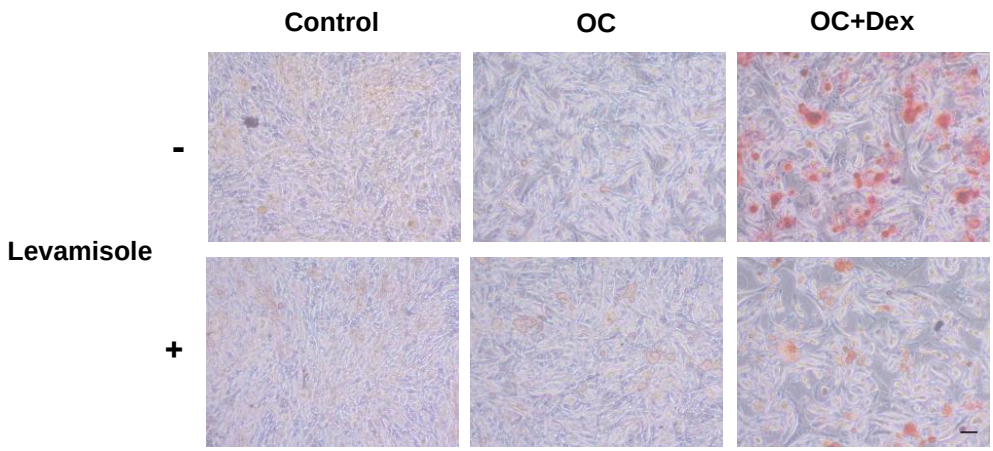

Figure 3.14 Effect of the ALP inhibitor levamisole on MDA-MB-231 mineralisation. Representative images (N=2) were captured at 10X magnification of Alizarin Red S stained MDA-MB-231 cells cultured for 14 days in control, OC or OC+Dex supplemented media in either the presence or absence of 100 µM levamisole. Positive Alizarin Red S staining was observed in OC+Dex cutured cells by day 14, which was reduced by the addition of levamisole. Scale bar represents 50 µm.

3.2.11 Bioinformatic analysis of ALP expression

In order to extend our *in vitro* findings of the importance of ALP activity on breast cancer cell mineralisation to patient data, we utilised a bioinformatics approach. We used Breast Cancer Gene-Expression Miner (Jézéquel et al., 2013), which is capable of pooling expression data from multiple datasets and correlating with clinical attributes, to analyse expression of ALP in breast cancer patients. We first looked at expression of ALP in patients with HER2+ tumours, as this is the molecular subtype most commonly associated with the presence of microcalcificaitons. No significant differences were observed in ALP expression according to HER2 status (Fig. 3.15 A). Comparing patients with triple-negative tumours did reveal a small but significant increase (Fig. 3.15 B). This is in keeping with our findings of high levels of ALP activity in the triple-negative MDA-MB-231 cell line (Fig. 3.10, 3.11). We next looked at expression of ALP in patients with metastatic lesions, as ALP has shown some promise as a marker for metastatic progression (Reale et al., 1995, Du et al., 2014). Using another bioinformatics tool, R2, we analysed expression of ALP by two separate clinical data tracks available within the software, “metastatic indicator” and “infiltrating ductal carcinoma v. metaplastic carcinoma”. Both analyses indicated a higher exppression of ALP in a metaplastic context (Fig 3.15 C,D).

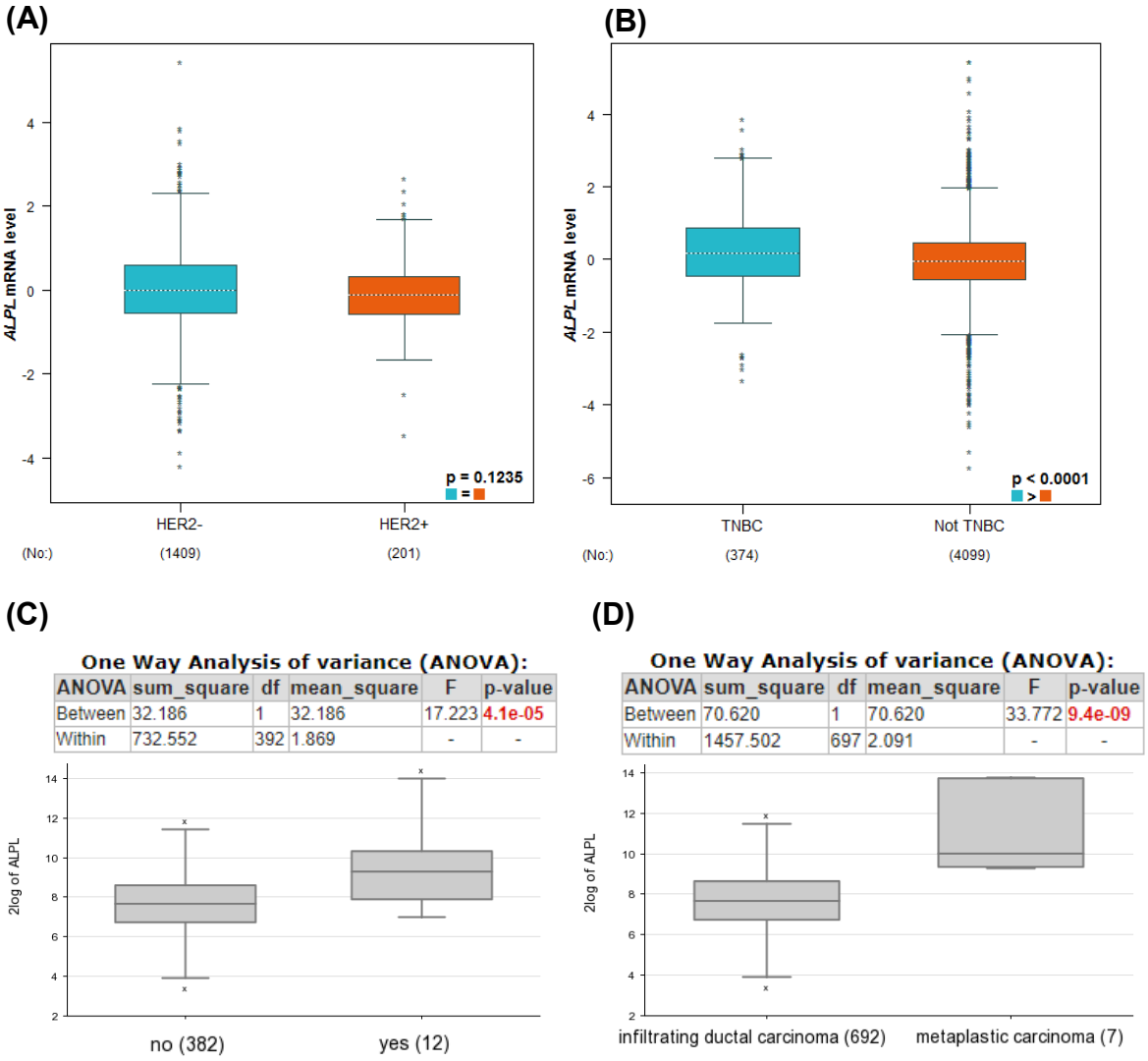

Figure 3.15 Bioinformatic analysis of ALP expression. Breast Cancer Gene-Expression Miner was used to compare levels of ALP expression in patients with and without HER2 amplification (A) and patients with or without triple-negative tumours (B**).** The R2 bioinformatics tool was used to analyse differential ALP expression in metastatic tumours (C,D). Reported P-values were computed by the online site.

3.2.12 Inorganic Pi and breast cancer cell mineralisation

In studies of both physiological and pathological mineralisation, ALP promotes calcium deposition by degrading the mineralisation inhibitor PPi and releasing free Pi, simultaneously reducing the levels of anti-calcification factors and increasing levels of pro-calcification factors. A recent study demonstrated a modified *in vitro* model of breast cancer calcification, utilising inorganic Pi instead of the organic β-glycerophosphate used in our model (Dang et al., 2017). To test the efficacy of free, inorganic- Pi in our model we cultured MDA-MB-231 cells with 50 µg/mL ascorbic acid and 10 mM sodium phosphate, both with and without dexamethasone.

Positive staining by both Alizarin Red S (Fig. 3.16 A) and von Kossa (Fig. 3.16 B) was observed beginning at day 7, increasing in intensity by day 14. Staining also appeared greater in cells cultured with both Pi and dexamethasone.

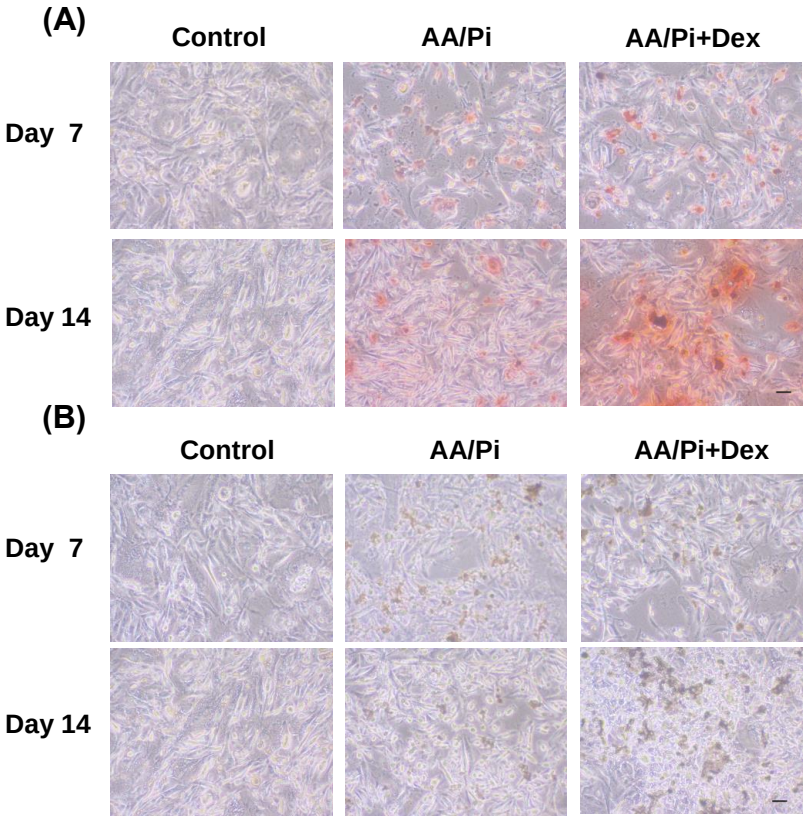

Figure 3.16 Inorganic Pi induced mineralisation of MDA-MB-231 cells. Representative images (N=2) were captured at 10X magnification of MDA-MB-231 cells cultured in control media, media supplemented with 50 µg/mL ascorbic acid and 10mM sodium phosphate (AA/Pi) or ascorbic acid, sodium phosphate and 100 nM dexamethasone (AA/Pi+Dex). Cells were fixed at days 7 and 14 and stained with Alizarin Red S (A) or von Kossa (B). Positve staining was observed for both AA/Pi and AA/Pi+Dex at both days 7 and 14, with AA/Pi+Dex cultured cells displaying more intense staining. Scale bar represents 50 µm.

Analysis of ALP activity of MDA-MB-231 cells cultured under inorganic Pi conditions revealed significant alterations, both between control and Pi stimulated samples, and between inorganic and organic Pi sources (Fig. 3.17). ALP activity of MDA-MB-231 cultured with AA/Pi+Dex rose five-fold compared to control samples at day 7 ($P < 0.01$). This increase appeared to be transient, as ALP activity in AA/Pi+Dex stimulated cells fell to 1.7 fold of control samples by day 14. This was a significant contrast to results of ALP assays carried out in cells cultured in calcification-promoting media with organic β-glycerophosphate, where ALP activity continually rose throughout the time course (Fig. 3.10).

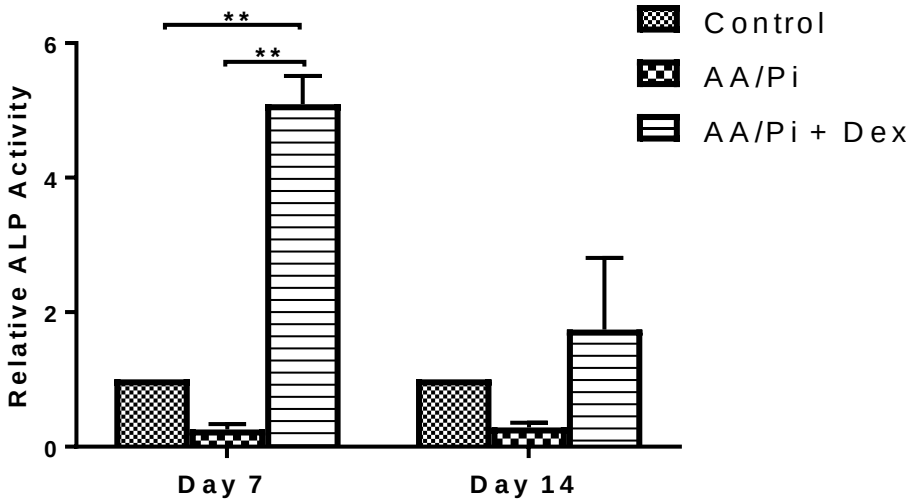

Figure 3.17 ALP activity of MDA-MB-231 cells under inorganic phosphate conditions. MDA-MB-231 cells were cultured in control media, media supplemented with 50 µg/mL ascorbic acid and 10 mM sodium phosphate (AA/Pi) or ascorbic acid, phosphate and 100 nM dexamethasone (AA/Pi+Dex). ALP activity was analysed at 7 and 14 days by incubation with the ALP substrate p-nitrophenyl phosphate (PNPP), monitoring absorbance at 405 nm. ALP activity was normalised to protein content, and expressed relative to control samples. Statistical significance was determined by two-way ANOVA (N = 2). **P<0.01

ALP results from SKBR3 cells cultured with inorganic Pi were largely the same as those from MDA-MB-231 cells. AA/Pi+Dex induced a significant increase in ALP activity in comparison to both control (3.15 fold, P < 0.0001) and AA/Pi (5.25 fold, P < 0.0001) stimulated cells at day 7, before dropping significantly. By day 14, ALP values were significantly lower in both AA/Pi and AA/Pi+Dex groups than control samples (~80% reduction, P < 0.001).

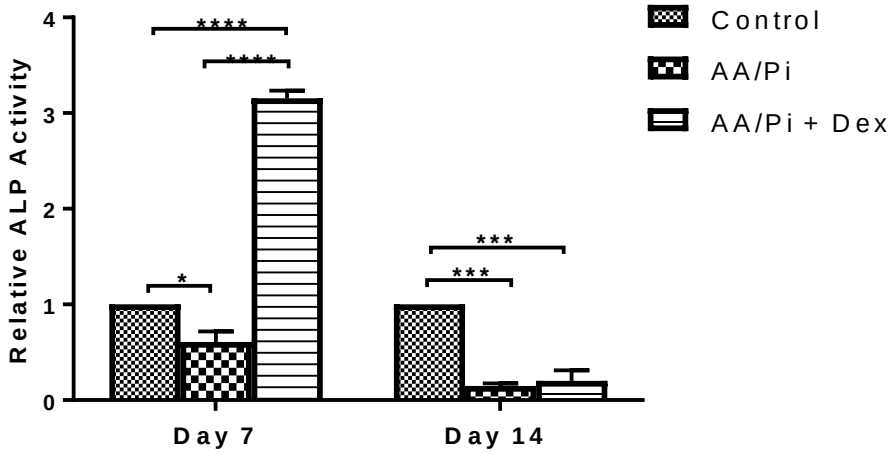

Figure 3.18 ALP activity of SKBR3 cells under inorganic phosphate conditions. SKBR3 cells were cultured in control media, media supplemented with 50 µg/mL ascorbic acid and 10 mM sodium phosphate (AA/Pi) or ascorbic acid, phosphate and 100 nM dexamethasone (AA/Pi+Dex). ALP activity was analysed at 7 and 14 days by incubation with the ALP substrate p-nitrophenyl phosphate (PNPP), monitoring absorbance at 405 nm. ALP activity was normalised to protein content, and expressed relative to control samples. Statistical significance was determined by two-way ANOVA (N = 2). *P<0.05, ***P<0.001, ****P<0.0001.

We finally investigated the mineralisation potential of MCF-7 cells in the presence of inorganic Pi. These cells had previously been found incapable of forming mineralisations in the presence of the organic phosphate source β-glycerophosphate (Fig. 3.2). In contrast to results observed under organic phosphate conditions, inorganic Pi sucessfully induced mineralisation in the MCF-7 cell line (Fig. 3.19). Positive Alizarin Red S staning was observed at days 7 and 14, in cells cultured in in both AA/Pi and AA/Pi+Dex.

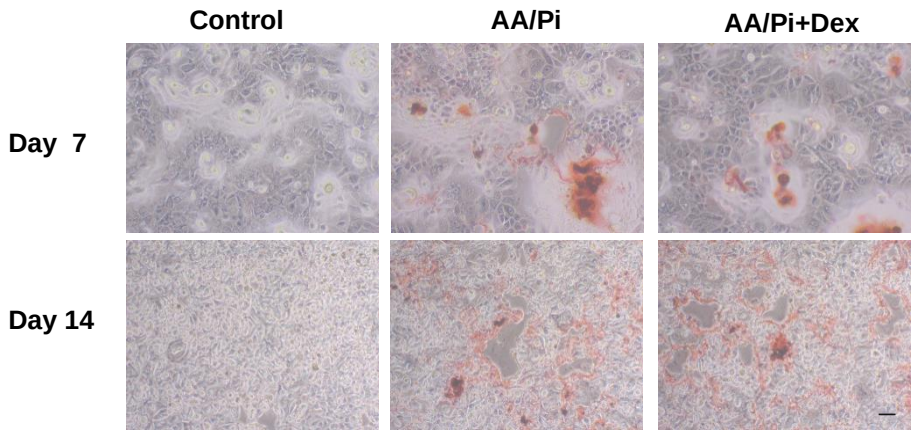

Figure 3.19 Inorganic Pi induced mineralisation of MCF-7 cells. Representative images (N=3) were captured at 10X magnification of MCF-7 cells cultured in control media, media supplemented with 50 µg/mL ascorbic acid and 10mM sodium phosphate (AA/Pi) or ascorbic acid, sodium phosphate and 100 nM dexamethasone (AA/Pi+Dex). Cells were fixed at days 7 and 14 and stained with Alizarin Red S. Positve staining was observed for both AA/Pi and AA/Pi+Dex at both days 7 and 14. Scale bar represents 50 µm.

3.3 Discussion

In addition to their routine use as mammographic indicators of possible breast cancer, microcalcifications have also shown significant promise as predictive and prognostic factors (Tabár et al., 2000, Tabar et al., 2004). Despite significant improvements in our understanding of microcalcification formation in recent years, many questions remain unanswered. Previous work from our lab has highlighted the role of an active, regulated cellular process with many similarities to physiological mineralisation in the formation of microcalcifications (Cox et al., 2012a, Cox et al., 2012b).

To date, the number of cell lines investigated for mineralisation potential is relatively small. In addition, much of the previous work from our lab has focused on the murine 4T1 cell line. Although results from this cell line yielded many key insights into the molecular mechanisms underlying formation of microcalcifications, we felt that the clinical relevance of our work would be improved by expansion of the model to include a variety of human derived cell lines. In particular, we sought a comprehensive analysis of the mineralisation potential of different subtypes of human breast cancer cells, which had not previously been carried out. The aim of this first chapter was to build on our previous findings by investigating a panel of human breast cancer cell lines representative of all major molecular subtypes, identify suitable cell lines for further study, develop a reliable and effective *in vitro* model of microcalcification formation and begin to probe the mechanisms responsible for calcium deposition. Our panel of cell lines was chosen to provide a broad representation of the highly heterogeneous makeup of breast cancer, with all major molecular subtypes included. The protocol that we used to induce mineralisation consists of prolonged incubation with ascorbic acid, β-glycerophosphate as a source of Pi and the synthetic glucocorticoid dexamethasone. These reagents are routinely used in studies of osteoblast mineralisation (Langenbach and Handschel, 2013) and were also shown in previous work from our lab to constitute an effective model of mineral deposition in breast cancer cell lines.

In keeping with previous work from this group (Cox et al., 2012a), we found the ability to mineralise *in vitro* to be highly dependent on the individual cell line with only two cell lines found to be capable of *in vitro* mineralisation.

Positive deposition of calcium was observed in both the HER2+ SKBR3 and the triple negative MDA-MB-231 cell lines, but not for any other tested cell line. Positive mineralisation was first observed in the SKBR3 cell by day 14 in both Alizarin Red S (Fig. 3.5 A) and von Kossa (Fig. 3.6 B) stained cells. The specific formulation of Alizarin used in our studies (2%, pH 4.4) has previously been optimised for hydroxyapatite staining (Shoji, 1993), the same calcium phosphate crystals found in type II calcifications, often associated with malignant disease. On the other hand, calcium oxalate (the principal component of benign type calcifications) will only stain with Alizarin at a pH of 7 (Proia and Brinn, 1985). This differential staining pattern indicates that the calcified deposits produced in our studies most likely consist of the clinically relevant calcium phosphate species hydroxyapatite. Further characterisation of our *in vitro* samples using Raman spectroscopy to confirm the presences of hydroxyapatite will be discussed in a later chapter (Fig. 5.22). Mineralisation was also confirmed via OCP assay (Fig. 3.5 C).

In contrast to MDA-MB-231 cells which required both OC and Dex, SKBR3 cells produced mineralisations in both OC and OC+Dex supplemented media. SKBR3 cells represent the HER2 subtype of breast cancer most commonly associated with the appearance of microcalcifications (Elias et al., 2014). Therefore, the ability to mineralise without Dex may reflect a greater innate inability to produce mineralisations than the MDA-MB-231 cell line which requires additional stimulation to begin the process of mineralisation.

Interestingly, we did not see positive results in either the HER2+ HCC1954 cell line (Fig. 3.6) or a HER2 overexpressing strain of the luminal MCF-7 cell line (Fig. 3.3). These results were intriguing as a large body of literature has shown a strong association between the presence of microcalcifications on mammography scans and HER2 overexpression. A recent microarray analysis found the *ERBB2* gene to be amongst the most differentially expressed between patients with highly suspicious calcifications versus those without (Shin et al., 2017). In addition, a meta-analysis encompassing a total of 17,745 breast cancers found that the presence of calcifications carried a pooled odds ratio of HER2 overexpression of 3.14, regardless of whether the detected calcification was found with or without an associated mass (Elias et al., 2014).

Calcification morphology may also be predictive of HER2 status. In one study, patients with calcifications of a suspicious morphology (pleomorphic, fine linear or branching) were 2.5 fold more likely to display HER2 overexpression than patients with more benign calcifications (amorphous, coarse heterogeneous) (Cen et al., 2017a). Although we did identify one HER2 overexpressing cell line capable of producing calcifications, it is unclear why the two other cell lines did not respond in a similar manner. Naseem et al. found microcalcifications in approximately 50% of HER2+ patients (Naseem et al., 2015). A similar figure of 56% was reported by Seo et al. (Seo et al., 2006). These results indicate that although there is a strong tendency for HER2+ tumours to exhibit calcifications, it is not a universal trait. It is likely that although HER2 may be contributing to the promotion of calcification, its expression is not sufficient by itself. This is evidenced by the lack of calcification in two HER2 expressing cell lines in our panel and by up to 50% of patients with HER2+ tumours. It is of interest that the SKBR3 cell line has a higher HER2 expression level than both the HCC1954 (Bashari et al., 2016, Conley et al., 2016) and HER2-MCF-7 (Pegram et al., 1997) cell lines, potentially explaining why it alone of all tested HER2+ cell lines was capable of *in vitro* mineralisation.

In addition to SKBR3, we also observed positive mineralisation in the MDA-MB-231 cell line. The MDA-MB-231 cell line is representative of the triple negative subtype, which are not commonly associated with the mammographic appearance of microcalcifications (Yang et al., 2008). When cultured with a combination of OC and dexamethasone, MDA-MB-231 cells produced calcified deposits, visible by day 14 (Fig 3.7). Positive red staining was observed in Alizarin Red S stained samples indicated a positive result for calcium rich deposits (Fig 3.7 A). Deposits of calcium was confirmed using the quantitative OCP calcium assay which detected statistically significant differences in calcium normalised to protein by day 21 onwards (Fig. 3.7 C). At its peak on day 21, calcium levels were increased 27-fold in OC+Dex treated cells compared with cells grown with control media ($P < 0.001$).

The finding of a positive mineralisation result in MDA-MB-231 (Fig. 3.7) cells was somewhat unexpected as these cells are known to form osteolytic lesions following bone metastasis (Gregory et al., 2013). Under normal physiological conditions, bone remodelling is controlled by a careful balance between osteoclastic bone resorption and osteoblastic bone formation (Rucci, 2008).

Establishment of metastatic lesions within the bone results in a dysregulation of this balance and leads to either the formation of osteolytic lesions and a loss of bone strength, or osteoblastic lesions associated with abnormal calcium deposition. Formation of these lesions causes the release of sequestered growth factors and stimulation of further tumour growth (Mundy, 2002). MDA-MB-231 cells are generally regarded as osteolytic lesion forming, as conditioned media derived from these cells promotes osteoblast apoptosis (Mastro et al., 2004), alters their differentiation and mineralisation capability (Barnes et al., 2004) and induces an inflammatory response (Kinder et al., 2008), all of which leads to a substantial alteration of normal bone remodelling.

A possible explanation for the formation of calcifications by a cancer cell line known for inducing bone loss may lie in the different microenvironment between a localised breast tumour with associated microcalcifications and an advanced bone metastatic lesion. In metastatic lesions, breast cancer cells exert much of their osteolytic activity indirectly by targeting local osteoclasts and osteoblasts (Gregory et al., 2013, Tiedemann et al., 2009), whereas in our model it is the cells themselves that are directly responsible for the formation of mineralisations. It is possible that a difference between indirect and direct effects of MDA-MB-231 cells may explain the different effect on mineralisation between the two settings.

Calcifications are relatively rare in triple-negative tumours. Yang et al. reported calcifications in only 15% of patients with triple negative tumours, suggesting that the low rate of ductal-carcinoma in situ (DCIS) observed amongst these patients may explain the relative rarity of calcification associated triple negative tumours (Yang et al., 2008). Many breast tumours start as small localised lesions known as DCIS that may progress to invasive tumours over time (Ben-Aharon et al., 2013). The molecular subtype of tumour strongly influences both the likelihood of progression to invasive disease and the speed at which this takes place, with several studies suggesting that triple negative tumours may progress at a significantly faster rate than average (Badve et al., 2011, Gorringe and Fox, 2017). In contrast, HER2+ tumours progress relatively slowly. In a direct comparison of the two tumour types, one study concluded that the speed of progression could be up to three times greater in triple negative tumours than HER2+ tumours (Perez et al., 2013).

As microcalcifications are strongly associated with the presence of DCIS (Hofvind et al., 2011), the significant differences in time spent at a DCIS stage between HER2+ and triple negative tumours may explain the different rates of associated microcalcifications observed between these two tumour types.

In addition, although MDA-MB-231 cells may seem unlikely to form calcifications based on their triple negative status, they do possess a number of other cellular characteristics that have been associated with the presence of microcalcifications in patient studies, including high vimentin expression and mesenchymal characteristics (Scimeca et al., 2014) and expression of Ca^{2+} channels TRPM7 (Mandavilli et al., 2013) and SPCA (Dang et al., 2017). This is supported by findings both from our work (Chapter 5) and others (Wilson et al., 2014) that MDA-MB-231 form microcalcifications *in vivo* following subcutaneous injection. The fact that MDA-MB-231 cells can mineralise in an *in vivo* setting without addition of any additional reagent highlights their suitability for usage in our studies.

We also investigated several ER+ luminal cell lines, including MCF-7 and ZR-75-1. Both of these cell lines tested negative for mineralisation potential. Identification of tumour receptor status is important in determining the most appropriate treatment strategy (Dunnwald et al., 2007). Although microcalcifications have a clear benefit in identifying HER2 overexpressing tumours (Naseem et al., 2015), their effectiveness in diagnosing ER and PR status is unclear, with several studies disagreeing on the association between calcifications and hormone receptor status (Killelea et al., 2013a, Gajdos et al., 2002, Griniatsos et al., 1995, Karamouzis et al., 2002, Naseem et al., 2015).

In a recent study Dang et al. observed positive mineralisation in MCF-7 cells, in contrast to our own findings (Dang et al., 2017). This discrepancy is explained by the modified version of our protocol utilised in their study, in which β-glycerophosphate was substituted with inorganic Pi. Usage of inorganic Pi results in an ALP independent mechanism of mineralisation, as the Pi necessary for calcium deposition is readily available to the cells without requiring ALP mediated degradation of β-glycerophosphate. We found similar results when we tested MCF-7 cells with both inorganic Pi (Fig. 3.19) or β-glycerophosphate with added exogenous ALP (Fig. 3.12).

In models of both physiological and pathological mineralisation, ALP plays a two-fold role in the induction of mineralisation. Degradation of PPi to free Pi results in both a reduction in an anti-mineralisation agent and an increase in an important pro-mineralisation factor, tipping the balance in favour of calcium deposition. Several studies have suggested that removal of inhibitory PPi may be of greater importance than the release of free Pi (O'Neill, 2006). Mice with a knockout mutation in the alkaline phosphatase 2 (*Akp2*) gene exhibit impaired skeletal mineralisation. Crossing *Akp2*$^{-/-}$ mice deficient in either *Enpp1 or Ank* results in a normalisation of extracellular PPi levels and mineralisation potential (Hessle et al., 2002, Harmey et al., 2004).

Although these findings indicate that MCF-7 cells may mineralise under appropriate conditions, we elected to utilise cells that were shown to be capable of mineralising under the influence of β-glycerophosphate for the remainder of our work. Utilising an organic source of Pi that requires ALP mediated degradation mimics the requirement of PPi degradation to yield positive mineralisation results and may result in a more selective mechanism of mineral deposition and a more physiologically relevant model. In addition, preliminary results from a Raman spectroscopy analysis suggest that the deposits formed by cells cultured in the organic β-glycerophosphate may be more representative of the microcalcifications found in breast cancer patient than those formed under the influence of inorganic Pi (data not shown).

The requirement for activation of ALP activity partially explains the cell line specific results observed in this chapter as levels ALP activity were significantly higher in the mineralising MDA-MB-231 and SKBR3 cell lines than the non-mineralising MCF-7 (Fig. 3.11). Similar results were found in a previous study, where ALP activity of mineralising 4T1 cells was significantly higher than the non-tumourigenic (and non-mineralising) MCF10A (Cox et al., 2012a). In addition to possessing naturally greater levels of ALP activity, both MDA-MB-231 and SKBR3 cells significantly increased ALP levels in OC+Dex media, indicating a greater ability of these cell lines to respond and adapt to mineralisation promoting conditions (Fig. 3.10, 3.11).

Interestingly, although both mineralising cell lines displayed alterations to ALP activity following incubation with mineralisation promoting media, there was some notable differences between the two cell lines.

ALP activity of MDA-MB-231 cells was highly responsive to dexamethasone, with significant increases observed from day 14 onwards as compared to control or OC media (Fig. 3.11). At day 7, OC+Dex treated cells displayed a 3-fold increase compared to control values. This augmentation of ALP activity increased over time, with the difference between control and OC+Dex values rising to a 6-fold difference by day 28. In contrast, ALP activity seemed less affected by the presence of OC or OC+Dex containing media in the SKBR3 cell line, as an approximate 6-fold increase was observed, but only at one-time point (day 7) in the OC+Dex group (Fig. 3.11 A). Interestingly, although MDA-MB-231 cells tended to possess a higher level of ALP activity compared to SKBR3 (249.7 v 31.98 mU/mg protein, $P < 0.05$), they were unable to mineralise in the absence of dexamethasone, unlike SKBR3, which mineralised in both the presence and absence of dexamethasone (although to a greater extent when dexamethasone was included).

If formation of microcalcifications were a simple function of cellular ALP activity, we would expect MDA-MB-231 cells to mineralise under both OC and OC+Dex conditions, similar to SKBR3. This highlights that a certain level of ALP activity is essential to mineralisation under conditions of organic Pi but this is not the sole determinant of which cell lines will successfully mineralise. Formation of microcalcifications is likely to involve a coordinated expression of bone associated proteins and the activation of ALP activity. This is evidenced by several papers that have noted increased levels of certain bone proteins in breast tumours, in particular those tumours presenting with calcifications. Bellachène et al. found high expression of bone sialoprotein, osteonectin and osteopontin in breast tumours with associated calcifications (Bellahcène and Castronovo, 1995, Bellahcène et al., 1994). Scimeca et al. found similar increases in osteopontin as well as bone morphogenetic protein 2 (Scimeca et al., 2014).

Another possible explanation of the dexamethasone-dependent mineralisation in MDA-MB-231 cells may lie in the cells expression of the enzyme ectonucleotide pyrophosphatase/phosphodiesterase 1 (ENPP1). As previously discussed, a balance between extracellular Pi and PPi regulates mineral deposition *in vivo* (Sapir-Koren and Livshits, 2011). ENPP1 is one of the key players in regulation of this balance via its role in degrading extracellular nucleotide triphosphates (most notably ATP) to yield the inhibitory PPi.

MDA-MB-231 cells have previously been shown to express a significantly higher level of ENPP1 than both MCF-7 and SKBR3 cells (Lau et al., 2013). The potential role of PPi and ENPP1 in our model will be explored in the next chapter.

The importance of ALP activity in the formation of microcalcifications was further shown by the significant decrease in positive Alizarin Red S staining in mineralising MDA-MB-231 cells treated with the ALP inhibitor levamisole (Fig. 3.14), and in the successful mineralisation results observed in MCF-7 cells when cultured with exogenous ALP (Fig. 3.12). Within the context of breast cancer, ALP has been shown to be a useful marker for a number of important clinical factors. Most notably, ALP may function as a marker of metastatic disease, with patients with bone metastases displaying significantly increased serum ALP levels (Reale et al., 1995, Singh et al., 2013, Ramaswamy et al., 2000). A recent meta-analysis showed a two-fold increase in serum levels of a skeletal-specific isoform of ALP in patients with osseous metastases versus patients with other forms of metastatic lesion (Du et al., 2014). Serum ALP levels are also predictive of bone metastasis in prostate cancer (Koo et al., 2015), a cancer with similar rate of bone metastases as breast cancer (Kakhki et al., 2013). Increased serum ALP is associated with dense breast tissue (Kim et al., 2015a), a known risk factor for developing breast cancer. Dense breast tissue has also been shown in some studies to display higher rates of calcification (Naseem et al., 2015, Skandalis et al., 2011). When combined with two other commonly used clinical lab measurements (haemoglobin and international normalized ratio) into a prognostic model, serum ALP levels were recently shown to predict patients with an increased risk of recurrence (Zhu et al., 2017). Similar results were reported previously by Keshaviah et al. who showed ALP levels to effectively predict tumour recurrence when combined with the cancer antigen Ca^{2+} 15-3 (Keshaviah et al., 2007). Finally, ALP may function as a prognostic marker in triple-negative breast cancer (Chen et al., 2016) and in patients undergoing surgery for metastatic breast cancer (Yoo et al., 2017). These associations are supported by our findings of high ALP activity in the triple-negative, metastatic MDA-MB-231 cell line (Fig. 3.11), and by bioinformatics analysis showing increased ALP expression in triple-negative tumours (Fig. 3.15 B) and metastatic tumours (Fig. 3.15 C, D).

In addition to demonstrating the MDA-MB-231 cell line as a suitable model system for the formation of microcalcifications, we also wanted to optimise some key characteristics of our cell culture environment to ensure optimal conditions for mineralisation. We first looked at the effect of glucose concentration on mammary calcification due to the pro-mineralisation effect high-glucose has been observed to exert on other forms of pathological soft-tissue calcification. In our studies, elevated glucose levels were observed to delay the onset of calcium deposition, with no positive staining observed in Alizarin Red S stained samples (Fig 3.8 B) until day 21 in comparison to MDA-MB-231 cells cultured in low-glucose media, which displayed positive staining by day 14.

The precise influence of glucose concentration on mineralisation is still not fully understood. In human alveolar bone-derived cells, high glucose concentrations upregulated expression of several genes associated with mineralisation including bone sialoprotein (BSP), osteocalcin (OCN) and Runx2 and increased deposited calcium (Garcia-Hernandez et al., 2012). Other studies have also demonstrated increased calcification under high glucose conditions (Li et al., 2007, Inagaki et al., 2010). For example, high glucose levels increased expression of the osteoblast transcription factor RUNX2, osteocalcin and BMP2 and enhanced calcification in bovine vascular smooth muscle cells (Chen et al., 2006a). However, other groups have found a decrease in mineralisation in response to elevated glucose (Balint et al., 2001, Zhen et al., 2010). Many of these studies on the effect of glucose concentration on mineralisation have utilised a variety of cell sources, which may help explain the apparent contradiction within their results as well as highlight the complexity and species specificity of cellular response to altered glucose levels.

We also investigated if coating tissue culture plates with a thin layer of collagen could further support the development of calcifications *in vitro*. No effect was observed on either calcium deposition (Fig. 3.9 A), or ALP activity (Fig. 3.9 B). Previous work from our lab also analysed any potential alteration in the development of microcalcifications by a collagen rich environment, by seeding 4T1 cells onto a 3D scaffold of collagen-glycosaminoglycan (Cox et al., 2012b), a model previously developed for bone tissue engineering research. Although positive mineralisation results were observed in these scaffolds, positive staining in a 3D environment was first observed at day 14, in comparison to day 11 when cells were grown as a monolayer.

However, this apparent delay in mineralisation may simply represent the time taken for cells seeded on the exterior of the scaffold to infiltrate within the structure, prior to commencement of mineral deposition. Matthews et al. observed significantly increased differentiation of both primary rat osteoblasts and MC3T3-E1 cells when grown in a 3D collagen gel (Matthews et al., 2014). Interestingly, this effect was not observed when cells were grown on collagen coated plates, suggesting that the 3D structure of a collagen network is essential for its pro-osteogenic effect. The coating procedure used in our study resulted in a thin, 2-dimensional layer of collagen, indicating that our findings of no significant effect on cellular mineralisation are in agreement with the work of Matthews et al. Previous studies on mammary calcification utilised 3D models and only used histological stains to confirm the presence of mineralisations within the scaffold, and did not use any quantitative measurements to assess any potential pro-osteogenic effect of growing within a collagen-enriched environment. As such, this study is the first to directly measure the effect of collagen coating on the *in vivo* development of microcalcifications. Due to the lack of significant changes, we elected to carry out the remainder of our studies using standard tissue-culture plates, without any additional coating.

Our studies have identified two additional mineralisation-capable cell lines, in addition to the three identified in previous studies; 4T1, 4T1.2 and Hs578Ts(i)8 (Cox et al., 2012a). So far, the majority of cell lines identified as mineralisation-capable are highly aggressive and tumourigenic. In a comprehensive analysis of the invasiveness and migratory capability of a panel of commonly used breast cancer cell lines, Zajchowski et al. classified MCF-7, SKBR3, ZR-75-1 as “weakly invasive” whilst MDA-MB-231 was found to be one of the most invasive (Zajchowski et al., 2001). The possible link between malignancy and the ability to mineralise *in vitro* is further evidenced by the fact that whilst the parental Hs578T was not capable of mineralising, the more invasive sub-clone Hs578Ts(i)8, generated through sequential passages through a Matrigel invasion chamber (Hughes et al., 2008) was successful in mineralising (Cox et al., 2012a).

Another property common to many mineralisation capable cell lines is their gene expression profile, which tends to be more mesenchymal/basal than non-mineralising cells. MDA-MB-231, Hs578Ts(i)8 and 4T1 have all been classed as either basal or claudin low (Holliday and Speirs, 2011). The mesenchymal-like phenotype of most mineralisation capable cells is interesting in light of the fact that

mesenchymal stem cells are capable of undergoing osteogenic differentiation when cultured in similar conditioned to those used in our studies (Birmingham et al., 2012). Other groups have also highlighted links between the presence of microcalcifications and a mesenchymal phenotype. Scimeca et al detected increased expression of the mesenchymal marker vimentin in patient samples with associated calcifications compared those without (Scimeca et al., 2014) and hypothesised that under certain conditions, breast cancer cells may be capable of acquiring mesenchymal properties and differentiating towards an osteoblast-like phenotype capable of mineralising.

3.4 Summary and conclusions

In the first phase of this thesis, we have achieved many of our short term goals, including identification of two novel mineralising breast cancer cell line and characterisation of their mineralisation characteristics, such as time of calcification, levels of deposited calcium and necessary conditions. This was done by a comprehensive analysis of a panel of human breast cancer cell lines, representative of all major molecular subtypes. These studies involved prolonged periods of up to 28 days under osteogenic conditions although mineralisation was often evident earlier. This is the first time such an analysis of human cell lines has been carried out and, to the best of our knowledge, the first identification of a HER2+ cell line capable of mineralisation.

The similarities in media requirements for successful mineralisation to those utilised in *in vitro* studies of osteoblasts, mesenchymal stem cells and other cell types capable of undergoing osteogenic differentiation are in agreement with previous work from our lab, and highlight the importance of an active and regulated cellular process underlying the formation of microcalcifications.

This concept of a link between a cellular mediated process and the development of calcifications is further underlined by our findings of the crucial nature of alkaline phosphatase activity, and by results from other groups demonstrating upregulation of various bone associated proteins, Ca^{2+} regulating channels and other known mediators of physiological mineralisation. Many of these other key players will be explored in the subsequent chapters.

In conclusion, our main findings from this chapter are as follows;

- Following a characterisation study of a representative panel of human breast cancer cell lines, two additional cell lines were added to the list of identified mineralisation-capable cell lines. The HER2+ SKBR3 and triple-negative MDA-MB-231 cell lines form calcified deposits when cultured with the appropriate agents.
- HER2 expression may be linked to development of calcifications but is not sufficient by itself to induce *in vitro* mineralisation.
- Alkaline phosphatase activity is essential to development of calcifications although is not the sole determining factor.
- Cell lines incapable of mineralising in the presence of β-glycerophosphate can be induced to form calcifications when cultured with inorganic Pi or exogenously added ALP.

Chapter 4.0

Microcalcifications as a result of loss of endogenous mineralisation inhibitors and alteration of Ca^{2+} transport pathways

4.1 Introduction

After establishing an effective, reproducible model of microcalcification formation in a human breast cancer cell line, we next sought to examine any potential links between the formation of microcalcifications in breast cancer and known mediators of physiological mineralisation. Previous work from our lab demonstrated the formation of microcalcifications in a murine breast cancer cell line to result from an active, regulated process (Cox et al., 2012a, Cox et al., 2012b). Results from the previous chapter support this hypothesis, in particular highlighting the importance of the ALP enzyme, suggesting that a similar mechanism is likely to be involved in our human derived cell model. Physiological mineralisation is a highly complex process and occurs as the result of a carefully orchestrated programme, with contributions from a large number of effector proteins, regulatory factors, homeostatic pathways and feedback loops.

4.1.1 Mineralisation associated proteins and breast cancer

Interestingly, many of the key players in physiological mineralisation are also found in close proximity to calcified deposits in a variety of pathological mineralisation diseases, suggesting a common pathway (Kirsch, 2006, Dhore et al., 2001). Breast microcalcifications display a similar pattern, with many studies highlighting strong expression of bone associated proteins such as BMP2, osteonectin, osteopontin, and bone sialoprotein in the vicinity of mammary microcalcifications (Bellahcène and Castronovo, 1995, Bellahcène et al., 1994, Scimeca et al., 2014, Oyama et al., 2002).

Although there seems to be significant evidence of an association between the expression of various bone associated proteins and the presence of mammary microcalcifications, an examination of any potential functional roles in calcification formation remains mostly unexplored. A few key players have been studied, perhaps most significantly, the role of ALP, with results from both the previous chapter in this thesis and earlier studies (Cox et al., 2012a, Cox et al., 2012b) showing a vital role for the ALP enzyme within our *in vitro* model. In addition, previous results from both our group and others show increased calcification in cells stimulated with recombinant BMP2 (Cox et al., 2012b, Dang et al., 2017).

Outside the context of microcalcifications, many of the key bone-associated proteins highlighted in these studies have been implicated in breast cancer. For instance, the mineralisation inhibitor matrix gla protein (MGP) which inhibits the development of vascular calcification by multiple mechanisms, including attenuation of BMP2-mediated osteogenic signalling and direct inhibition of calcium crystal growth (Proudfoot and Shanahan, 2006) may also be significant in breast cancer, as high MGP expression is associated with increased relapse-free survival (RFS) in luminal breast cancer patients (Tuo and Ye, 2017) and repression of MGP in MCF-7 breast cancer cells via miR-155 results in increased proliferation and invasion (Tiago et al., 2016).

Another important factor in both osteogenesis and breast cancer is the runt-related transcription factor 2 (RUNX2) which acts as a master transcription factor for osteogenic differentiation in osteoblasts, mesenchymal stem cells and vascular smooth muscle cells (Vimalraj et al., 2015, Bruderer et al., 2014). RUNX2 expression is increased in breast tumours compared to normal breast tissue and is particularly highly expressed in aggressive, invasive cell lines (Chang et al., 2014). Knockdown of RUNX2 in MDA-MB-231 cells significantly reduces expression of MMP2, MMP13, and vascular endothelial growth factor (VEGF), resulting in decreased invasive ability (Pratap et al., 2005).

4.1.2 Calcium/Magnesium balance

In addition to the important regulatory role played by protein inducers/inhibitors, development of calcifications is also strongly influenced by the local concentration of Pi and Ca^{2+}, which precipitate under appropriate conditions to form calcium phosphate mineral deposits, most notably hydroxyapatite. In our *in vitro* studies, β-glycerophosphate acts as an organic Pi donor following degradation by the ALP enzyme. As discussed in the previous chapter, the pro-mineralisation activity of Pi ions is counteracted by a careful balance of PPi.

In contrast to Pi, which requires supplementation to reach concentrations conducive to mineralisation, cell culture media typically contains a sufficient Ca^{2+} concentration (1.8 mM in standard DMEM). Some studies have indicated that an elevated Ca^{2+} level may promote the formation of calcifications (Yang et al., 2004) although this theory has not been tested in the context of mammary calcifications.

Ca^{2+} homeostasis is modulated by a wide variety of channels and transport proteins and dysregulation of Ca^{2+} signalling has been suggested as an important contributor to tumourigenesis (Chen et al., 2013). The biological effects of Ca^{2+} are, to an extent, antagonised by the presence of Mg^{2+} ions (Jahnen-Dechent and Ketteler, 2012). Mg^{2+} seems to act as a potent inhibitor of vascular calcification as several clinical trials have shown decreased incidence of coronary artery calcification in patients with high intakes of dietary magnesium (Posadas-Sanchez et al., 2016, Hruby et al., 2014), whilst *in vitro* studies have demonstrated a number of anti-calcification effects including downregulation of ALP activity and decreased expression of osteogenic factors (Bai et al., 2015, Xu et al., 2015a). Magnesium has also been linked to breast cancer, with some studies suggesting an imbalance in serum Ca^{2+}/Mg^{2+} ratios to be associated with increased risk of breast cancer (Tao et al., 2016, Abdelgawad et al., 2015).

A key player in the regulation of cellular Mg^{2+} homeostasis is the transient receptor potential cation channel, subfamily M, member 7 (TRPM7) protein. This cation channel is permeable to a range of divalent cations, although predominantly conducts Ca^{2+} and Mg^{2+}. TRPM7 channel activity can be modulated by a variety of factors, including mechanical force, intracellular Mg^{2+} concentration, growth factors and reactive oxygen species (Visser et al., 2014). TRPM7 is often observed to exert a protective effect in studies of pathological calcification via its role in mediating Mg^{2+} influx, which acts to downregulate pro-osteogenic signalling pathways and attenuate development of a mineralisation-competent phenotype (Louvet et al., 2013, Montezano et al., 2010, Sonou et al., 2017).

However, a recent study found that that TRPM7 channel activity promoted IL-18 mediated vascular calcification in rat vascular smooth muscle cells (Zhang et al., 2017). In addition, Mandavilli demonstrated high immunohistochemical staining for the TRPM7 protein in patients with calcification associated breast tumours (Mandavilli et al., 2013). Within the context of breast cancer, TRPM7 has been linked to proliferation (Guilbert et al., 2009), EMT (Davis et al., 2014) and tumour metastasis (Middelbeek et al., 2012). Considering the important role in both pathological calcification and breast cancer, we hypothesised a potential role for the channel in the development of microcalcifications.

In summary, a significant body of evidence now exists to suggest a link between certain bone associated proteins, including MGP, BMP2 and RUNX2, and the development of mammary calcifications. However, direct *in vitro* evidence is lacking for most of these factors. The aim of this chapter therefore, will be to investigate the expression and function of known mediators and inhibitors of mineralisation within our *in vitro* model and to explore any potential role for TRPM7 and other Ca^{2+} transport proteins.

4.1.3 Aims of this chapter

The specific aims of this chapter were as follows

- Investigate potential roles for known inhibitors of pathological calcification, including PPi and Mg^{2+}.
- Analyse changes in expression of mineralisation associated genes and their potential contribution.
- Examine if altered Ca^{2+} levels can initiate or promote development of microcalcifications.
- Analyse potential roles for TRPM7 and other Ca^{2+} transport proteins.

4.2 Results

4.2.1 BMP-2 expression in mineralising MDA-MB-231 cells

The BMP family of proteins are potent regulators of osteoblast differentiation and activity (Dhore et al., 2001) and have also been implicated in several pro-oncogenic mechanism in breast cancer, including apoptotic resistance and angiogenesis (Tuo and Ye, 2017). We started our investigation into the role of BMP2 in microcalcification formation by assessing BMP2 expression in OC+Dex treated cells by qPCR (Fig 4.1). BMP2 expression was increased approximately 3-fold after 3 days incubation with OC+Dex media, in comparison to control values at the same time point ($P < 0.01$). This increase in expression was transient and returned to control values by day 7.

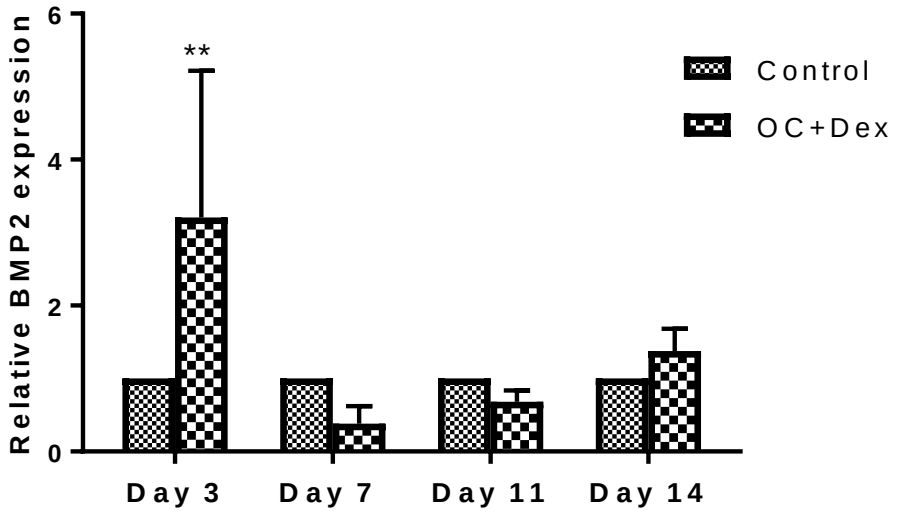

Figure 4.1 Expression of BMP2 in mineralising MDA-MB-231 cells. qPCR analysis of BMP2 expression in mineralising MDA-MB-231 cells at the indicated time points. BMP2 expression is increased 3 fold in OC+Dex stimulated cells at day 3. All data points represent mean + SD (N=3). Statistical significance was determined by two-way ANOVA. **P<0.01.

After establishing upregulation of BMP2 in mineralising breast cancer cells, we hypothesised that BMP2 could be helping to promote the development of microcalcifications. To test this hypothesis, we cultured MDA-MB-231 cells in OC+Dex media with or without recombinant BMP2, and examined for mineralisation by Alizarin Red S staining and by quantification of deposited calcium. BMP2 was used at a concentration of either 10 or 100 ng/mL, which have previously been shown to induce osteoblastic differentiation (Schurgers et al., 2008, Tuo and Ye, 2017, Tiago et al., 2016).

Although our lower tested concentration of 10 ng/mL of BMP2 had no significant impact on MDA-MB-231 mineralisation, the higher concentration of 100 ng/mL significantly increased both Alizarin Red S staining (Fig. 4.2 A) and deposited calcium (Fig. 4.2 B) in OC+Dex treated MDA-MB-231 cells after 28 days. Calcium deposition was increased 2.4-fold in cells treated with 100 ng/mL compared to OC+Dex alone (177 v 433 ppm/mg, $P < 0.05$). No positive Alizarin Red S staining was detected in cells cultured in OC, even at the highest tested concentration of BMP2, indicating that although BMP2 may augment the development of microcalcifications, it does not replace the pro-osteogenic signal generated by dexamethasone.

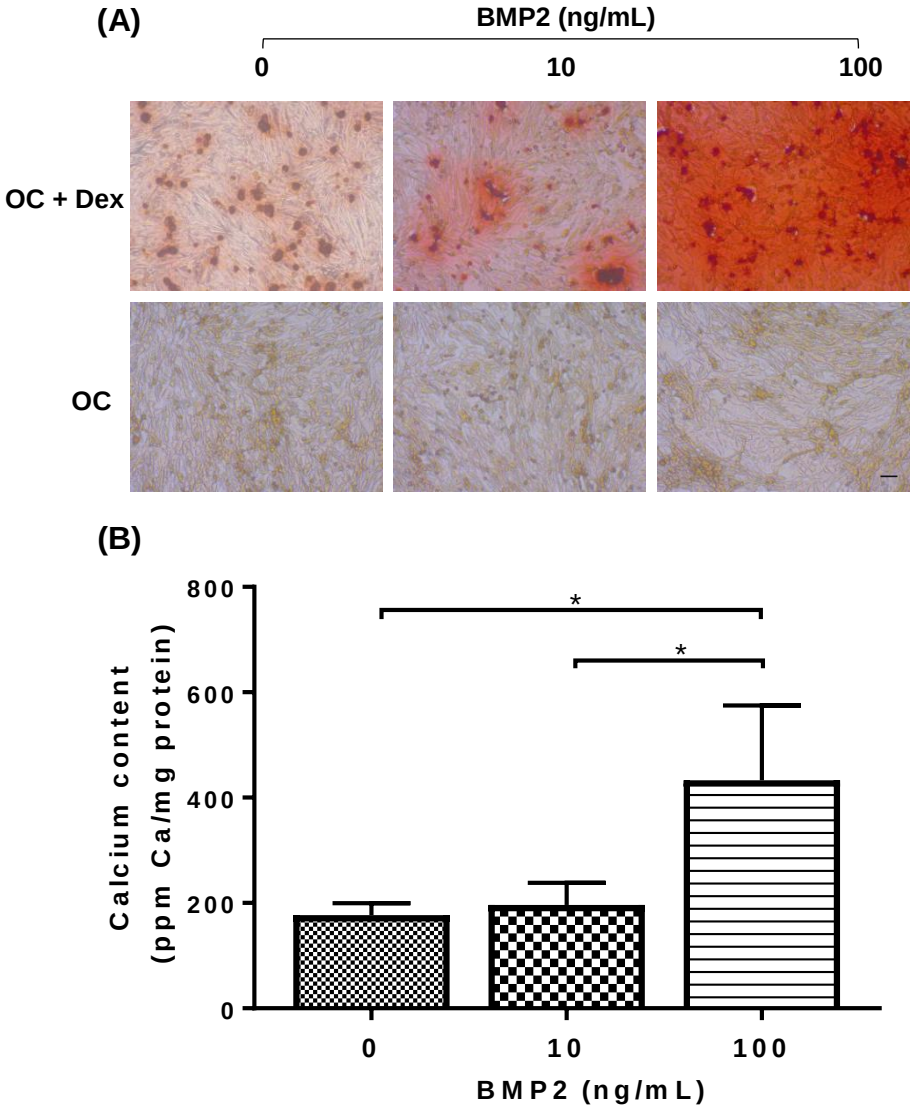

Figure 4.2 BMP2 promotes MDA-MB-231 calcification. Representative images (10X magnification) of Alizarin Red S stained MDA-MB-231 cells cultured in OC/OC+Dex media and rh-BMP2 at the indicated concentration for 28 days (A). Calcium content as measured by OCP assay, normalised to protein content (B). Significant increases in deposited calcium were observed in cells cultured with 100 ng/mL. All data points represent mean + SD (N=3). Statistical significance was determined by one-way ANOVA. *P<0.05. Scale bar represents 50 µm.

We next examined the effect of BMP2 on ALP activity in MDA-MB-231 cells. Similar to the results of our calcium quantification study, only the higher concentration of 100 ng/mL was observed to influence ALP activity, with treated cells displaying a 50% increase ($P < 0.001$) compared to cells grown in OC+Dex media or OC+Dex media with 10 ng/mL BMP2 (Fig. 4.3). Exogenous BMP2 at a concentration of 10 ng/mL did not appear to stimulate ALP activity.

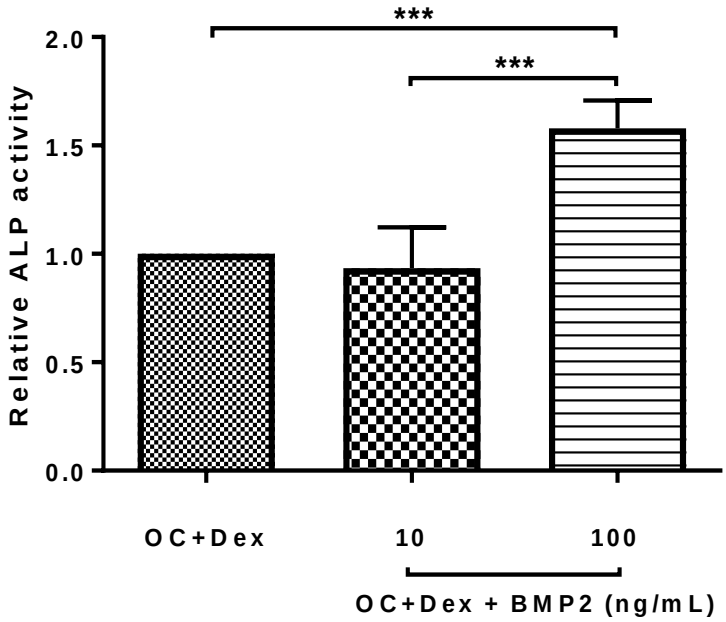

Figure 4.3 BMP2 stimulates MDA-MB-231 alkaline phosphatase activity. ALP activity of MDA-MB-231 cells cultured for 28 days in OC+Dex supplemented media with rh-BMP2 at the indicated concentration. ALP activity was increased by 50% in cells cultured with 100 ng/mL BMP2. All data points represent mean + SD (N=4). Statistical significance was determined by one-way ANOVA. ***P<0.05.

Due to the significant pro-mineralisation effect of exogenous BMP2 observed in MDA-MB-231 cells, we wondered if addition of BMP2 to previously non-mineralising cell lines could promote the development of calcifications. Despite its mineralisation promoting effect in MDA-MB-231 cells, BMP2 did not alter the mineralisation capability of the luminal MCF-7 cell line, with no positive Alizarin Red S staining observed following addition of either 10 or 100 ng/mL of recombinant BMP2 (Fig. 4.4).

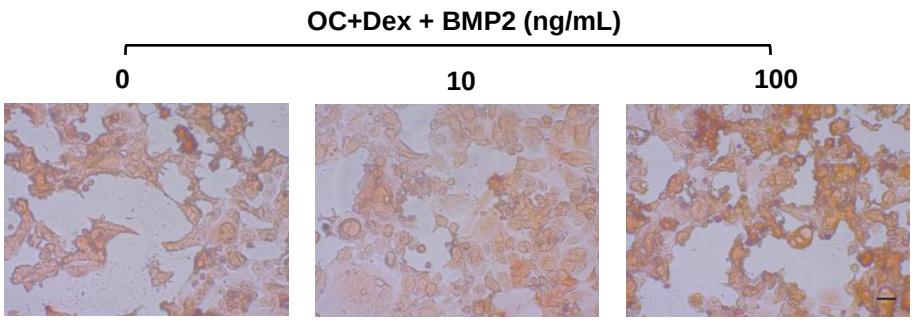

Figure 4.4 BMP2 does not alter mineralisation capability of luminal MCF-7 cells. Representative images (10X magnification) of Alizarin Red S stained MCF-7 cells cultured in OC/OC+Dex media and rh-BMP2 at the indicated concentration for 28 days (A). No significant alteration in staining was observed between any treatment group (N=3). Scale bar represents 50 µm.

4.2.2 Loss of ENPP1 expression in mineralising MDA-MB-231 cultures

Results from our previous chapter showed that onset of mineralisation is accompanied by activation of the ALP enzyme, as measured by enzymatic assay and qPCR (Fig. 3.11). ALP is a key regulator of mineralisation via its activity in reducing levels of the potent anti-calcification molecule PPi and in turn, increasing levels of free Pi to promote development of calcium phosphate precipitation. PPi is predominantly produced from ATP, which is exported to the extracellular environment where it can be subsequently degraded to PPi by the ectonucleotide pyrophosphatase/ phosphodiesterase 1 (ENPP1) enzyme (Villa-Bellosta and Egido, 2017).

As we have already demonstrated the importance of increased ALP activity in our model, we next decided to examine the potential role of ENPP1 and PPi in breast calcifications. We first examined expression of ENPP1 over a 14-day time course in mineralising MDA-MB-231 cells. Treatment with OC+Dex strongly suppressed expression of ENPP1 by over 50% at all examined time points, with an 80% decrease observed by day 14 (Fig 4.5 B, $P < 0.0001$).

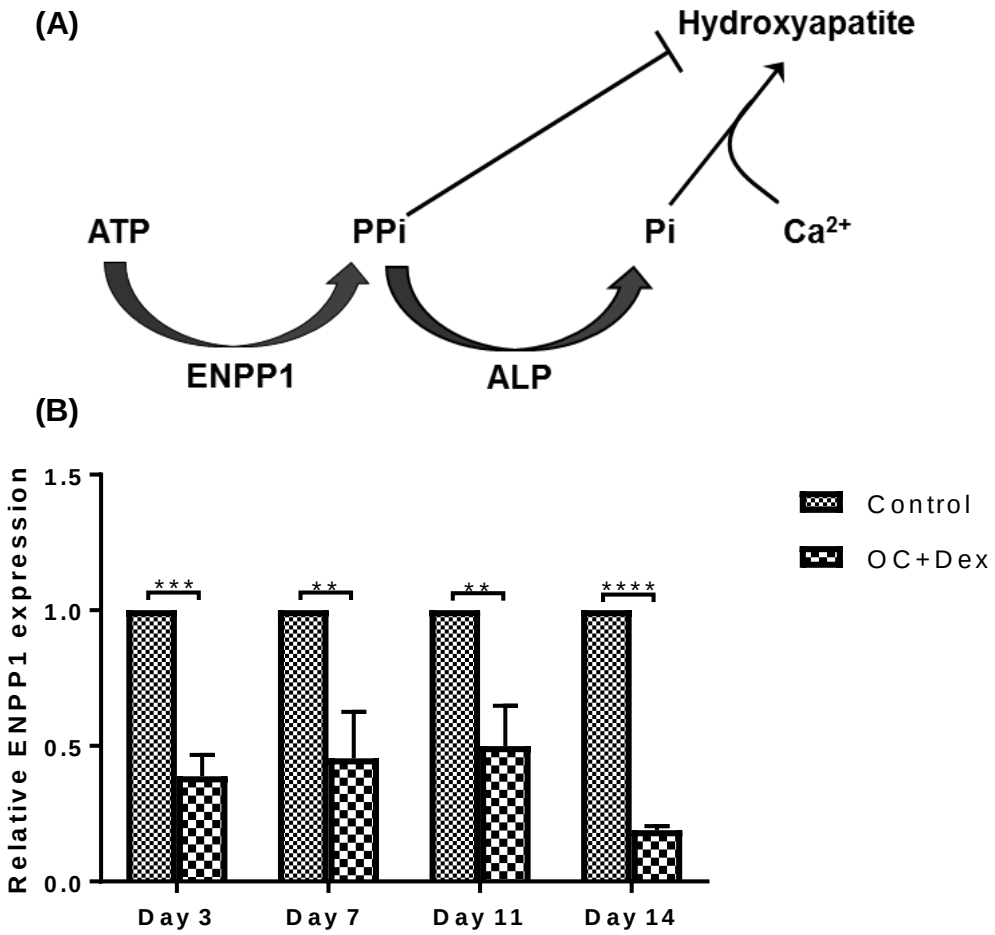

Figure 4.5 Onset of MDA-MB-231 mineralisation is accompanied by downregulation on ENPP1. The relationship between the mineralisation-inhibiting pyrophosphate (PPi) and mineralisation-promoting phosphate (Pi) in the formation of hydroxyapatite calcifications is detailed (A). qPCR analysis of ENPP1 revealed significant decreases in expression in OC+Dex treated cells at all time points (B). Each time point represents the mean + SD (N=3). Statistical significance was determined by two-way ANOVA, **P<0.01, ***P<0.001, ****P<0.0001.

As the loss of ENPP1 expression from mineralising MDA-MB-231 cells was likely to result in decreased levels of the anti-mineralisation agent PPi, we next examined the direct effect of PPi on mineralising cell cultures. MDA-MB-231 cells cultured in OC+Dex media displayed strong Alizarin Red S staining by day 14, as expected. Addition of sodium PPi at either 100 or 200 µM markedly decreased positive staining, indicating a decreased ability to produce microcalcifications under high-PPi conditions (Fig 4.6 A). PPi also blocked the increased ALP activity seen in cells grown in OC+Dex media (Fig. 4.6 B). Finally, as ALP activity contributes to mineralisation in part by degradation of PPi and reduction of its inhibitory effect (Sapir-Koren and Livshits, 2011), we treated PPi with ALP prior to using it in our mineralisation studies.

PPi that had been previously treated with ALP was significantly less effective at inhibiting mineralisation, as evidenced by the greater level of Alizarin Red S staining compared to cells grown in OC+Dex media with untreated-PPi (Fig. 4.6 C). We did note that although ALP treatment reduces the inhibitory effect of PPi, cells grown with ALP-treated PPi still displayed lower levels of Alizarin Red S staining than cells grown without any PPi, most likely indicating incomplete degradation of PPi.

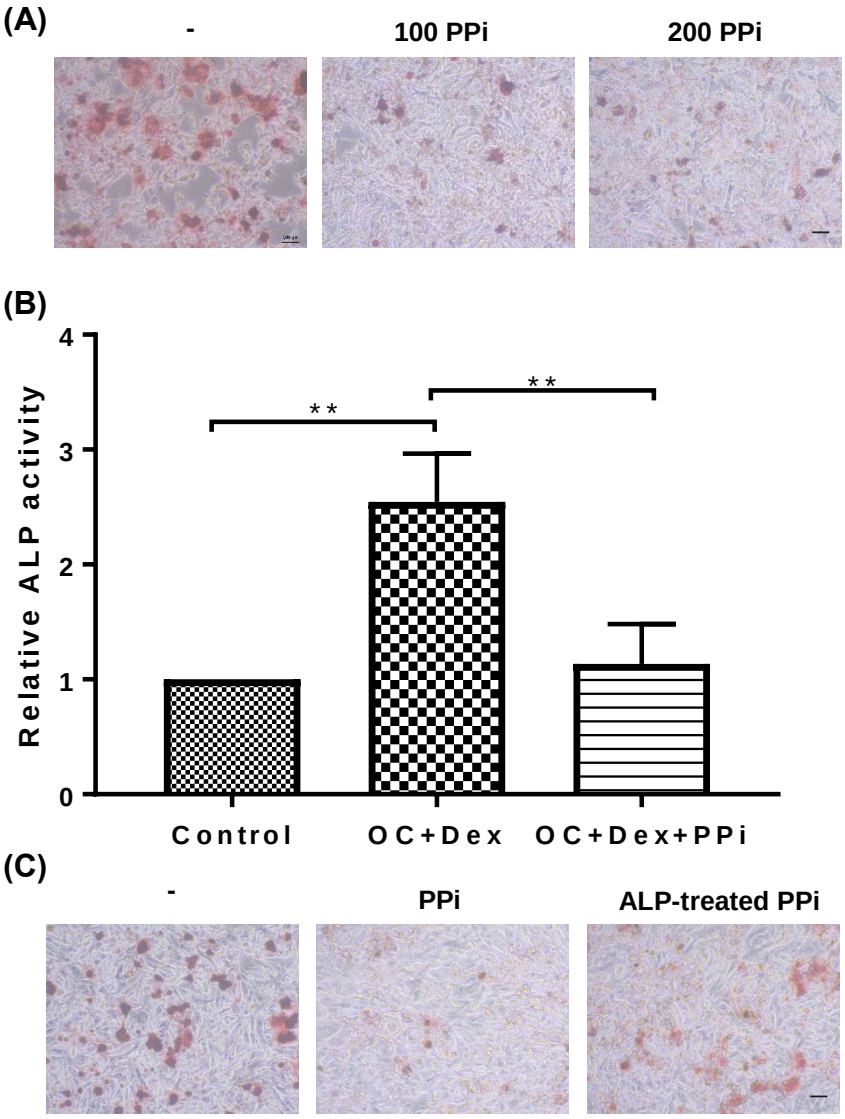

Figure 4.6 Anti-mineralisation effect of PPi in MDA-MB-231 cells. Representative images (10X magnification) of Alizarin Red S stained MDA-MB-231 cells cultured for 14 days in OC+Dex media supplemented with PPi at the indicated concentration (A). ALP activity, as measured at day 7 by incubation with the chromogenic substrate para-nitrophenyl phosphate also showed attenuation of OC+Dex mediated increase with 100 µM PPi (B). PPi treated with 1U/mL bovine ALP had a reduced, but still present inhibitory effect on MDA-MB-231 mineralisation (C). Each point represents mean + SD (N=3). Statistical significance was determined by one-way ANOVA. **P<0.01. Scale bar represents 50 µm.

4.2.3 Decreased MGP expression in mineralising MDA-MB-231 cells

In addition to PPi, several other mineralisation inhibitors act to keep pathological mineralisation from developing and spreading. These include Mg^{2+}, fetuin-A and matrix gla protein (MGP) (Kirsch, 2006). MGP is a vitamin-K dependent calcification inhibitor that binds Ca^{2+} with high affinity through its gamma-carboxyglutamic (GLA) domain (Schurgers et al., 2008). MGP may also play a role in tumour development (Gheorghe and Craciun, 2016). We observed a significant reduction in MGP expression in MDA-MB-231 cells cultured in OC+Dex media at all tested time points, with expression at day 14 being decreased by approximately 70% (Fig 4.7, $P < 0.0001$). This decrease was also observed to be time-dependent, as levels at day 14 were significantly lower than days 3 and 7 ($P < 0.01$).

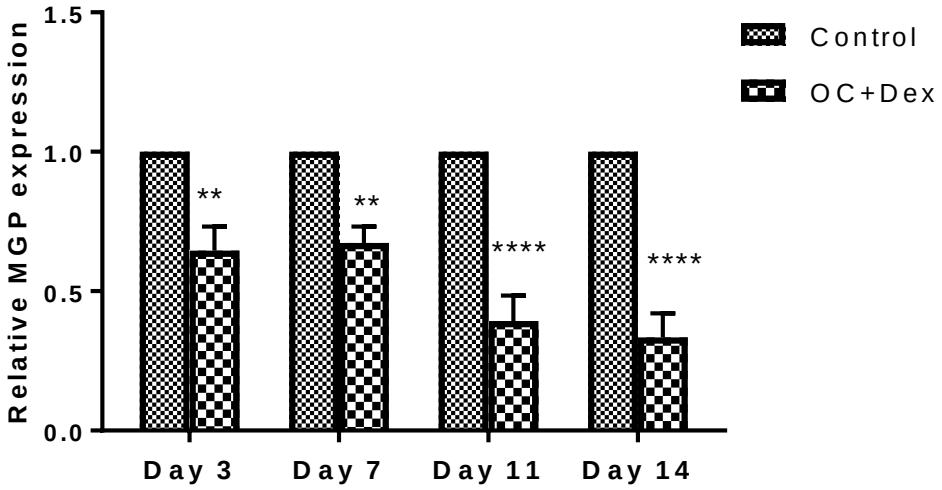

Figure 4.7 OC+Dex decreases MGP expression in MDA-MB-231 cells. MGP expression in mineralising MDA-MB-231 cells as analysed by qPCR at the indicated time points. OC+Dex potently decreased MGP expression at all tested time points. Each point represents mean + SD (N=3). Statistical significance was determined by two-way ANOVA. **P<0.01, ****P<0.0001.

4.2.4 RUNX2 and MDA-MB-231 mineralisation

The RUNX2 transcription factor is vital for generation of mature osteoblasts (Franceschi et al., 2003), and also plays a role in development of vascular calcification (Lin et al., 2015). RUNX2 is also upregulated in invasive breast tumours and promotes invasion and metastasis (Vishal et al., 2017). To examine any potential role for RUNX2 in the development of microcalcifications, we first analysed RUNX2 expression in our two mineralisation-capable cell lines (MDA-MB-231 and SKBR3) and a non-mineralising cell line (MCF-7).

In agreement with previous studies of increased RUNX2 expression in invasive breast cancer cell lines, we observed approximately 7-fold greater RUNX2 expression in MDA-MB-231 cells than both SKBR3 and MCF-7 cell lines ($P < 0.05$).

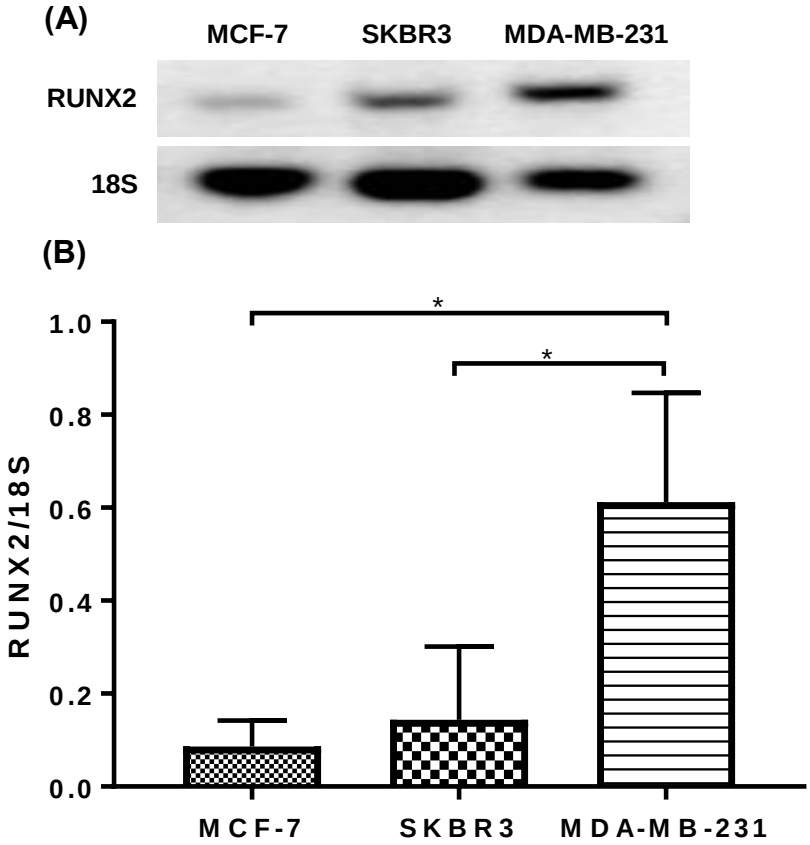

Figure 4.8 Elevated RUNX2 expression in MDA-MB-231 cells. Gel electrophoresis images (1.2% agarose) of RUNX2 and 18S PCR products from mRNA isolated from confluent, unstimulated cell cultures (A). Expression of RUNX2 in the indicated cell lines was analysed by densitometry (B). Each point represents mean + SD (N=3). Statistical significance was analysed by one one-way ANOVA. *P<0.05.

We next investigated any potential alterations in RUNX2 expression during the mineralisation process. qPCR analysis of OC+Dex stimulated MDA-MB-231 cells revealed a 50% upregulation at the two earliest time points tested (Fig. 4.9; days 3 & 7, $P < 0.05$).

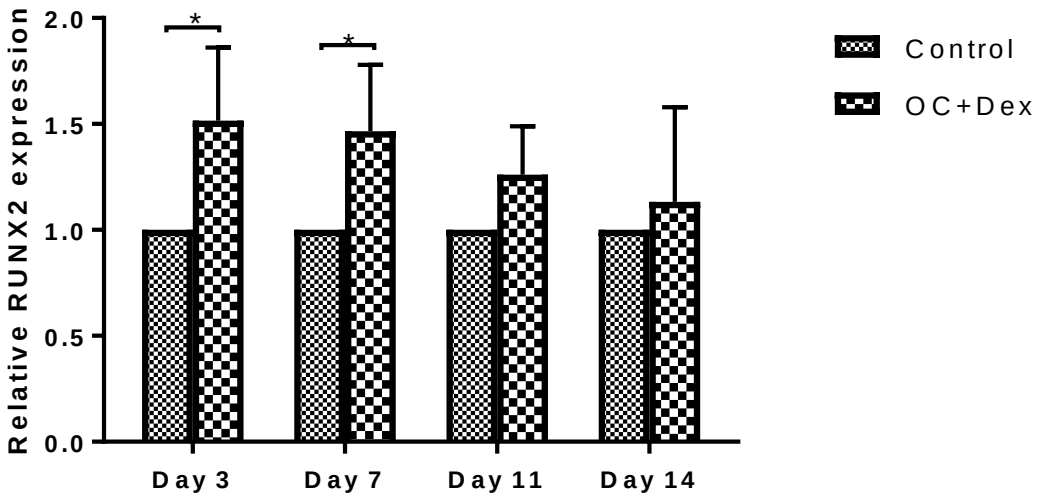

Figure 4.9 OC+Dex increases RUNX2 expression in MDA-MB-231 cells. RUNX2 expression in mineralising MDA-MB-231 cells as analysed by qPCR at the indicated time points. OC+Dex potently increased RUNX2 expression at days 3 and 7. Each point represents mean + SD (N=4). Statistical significance was determined by two-way ANOVA. *P<0.05.

To investigate a potential role for RUNX2 in the development of breast tumour mineralisations, we used a siRNA approach to knock down RUNX2 expression in MDA-MB-231 cells. Cells were transfected with either a RUNX2 targeting or a negative-control siRNA. RUNX2 expression was decreased by approximately 60% 72 hours post-transfection, as measured by qPCR (Fig. 4.10 A). After a 72-hour transfection period, cells were switched to OC+Dex supplemented media, with mineralisation assessed at day 14. Alizarin Red S staining revealed significant red staining in both control and RUNX2-siRNA transfected wells (Fig. 4.10 B). Quantification of extracted calcium revealed a 20% decrease in cells transfected with a RUNX2-targeting siRNA versus those transfected with a control-siRNA (Fig. 4.10 C).

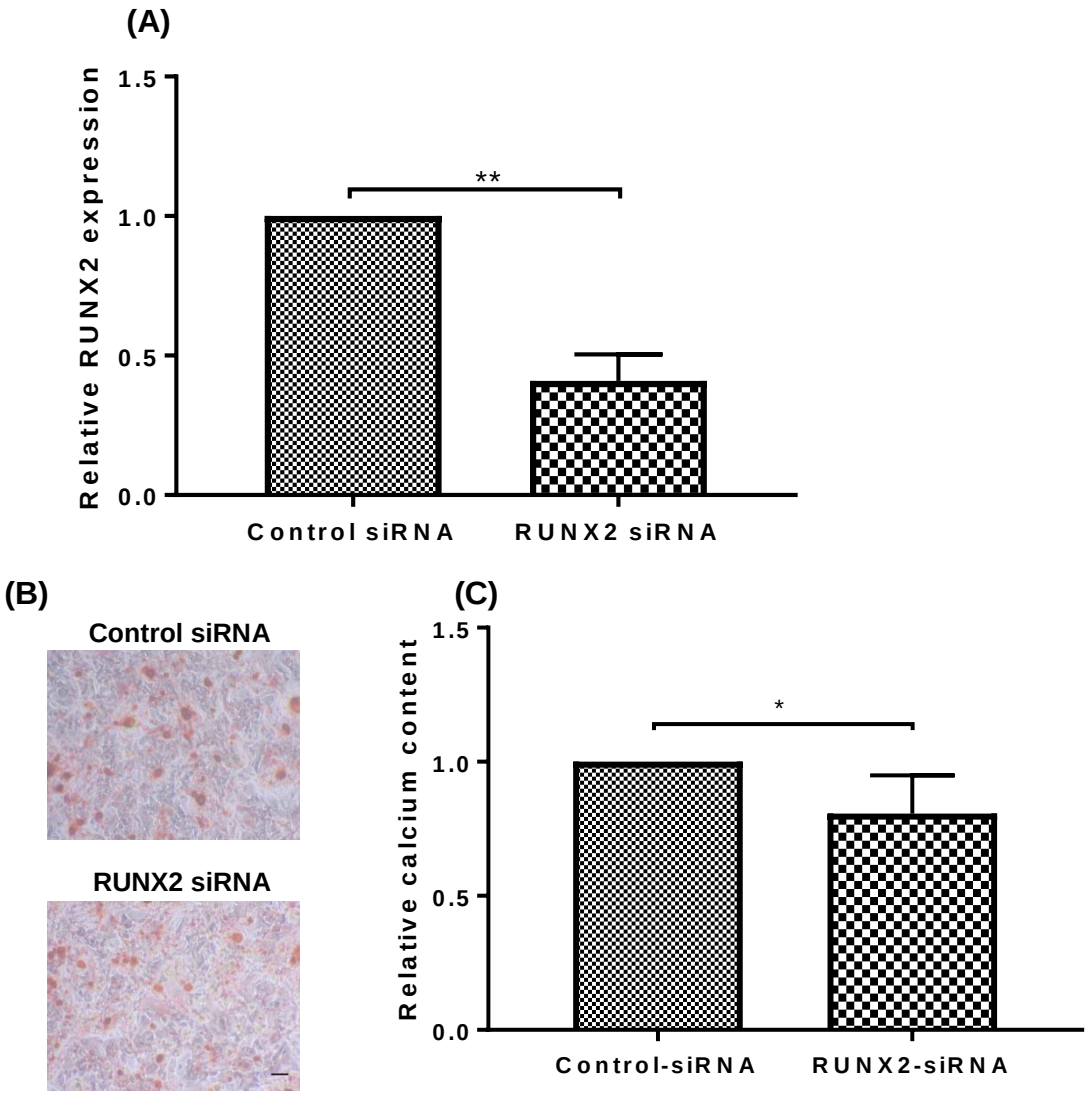

Figure 4.10 siRNA knockdown of RUNX2 decreases MDA-MB-231 mineralisation. RUNX2 knockdown efficiency in MDA-MB-231 cells transfected with a RUNX2 targeting or a negative-control siRNA, as assessed by qPCR (A). Representative images (10X magnification) of Alizarin Red S stained cells cultured post siRNA transfection for 14 days in OC+Dex media (B). Calcium content as measured by OCP assay, normalised to protein content showed a significant decrease in RUNX2-siRNA treated cells (C). Each data point represents mean + SD (qPCR N=3, OCP N=5). Statistical significance was determined by t-test. *P<0.05, **P<0.01. Scale bar represents 50 µm.

Considering the reduction in calcification observed in RUNX2-siRNA treated cells, we next sought to determine if mineralisation could be increased via upregulation of the RUNX2 gene. MDA-MB-231 cells were transfected with a plasmid containing RUNX2 cDNA under control of a CMV promoter. This plasmid contained a full-length copy of the mouse RUNX2 cDNA, which shares 93% homology with the human mRNA (Zhang et al., 2000) and has previously been used successfully to upregulate RUNX2 expression in human cells (Jiménez et al., 1999). As a control, replicate wells were transfected with a control plasmid containing GFP (CMV-GFP).

RUNX2 expression, examined by qPCR 72-hours post transfection, showed an 80-fold increase ($P < 0.01$) in cells transfected with CMV-RUNX2 compared to CMV-GFP, indicating successful transfection and target upregulation (Fig. 4.11 A). Following transfection, cells were then switched to OC+Dex supplemented media and cultured for 14 days prior to analysis of deposited calcium levels. Despite a significant increase in RUNX2 expression, this did not alter the development of calcifications in MDA-MB-231 cells, as no significant difference was observed in calcium levels between control or RUNX2 transfected cells (Fig 4.11 B).

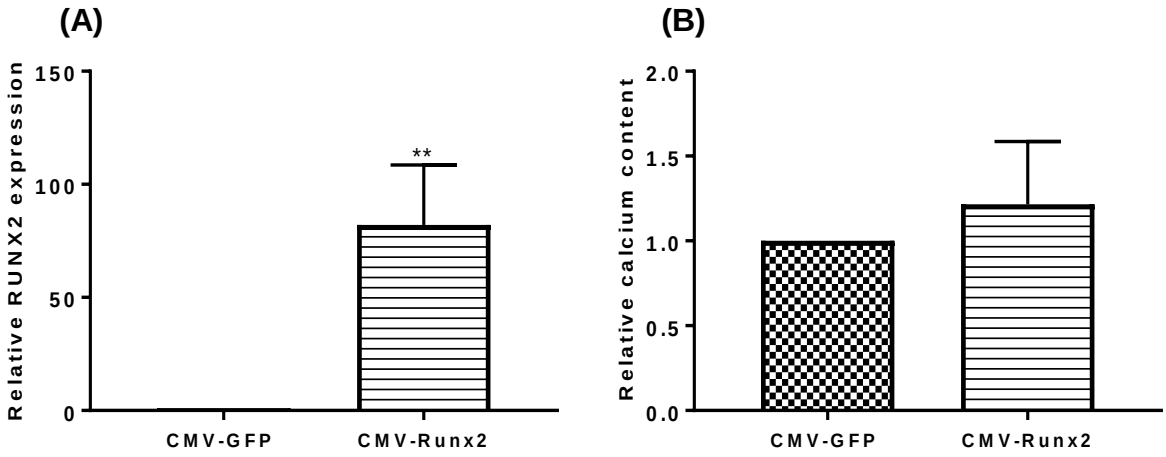

Figure 4.11 Overexpression of RUNX2 does not alter MDA-MB-231 mineralisation. Expression of RUNX2 in MDA-MB-231 cells 72-hours post transfection with a plasmid containing full-length mouse RUNX2 cDNA under the control of a CMV promoter (CMV-RUNX2) or a control plasmid containing GFP (CMV-GFP) as measured by qPCR (A). Calcium content, as measured by OCP assay normalised to protein content, in cells cultured for 14 days post transfection in OC+Dex media did not reveal any significant alterations (B). All data points represent mean + SD (qPCR N=3, calcium N=6). Statistical significance was determined by t-test. **P<0.01

4.2.5 Role of intracellular Ca^{2+} accumulation and TRPM7 channel activity in microcalcification formation

Malignancy associated microcalcifications are composed of calcium phosphate crystals, most commonly hydroxyapatite (Tse et al., 2008). In the previous chapter, we investigated the effect of Pi on the *in vivo* formation of calcifications. We next sought to examine the role of Ca^{2+}. Standard DMEM media contains 1.8 mM Ca^{2+}. This is slightly lower than serum Ca^{2+} levels which are typically between 2.2 and 2.7 mM (Abdelgawad et al., 2015). To assess how elevated serum Ca^{2+} levels may impact the development of calcifications, we supplemented DMEM media with calcium chloride to either 2.2 or 2.7 mM, representing a 25 and 50 % increase in available Ca^{2+}, respectively.

Cells were cultured in this high- Ca^{2+} media, supplemented with OC or OC+Dex reagents for 14 days before assessing for mineralisation. Cells grown in OC media did not display any Alizarin Red S staining at either elevated Ca^{2+} levels, indicating that increased Ca^{2+} cannot promote mineralisation in the absence of dexamethasone stimulation (Fig. 4.12 A). In contrast, cells grown in OC+Dex media displayed significantly increased staining when cultured at 2.2 or 2.7 mM Ca^{2+} compared to basal 1.8 mM. This was confirmed via quantification of extracted calcium deposits, with cells grown at 2.7 mM Ca^{2+} displaying an almost 4-fold increase in calcium measurements (Fig. 4.12 A, $P < 0.05$). Cells grown at 2.2 mM Ca^{2+} displayed a trend towards increased calcification although this did not reach statistical significance (2.5-fold increase, P=0.18).

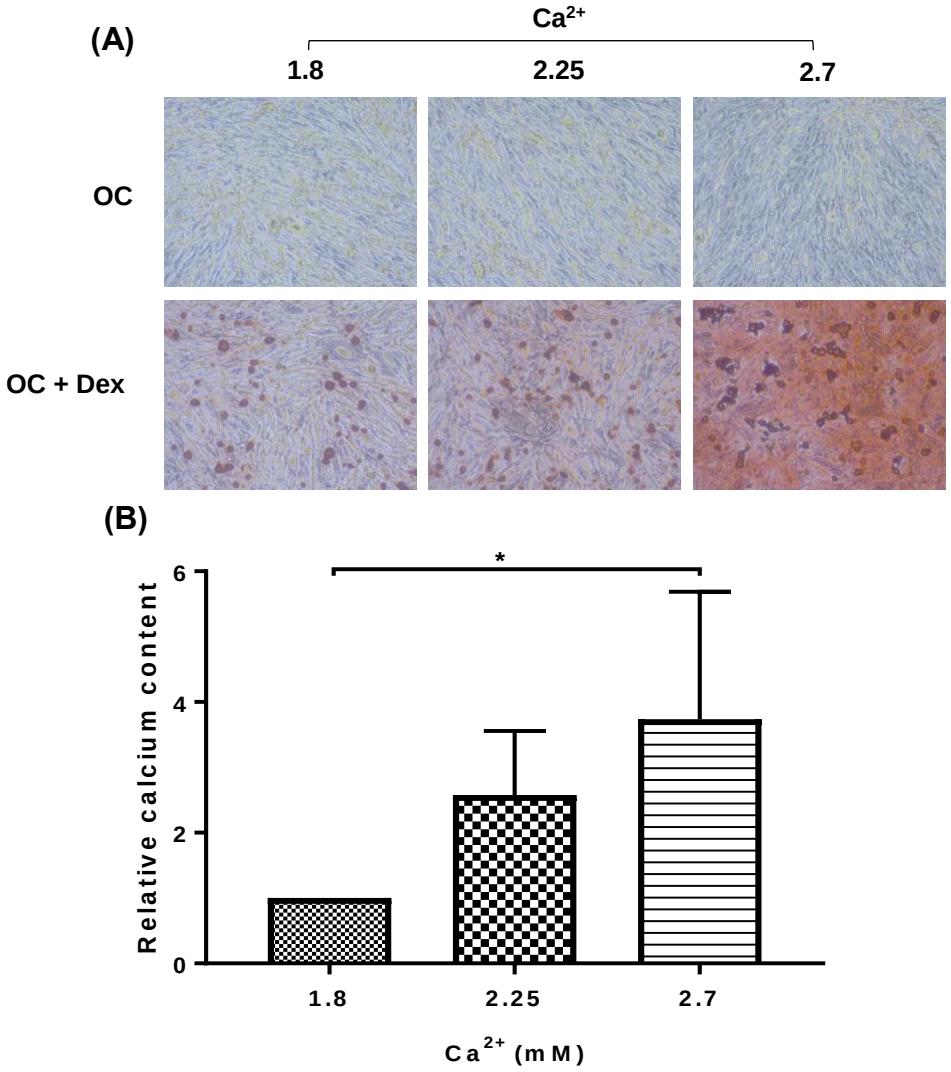

Figure 4.12 Effect of increased Ca2+ levels on MDA-MB-231 mineralisation. Representative images (10X magnification) of Alizarin Red S stained MDA-MB-231 cells cultured for 14 days in either OC or OC+Dex media at the indicated Ca^{2+} concentration (A). Basal Ca^{2+}concentration in DMEM (1.8 mM) was supplemented with calcium chloride to the indicated concentrations. Calcium content, as measured by OCP assay normalised to protein content revealed increased mineralisation in OC+Dex cultured cells at 2.7 mM Ca^{2+} (B). Each point represents mean + SD (N=4). Statistical significance was determined by one-way ANOVA. *P<0.05. Scale bar represents 50 µm.

After observing the increased levels of mineralisation in cells cultured in high Ca^{2+} conditions, we next examined if alterations in intracellular Ca^{2+} levels may be involved in the development of mineralisations. BAPTA-AM is a membrane-permeable chelator complex, consisting of the chelator compound BAPTA bound to an acetoxymethyl (AM) group by ester linkage. BAPTA-AM is inactive until it crosses the cell membrane and has its AM group removed by cellular esterases. This limits the compounds activity to an intracellular context and allows for blockade of intracellular rises in Ca^{2+}. BAPTA-AM decreased MDA-MB-231 mineralisation in a dose-dependent manner, with cells cultured in 10 µM displaying an almost 80% reduction in calcium deposition (Fig. 4.13 A, $P < 0.05$). 5 µM displayed a strong trend towards reduced calcification, but this did not reach statistical significance. Chelation of intracellular Ca^{2+} also decreased cellular ALP activity (Fig. 4.13 B). Cells cultured in 5 µM BAPTA-AM had a 25% reduced ALP activity, although similar to results from our calcification assay, this fell just short of statistical significance (P=0.0505). 10 µM BAPTA-AM reduced ALP activity of MDA-MB-231 cells by almost 50% ($P < 0.01$).

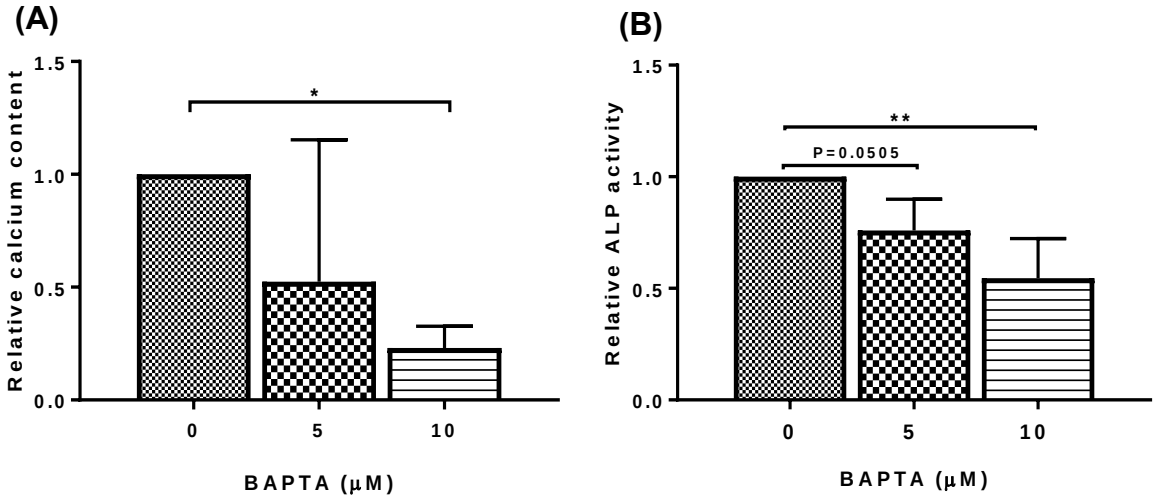

Figure 4.13 MDA-MB-231 mineralisation is inhibited by intracellular Ca^{2+} chelation. Calcium content, as measured by OCP assay normalised to protein content of MDA-MB-231 cells cultured for 14 days in OC+Dex media with BAPTA-AM at the indicated concentration (B). Significant decreases were observed in cells cultured with 10 µM. Similar decreases were also observed in ALP activity at day 14 (B). Each point represents mean + SD (N=4). Statistical significance was determined by one-way ANOVA. *P<0.05, **P<0.01

These results suggest that an intracellular accumulation of Ca^{2+} is an important step in the development of microcalcifications, which concurs with previous studies (Kapustin et al., 2011). Intracellular Ca^{2+} influx in tumour cells is a complex relationship between many different Ca^{2+} pumps, channels and transport proteins (Stewart et al., 2015).

Several members of the transient receptor potential (TRP) family of ion channels have been implicated in the development and spread of breast tumours and may constitute novel therapeutic targets (Ouadid-Ahidouch et al., 2012). Of particular interest, the transient receptor potential melastatin type 7 (TRPM7) channel has been shown to be an important regulator of Ca^{2+} influx in breast cancer (Guilbert et al., 2009) and has also been shown to be highly expressed in breast tumours with associated microcalcifications (Mandavilli et al., 2013). We hypothesised that TRPM7 may play a role in the intracellular influx of Ca^{2+} leading to onset of mineralisation. Using qPCR, we examined expression of both TRPM7 and the related TRPC1 channel, which has also been shown to be highly expressed in calcification associated breast tumours (Mandavilli et al., 2013). Expression of TRPM7 was observed to increase in a time-dependent manner over a 14-day time course (Fig. 4.14 A, 1.6-fold compared to control at day 14, $P < 0.001$). Expression of TRPC1 was also upregulated, albeit in a transient fashion (2-fold increase at day 7, $P < 0.05$).

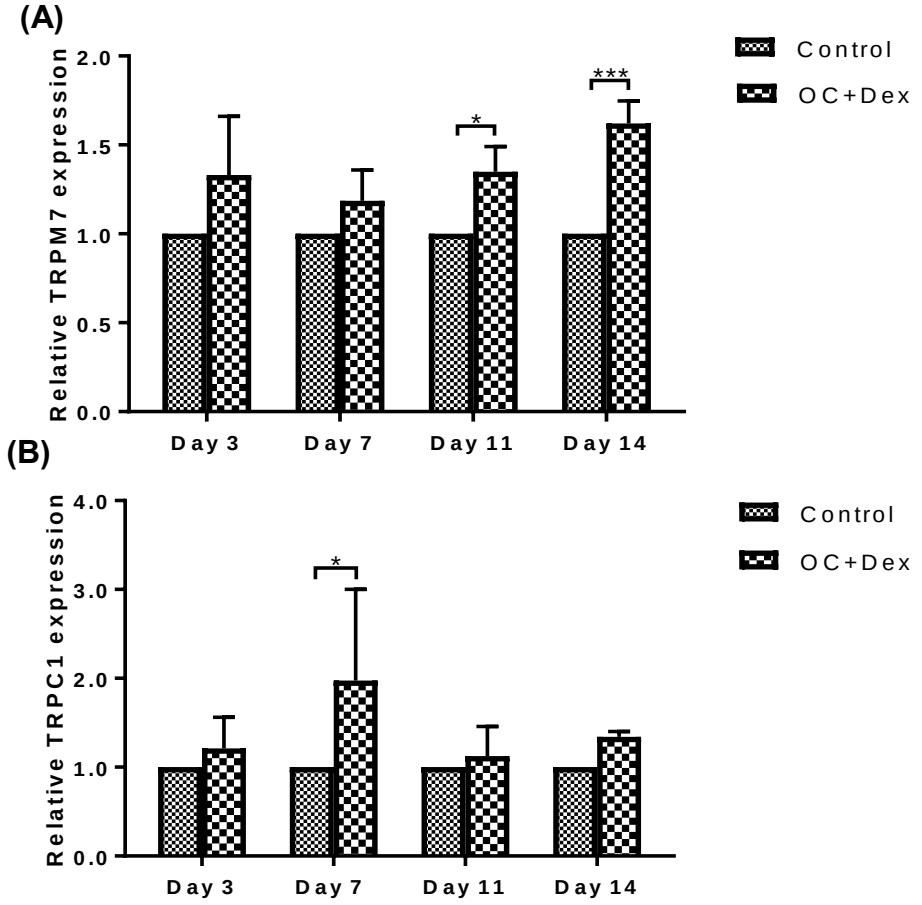

Figure 4.14 Upregulation of TRPM7 and TRPC1 channels during MDA-MB-231 mineralisation. Expression of TRPM7 (A) and TRPC1 (B) in MDA-MB-231 cells cultured for 14 days in OC+Dex supplemented media was examined by qPCR at the indicated time points. Each data point represents the mean + SD (N=3). Statistical significance was determined by two-way ANOVA. *P<0.05, ***P<0.001.

To examine a potential role for the TRPM7 channel in the generation of microcalcifications, we tested the ability of MDA-MB-231 cells to mineralise under the effect of the TRP channel modulator 2-APB. Although no difference in Alizarin Red S staining was observed for the two lowest tested concentrations (10 µM and 100 µM), the higher concentrations of 150 µM and 200 µM noticeably decreased staining, indicating an inhibition of calcium deposition (Fig. 4.15 A). Quantitative measurement of calcium content revealed a slight increase in calcium at 10 µM 2-APB, although this did not reach statistical significance (Fig. 4.15 B). 150 and 200 µM 2-APB both significantly decreased calcium, with 200 µM leading to a total inhibition of mineralisation (97% decrease compared to control, P<0.05).

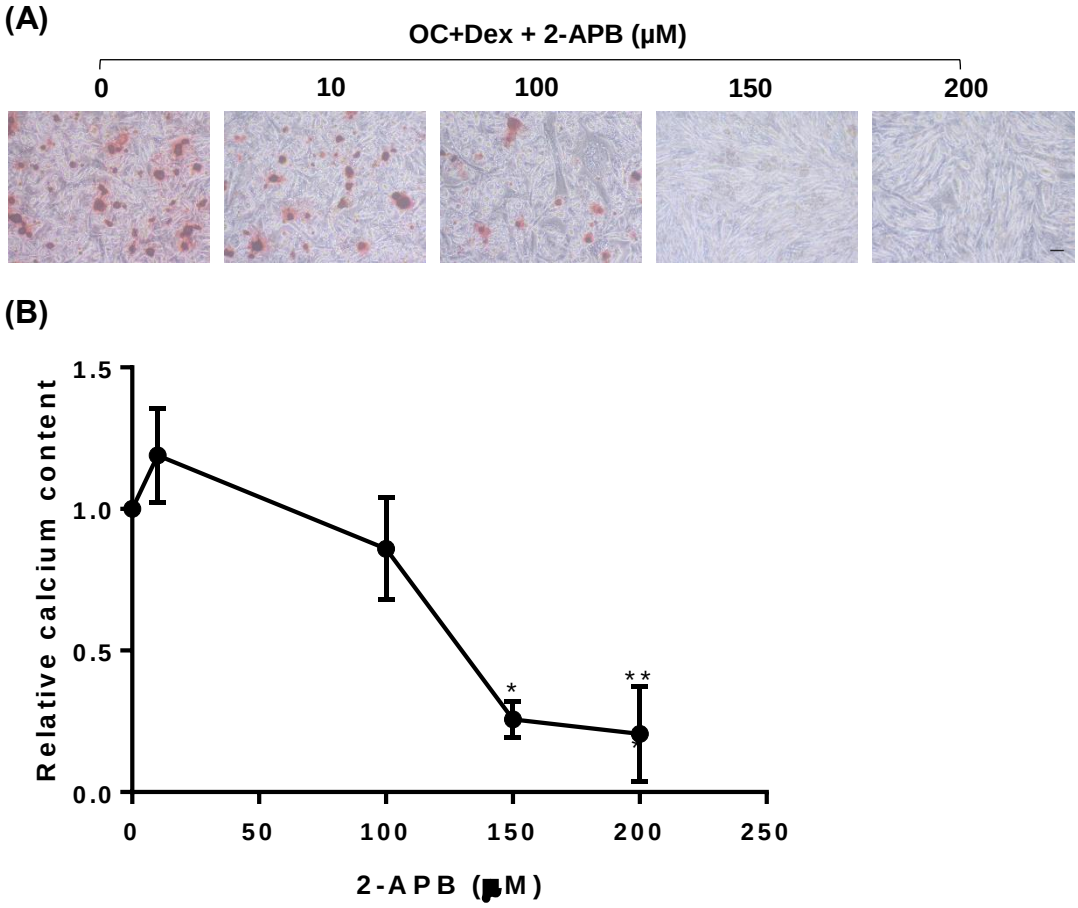

Figure 4.15 Inhibition of MDA-MB-231 mineralisation by the TRP channel modulator 2-APB. Representative images (10X magnification) of Alizarin Red S stained MDA-MB-231 cells cultured for 28 days in OC+Dex media with 2-APB at the indicated concentration (A). Measurement of calcium content of cell monolayers showed significantly decreased calcium at 150 and 200 µM (B). Calcium content was normalised to protein content, and expressed relative to control values. Each data point represents the mean + SD (N=4). Statistical significance was determined by one-way ANOVA. *P<0.05, **P<0.01. Scale bar represents 50 µm.

Although these results indicated a possible role for the TRPM7 channel in microcalcification development, it is important to note that 2-APB is not a specific TRPM7 inhibitor. Other studies have utilised 2-APB to block TRPM7 activity at concentrations ranging from 10 to 500 µM (Chokshi et al., 2012, Guilbert et al., 2009, Li et al., 2006). However, 2-APB has been shown to block several other TRP family members at these concentrations, including TRPM2 (Togashi et al., 2008) and TRPC5 (Xu et al., 2005) as well as activating TRPV1, TRPV2, and TRPV3 (Hu et al., 2004). To address any potential issues with the selectivity of 2-APB, we repeated the experiment using NS8593, a TRPM7 inhibitor with significantly improved specificity (Chubanov et al., 2012). Results with NS8593 were even more significant, with all tested concentrations leading to a significant decrease in both Alizarin Red S staining and calcium content (Fig. 4.16). NS8593 effectively blocked calcium deposition by 65% even in the lowest tested concentration of 2 µM, which roughly corresponds to the IC50 of the TRPM7 channel (Chubanov et al., 2012).

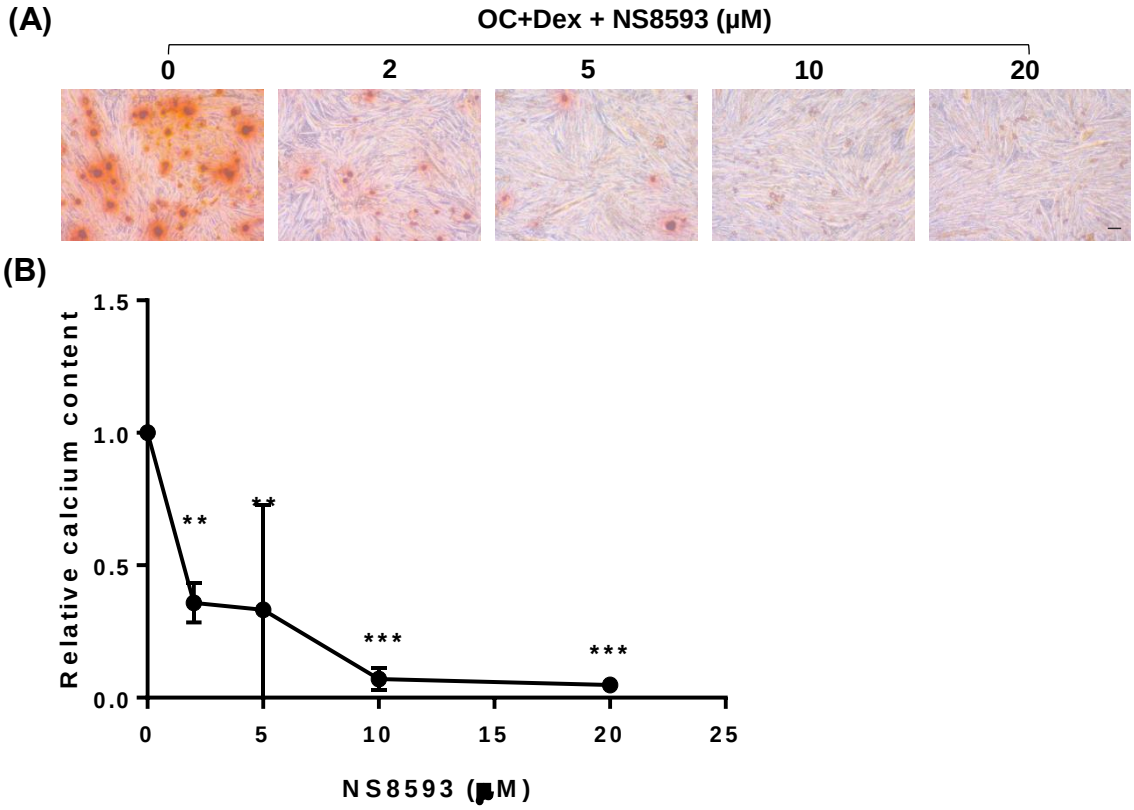

Figure 4.16 Inhibition of MDA-MB-231 mineralisation by the TRPM7 channel inhibitor NS8593. Representative images (10X magnification) of Alizarin Red S stained MDA-MB-231 cells cultured for 28 days in OC+Dex media with NS8593 at the indicated concentration (A). Alizarin Red S staining revealed decreased calcium deposition at all tested concentrations. Measurement of calcium content of cell monolayers also showed significant decreases (B). Calcium content was normalised to protein content, and expressed relative to control values. Each data point represents the mean + SD (N=3). Statistical significance was determined by one-way ANOVA. **P<0.01, ***P<0.001. Scale bar represents 50 µm.

We next examined the effect of TRPM7 inhibition on ALP activity. For both inhibitors, the second highest concentration from our previous dose-response experiments was selected for further study. Both TRPM7 inhibitors significantly decreased ALP activity in mineralising MDA-MB-231 cells (Fig 4.17). Similar to results from our mineralisation assays, the more selective NS8593 was markedly more effective at inhibiting ALP activity, with a dose of 10 µM decreasing ALP activity by approximately 80% (P<0.0001) compared to an 18% reduction by 150 µM 2-APB (P<0.01).

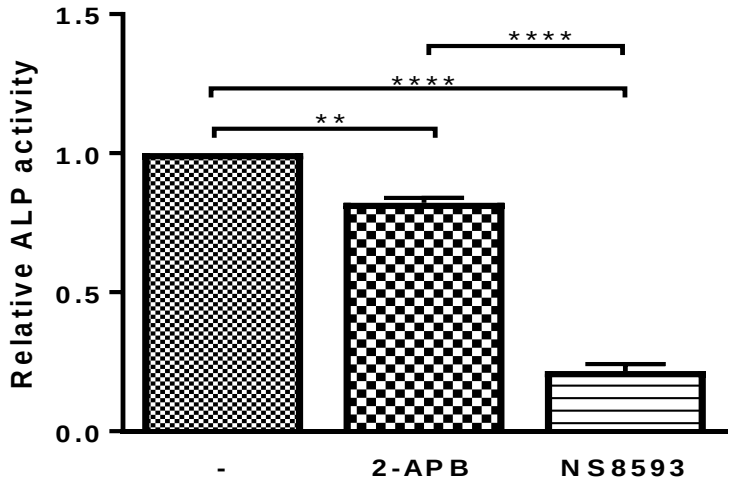

Figure 4.17 Inhibition of MDA-MB-231 ALP activity by the 2-APB and NS8593. ALP activity of MDA-MB-231 cells cultured for 14 days in OC+Dex supplemented media with 2-APB (150 µM), NS8593 (10 µM) or DMSO vehicle control. ALP activity was measured by incubation with the ALP substrate PNPP, normalised to protein content and expressed relative to vehicle-control treated cells. Each data point represents the mean + SD (N=2). Statistical significance was determined by t-test. **P<0.01, ****P<0.0001.

Finally, we verified our findings from inhibitor studies using siRNA to knockdown TRPM7 in mineralising MDA-MB-231 cells. Knockdown efficiency, as measured by qPCR at 72 hours, was 60% (Fig. 4.18 A). Following a 72-hour incubation period with siRNA complexes, cells were switched to OC+Dex supplemented media for 14 days. Knockdown of TRPM7 decreased calcium deposition by approximately 25% at day 14 (Fig. 4.18 C). A decrease in Alizarin Red S staining was also noted (Fig. 4.18 B).

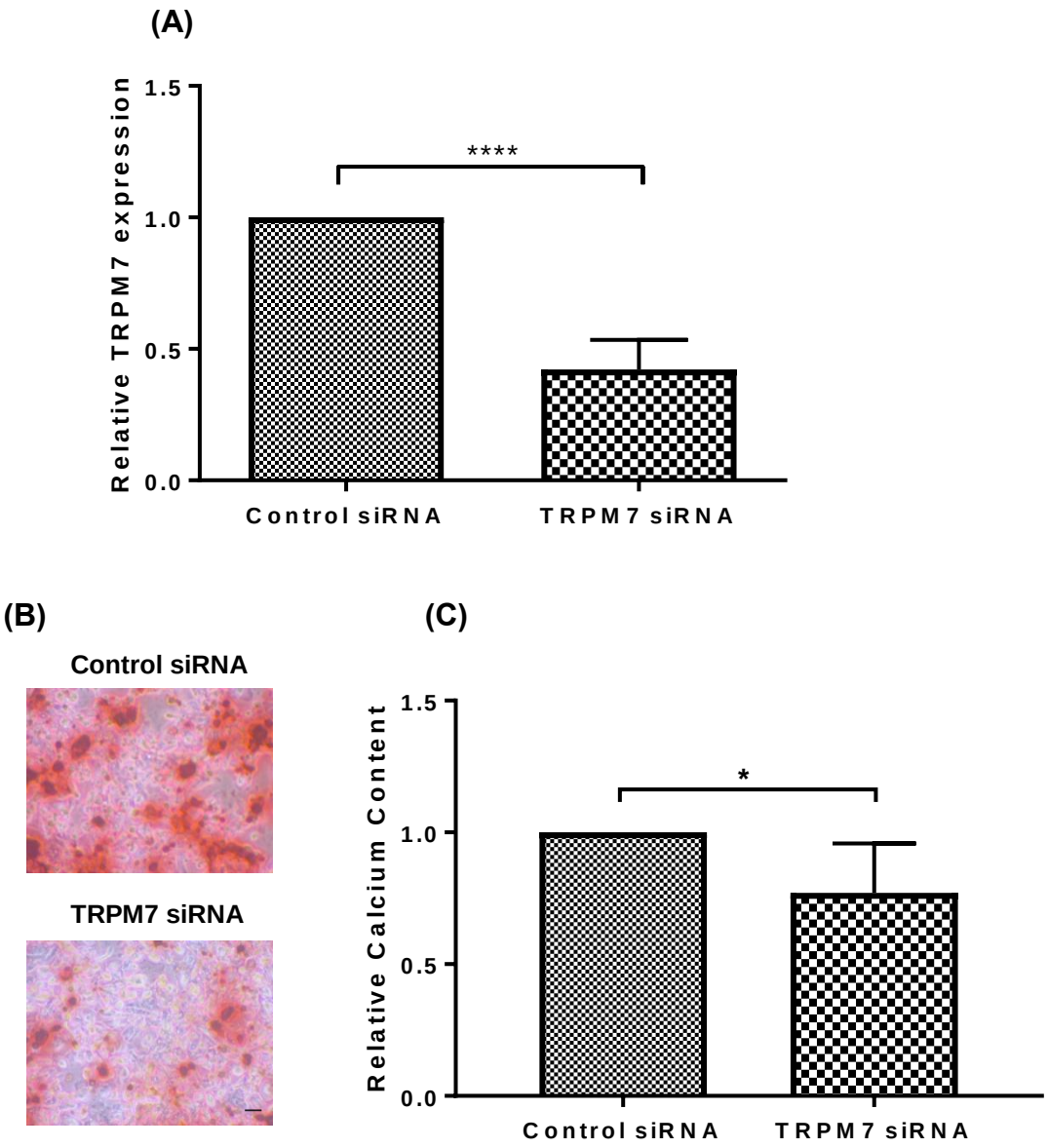

Figure 4.18 siRNA knockdown of TRPM7 reduces MDA-MB-231 mineralisation. TRPM7 knockdown efficiency in MDA-MB-231 cells transfected with a TRPM7 targeting or a negative-control siRNA, as assessed by qPCR (A). Representative images (10X magnification) of Alizarin Red S stained cells cultured post siRNA transfection for 14 days in OC+Dex media (B). Calcium content was normalised to protein content, and expressed relative to control values (C). Reduced mineralisation was demonstrated by Alizarin Red S staining (B) and quantitative calcium measurement (C) at day 14. Each data point represents the mean + SD (N=5). Statistical significance was determined by t-test. *P<0.05, ****P<0.0001. Scale bar represents 50 µm.

4.2.6 Breast calcifications and magnesium

Interestingly, although we have shown evidence of a role for the TRPM7 channel in promoting calcification of breast cancer cells, studies of other forms of pathogenic mineralisation have actually shown TRPM7 to act in a protective manner. In addition to mediating influx of Ca^{2+} ions, TRPM7 is also permeable to a range of other divalent cations including Mg^{2+}, Zn^{2+}, Mn^{2+}, and Co^{2+} (Monteilh-Zoller et al., 2003). In studies of vascular calcification, TRPM7 has been shown to exert a protective effect by promoting influx of Mg^{2+}, a potent inhibitor of calcium deposition (Sonou et al., 2017, Louvet et al., 2013, Montezano et al., 2010).

We first examined if Mg^{2+} had the same protective effect in our model as has been demonstrated in other studies. MDA-MB-231 cells were cultured under mineralising conditions in DMEM media with unaltered Mg^{2+} levels (0.8 mM) or DMEM supplemented with magnesium chloride to yield a total Mg^{2+} concentration of 1.5 or 3 mM. These concentrations have previously been used in other studies of the anti-mineralisation effect of Mg^{2+} (Xu et al., 2015a, Montezano et al., 2010). Cells were cultured for up to 28 days under these conditions before assessment of mineralisation.

Similar to results from studies in other cell types, we observed a strong reduction in mineralisation in cells cultured under increased Mg^{2+} conditions. Alizarin Red S staining was very faint in 1.5 and 3 mM groups compared to 0.8 (Fig. 4.19 A). These results were confirmed by measurement of deposited calcium (Fig. 4.19 B), with an approximate 80% reduction observed at day 21 for both increased Mg^{2+} groups ($P<0.05$), and a 70% and 90% reduction for 1.5 and 3 mM respectively at day 28 ($P<0.0001$). Increased Mg^{2+} also potently inhibited mineralisation in cells mineralised with inorganic Pi (Fig. 4.19 C), rather than our standard OC+Dex formulation (containing organic β-glycerophosphate). Addition of extra Mg^{2+} had no observable effect on cells grown in standard DMEM media without OC+Dex supplementation, with no mineralisation observable in any group (Fig. 4.20).

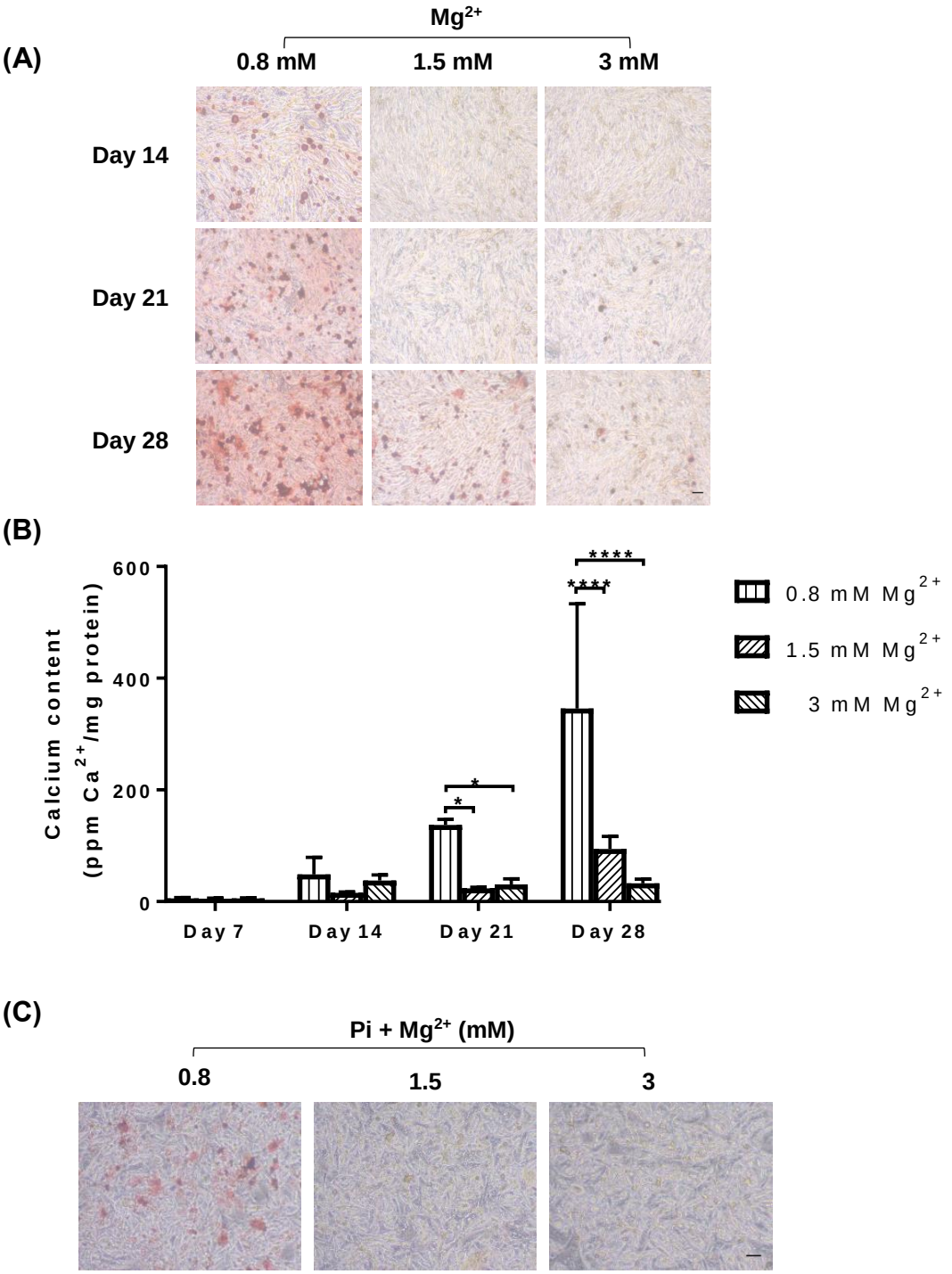

Figure 4.19 Magnesium potently inhibits development of MDA-MB-231 calcifications. Representative images (10X magnification) of Alizarin Red S stained MDA-MB-231 cells cultured for 28 days in OC+Dex media with Mg^{2+} at the indicated concentration (A). Magnesium chloride was used to adjust total Mg^{2+} concentration from basal (0.8 mM) to 1.5 or 3 mM. Measurement of calcium content of cell monolayers demonstrated an almost total inhibition of mineralisation under increased Mg^{2+} conditions (B). Alizarin Red S stained images of MDA-MB-231 showing strong anti-mineralisation effect of Mg^{2+} under inorganic Pi conditions (C). Each data point represents the mean + SD (N=2). Statistical significance was determined by one-way ANOVA. **P<0.01, ***P<0.001. Scale bar represents 50 µm.

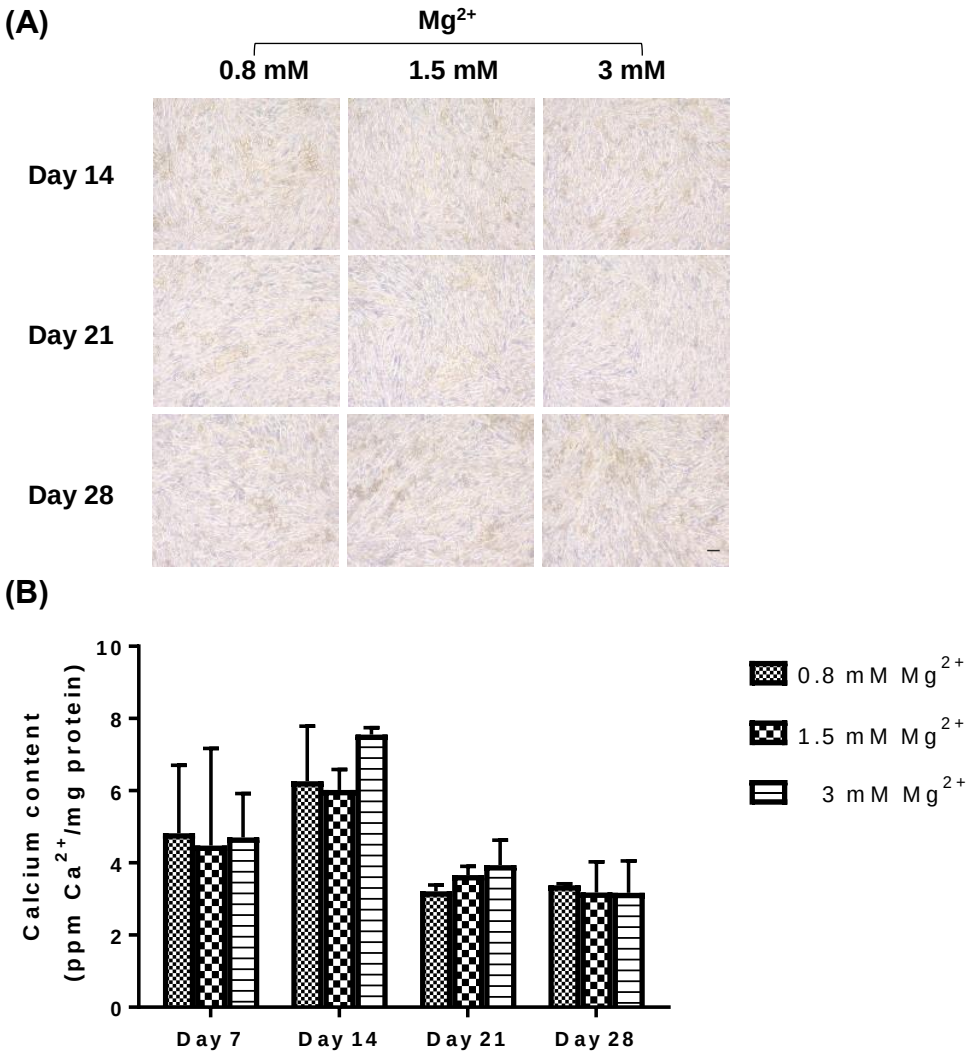

Figure 4.20 Magnesium does not affect MDA-MB-231 cultured in non-calcifying media. Representative images (10X magnification) of Alizarin Red S stained MDA-MB-231 cells cultured for 28 days in standard DMEM media with Mg^{2+} at the indicated concentration (A). Magnesium chloride was used to adjust total Mg^{2+} concentration from basal (0.8 mM) to 1.5 or 3 mM. No significant differences were observed in Alizarin staining or by measurement of calcium content of cell monolayers (B). Each data point represents the mean + SD (N=2). Statistical significance was determined by one-way ANOVA. Scale bar represents 50 µm.

Analysis of ALP activity also revealed a significant influence for Mg^{2+} concentration Cells cultured for 14 days in OC+Dex media experienced a two-fold increase in ALP activity compared to cells grown in control media. This increase was almost totally abolished at 1.5 or 3 mM Mg^{2+} (Fig. 4.21). Increased Mg^{2+} also decreased ALP activity by approximately 50% in control cells, although this did not reach statistical significance.

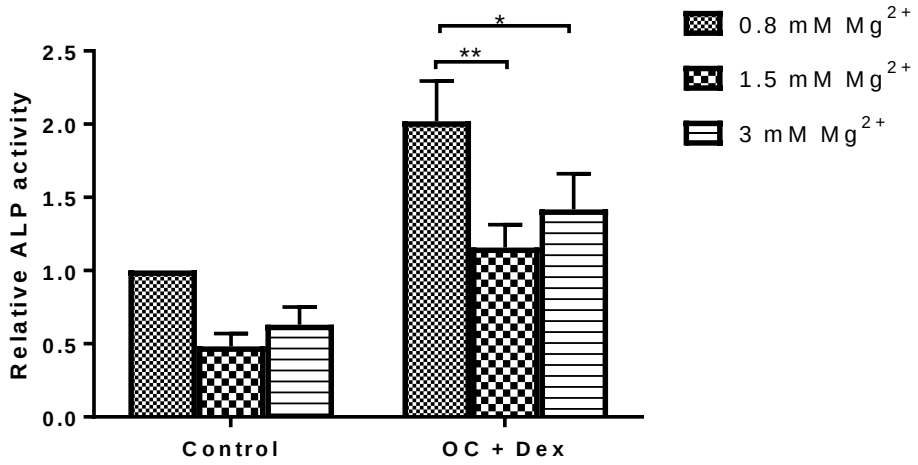

Figure 4.21 Magnesium alters ALP activity in MDA-MB-231 cells. ALP activity of MDA-MB-231 cells cultured for 14 days in control media or OC+Dex supplemented media at the indicated Mg^{2+} concentration. Cells were lysed and ALP activity was measured by incubation with the ALP substrate p-nitrophenyl phosphate (PNPP), monitoring absorbance at 405 nm. ALP activity was normalised to protein content and expressed relative to vehicle-control treated cells. Each data point represents the mean + SD (N=3). Statistical significance was determined by two-way ANOVA *P<0.05.

After demonstrating a clear anti-mineralisation effect for Mg^{2+} in the development of breast calcifications, we next sought to investigate any potential interaction between this protective effect and activity of the TRPM7 channel. TRPM7 exerts a protective effect on several forms of pathological calcification, primarily through its role in Mg^{2+} influx (Montezano et al., 2010, Louvet et al., 2013). To test this, we once again cultured MDA-MB-231 cells with OC+Dex media with increased Mg^{2+} (1.5 mM), and either TRPM7 inhibitor or vehicle control. Similar to previous results, addition of extra Mg^{2+} almost totally abolished calcium deposition, as measured by both Alizarin Red S staining (Fig. 4.22 A) and calcium measurement (Fig. 4.22 B, C). Addition of either TRPM7 inhibitor had no effect on MDA-MB-231 mineralisation and did not attenuate the anti-mineralisation effect of Mg^{2+}. Indeed, higher doses of the two inhibitor compounds even seemed to further decrease deposited calcium compared to Mg^{2+} alone. This is in contrast to other studies which have shown a partial reversal of Mg^{2+}'s anti-mineralisation effect upon inhibition of TRPM7 channel activity (Montezano et al., 2010, Louvet et al., 2013).

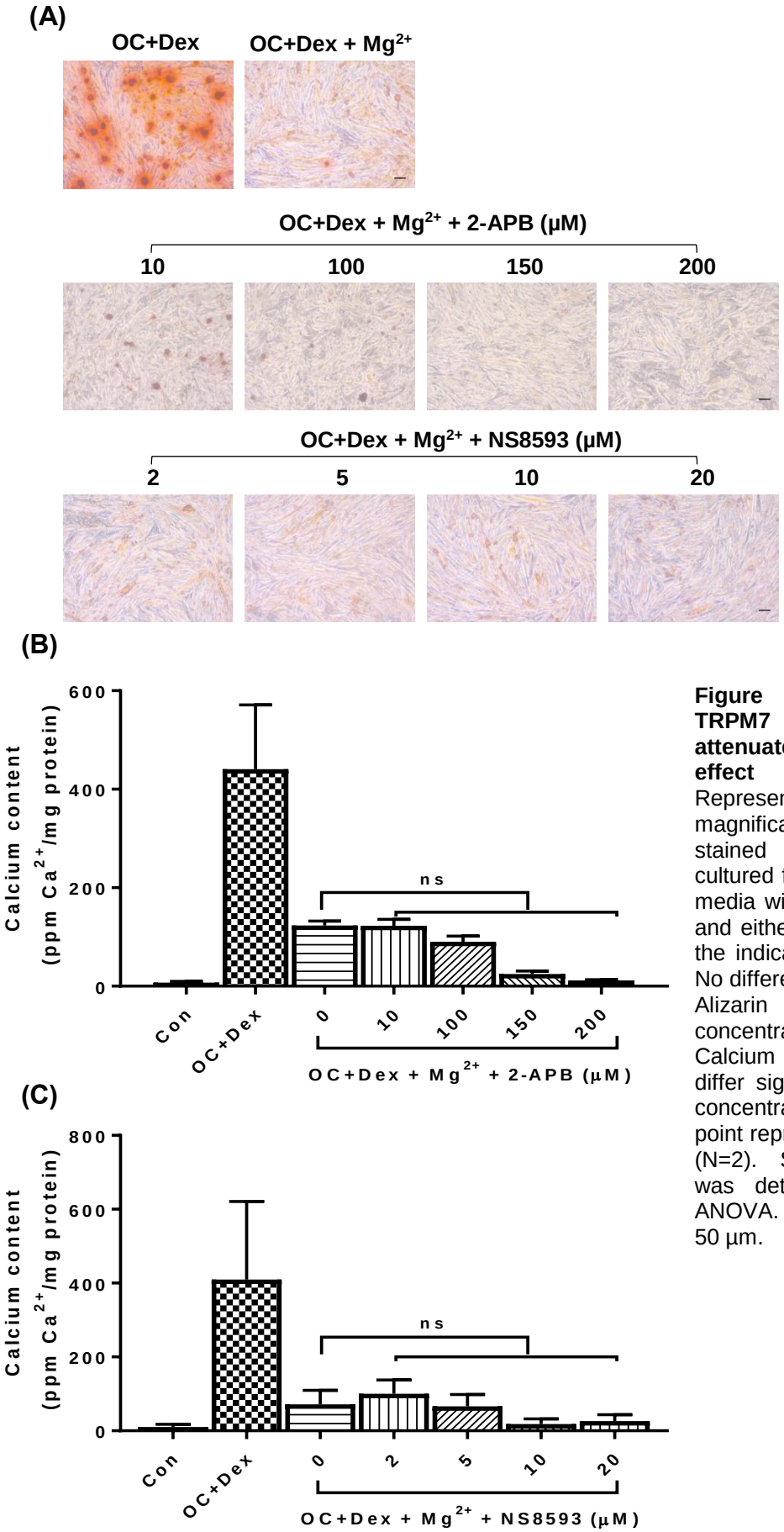

Figure 4.22 Inhibition of TRPM7 channel does not attenuate anti-mineralisation effect of magnesium. Representative images (40X magnification) of Alizarin Red S stained MDA-MB-231 cells cultured for 28 days in OC+Dex media with 1.5 mM magnesium and either 2-APB or NS8593 at the indicated concentration (A). No differences were observed in Alizarin staining at any concentration of either inhibitor. Calcium content also did not differ significantly between any concentration (B). Each data point represents the mean + SD (N=2). Statistical significance was determined by one-way ANOVA. Scale bar represents 50 µm.

We also investigated any potential link between either Mg^{2+} or TRPM7 inhibition and cell proliferation. Previous studies have shown conflicting results on the importance of the TRPM7 channel in regulating breast cancer proliferation (Guilbert et al., 2009, Middelbeek et al., 2012). Analysis of MDA-MB-231 cells cultured in either 1.5 mM Mg^{2+} or 10 µM NS8593 for 72 hours did not reveal any significant differences in proliferation, as measured by MTT assay (Fig. 4.23).

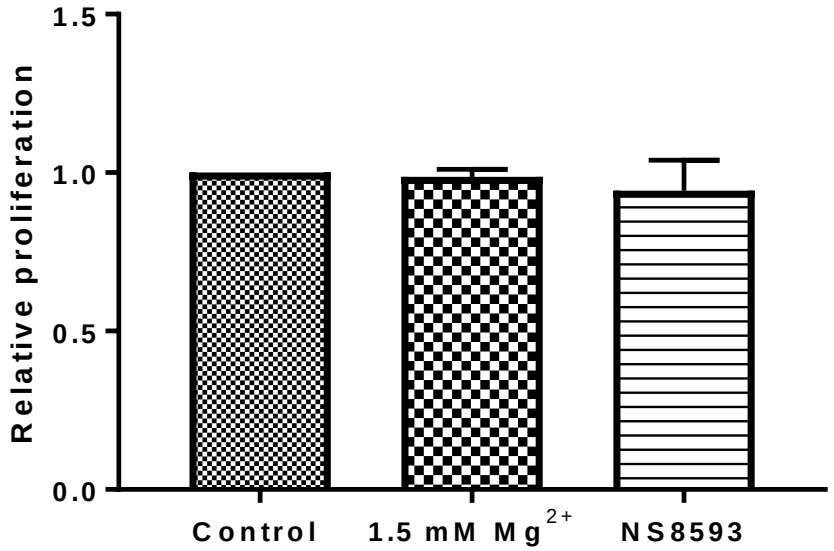

Figure 4.23 MDA-MB-231 proliferation is not affected by magnesium or inhibition of the TRPM7 channel. Proliferation of MDA-MB-231 cells cultured for 48 hours in control media, high-Mg^{2+} media (1.5 mM) or 10 µM NS8593 was measured via MTT assay. No significant difference was observed between any treatment group. Each data point represents the mean + SD (N=3). Statistical significance was determined by one-way ANOVA.

4.2.7 PMCA channels and MDA-MB-231 mineralisation

In addition to Ca^{2+} influx channels such as TRPM7, we also wanted to investigate a possible role for Ca^{2+} efflux channels. A recent study utilising a modified version of our model demonstrated a role for the secretory pathway calcium ATPase (SPCA) channels SPCA1 and SPCA2 in the formation of microcalcifications (Dang et al., 2017). SPCA pumps use ATP hydrolysis to drive active Ca^{2+} transport into the Golgi compartment (Vandecaetsbeek et al., 2011). Intracellular Ca^{2+} levels are also regulated by a second set of ATPase pumps, the plasma membrane Ca^{2+} ATPases (PMCA1 – PMCA4) family which exports Ca^{2+} through the plasma membrane to the extracellular environment.

PMCA2 is essential for lactation through its role in pumping Ca^{2+} ions into the milk duct (Reinhardt et al., 2004) and has also previously been suggested to play a role in the development of microcalcifications, likely via promoting the accumulation of Ca^{2+} within the ductal lumen (Cross et al., 2014).

To test this hypothesis, we performed siRNA knockdown of PMCA1 and PMCA2. Knockdown efficiency, as confirmed by qPCR 72 hours post-transfection, was approximately 75% and 65% for PMCA1 and PMCA2 respectively (Fig. 4.24 A, C). Following transfection, siRNA treated cells were switched to OC+Dex media for 14 days before assessment of mineralisation. Cells treated with PMCA1-siRNA did not display any alteration in calcium deposition compared to control-siRNA treated cells (Fig. 4.24 B). However, cells treated with PMCA2-siRNA displayed approximately 30% decreased mineralisation compared to control-siRNA treated cells (Fig. 4.24 D). Knockdown of PMCA2 was also observed to result in markedly lower Alizarin Red S staining (Fig. 4.24 D).

Finally, we examined expression of both PMCA1 and PMCA2 in mineralising MDA-MB-231 cells. Although we did observe a strong trend towards increased PMCA1 expression in cells grown with OC+Dex media, these did not reach statistical significance (Fig. 4.25 A). We also did not observe any significant differences in PMCA2 expression (Fig. 4.25 B)

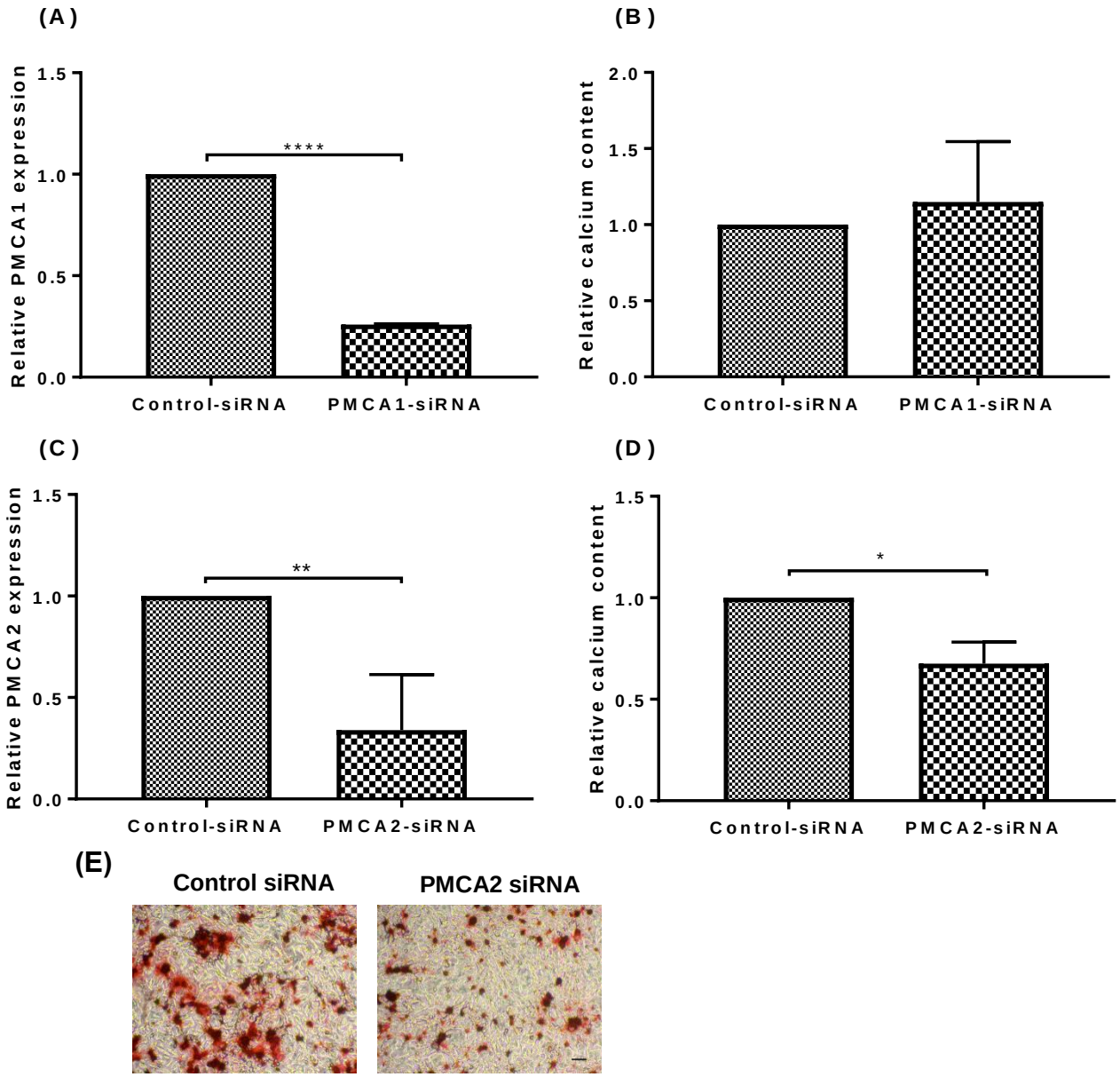

Figure 4.24 PMCA1/2 and MDA-MB-231 mineralisation. qPCR analysis of knockdown efficiency in MDA-MB-231 cells transfected with PMCA1 (A) or PMCA2 (C) targeting or a negative-control siRNA. Calcium content of MDA-MB-231 cells cultured for 14 days in OC+Dex media revealed a significant decrease in cells transfected with PMCA2-siRNA (D) but not PMCA1-siRNA (C). Calcium content was analysed by OCP, normalised to protein content, and expressed relative to control values. Reduced mineralisation in PMCA2-siRNA treated cells was confirmed by Alizarin Red S staining, representative image shown at 10X magnification (E). Each data point represents the mean + SD (PMCA1 calcium N=4, qPCR N=2, PMCA2 calcium + qPCR N=3). Statistical significance was determined by t-test. *P<0.05, ****P<0.0001. Scale bar represents 50 µm.

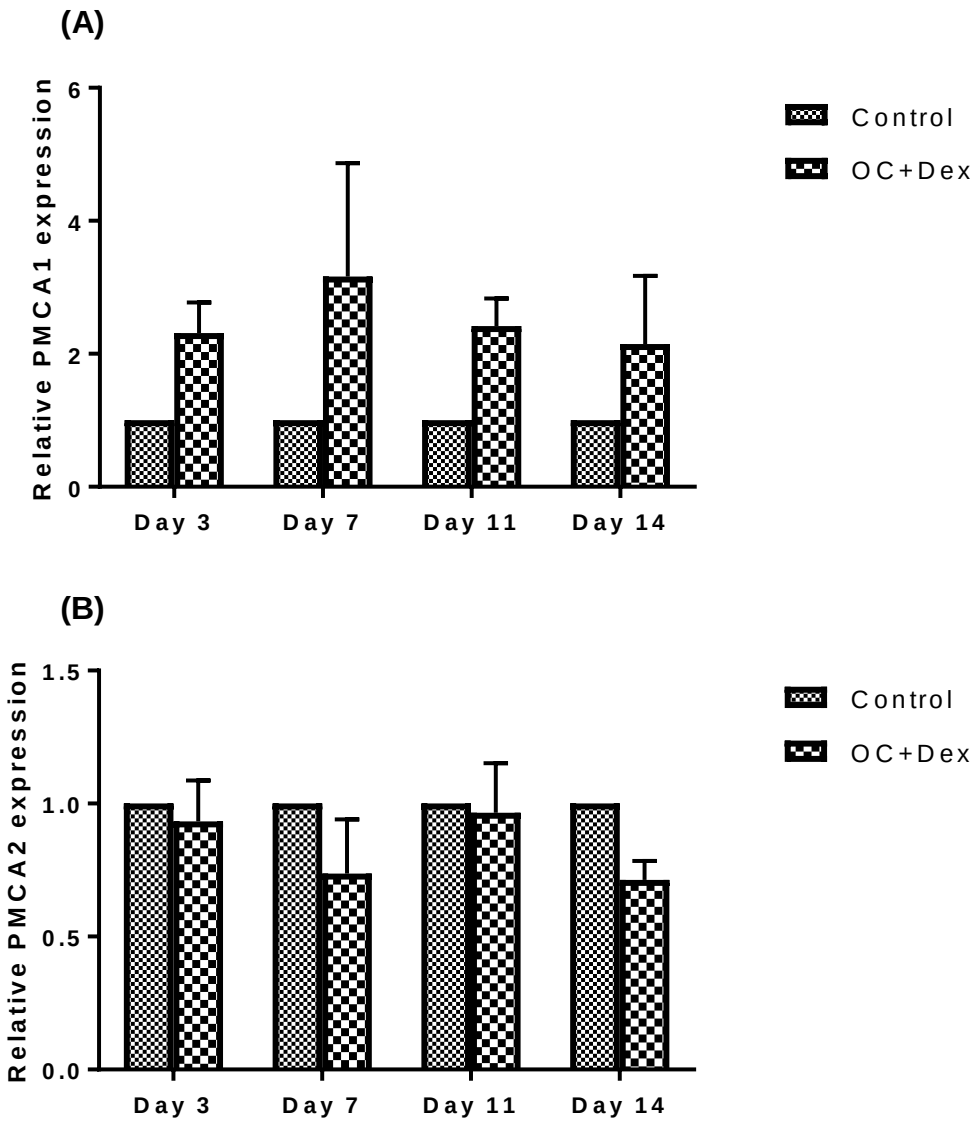

Figure 4.25 Expression of PMCA1/2 in mineralising MDA-MB-231 cells. Expression of PMCA1 (A) and PMCA2 (B) in MDA-MB-231 cells cultured for 14 days in OC+Dex supplemented media was examined by qPCR at the indicated time points. Each data point represents the mean + SD (N=4). Statistical significance was determined by two-way ANOVA.

4.3 Discussion

In a recent review of Ca^{2+} signalling pathways in breast cancer, Cross et al. proposed a mechanism of microcalcification formation, involving a dysregulation of Ca^{2+} transport in conjunction with “abnormal expression of bone matrix proteins” (Cross et al., 2014). This potential model is supported by numerous patient studies highlighting increased expression of bone associated proteins including BMP2, osteonectin, osteopontin, and bone sialoprotein (Bellahcène and Castronovo, 1995, Bellahcène et al., 1994, Scimeca et al., 2014, Oyama et al., 2002) as well as the Ca^{2+} channels TRPC1 and TRPM7 (Mandavilli et al., 2013) in the vicinity of microcalcifications. However, this theory remains untested. The aim of this chapter therefore was to utilise our *in vitro* model to explore potential roles for both markers of physiological osteoblastic mineralisation, and cellular Ca^{2+} transport proteins in the development of breast calcifications.

We began with BMP2, which has previously been shown to promote mineralisation of breast cancer cells in studies from both our lab and other groups (Cox et al., 2012b, Dang et al., 2017). Our findings were in agreement with these previous studies, with MDA-MB-231 cells cultured with 100 ng/mL of rh-BMP2 displaying a 2.4-fold increase in deposited calcium (Fig. 4.2 B) and 50% greater ALP activity (Fig. 4.3). A novel finding from our BMP2 studies was the lack of positive mineralisation in the non-mineralising MCF-7 cell line when BMP2 was included in their growth media (Fig. 4.4). These results indicate that although BMP2 promotes and increases mineralisation in cell lines that are capable of undergoing *in vitro* mineralisation, it does not in of itself induce their formation. MDA-MB-231 cells have previously been shown to produce significantly greater amounts of endogenous BMP2 than MCF-7 cells (Arnold et al., 1999).

The role of BMP2 in breast cancer is complex and incompletely understood, with much contradiction within the literature. Stimulation of MCF-7 and MDA-MB-231 cells with BMP2 has been shown to inhibit proliferation, promote apoptosis and decrease their tumour formation in a nude mice xenograft model (Chen et al., 2012, Ghosh-Choudhury et al., 2000b). Other studies have also shown BMP2 to exert a potent anti-proliferative effect on breast cancer cells (Ghosh-Choudhury et al., 2000a, Arnold et al., 1999, Soda et al., 1998). Although these results suggest that BMP2 acts as a tumour suppressor, other studies have found contradictory results.

A recent study by Huang et al. provided a comprehensive analysis of induction of both EMT and cell stemness in BMP2 stimulated MCF-7 cells, demonstrating a significant increase in tumourigenic properties (Huang et al., 2017). Noting the discrepancy between their findings of increased tumour growth following BMP2 stimulation versus the decreased growth observed in other studies (Chen et al., 2012, Ye et al., 2013), the authors noted that induction of apoptosis may play a more important role at an early stage of tumour development, with a low number of tumour cells, before development of EMT and stemness take over as the dominant factor in tumour response to BMP2 stimulation. In addition, BMP2 overexpression promotes migration and invasion in the MCF-7 cell line, as well as supporting estrogen-independent growth in a xenograft model (Clement et al., 2005). Interestingly, the BMP2 overexpressing MCF-7 sub-clones were observed to form calcified deposits in xenograft models, further highlighting the importance of BMP2 in the development of microcalcifications. A recent literature review of the often-contradictory studies on the role of BMP2 in tumour growth noted that studies showing a tumour promoting effect for BMP2 tended to be more comprehensive, examining both “the invasiveness and migration properties of tumour cells in addition to proliferation” and concluding that the overall balance of data supported a pro-tumourigenic role for BMP2 (Tian et al., 2017).

Although other studies have highlighted a pro-mineralisation effect of BMP2 in breast calcification (Cox et al., 2012b, Dang et al., 2017), this is the first study to demonstrate its upregulation during formation of microcalcifications. If BMP2 does indeed exert a pro-tumourigenic effect on breast tumours, the increase in BMP2 expression we observed (Fig. 4.1) in mineralising MDA-MB-231 cells may be clinically relevant. A study by Tan et al. provided strong evidence for a link between expression of bone associated genes and acquisition of a bone metastatic capability (Tan et al., 2016). Co-stimulation of breast cancer cells with fibroblast conditioned media and BMP2 induced an EMT effect resulting in generation of osteoblast-like breast cancer cells. This phenotype was accompanied by upregulation of a host of bone associated genes including RUNX2 and acquisition of an osteomimetic phenotype, as well as an increase in proliferation, drug resistance and migration towards osteoblast cells, indicating a propensity towards bone metastasis.

As an increase in RUNX2 was also observed in mineralising MDA-MB-231 cells (Fig. 4.9), alterations in gene expression observed within our model leading to deposition of calcium may alter cellular metastatic ability, although this theory has not been directly examined and will require significant further work.

To the best of our knowledge, no studies have looked at a possible link between the presence of microcalcifications in primary breast tumours and the later development of bone metastases, it is tempting to speculate that upregulation of bone associated proteins within mineralising breast tumour cells may result in a bone-homing phenotype and an increased capability to spread and thrive within the skeletal system. Interestingly, previous studies from our lab found that 4T1.2, a sub-clone of the murine 4T1 cell line that preferentially metastasizes to the bone (Lelekakis et al., 1999), more readily developed calcifications when injected into the mammary fat pad of BALB/c mice than their parental 4T1 line (Cox et al., 2012a).

BMP2 also remains the only mineralisation associated gene with direct *in vivo* evidence as a promoter of microcalcification formation. In addition to the previously mentioned study of BMP2-overexpressing MCF-7 cells (Clement et al., 2005), results from Liu et al. demonstrated that subcutaneous implantation of human-BMP2 transfected R3230 rat tumour cells into the mammary fat pad of a Fischer 344 rat results in large areas of calcification in all mice implanted with the transduced cells (Liu et al., 2008). Interestingly, when rats were implanted bilaterally (one fat pad with transfected cells, the other with untransfected), calcifications were observed not only in the fat pad with BMP2 expressing cells, but also in the untransfected side, indicating that BMP signalling can act humorally to induce microcalcification formation. A second study by the same group demonstrated that transfection wasn't necessary: a single intraperitoneal injection of BMP2 into Fischer 344 rats bearing syngeneic R3230 breast tumours was sufficient to induce microcalcification formation in a dose and time dependent manner (Liu et al., 2010).

In addition to BMP2, we also examined the role of the osteogenic transcription factor RUNX2 in formation of microcalcifications. RUNX2 acts as a "master regulator" of chondrocyte and osteoblast differentiation (Komori, 2009) and also appears to be an important driver of pathological calcification, as studies have shown high RUNX2 expression in calcified atherosclerotic lesions (Byon et al., 2011). In addition, RUNX2-deficient vascular smooth-muscle cells fail to mineralise both *in vitro* and *in vivo* (Lin et al., 2015, Sun et al., 2012).

RUNX2 is highly expressed in triple-negative breast tumours and appears to act as marker within this subtype (McDonald et al., 2014, Das et al., 2009). We found significantly greater RUNX2 expression in the triple-negative MDA-MB-231 cell line than SKBR3 or MCF-7, in agreement with other studies (Leong et al., 2010). RUNX2 expression was further increased following stimulation with OC+Dex media (Fig. 4.9). Previous work from our group examined expression of RUNX2 in mineralising 4T1 murine breast cancer cells, but no increase in expression was observed (Cox et al., 2012b). This difference may potentially be explained by the murine origin of the cell line utilised in previous work, compared to the exclusively human derived cell lines used in our studies. This therefore represents the first report of an increase in this vital osteogenic transcription factor in the context of breast calcification.

In addition to changes in expression, we also sought to demonstrate a functional role for RUNX2 in the formation of microcalcifications. Although we did not observe a total inhibition of calcification in siRNA treated cells (20% reduction in comparison to control siRNA treated cells, Fig. 4.10), we assessed mineralisation a relatively long time period after transfection (72 hours transfection & 14 days in OC+Dex media), by which point RUNX2 expression was likely to have recovered. Repeating the experiment with a longer acting knockdown strategy, like a shRNA containing plasmid may yield more conclusive results. Unexpectedly, despite the decrease in calcification observed in MDA-MB-231 with suppressed RUNX2 expression, we did not observe any increases in cells transfected with a RUNX2 expressing plasmid (Fig. 4.11). This may be due to the already high level of RUNX2 expression in MDA-MB-231 cells (Fig. 4.8).

In breast cancer, RUNX2 significantly influences development of metastases. Knockdown of RUNX2 in MDA-MB-231 cells has a significant effect on their tumourigenic properties including reductions in metalloproteinase expression, migration and invasion whilst RUNX2 overexpression in MCF-7 cells increases migration (Leong et al., 2010, Pratap et al., 2005, Mendoza-Villanueva et al., 2010). The presence of mammographic calcifications has been associated in some studies with an increased risk of positive lymph-node status (Cen et al., 2017a, Tabar et al., 2004, Jiang et al., 2011). In addition, stimulation of breast cancer cells with hydroxyapatite nanoparticles increases migration in a scratch wound assay (Cox et al., 2012a) and upregulates metalloproteinase activity (Morgan et al., 2001), two key markers of increased migration and invasion.

If our *in vitro* findings of increased RUNX2 in mineralising breast cancer cells are truly indicative of the *in vivo* mechanism of microcalcification formation, altered RUNX2 signalling may play a role in the increased invasion capability of mineralisation associated tumours.

In addition to the mineralisation promoting bone associated genes BMP2 and RUNX2, we also investigated potential roles for two genes typically recognised as anti-mineralisation factors. Both ENPP1 and MGP were observed to be significantly decreased in mineralising MDA-MB-231 cells (Fig. 4.5, 4.7), indicating a shift towards a mineralisation-capable phenotype. MGP is a vitamin K-dependent calcification inhibitor, which inhibits mineralisation through a variety of mechanisms including binding Ca^{2+} ions, direct inhibition of crystal growth and modulation of osteogenic signalling pathways (Proudfoot and Shanahan, 2006). The importance of MGP in preventing ectopic mineralisation is evidenced by *Mgp*$^{-/-}$ mice, which develop extensive vascular calcification and typically die after 2 months (Luo et al., 1997, El-Maadawy et al., 2003). MGP acts as a tumour suppressor gene in ER+ breast cancer as loss of MGP expression increases proliferation in MCF-7 cells (Tiago et al., 2016) whereas high expression is associated with increased RFS in patients with luminal breast tumours (Tuo and Ye, 2017). Part of the anti-mineralisation effect of MGP comes from its ability to bind to and modulate BMP2 (Zebboudj et al., 2002). Therefore, a decrease in MGP expression in breast tumours may limit their capacity to control the previously discussed pro-tumourigenic effects of BMP2.

In the previous chapter, we demonstrated the vital role of ALP activity in our *in vitro* model. ALP promotes mineralisation by degrading PPi, which simultaneously increases levels of free Pi and deceases concentrations of the mineralisation inhibitor PPi. The primary enzyme responsible for maintenance of PPi concentrations is the transmembrane ENPP1 protein which produced PPi through hydrolysis of extracellular nucleotide triphosphates, most notably ATP. Similar to *Mgp*$^{-/-}$ mice, *Enpp1*$^{-/-}$ mice display widespread ectopic mineralisation (Hajjawi et al., 2014). PPi inhibits mineralisation through binding to hydroxyapatite crystals and preventing further growth, as well as upregulating expression of the mineralisation inhibitor protein osteopontin (Addison et al., 2007).

Interestingly, ENPP1 can also positively regulate mineralisation in certain contexts as osteoblast specific deletion of ENPP1 results in improperly differentiated and inactive osteoblasts (Nam et al., 2011). Stimulation of MDA-MB-231 cells with OC+Dex media was observed in our studies to significantly reduce expression of ENPP1 (Fig. 4.5 B). The reduced ENPP1 activity we observed in mineralising breast cancer cells would result in a lowered extracellular concentration of PPi and a loss of its inhibitory effect. In combination with the increased ALP activity demonstrated in the previous chapter, this decrease in ENPP1 activity acts in tandem by simultaneously decreasing the amount of PPi produced and increasing the enzymes necessary to degrade any PPi that is made.

The importance of PPi levels in regulating development of breast mineralisations is highlighted by the strong inhibition of calcium deposition in MDA-MB-231 cells cultured in OC+Dex media with exogenous PPi (Fig. 4.6A). In addition, exogenous PPi completely blocked the increase in ALP activity observed in OC+Dex stimulated MDA-MB-231 cells (Fig. 4.6 B). These results show that PPi exerts a strong anti-mineralisation effect in our *in vitro* model, similar to its role in other models of pathological calcification. MDA-MB-231 cells have previously been shown to express a significantly higher level of ENPP1 than both MCF-7 and SKBR3 cells (Lau et al., 2013). Although we did not test this hypothesis, it is possible that the high expression of ENPP1 in the MDA-MB-231 cell line would result in a significant production of extracellular PPi, initially forming an inhibitory roadblock to mineralisation. However, as we demonstrated by qPCR, OC+Dex stimulation appears to be a potent suppressor of ENPP1 expression, thus overcoming this initial inhibition and allowing for mineralisation to proceed.

In this way, results from our qPCR studies show that onset of mineralisation in the MDA-MB-231 cell line is preceded not only by upregulation of mineralisation promoting factors (ALP, BMP2, RUNX2) but also by a concurrent downregulation of inhibitory factors (MGP, ENPP1). High ENPP1 expression may also partly explain the requirement of dexamethasone for MDA-MB-231 mineralisation in contrast to SKBR3 cells, which express lower ENPP1 and mineralise in OC media alone. However, varying expression of ENPP1 cannot be the primary cause behind our finding of positive mineralisation being restricted to certain cell lines, as the (non-mineralising) MCF-7 cell line also expresses low levels of ENNP1.

In contrast to MGP, in which decreased expression is associated with a worse prognosis (Tuo and Ye, 2017), the decrease in ENPP1 expression we observe in our model may decrease the tumourigenic capability of MDA-MB-231 cells. ENPP1 is a powerful driver of invasion in breast cancer cells and is highly upregulated in breast cancer cell lines capable of forming bone metastases (MDA-MB-231, MDA-MB-468) relative to cell lines that do not form bone metastases (MCF-7, SKBR3), (Lau et al., 2013). In addition, loss of ENPP1 repression by miR-27b increases drug resistance and cancer stem cell properties in MCF-7 cells (Takahashi et al., 2015). In summary, ENPP1 appears to act as an inhibitor of microcalcification formation via production of PPi, and its differential expression between cell lines may play a role in response to mineralisation promoting conditions.

In addition to exploring functional roles for bone associated proteins in the development of breast calcifications, our second aim for this chapter was to examine how alterations in the Ca^{2+} handling system of breast cancer cells could potentially contribute to mineralisation. Ca^{2+} plays diverse roles in tumour biology and can act in either a pro- or anti-tumourigenic capacity. Increased intracellular Ca^{2+} is an important step in induction of apoptosis and increased Ca^{2+} efflux capacity has been linked to drug resistance (Dubois et al., 2013). On the other hand, Ca^{2+} influx can also promote tumourigenic effects including EMT, (Davis et al., 2014), increased proliferation (Guilbert et al., 2009) and invasion (Meng et al., 2013). High Ca^{2+} levels increase proliferation in MCF-7 cells through the TRPC1 channel (El Hiani et al., 2009a, El Hiani et al., 2009b). This channel has previously been shown to be highly expressed in breast tumours with associated microcalcifications (Mandavilli et al., 2013). Although we did not explore a functional role for the TRPC1 channel in cell mineralisation, it is interesting to note that we did observe an increase in TRPC1 expression in MDA-MB-231 cells cultured in OC+Dex media (Fig. 4.14). Ca^{2+} influx may also play a role in the upregulation of inflammatory markers observed in hydroxyapatite stimulated breast cancer cells (Morgan et al., 2001, Morgan et al., 2004), a hypothesis that will be further explored in the next chapter.

High intake of dietary calcium appears to be protective against breast cancer, as a recent meta-analysis found evidence of an inverse dose–response association between calcium intake and breast cancer, especially in premenopausal women (Hidayat et al., 2016).

Although we could not find any data in the literature on a potential link between altered serum Ca^{2+} levels and mammary calcifications, increased serum Ca^{2+} levels may promote development of other forms of pathological calcification (Wang et al., 2010a). We did observe a significant increase in mineralisation in cells cultured in 2.7 mM versus 1.8 mM Ca^{2+} (Fig. 4.12). Although this finding of increased calcification in cells cultured in a high Ca^{2+} environment is not surprising, it was interesting to note that increased Ca^{2+} did not induce mineralisation in cells cultured in OC without dexamethasone, indicating that mineralisation cannot proceed based on a simple increase in available extracellular Ca^{2+} without a source of Pi.

Although previous work from our lab established a vital role for influx of Pi ions via type III Na(+)/Pi channels Pit-1 and Pit-2 in the development of microcalcifications (Cox et al., 2012a), the significance of Ca^{2+} influx has not been previously explored. Kapustin et al. reported that mineralisation in VSMCs can be inhibited by blocking intracellular Ca^{2+} accumulation either by the intracellular Ca^{2+} chelator BAPTA-AM or the T-type Ca^{2+} channel blocker nickel chloride (Kapustin et al., 2011). We observed similar effects, with significant reductions in calcium deposition in cells treated with BAPTA-AM (Fig. 4.13). Interestingly, ALP activity was also decreased in BAPTA-AM treated cells, indicating that ALP expression may be Ca^{2+} regulated in MDA-MB-231 cells. Additionally, hydroxyapatite crystals have been shown to induce Ca^{2+} influx into a variety of cell types (Nguyen et al., 2012, Halverson et al., 1998, McCarthy et al., 1998, Ewence et al., 2008). If a rise in intracellular Ca^{2+} is involved in mineralisation, then the initial deposition of hydroxyapatite could promote intracellular Ca^{2+} accumulation, creating a self-sustaining loop and possibly inducing osteogenic changes in nearby cells.

The decreased mineralisation observed in BAPTA-AM treated cells indicates that intracellular influx and accumulation of Ca^{2+} is an important step in the initiation of cell mineralisation, similar to previous reports. A wide range of possible Ca^{2+} transport channels may be involved in this intracellular flow of Ca^{2+}, but we chose to focus on the TRPM7 channel, which was previously shown to be upregulated in breast tumours with associated calcifications (Mandavilli et al., 2013). Deposition of Ca^{2+} in our MDA-MB-231 model was significantly decreased by two different TRPM7 channel inhibitors (Fig. 4.15, 4.16). and also by siRNA knockdown (Fig. 4.18) of the channel.

Interestingly, many of the previous studies on TRPM7 and calcification have shown it to exert a protective effect. TRPM7 is a non-selective cation channel, permeable to a range of ions and acts as an important regulator of Mg^{2+} homeostasis (Ryazanova et al., 2010). This role in Mg^{2+} influx seems to be essential to TRPM7 mediated protection.

In vitro studies of vascular calcification have shown that increasing Mg^{2+} concentration upregulates expression of calcification inhibitors including MGP and osteopontin, as well as decreasing RUNX2 expression, suppressing ALP activity and leading to an overall reduction in levels of deposited calcium (Xu et al., 2015a, Montezano et al., 2010, Montes de Oca et al., 2014). Blockade of TRPM7 activity with the one of the same inhibitors used in our studies (2-APB) attenuates many of these anti-mineralisation effects and allows for calcification to proceed. In agreement with previous studies of other forms of pathological calcification, we found a potent anti-mineralisation effect of Mg^{2+} in our *in vitro* model, with an almost total suppression of calcium deposition in MDA-MB-231 cells cultured in either 1.5 or 3 mM Mg^{2+} (Fig. 4.19), as well as significant reductions in ALP activity (Fig. 4.21).

However, the anti-mineralisation effect of Mg^{2+} did not appear to be TRPM7 dependent in our model, as inhibition of TRPM7 channel did not reverse the suppression of mineralisation observed in MDA-MB-231 cells grown in OC+Dex media with increased Mg^{2+} levels (Fig. 4.22). Although this finding is in disagreement with some of the literature, recently Zhang et al. demonstrated a pro-calcification effect for TRPM7 in VSMCs (Zhang et al., 2017). VSMCs grown in a calcifying media containing the same concentration of β-glycerophosphate used in our studies (although without dexamethasone) displayed a dose-dependent increase in calcification when stimulated with IL-18. This increase was completely blocked by either the TRPM7 inhibitor 2-APB or siRNA knockdown of TRPM7. In addition, many of the key findings from this study match those of our own. For example, not only was TRPM7 expression increased by the presence of calcifying media but the addition of 2-APB decreased both calcification and ALP activity. In summary, although previous studies have tended to show an anti-mineralisation effect of TRPM7 in vascular calcification we have shown strong evidence of a pro-calcification effect for the channel in the context of breast microcalcifications.

Some studies have suggested that breast cancer patients are likely to have lower serum Mg^{2+} levels than control (Abdelgawad et al., 2015, Sartori et al., 1992). Decreased serum concentrations would result in a reduction of the anti-mineralisation effect of Mg^{2+} and may promote the development of microcalcifications. Studies in vascular calcification have drawn similar conclusions, with significantly lower serum Mg^{2+} levels found in patients with calcifications than those without (Ishimura et al., 2007). Outside its role in inhibiting their formation, several recent studies have shown other interesting links between Mg^{2+} and microcalcifications. Scimeca et al. used energy dispersive x-ray microanalysis to probe the chemical composition of microcalcifications in a group of patients with either benign or malignant breast lesions and identified significant amounts of magnesium substituted hydroxyapatite, a novel form of microcalcification which was only found in malignant lesions (Scimeca et al., 2014). This was followed by a study using X-ray diffraction, which found small amounts of the magnesium-containing calcium phosphate crystal whitlockite in calcification samples from breast cancer patients (Scott et al., 2016). The percentage of whitlockite found in samples increased significantly from benign to *in situ* lesions to invasive tumours. The clinical significance of these findings are not yet fully understood although a recent study found increased osteogenic differentiation of mesenchymal stem cells cultured on synthetic whitlockite nanoparticles (Kim et al., 2017), suggesting that an initial deposition of whitlockite by breast cancer cells could promote further development of microcalcifications.

Whitlockite is formed under acidic conditions (Jang et al., 2014). As tumour cells are known to acidify their extracellular environment (Kato et al., 2005), altered pH conditions in the tumour vicinity could promote the development of whitlockite deposits and may explain the greater concentration of this novel form of microcalcification in invasive versus benign lesions. Interestingly, a recent report by Zheng et al. showed that inhibition of carbonic anhydrase 1 (CA1) partially inhibits mineralisation in 4T1 cells (Zheng et al., 2015). As many carbonic anhydrase isoforms are important regulators of tumour pH (Kato et al., 2005), increased activity of these enzymes may be important in creating the extracellular conditions conducive to formation of whitlockite deposits.

Carbonic anhydrase activity may also promote development of hydroxyapatite calcifications indirectly by facilitating calcium carbonate deposition which can act as a seed for subsequent hydroxyapatite formation (Adeva-Andany et al., 2015).

We did observe a significant reduction in ALP activity in cells cultured under high-Mg^{2+} conditions, which is in agreement with previous studies (Xu et al., 2015a), and is likely to form part of Mg^{2+}'s protective effect. However, as Mg^{2+} also inhibited mineralisation in cells cultured with inorganic Pi (a non ALP-dependent model of mineralisation), this cannot be the sole mechanism responsible. We also did not find Mg^{2+}'s protective effect in our model to be dependent on the TRPM7 channel, in contrast to several previous studies (Montezano et al., 2010, Sonou et al., 2017).

Finally, we looked at potential role for the PMCA1 and PMCA2 Ca^{2+} transporters. Although siRNA knockdown of PMCA1 did not alter calcium deposition in MDA-MB-231 cells, knockdown of PCMA2 decreased calcium deposition by approximately 30% (Fig. 4.24D). Although we were unable to further investigate any potential mechanisms for PMCA2 mediated calcification, it is of interest that expression of PMCA2 is strongly correlated with HER2, and PMCA2 regulates proliferation, HER2 signalling and localization as well as proliferation in the HER2+ SKBR3 cell lines (Jeong et al., 2016). As microcalcifications are most commonly found in HER2+ tumours (Cen et al., 2017a), the association between PMCA2 and HER2 further supports a possible role for PMCA2 in the development of microcalcifications.

Interestingly, in the course of this chapter we have shown evidence for the involvement of both Ca^{2+} influx (TRPM7) and Ca^{2+} efflux (PMCA2) channels. TRPM7 is expressed in the ductal epithelial layer, and is increased in tumour compared to normal tissue (Ouadid-Ahidouch et al., 2012, Guilbert et al., 2009). We could not find any reports in the literature on the cellular localisation of TRPM7 in breast epithelial cells, but if TRPM7 were to be expressed at the basolateral side then it could facilitate Ca^{2+} entry and accumulation within the cell before PMCA2 pumps the Ca^{2+} back out of the cell, into the ductal lumen. In this way, both Ca^{2+} influx (TRPM7) and efflux (PMCA2) channels could be involved in transepithelial movement of Ca^{2+} across the epithelial cell barrier and into the lumen of the duct, facilitating formation of calcifications. This transepithelial flow of Ca^{2+} would, to some extent, mimic the normal physiological function of breast tissue, lactation.

Calcifications can also sometimes be found during lactation (Joshi et al., 2013), when breast epithelial cells undergo considerable remodelling of tissue architecture and increased expression of Ca^{2+} transport proteins.

Following entry to the epithelial cell layer at the basolateral side, Ca^{2+} is either directly exported out of the cell into the ductal lumen by PMCA2 or diverted into the Golgi system by two the secretory pathway calcium-ATPases, SPCA1 and SPCA2, before release via exocytosis (VanHouten et al., 2007). A recent study by Dang et al. showed that overexpression of SPCA proteins significantly increases calcium deposition in breast cancer cells (Dang et al., 2017). Although our findings of a role for PMCA2 in MDA-MB-231 mineralisation are preliminary, it is of interest that both our group and others have now shown evidence for a pro-mineralisation effect of Ca^{2+} channels known to be important in lactation. Although we did not examine changes in intracellular Ca^{2+} concentration, measurement of any such changes may shed light on the precise role of intracellular Ca^{2+} levels on the development of microcalcifications. Similar approaches have been used to demonstrate increased cytosolic Ca^{2+} in models of vascular calcification (Kapustin et al., 2011, Rodenbeck et al., 2017).

Cross et al. recently proposed that microcalcifications could arise from a combination of abnormal expression of bone associated proteins combined with altered Ca^{2+} secretion in the absence of Ca^{2+} buffer proteins (Cross et al., 2014). In this chapter, we have shown evidence in support of this theory, with altered expression patterns observed in several key calcification inhibitors and promoters. Although many of these factors have previously been hypothesised to play a role in mammary calcification, this represents the first direct *in vitro* evidence in their favour and further supports the concept of an active, cell mediated process underlying the formation of breast microcalcifications.

4.4 Summary and conclusions

In conclusion, our main findings from this chapter are as follows;

- BMP2 is upregulated in OC+Dex treated MDA-MB-231 cells and promotes ALP activity and mineralisation.
- PPi is an effective inhibitor of breast cancer mineralisation. Decreased ENPP1 expression in mineralising cells may lead to lower levels of this important inhibitor molecule.
- RUNX2 is highly expressed in MDA-MB-231 cells and is further increased by OC+Dex. Knockdown of RUNX2 expression in MDA-MB-231 cells decreases calcification although overexpression by a RUNX2-expressing plasmid does not have any significant effect.
- TRPM7 promotes formation of MDA-MB-231 mineralisation, likely by supporting intracellular Ca^{2+} accumulation.
- Increased Mg^{2+} levels strongly inhibit MDA-MB-231 ALP activity and mineralisation. This effect is not dependent on TRPM7 activity.
- Knockdown of PMCA2 decreases formation of microcalcifications.

Chapter 5.0

Inflammation and cancer stemness: Investigating potential tumour promoting effects of microcalcifications

5.1 Introduction

5.1.1 Tumour promoting effects of microcalcifications

The presence of mammographic calcifications has been linked to a variety of negative prognostic factors, including tumour grade, lymph node involvement and risk of recurrence (Table 1.2). In particular, studies from Tabar et al. have shown an unusually aggressive nature for small tumours presenting with associated calcifications (Tabár et al., 2000, Tabar et al., 2004). One potential explanation for this association is a direct stimulatory effect of calcifications on the tumour and/or surrounding tissue.

In the previous two chapters, we showed altered expression of a number of genes in mineralising breast cancer cells. Although most of these genes are most commonly studied within the context of mineralisation, they have all been found to also play active roles in regulation of breast tumourigenesis. For example, we found high expression of RUNX2 in MDA-MB-231 (Fig. 4.8) which was further increased following 72 hours culture in OC+Dex media (Fig. 4.9). Although best known as a master-regulator of osteoblast differentiation, RUNX2 expression in breast tumours has also been linked to tumour invasion and metastasis (Wysokinski et al., 2015). It is possible that the altered expression profile we observed in mineralising breast cancer cells could affect tumour behaviour and promote a more aggressive phenotype. This theory is supported by increased expression of several proteins known to promote tumour progression in breast tumours with associated calcifications (Scimeca et al., 2014, Bellahcène and Castronovo, 1995, Bellahcène et al., 1994).

A direct effect of calcifications on the tumour is also possible as stimulation of breast cancer cells with exogenous hydroxyapatite (HA) nanoparticles results in upregulation of numerous inflammatory mediators, including COX2, prostaglandins, matrix metalloproteinases and IL-1β (Cooke et al., 2003, Morgan et al., 2001). This mechanism is believed to be a Ca^{2+} signalling dependent process, based on findings from studies using fibroblasts in which a two-phase increase in intracellular Ca^{2+} is observed (Halverson et al., 1998). An initial transient spike in intracellular Ca^{2+}, likely caused by direct activation of ion channels on the cell membrane, followed by phagocytosis and dissolution of the HA crystal resulting in a slower-acting but sustained rise in Ca^{2+} over a number of hours.

HA stimulation may also increase proliferation (Morgan et al., 2001) and migration (Cox et al., 2012a) in breast cancer cells.

In the previous two chapters we established an *in vitro* model of mammary calcification using human breast cancer cell lines and utilised it to probe the involvement of various promoters and inhibitors or physiological mineralisation as well as tumour micro-environmental factors. In this final chapter, we aim to investigate potential links between mammary calcifications and tumour promoting effects, in particular inflammation and the promotion of cancer stemness.

In addition, we will present results from a Raman spectroscopy analysis of the chemical composition of *in vitro* calcification samples produced during this thesis as well as confirm the *in vivo* mineralisation potential of the MDA-MB-231 cell line. It is hoped that this will further support the applicability of our *in vitro* model and demonstrate its clinical relevance.

5.1.2 Aims of this chapter

The primary aims of this chapter are as follows.

- Characterise the inflammatory output of HA stimulated breast cancer cells
- Investigate the influence of inflammatory cytokines on the formation of microcalcifications
- Explore any links between mammary calcifications and cancer stemness
- Utilise Raman spectroscopy to characterise the chemical composition of *in vitro* calcification samples
- Confirm the *in vivo* mineralisation potential of the MDA-MB-231 cell line

5.2 Results

5.2.1 Inflammatory effect of hydroxyapatite on breast cancer cells

Several previous studies have found significant upregulation of inflammatory markers in breast cancer cells treated with HA (Cooke et al., 2003, Morgan et al., 2001). However, the number of genes analysed is relatively small and only includes COX2, IL-1β, MMP1, MMP2 and MMP9. In addition, the effects of HA stimulation on the triple-negative MDA-MB-231 cell line has not been previously examined. We therefore sought to increase the number of cells with a characterised response to HA stimulation, and expand the number of inflammatory markers studied..

We began by examining expression of COX2, an inflammatory mediator previously shown to be significantly upregulated in HA treated MCF-7 and Hs578T breast cancer cells (Cooke et al., 2003). Serum-starved (0.5 % FBS overnight) MDA-MB-231 cells were incubated with HA at a concentration of 50, 100, or 200 µg/cm^2. HA concentration was measured in µg/cm^2 as the crystals are comprised of an insoluble precipitate which rapidly sinks to the bottom of a tissue culture plate once added. Calculating HA concentration by surface area, rather than volume allowed for a consistent exposure between different plate sizes. Exposure to HA significantly upregulated COX2 expression in MDA-MB-231 cells, with all tested concentrations (Fig. 5.1) HA used at a concentration of 200 µg/cm^2 had the greatest effect, with a 5.3-fold increase in COX2 expression compared to control (**$P<0.01$) although this was not found to be significantly greater than other concentrations.

A previous dose-response of COX2 stimulation by HA showed maximum upregulation between 100 and 180 µg/cm^2 (Cooke et al., 2003). Based on this, and our finding of no major differences between any of our tested concentrations, we elected to continue the rest our study using HA at a concentration of 100 µg/cm^2.

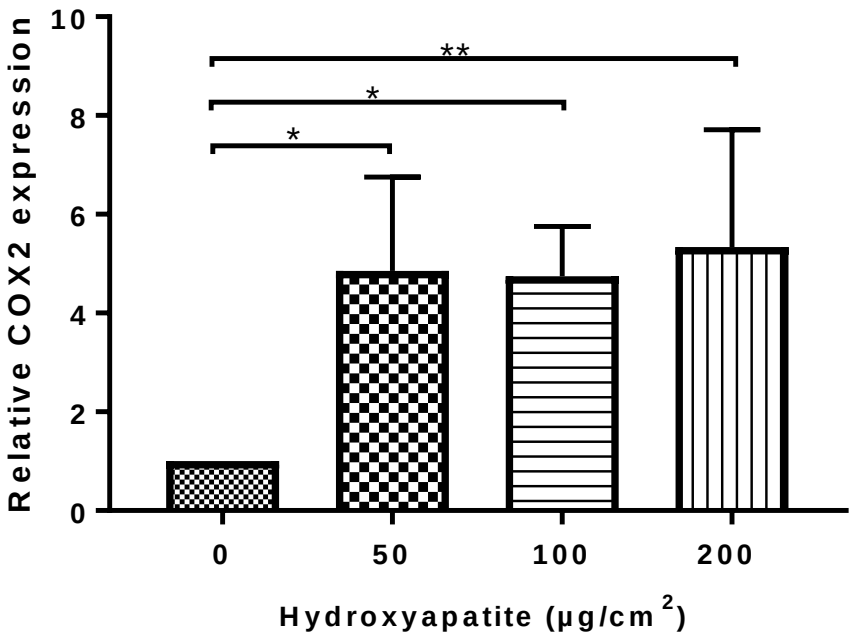

Figure 5.1 Hydroxyapatite upregulates COX2 in MDA-MB-231 cells. qPCR analysis of COX2 expression in serum-starved MDA-MB-231 cells treated with 50, 100 or 200 µg/cm^2 HA for 24 hours. Each point represents mean + SD (N=4). Statistical significance was determined by one-way ANOVA. *P<0.05, **P<0.01.

We next decided to investigate expression of IL-6, which has been highlighted in other studies of pathological calcification (Fukuyo et al., 2014), HA–induced inflammatory conditions (Jin et al., 2011) and breast cancer (Knupfer and Preiss, 2007). Stimulation of serum-starved MDA-MB-231 cells with 100 µg/cm^2 HA resulted in a 3.7-fold increase in IL-6 expression after 24 hours (Fig. 5.2 A). Robust induction of IL-6 expression was also confirmed in cells grown in full serum media (10% FBS), with similar levels of upregulation observed. Increased IL-6 production was also confirmed by ELISA analysis, with IL-6 levels in conditioned media from HA-stimulated cells increased to 565.4 ± 53 pg/mL, compared to 245.1 ± 49.99 pg/mL in control samples (Fig. 5.2 B).

Stimulation of breast cancer cells by HA nanoparticles has previously been shown to require direct cell-crystal contact, phagocytosis and intracellular crystal dissolution (Cooke et al., 2003). Blockade of this interaction inhibits the mitogenic effect of HA in breast cancer cells. However, a potential role for Ca^{2+} influx has not previously been explored in its inflammatory effect.

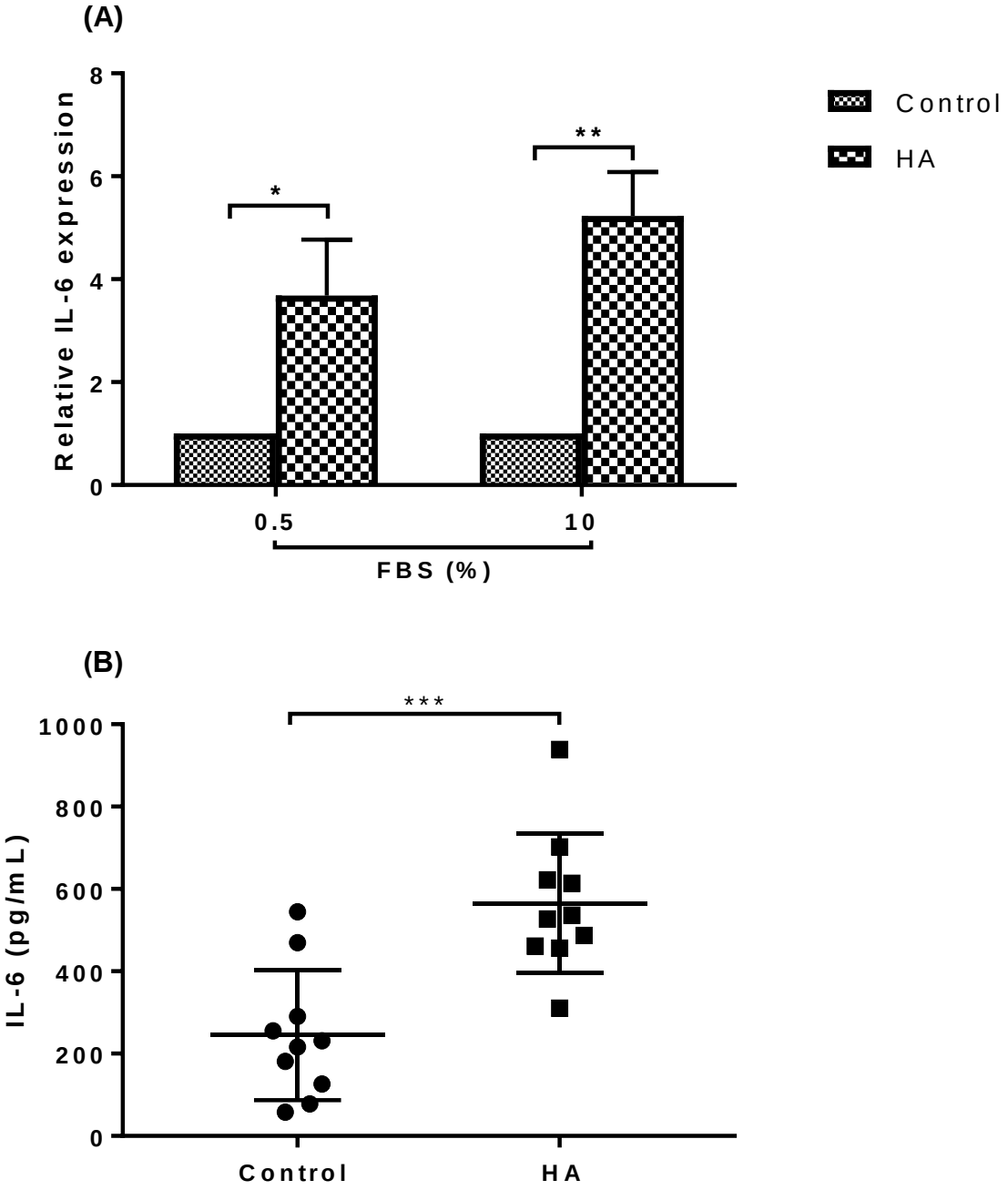

Figure 5.2 Hydroxyapatite upregulates IL-6 in MDA-MB-231 cells. qPCR analysis of IL-6 expression in cells grown in 0.5 or 10 % FBS media stimulated for 24 hours with 100 µg/cm^2 HA (A). Increased IL-6 expression was confirmed by ELISA in 0.5% FBS samples (B). Each point represents mean + SD (qPCR, N=3. ELISA, N=10). Statistical significance was determined by one-way ANOVA. *P<0.05, **P<0.01, ***P<0.001.

We next examined HA-stimulation of IL-6 in cells in the presence of the intracellular Ca^{2+} chelator BAPTA-AM, shown in the previous chapter to inhibit MDA-MB-231 mineralisation (Fig. 4.13). We found that inhibition of intracellular Ca^{2+} accumulation by administering BAPTA-AM 4 hours prior to HA exposure completely blocked any increase in IL-6 expression. qPCR analysis showed a 3.8-fold increase in IL-6 expression in HA-stimulated MDA-MB-231 cells (Fig. 5.3 A).

No significant increases were seen in cells pre-treated with BAPTA-AM. Similar results were seen by ELISA analysis, with a significant increase in IL-6 levels of conditioned media taken from HA-treated cells that was blocked by prior treatment with BAPTA-AM (Fig. 5.3 B). In addition to crystal dissolution, HA may also raise intracellular Ca^{2+} levels by direct activation of membrane bound ion channels (Halverson et al., 1998). Intake of Ca^{2+} via the TRPM7 channel, which was shown in the previous chapter to be involved in formation of microcalcifications (Fig. 4.15-4.18), has also been demonstrated to regulate activation of signal transducer and activator of transcription factor 3 (STAT3), an important component of the IL-6 signalling pathway (Davis et al., 2014). We hypothesised that activation of TRPM7 activity could be involved in induction of IL-6 expression by HA. Inhibition of TRPM7-mediated Ca^{2+} influx by prior treatment with NS8593 did not alter expression of IL-6 in HA-stimulated MDA-MB-231 cells, indicating that activation of the TRPM7 channel is not involved in the inflammatory effect of HA in breast cancer (Fig. 5.3).

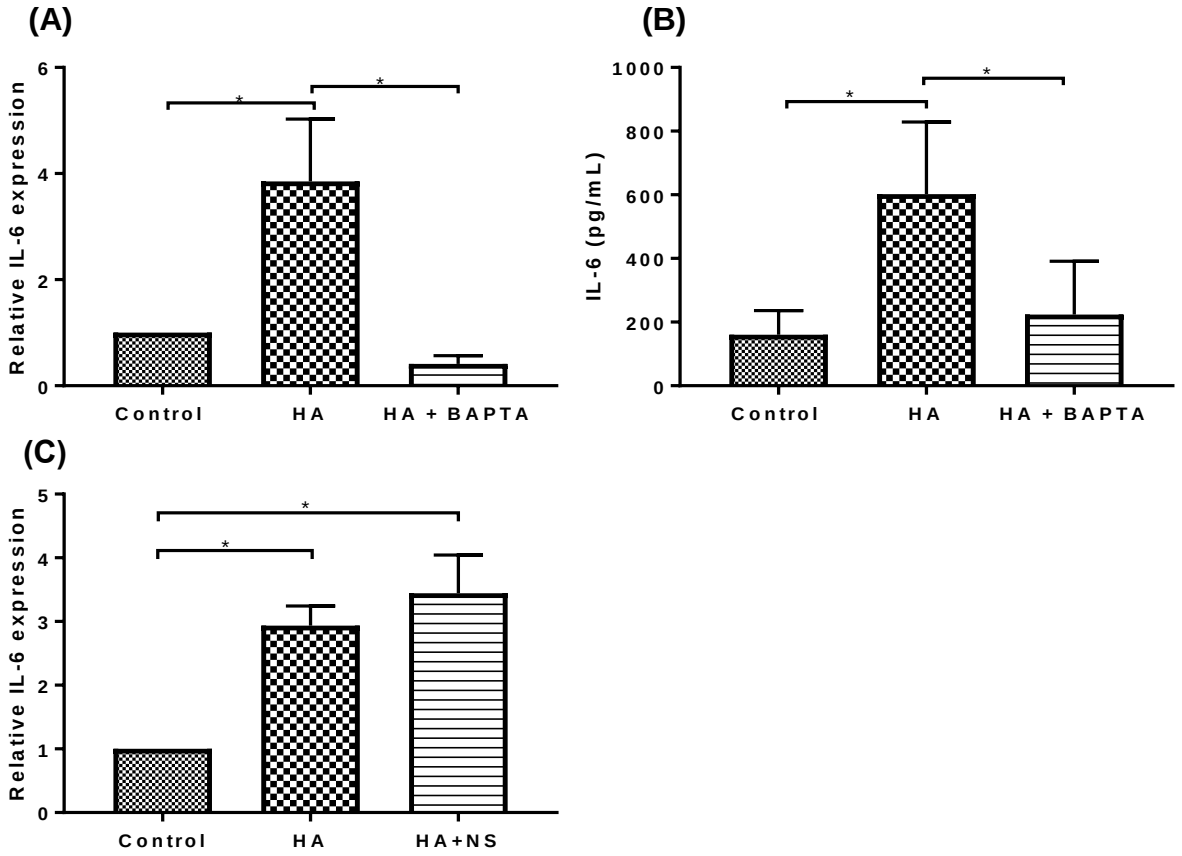

Figure 5.3 Upregulation of IL-6 in hydroxyapatite-stimulated cells is inhibited by intracellular Ca^{2+} chelation. IL-6 production in serum starved MDA-MB-231 24 hours post stimulation with 100 µg/cm^2 HA was assessed by qPCR (A) and ELISA (B). Cells were treated with 20 µM BAPTA-AM or vehicle control 4 hours prior to HA stimulation. HA induced an approximate 4-fold increase in IL-6 levels, which was blocked by prior treatment with BAPTA-AM. Upregulation of IL-6 was unaffected by inhibition of TRPM7 by 20 µM NS8593 (C). Each point represents mean + SD (N=3, qPCR. N=4, ELISA). Statistical significance was determined by one-way ANOVA. *P<0.05.

5.2.2 THP-1 monocytes and HA stimulation

Secretion of inflammatory cytokines from tumour cells can influence other cells in the microenvironment. Tumour associated macrophages (TAMs) can comprise up to 50% of a tumours volume (Vinogradov et al., 2014) and are potent promoters of tumour growth and metastasis. The human monocytic THP-1 cell line can be differentiated into macrophages by stimulation with phorbol 12-myristate 13-acetate (PMA) and used as *in vitro* studies of TAM function (Genin et al., 2015).

We first tested the effect of direct HA stimulation on THP-1 macrophages (Fig. 5.4 A). IL- 1β was highly upregulated in HA stimulated THP-1 cells (6.4-fold increase, $P < 0.0001$). In contrast, although IL-6 and COX2 were both strongly upregulated in MDA-MB-231 cells, HA stimulation did not have any significant effect on either of these genes in the THP-1 cell line. To test if the increased expression of inflammatory markers observed in HA stimulated MDA-MB-231 cells could influence TAMs, we stimulated MDA-MB-231 cells for 24 hours in serum-free media with HA and used the conditioned media (CM) to stimulate PMA-derived THP-1 macrophages (Fig. 5.4 A). Control media was generated by culturing MDA-MB-231 cells in serum-free media for 24 hours. Control CM increased IL-6 expression in THP-1 3.6-fold ($P < 0.05$), COX2 expression 2.5-fold ($P < 0.05$) and IL- β 4-fold (n.s). In all three tested genes, expression tended to be increased to a greater extent by conditioned media from HA stimulated MDA-MB-231 cells, however none of these changes were found significant.

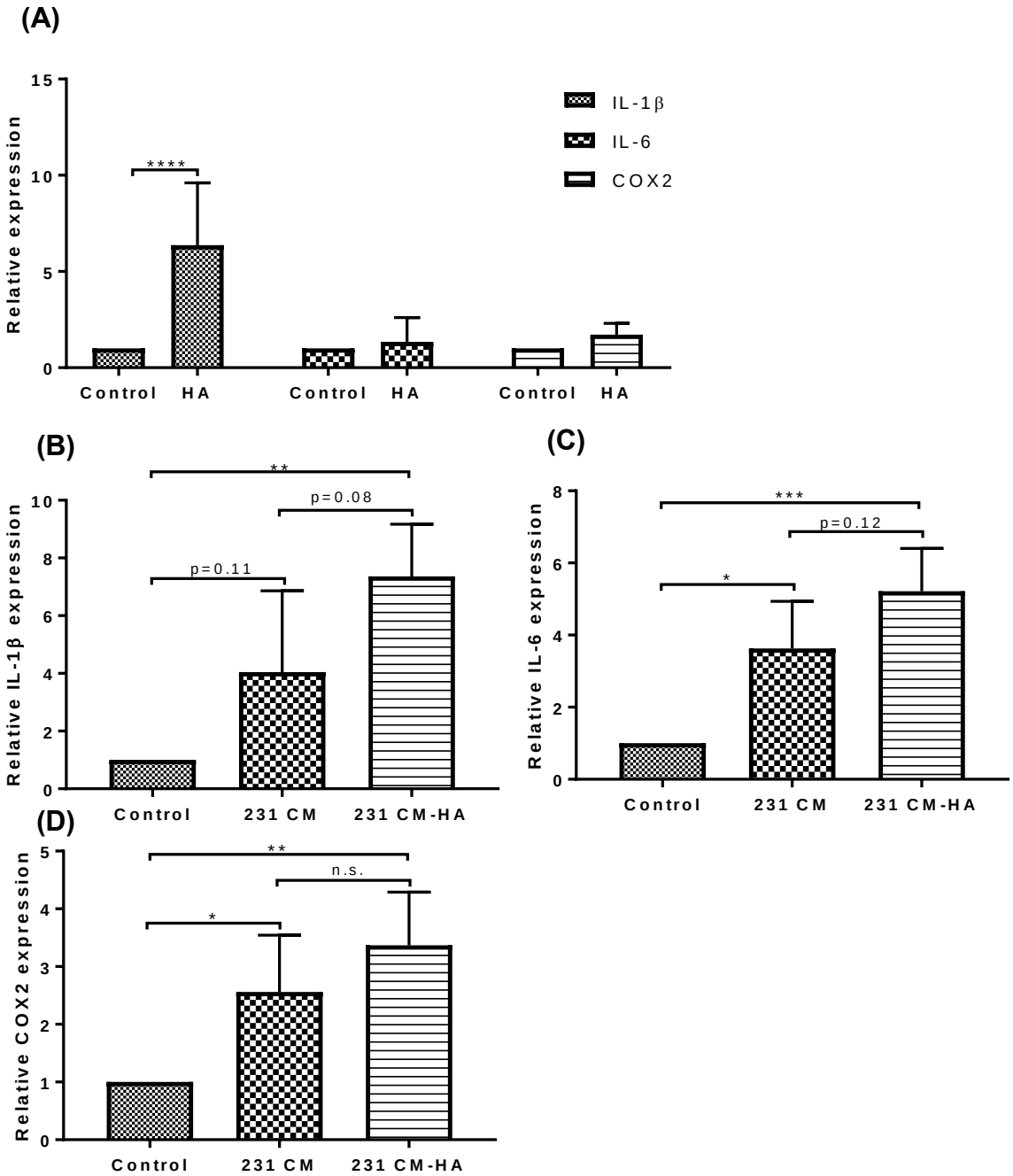

Figure 5.4 Increased expression of inflammatory markers in THP-1 macrophages following stimulation with HA or MDA-MB-231 conditioned media. PMA-derived THP-1 macrophages were treated with 100 µg/cm^2 HA or conditioned media from MDA-MB-231 cells for 24 hours. Direct stimulation with HA increased IL- β significantly (A). Conditioned media from MDA-MB-231 cells (231 CM) increased expression in all three markers with media taken from HA stimulated cells (231 CM-HA) tending to induce a greater increase (B). All data points represent the mean + SD (A N=5, B N=4). Statistical significance was determined by one-way ANOVA. *P<0.05, **P<0.01, ***P<0.001, ****P<0.0001.

5.2.3 Inflammatory cytokines and formation of microcalcifications

After demonstrating significant upregulation of IL-6 in HA-stimulated breast cancer cells, we next wanted to determine if IL-6 played any role in the formation of mineralisations. IL-6 signals through a receptor complex consisting of the gp130 subunit, common to several cytokine receptors, and the IL-6 receptor. IL-6 can also bind to a soluble form of the IL-6 receptor (sIL-6R), produced by enzymatic cleavage or alternative splicing to activate an alternative, trans-signalling pathway (Fig. 5.5 A) (Mihara et al., 2012). MDA-MB-231 cells have been shown to express high levels of IL-6, and the gp130 receptor subunit although studies have disagreed on their expression level of IL-6R (Zhong et al., 2016, Douglas et al., 1997, Bharti et al., 2015, Casneuf et al., 2016). As the MDA-MB-231 cell line may not express membrane bound IL-6R, and addition of exogenous sIL-6R has previously been shown to activate IL-6 signalling in cells without sufficient IL-6R, we tested the effect of both IL-6 and sIL-6R on MDA-MB-231 mineralisation.

MDA-MB-231 cells were cultured with OC+Dex and either IL-6, sIL-6R or a combination of both at a concentration of 100 ng/mL. Whilst IL-6 had no significant impact on calcium deposition, addition of sIL-6R at 100 ng/mL significantly increased MDA-MB-231 calcification as measured by Alizarin Red S staining and quantitative analysis (Fig. 5.5 B, C). Unusually, when sIL-6R was used in combination with IL-6, the increase in mineralisation was repressed. Analysis of ALP activity did not reveal any significant differences between cells cultured with IL-6 or sIL-6R (Fig. 5.5 D).

We also assessed mineralisation in cells cultured in OC media without dexamethasone. As previously seen, no positive Alizarin Red S staining was observed in cells cultured in OC media alone (Fig. 5.6 A). Addition of either IL-6 or sIL-6R did not induce MDA-MB-231 mineralisation, although positive staining was observed in cells cultured with both, indicating the first time we observed a positive mineralisation results in MDA-MB-231 cells without either dexamethasone or exogenous ALP. Positive mineralisation was confirmed by OCP assay, which confirmed a significant increase in calcium deposition in cells cultured with both IL-6 and sIL-6R compared to control values: calcium content of cells from IL-6/sIL-6R was increased over 3-fold compared to control samples (181 v 50 ppm/mg, $P < 0.05$).

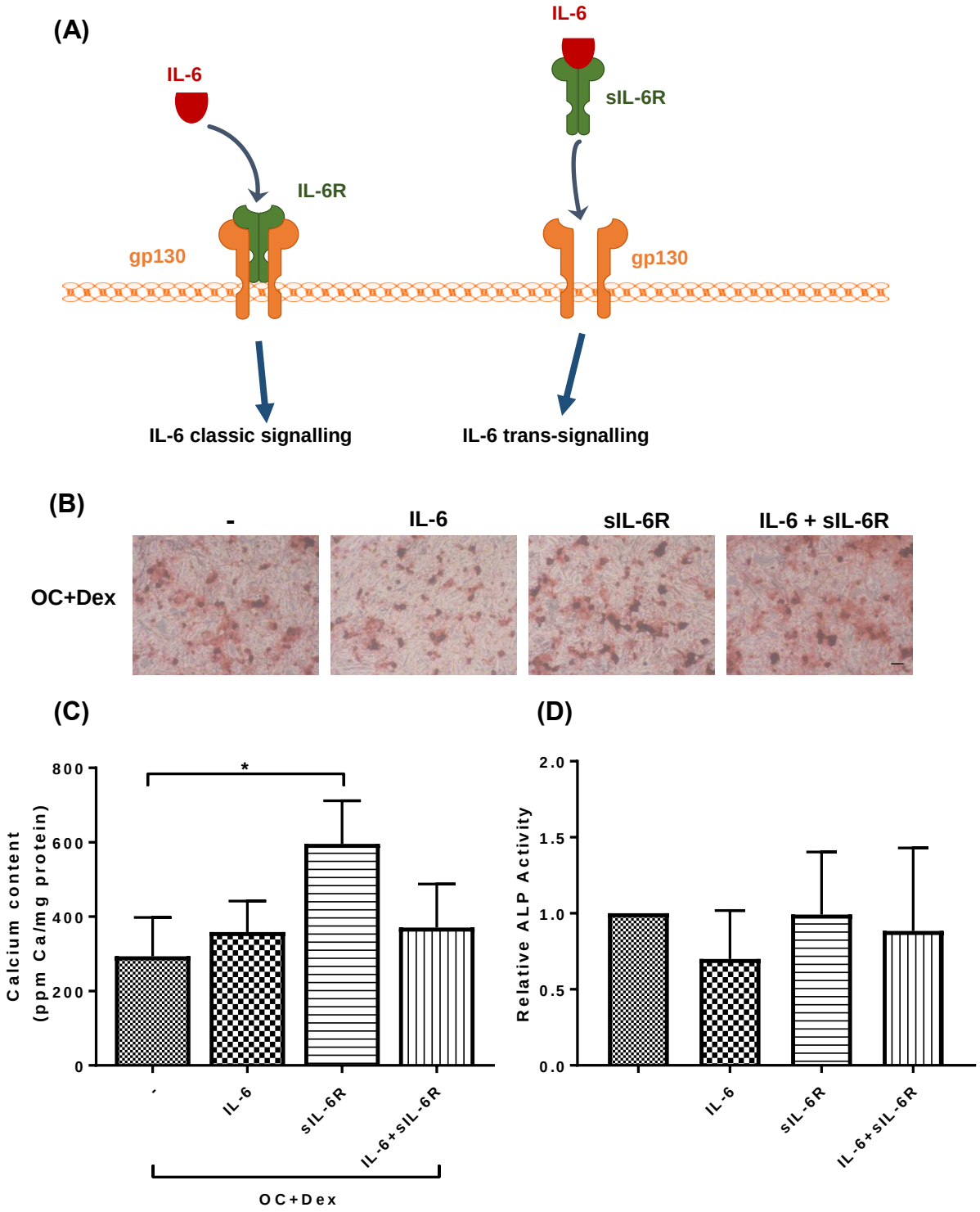

Figure 5.5 sIL-6R promotes MDA-MB-231 mineralisation. IL-6 activated either a classic or trans-signalling pathway depending on the presence of membrane-bound or soluble IL-6R (A). Representative images (10X) were captured of Alizarin Red S stained MDA-MB-231 cells following 28 days incubation with OC+Dex and the indicated cytokines (A). All cytokines were tested at 100 ng/mL. Addition of sIL-6R at 100ng/mL increased MDA-MB-231 calcification as measured by OCP assay (C). No difference was found in ALP activity of cells cultured for 14 days with the indicated cytokines (D). Each point represents mean + SD. (OCP N=3, ALP N=4). Statistical significance was determined by one-way ANOVA *P<0.05. Scale bar represents 50 µm.

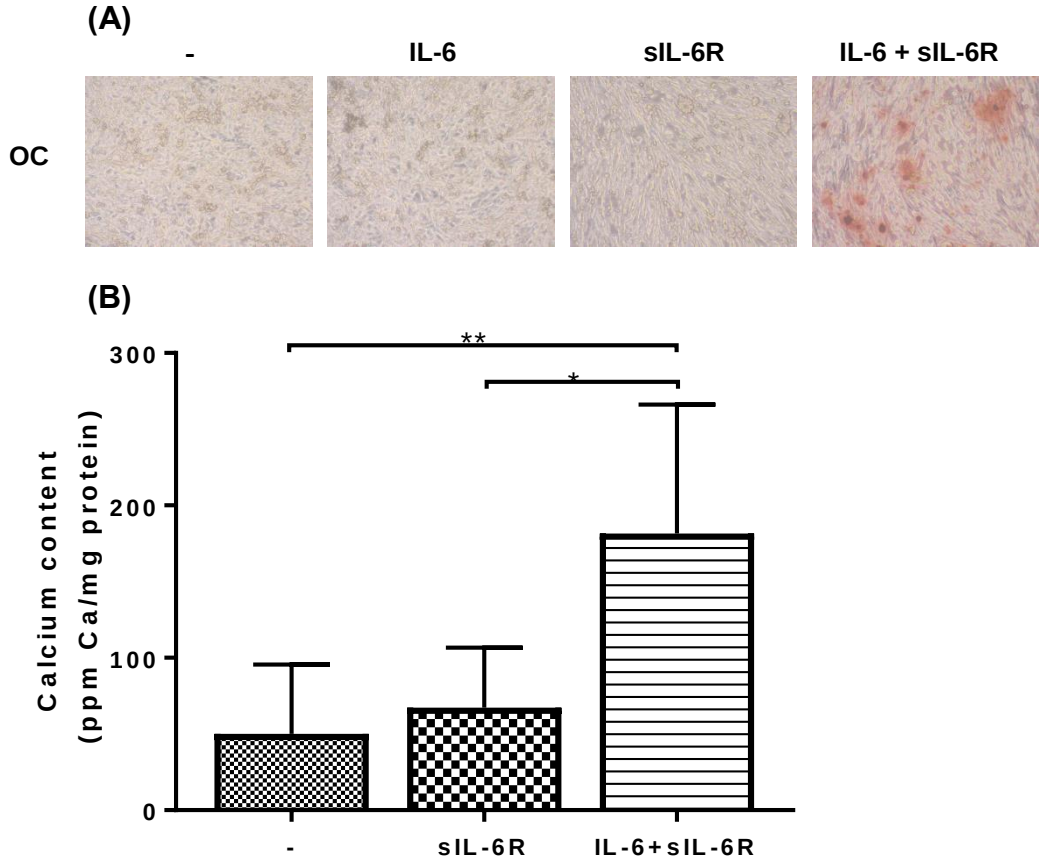

Figure 5.6 Activation of IL-6 trans-signalling pathway promotes MDA-MB-231 mineralisation. Representative images (10X) were captured of Alizarin Red S stained MDA-MB-231 cells following 28 days incubation with OC and the indicated cytokines (A). IL-6 and sIL-6R were used at 100 ng/mL. Addition of IL-6/sIL-6R at 100ng/mL increased MDA-MB-231 calcification as measured by OCP assay (B). Each point represents mean + SD. (N=4). Statistical significance was determined by one-way ANOVA *P<0.05, **P<0.05. Scale bar represents 50 µm.

Stimulation of IL-6 signalling results in activation of several downstream signalling pathways including recruitment of Janus kinases (JAK) and phosphorylation of STAT3 (Scheller et al., 2011). As we did not observe any stimulatory effect for IL-6 alone in the MDA-MB-231 cell line, we examined changes in STAT3 phosphorylation in MDA-MB-231 cells by western blot. Although stimulation by IL-6 or sIL-6R alone did not cause any change in pSTAT3, co-stimulation of the two resulted in increased STAT3 phosphorylation in MDA-MB-231 cells (Fig. 5.7 A). Some studies have also found that despite high expression of IL-6 by the MDA-MB-231 cell line, they are unresponsive to stimulation with exogenous IL-6 and may not express IL-6R (Casneuf et al., 2016, Zhong et al., 2016). However, there is some disagreement in the literature with other studies finding significant levels of IL-6R in the MDA-MB-231 cell line (Chiu et al., 1996, Bharti et al., 2017).

In the hope of addressing this discrepancy, we next examined expression of three components of the IL-6 signalling pathway; the gp130 receptor subunit and both membrane-bound and soluble IL-6R in both MDA-MB-231 and SKBR3 cells. Expression of IL-6 signalling genes was also investigated in cells cultured in control or OC+Dex media. Although we observed high expression of gp130 in both MDA-MB-231 and SKBR3 cells, expression of both membrane-bound and soluble IL-6R was only found in SKBR3 cells (Fig. 5.7 A). The presence of OC+Dex media also appeared to slightly increase levels of IL-6R in SKBR3 cells.

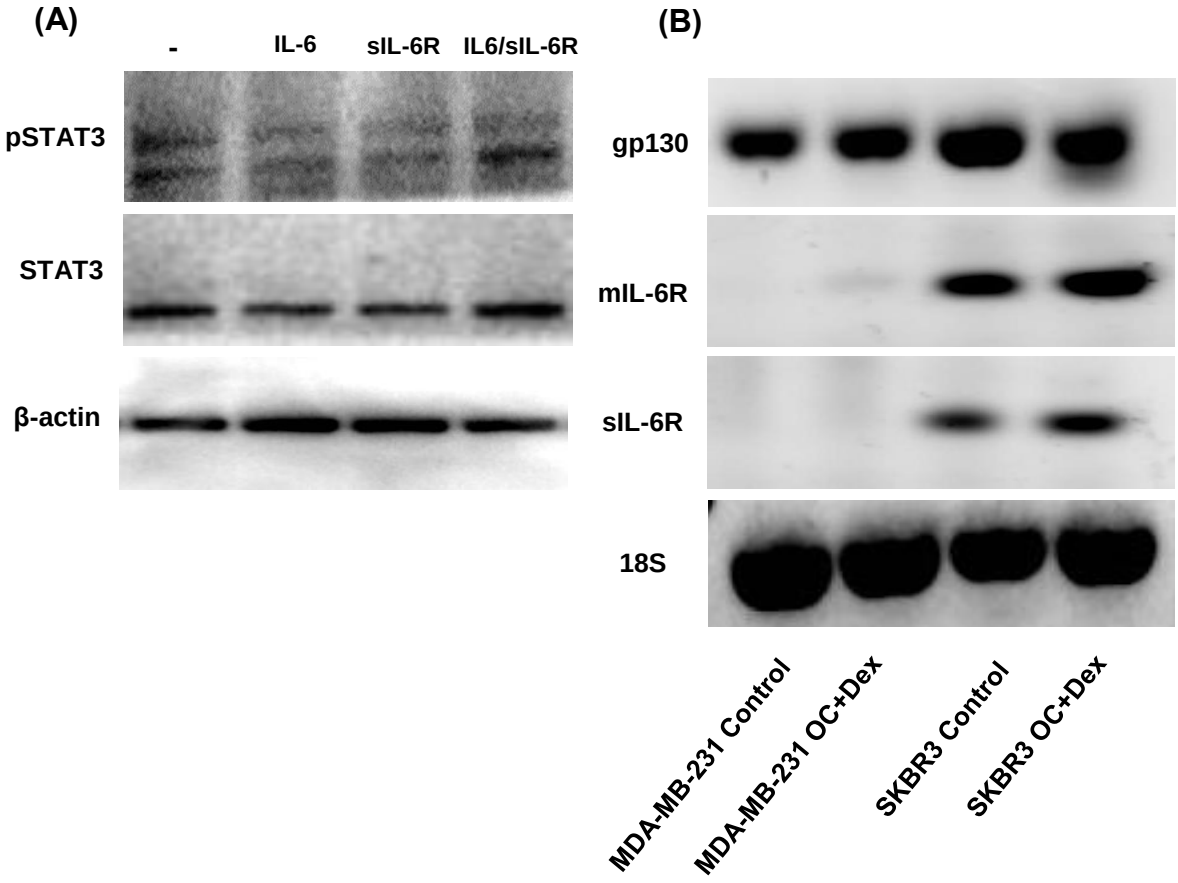

Figure 5.7 MDA-MB-231 cells are unresponsive to IL-6 without sIL-6R co-stimulation. The level of phosphorylated STAT3 (pSTAT3) versus total STAT3 in MDA-MB-231 cells was examined by western blot 24 hours after stimulation with 100 ng/mL of IL-6, sIL-6R or both (A). Expression of IL-6 signalling pathway components gp130, membrane-bound IL-6R (mIL-6R) and soluble IL-6R (sIL-6R) was examined in MDA-MB-231 and SKBR3 cells, cultured in control and OC+Dex media for 72 hours was examined by PCR and visualised by agarose gel electrophoresis.

In agreement with previous studies (Garcia et al., 2001), both cell lines displayed a significant level of constitutive STAT3 phosphorylation The presence of OC+Dex media did not result in any alteration in pSTAT3 in MDA-MB-231 cell line (Fig. 5.8 A). In contrast, OC+Dex media enhanced STAT3 phosphorylation almost 3-fold in the SKBR3 cell line. (Fig. 5.8 B, C).

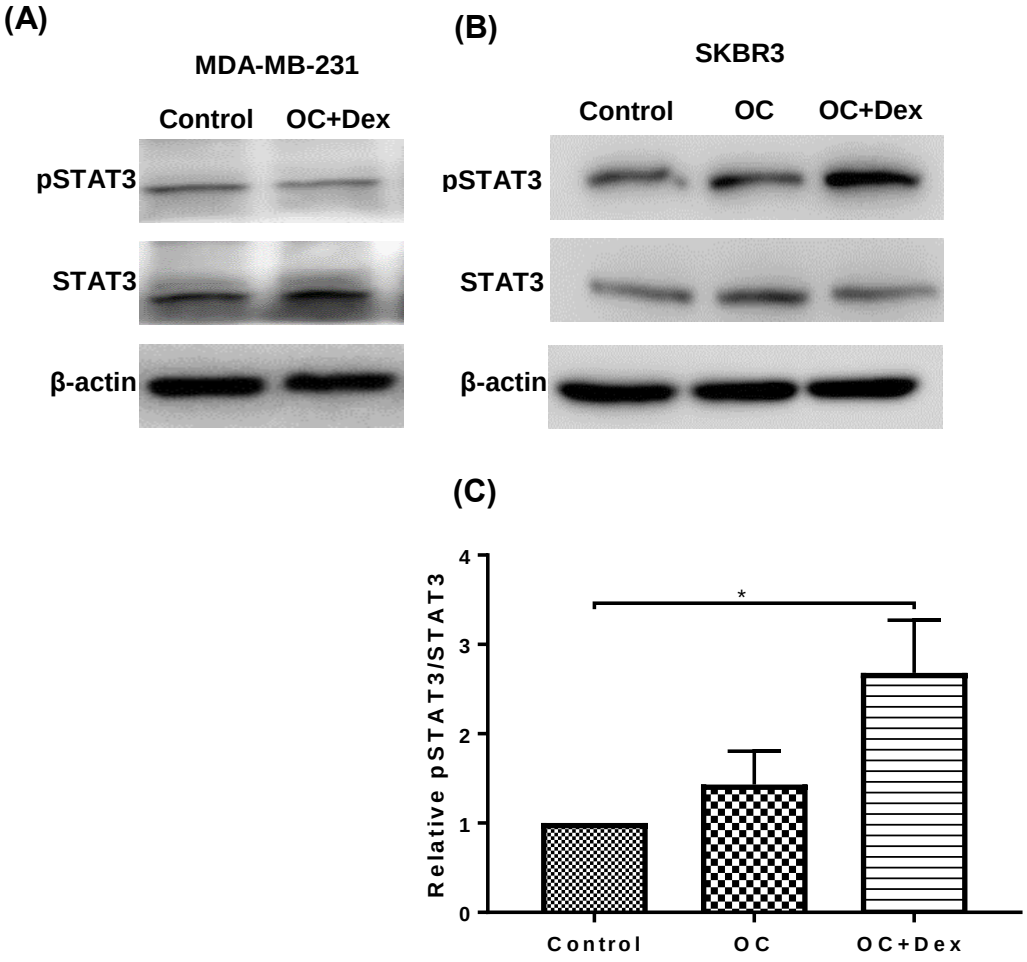

Figure 5.8 OC+Dex promotes STAT3 phosphorylation in SKBR3 cells. Levels of phosphorylated STAT3 versus total STAT3 was examined by western blot in MDA-MB-231 (A) and SKBR3 (B) cells. Cells were cultured in control and OC+Dex (MDA-MB-231) or control, OC and OC+Dex media (SKBR3) for 72 hours prior to analysis. Densitometry revealed significant increases in STAT3 phosphorylation in SKBR3 cells cultured in OC+Dex media (C). Each point represents mean + SD. (N=3). Statistical significance was determined by one-way ANOVA *P<0.05.

Finally, we examined the effect of inhibiting pSTAT3 on the formation of calcifications as a similar strategy was previously shown to reduce osteogenic transformation and calcium mineralisation in a study of adipose derived stromal cells (Huh and Lee, 2013). Administration of the pSTAT3 inhibitor JSI-124 at a concentration of 100 nM decreased calcium deposition and ALP activity in MDA-MB-231 cells by approximately 70% and 40% respectively (Fig. 5.9 A, B). Unusually, despite functioning as an inhibitor of STAT3 phosphorylation and successfully inhibiting mineralisation, we did not observe any detectable decrease in pSTAT3 levels in MDA-MB-231 cells treated for 24 hours with JSI-124 (Fig. 5.9 C, D).

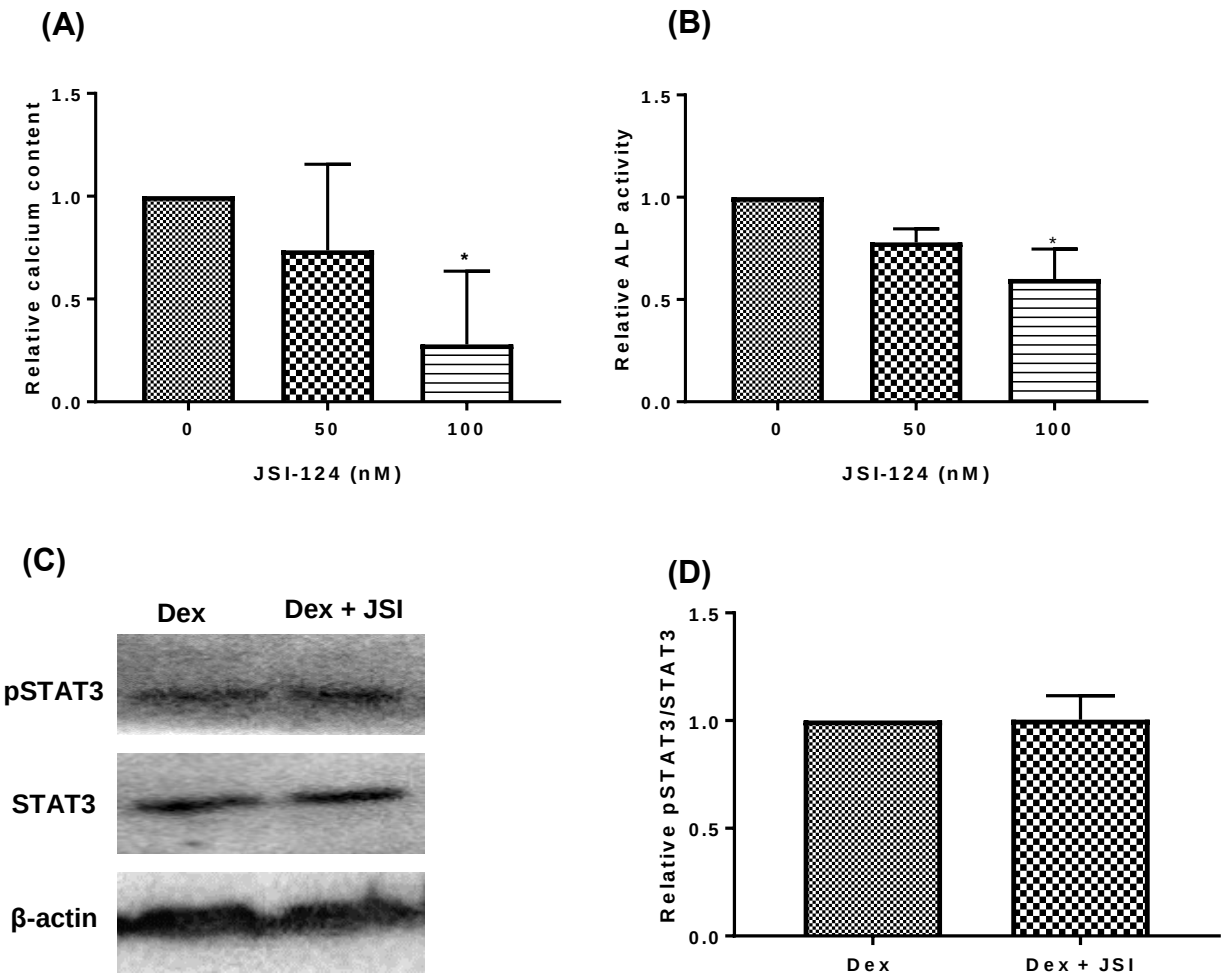

Figure 5.9 JSI-124 and MDA-MB-231 mineralisation. MDA-MB-231 cells grown in OC+Dex media with 100 nM JSI-124 or vehicle control for 14 days displayed significantly reduced mineralisation (A) and ALP activity (B). Analysis of pSTAT3 levels by western blot did not reveal any detectable changes after 24 hours (C, D). Each point represents mean + SD. (A,C,D N=3, B N=2). Statistical significance was determined by one-way ANOVA or student t-test *P<0.05.

We also examined two other inflammatory cytokines for possible roles in formation of microcalcifications. IL-1β and TNF-α have previously been shown to both promote and inhibit vascular calcification, depending on concentration (Lencel et al., 2010). We cultured MDA-MB-231 cells for 28 days in OC+Dex media, with IL-1β and TNF-α at various concentrations. We observed a highly significant inhibitory effect for both cytokines in the development of breast calcifications. We first tested each cytokine individually at relatively high concentrations (10 and 100 ng/mL). A complete absence of positive Alizarin Red S staining was observed in cells cultured with either cytokine at both tested concentrations (Fig. 5.10 A). We next tested both cytokine in OC media without dexamethasone, as some studies have shown that these inflammatory cytokine can replace the osteogenic signal of dexamethasone in *in vitro* models of mineralisation in other cell types, similar to our previous findings with IL-6+sIL-6R (Ferreira et al., 2013). Our results in contrast, did not show any pro-osteogenic effect of either IL-1β or TNF-α in OC media alone, with no positive Alizarin Red S staining observed in MDA-MB-231 cells cultured for 28 days in OC media with 10 or 100 ng/mL IL-1β or TNF-α (Fig. 5.10 B).

We also tested the cytokines in combination and at lower concentrations, as some studies have shown lower concentrations to promote a greater osteogenic effect (Huang et al., 2011). Results were similar to those seen with higher doses, with both IL-1β and TNF-α completely blocking MDA-MB-231 mineralisation even at a concentration of only 0.1 ng/mL (Fig. 5.10 C). A combination of both cytokines at 0.1, 0.5 or 1 ng/mL also inhibited mineralisation.

Finally, we examined the effect of IL-1β and TNF-α on ALP activity. Analysis of ALP activity in MDA-MB-231 cells cultured in OC+Dex media for 14 days showed significant decreases when either cytokine was included. IL-1β at a concentration of 10 or 100 ng/mL decreased ALP activity by 60 and 70% respectively (Fig. 5.11 A), whilst TNF-α was even more effective, with 100 ng/mL TNF-α decreasing ALP activity by almost 95% ($P < 0.01$, Fig. 5.11 B).

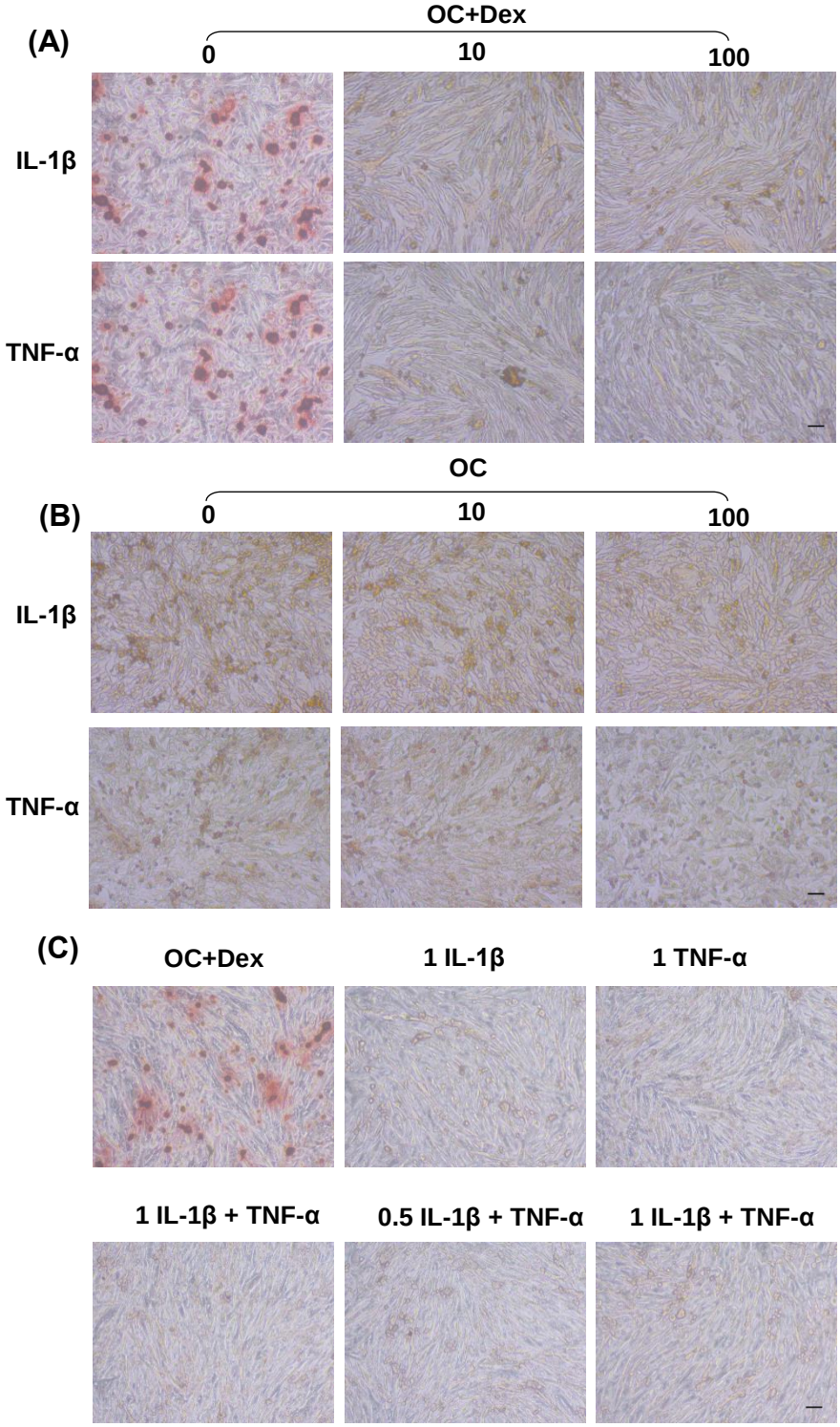

Figure 5.10 Suppression of MDA-MB-231 mineralisation by inflammatory cytokines IL-1β and TNF-α. Representative images (N=2) shown at 10X magnification of MDA-MB-231 cells grown for 28 days in OC+Dex media with IL-1β and TNF-α at the indicated concentrations (ng/mL) showed a complete loss of Alizarin Red S staining in cells grown in the presence of any tested concentration of cytokines (A). Neither cytokine induced mineralisation in cells grown in OC media without dexamethasone (B). Low dose and combination treatment of both cytokines also decreased Alizarin Red S staining (C). Scale bar represents 50 µm.

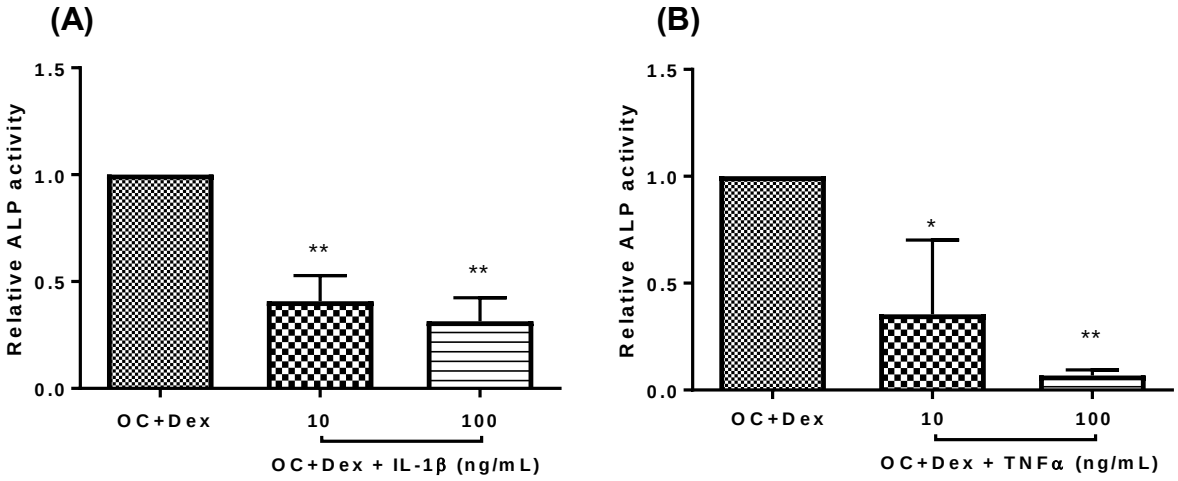

Figure 5.11 Suppression of MDA-MB-231 ALP activity by inflammatory cytokines IL-1β and TNF-α. Analysis of ALP activity in MDA-MB-231 cells cultured for 14 days in OC+Dex media with IL-1β (A) or TNF-α (B) at the indicated concentration revealed significant decreases for both cytokines. Each point represents mean + SD. (N=3). Statistical significance was determined by one-way ANOVA *P<0.05, **P<0.05.

5.2.4 Microcalcifications and cancer stem cells

Cancer stem cells (CSCs) are cancer cells that display features typical of normal stem cells, including self-renewal and differentiation into multiple cell types (Borah et al., 2015). CSCs are an active area of research, as their enhanced ability to form new tumours make them a significant contributor to metastasis and recurrence (Chang, 2016). Tumoursphere cultures have been shown to be an effective *in vitro* model of cancer stemness (Lee et al., 2016). Tumourspheres are generated by forcing adherent cancer cells to grow as a suspension culture by seeding cells into tissue-culture plates coated with the hydrogel poly2-hydroxyethyl methacrylate (pHEMA), which forms a highly hydrophilic layer that prevents cell adhesion. Cells are grown in a serum free media (DMEM/F12) supplemented with EGF and the serum-free supplement B27. Breast cancer cell lines grown as tumoursphere cultures are enriched for cells with stem-cell properties and have enhanced tumourgenicity (Wang et al., 2014).

Cancer stemness is closely associated with another pro-tumourigenic pathway, epithelial-mesenchymal transition (EMT). EMT results in a loss of cellular adhesion and acquisition of a migratory, invasive phenotype (Felipe Lima et al., 2016) and has previously been suggested to play a role in formation of microcalcifications. Scimeca et al. found greater immunohistochemical staining for the mesenchymal marker vimentin in breast tumours with associated calcifications than those without and suggested that acquisition of a mesenchymal phenotype could lead to generation of breast cancer cells with osteoblast like activity and deposition of calcium (Scimeca et al., 2014).

We first examined if culturing breast cancer cells could promote the formation of cancer stem cells. We seeded MDA-MB-231 cells into pHEMA coated plates and cultured them for 7 days in either the presence or absence of OC+Dex supplementation. Formation of tumourspheres was assessed by light microscopy at days 3, 5 and 7. We observed successful formation of tumourspheres in the MDA-MB-231 cell line (Fig. 5.12). After 3 days, cells grown in control media displayed a tumoursphere forming efficiency (TFE, calculated by dividing the number of spheres counted by the number of cells initially seeded and expressed as a percentage) of 0.47. This remained largely stable, and did not increase over time. In contrast, cells cultured in media with OC+Dex supplementation had a TFE of 0.835, which continually increased over the course of the experiment. By day 7, cells in OC+Dex media formed 3.5 times more spheres than those in control media ($P > 0.05$).

We next repeated the experiment with another mineralisation capable cell lines, the HER2+ SKBR3. Results were largely the same, with a continual increase in sphere formation in cells cultured in OC+Dex media versus control (Fig. 5.13). SKBR3 cells grown in control media also displayed a slightly higher TFE than MDA-MB-231 cells.

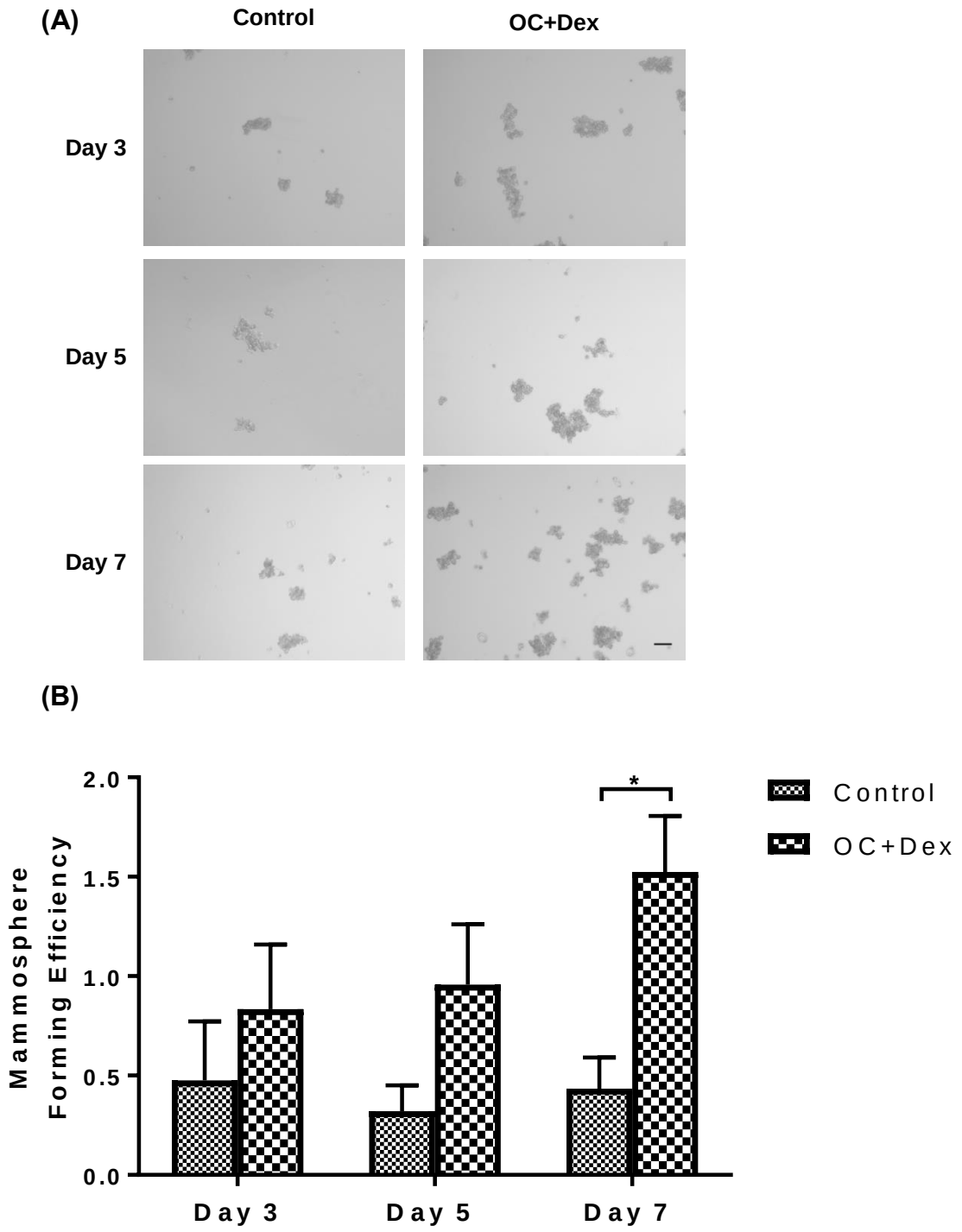

Figure 5.12 Tumoursphere formation in MDA-MB-231 cells. Representative images (10X magnification) of MDA-MB-231 cells cultured in non-adherent pHEMA coated plates (A). Analysis of sphere formation by counting under light microscopy reveals significant increases in sphere formation in cells cultured with OC+Dex media (B). Each point represents mean + SD. (N=4). Statistical significance was determined by two-way ANOVA *P<0.05. Scale bar represents 50 µm.

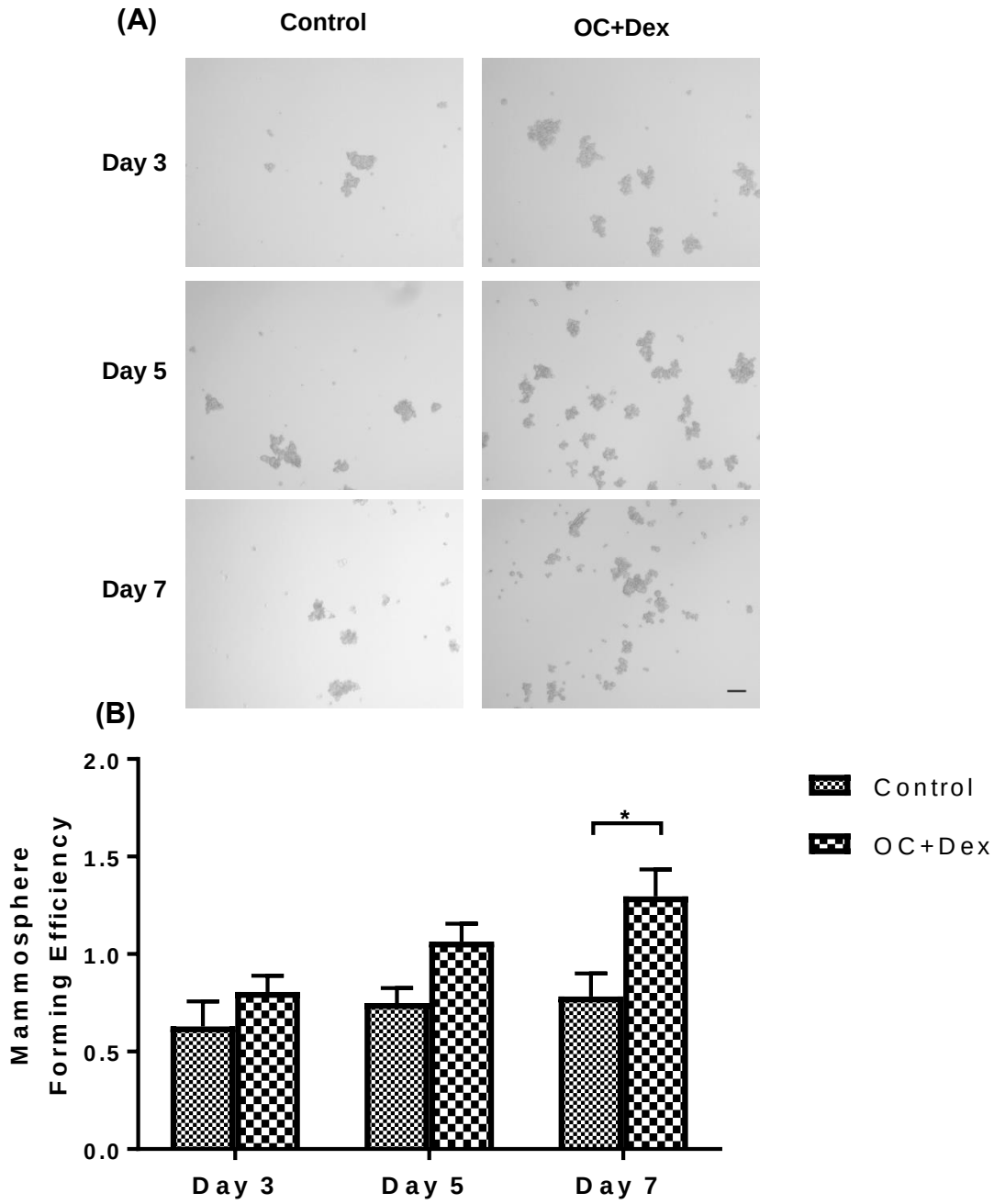

Figure 5.13 Tumoursphere formation in SKBR3 cells. Representative images (10X magnification) of SKBR3 cells cultured in non-adherent pHEMA coated plates (A). Analysis of sphere formation by counting under light microscopy reveals significant increases in sphere formation in cells cultured with OC+Dex media (B). Each point represents mean + SD (N=3). Statistical significance was determined by two-way ANOVA. *P<0.05. Scale bar represents 50 µm.

Although the 7 day length of our tumoursphere assay was shorter than the time frame at which initial mineralisation is usually observed in the MDA-MB-231 cell line (day 11 -14), we collected tumourspheres at the end of each assay to examine if any calcifications has been formed within the spheres. Tumourspheres were collected and deposited onto poly-lysine coated microscope slides using a cytocentrifuge and stained with Alizarin Red S, following normal procedure.

Although the deposited layer was significantly denser in cells from OC+Dex media (confirming a greater number of viable tumourspheres in these wells, as compared to controls) no noticeable staining was observed in either control or OC+Dex sides (Fig. 5.14 A). We also stained the pHEMA coated plates to check for any calcifications that may have formed on the tumourspheres before falling to the bottom of the plates. No positive staining was observed in any of the plates (data not shown), although it is worth noting that if any calcifications potentially did form, due to the low number of cells seeded per well (5,000) they would likely be extremely small and low in number, and possibly beyond the detection capability of this stain. In addition, the pHEMA coating absorbed a significant amount of the Alizarin Red S stain, resulting in a uniform orange colour across all wells, further complicating identification of any areas of positive staining. A separated set of replicates were pelleted, and incubated with nitric acid for 1 hour to extract any deposited calcium on the surface of tumourspheres. No increases in calcium content was observed in cells incubated in OC+Dex media (Fig. 5.14 B).

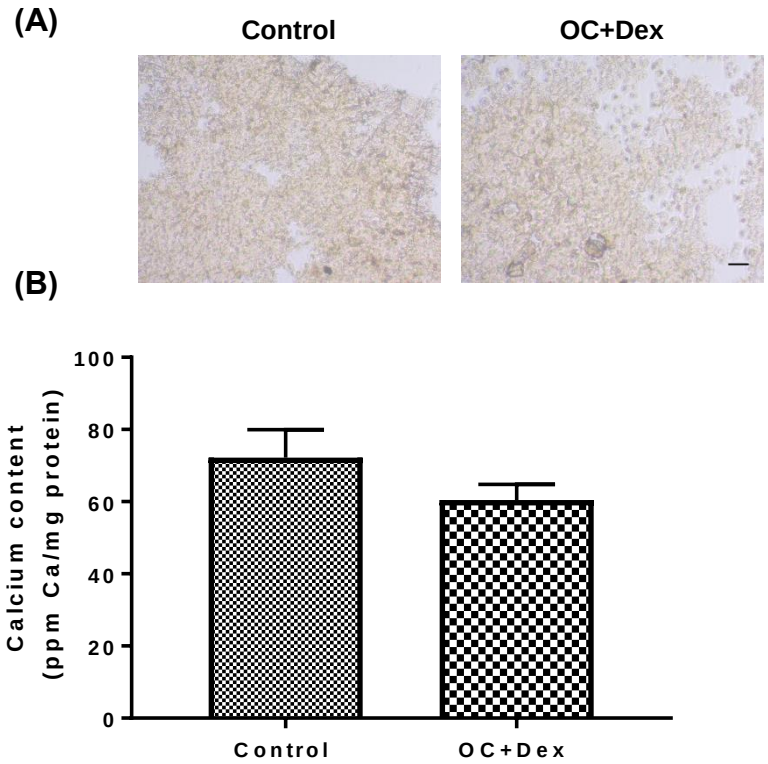

Figure 5.14 MDA-MB-231 do not mineralise as tumoursphere cultures. Alizarin Red S staining MDA-MB-231 cells grown as tumourspheres for 7 days and cytospun onto poly-lysine coated slides does not show any evidence of mineralisation (A). Representative images (N=3) are shown here at 10X magnification. OCP analysis of calcium content of pelleted tumourspheres also showed no significant difference. All data points represent mean + SD (N=3). Statistical significance was analysed by student t-test. Scale bar represents 50 µm.

Cell stemness is often correlated with changes in expression in a number of transcription factors, including Nanog, Oct4 and Sox2 (Apostolou et al., 2012). Similarly, the EMT process is often characterised by a decrease in epithelial markers (E-cadherin) and an increase in mesenchymal markers (Vimentin, Snail, Twist) (Zeisberg and Neilson, 2009). We next examined the effect of OC+Dex media on expression of a panel of markers for both cell stemness and EMT.

Expression of both E-cadherin and vimentin was decreased by a small but statistically significant amount (Fig. 5.15 A). Decreased expression of the EMT transcription factors Snail and Twist was also observed, although only Twist was found to be significant. Results were similar for markers of stemness, with significant decreases in Sox2 and Oct4, and a trend towards decreased Nanog (Fig. 5.15 B).

We also examined expression of these genes in the SKBR3 cell line. Note, we were unable to examine expression of E-cadherin in the SKBR3 cell line, as expression was only detected at high Ct values, which are unlikely to be reliable. No significant changes were detected in the mesenchymal markers vimentin and Snail (Fig. 5.16 A). Stemness markers displayed a trend towards decreased expression although only Sox2 was found to be significant (Fig. 5.16 B).

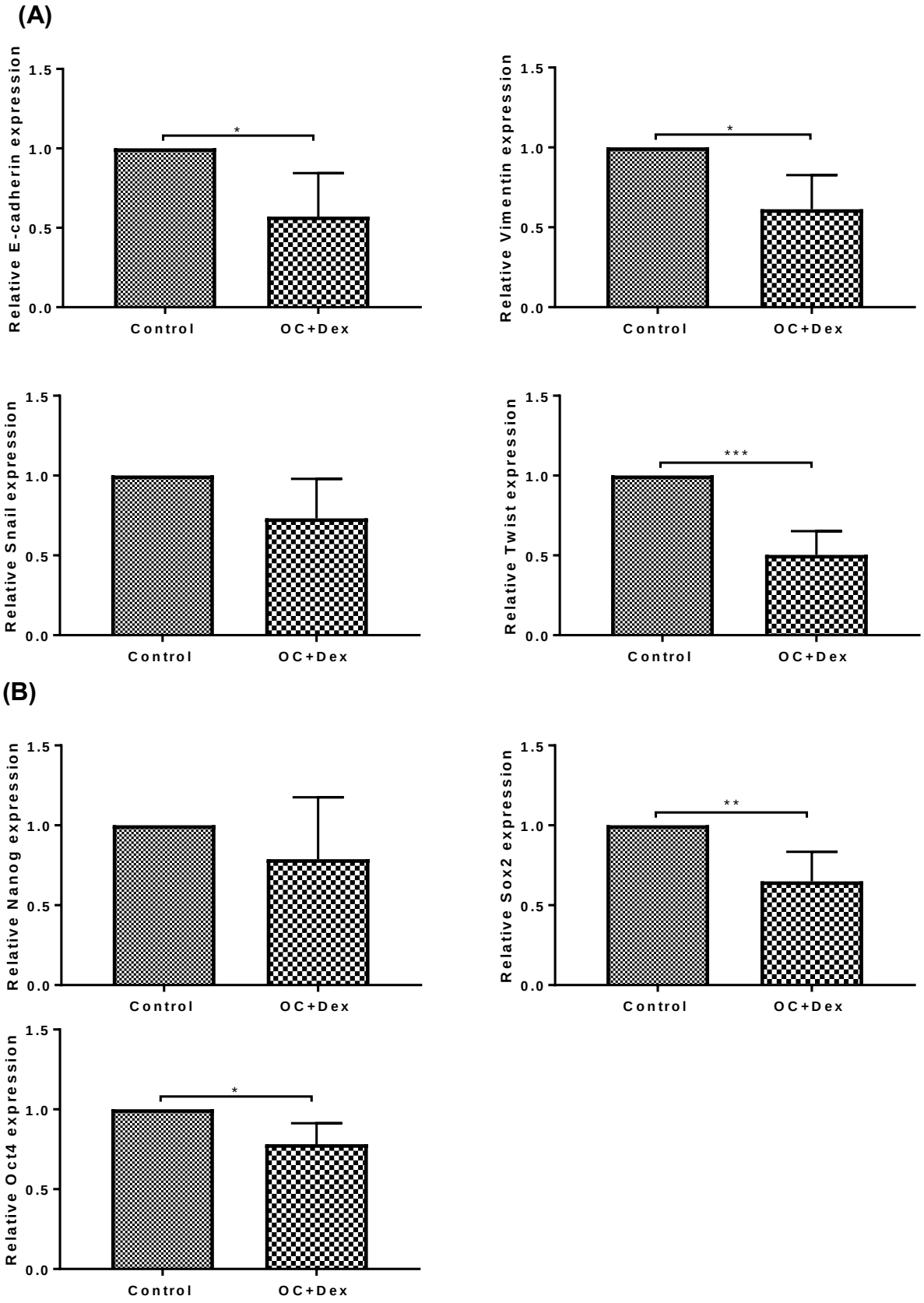

Figure 5.15 Effect of OC+Dex on expression of EMT and cancer stemness markers in MDA-MB-231 cells. Expression of markers of EMT (A) and cancer stemness (B) in MDA-MB-231 cells was analysed following 72-hours culture in control or OC+Dex media. Each point represents mean + SD. (N=4). All statistical significance was analysed by student t-test. *P<0.05.

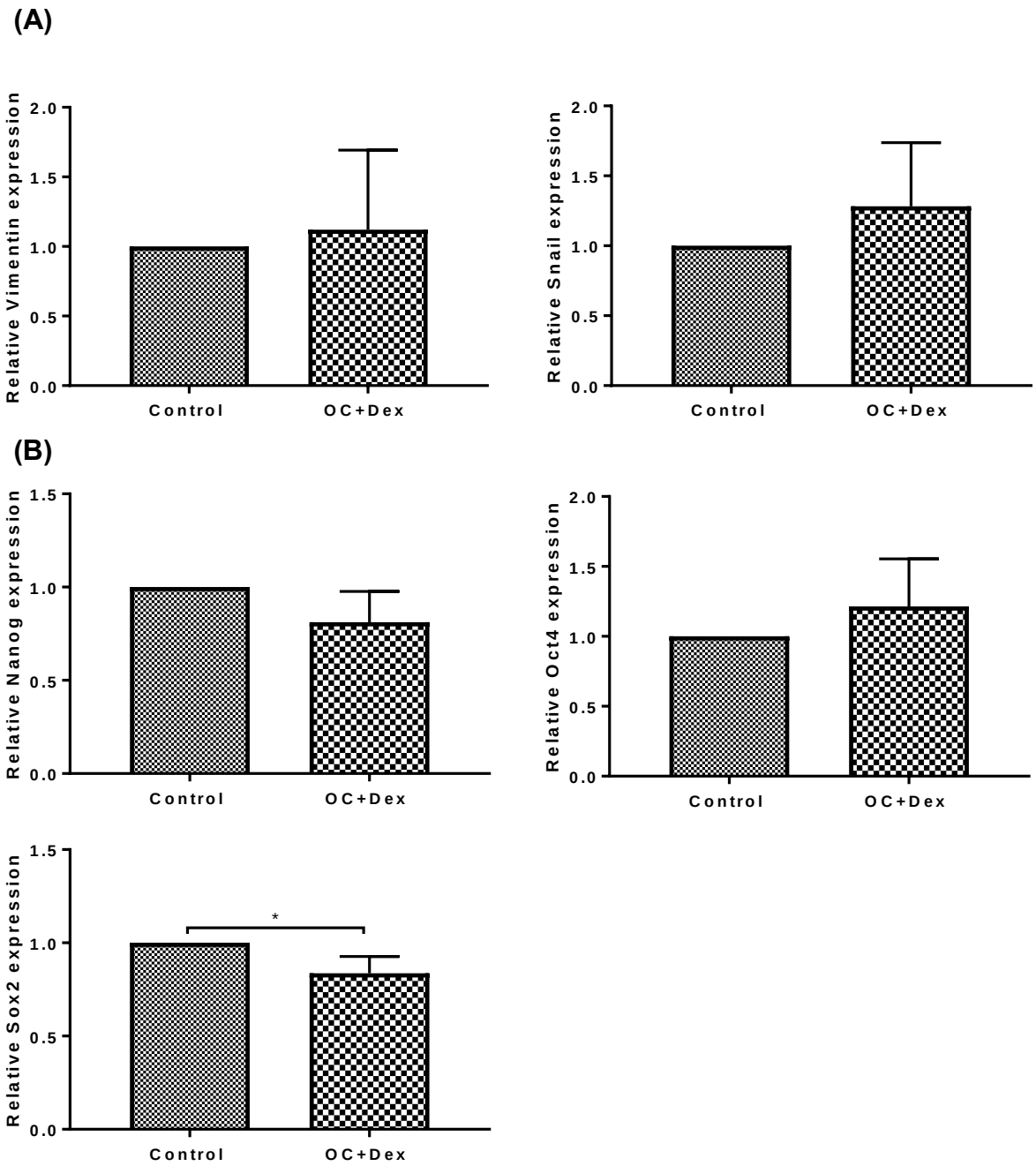

Figure 5.16 Effect of OC+Dex on expression of EMT and cancer stemness markers in SKBR3 cells. Expression of markers of EMT (A) and cancer stemness (B) in SKBR3 cells was analysed following 72-hours culture in control or OC+Dex media. Each point represents mean + SD. (N=4). All statistical significance was analysed by student t-test. *P<0.05

TRPM7 channel activity has been shown to regulate glioma stem cell formation (Liu et al., 2014) and maintain progenitor-like features in neuroblastoma (Middelbeek et al., 2012). However, to the best of our knowledge, a possible role for the channel in breast cancer stem cells has not been investigated. We first analysed if inhibition of TRPM7 by the NS8593 compound previously used within our studies could alter formation of MDA-MB-231 tumourspheres. MDA-MB-231 cells were cultured in control or OC+Dex media, in the presence of absence of 20 µM NS8593. Formation of tumourspheres was assessed after 7 days (Fig. 5.17). As seen previously, cells cultured in OC+Dex media formed significantly more tumourspheres than cells in control media (2.5-fold increase, $P < 0.05$). Inhibition of TRPM7 partially blocked this increase (1.9-fold increase). Compared to cells grown in OC+Dex media alone, cells grown in OC+Dex media with NS8593 displayed a trend towards decreased sphere formation, with approximately 25% fewer tumourspheres counted at day 7, although this trend did not reach statistical significance ($P=0.46$). Addition of 20 µM NS8593 to cells in control media decreased tumoursphere formation by 30%, although this effect was also not found significant.

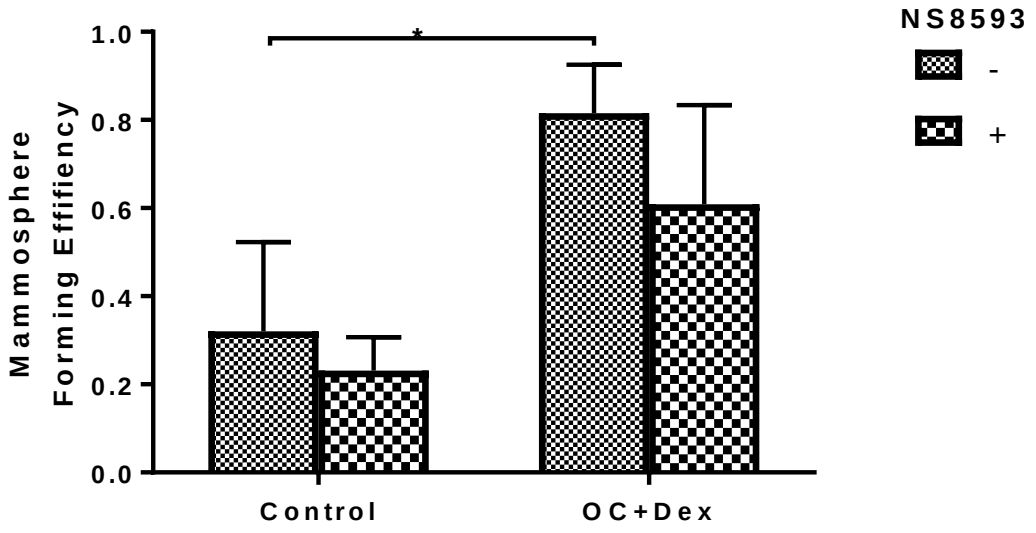

Figure 5.17 Effect of TRPM7 channel inhibition on MDA-MB-231 tumoursphere formation. Analysis of sphere formation in MDA-MB-231 cells cultured in non-adherent pHEMA coated plates for 7 days in control or OC+Dex media, with 20 µM of the TRPM7 inhibitor NS8593 or vehicle control. Each point represents mean + SD. (N=3). Statistical significance was determined by two-way ANOVA, *P<0.05.

As a trend was observed towards decreased tumoursphere formation in MDA-MB-231 cells with inhibited TRPM7 function, we elected to try another approach. MDA-MB-231 cells were transfected with TRPM7 siRNA or a negative control siRNA. Results from our previous chapter showed a 60% decrease in TRPM7 expression 72 hours post-transfection (Fig. 4.18 A). Cells were harvested at this point and assayed for tumoursphere formation. We also chose to use a shorter time-point for this experiment to ensure that any alteration in sphere formation was captured in the time frame in which siRNA knockdown was likely to still be active.

Cells treated with a control siRNA and grown in OC+Dex media formed almost twice as many tumourspheres (1.9-fold increase, $P < 0.05$) as those grown in control media (Fig. 5.18). Cells treated with a TRPM7 targeting siRNA did not exhibit as great of an increase in tumoursphere formation (1.35-fold) following incubation with OC+Dex media. Similar to results with NS8593, a direct comparison between the sphere forming capability of control-siRNA and TRPM7-siRNA in either control or OC+Dex media showed a trend towards decreased formation, although neither reached statistical significance.

Finally, we analysed expression of a panel of EMT and cancer stemness markers in MDA-MB-231 cells transfected with TRPM7 siRNA. Loss of TRPM7 expression had a significant effect on expression of EMT markers (Fig. 5.19 A). Expression of the mesenchymal markers vimentin and Snail were significantly decreased by 25 and 30% respectively, whilst the epithelial marker E-cadherin was upregulated almost 2-fold. Decreased expression of the EMT transcription factor Twist did not reach statistical significance ($P=0.1825$).

In an analysis of stemness markers, downregulation of all three tested markers (Nanog, Sox2 and Oct4) also did not reach the level of statistical significance (Fig. 5.19 B).

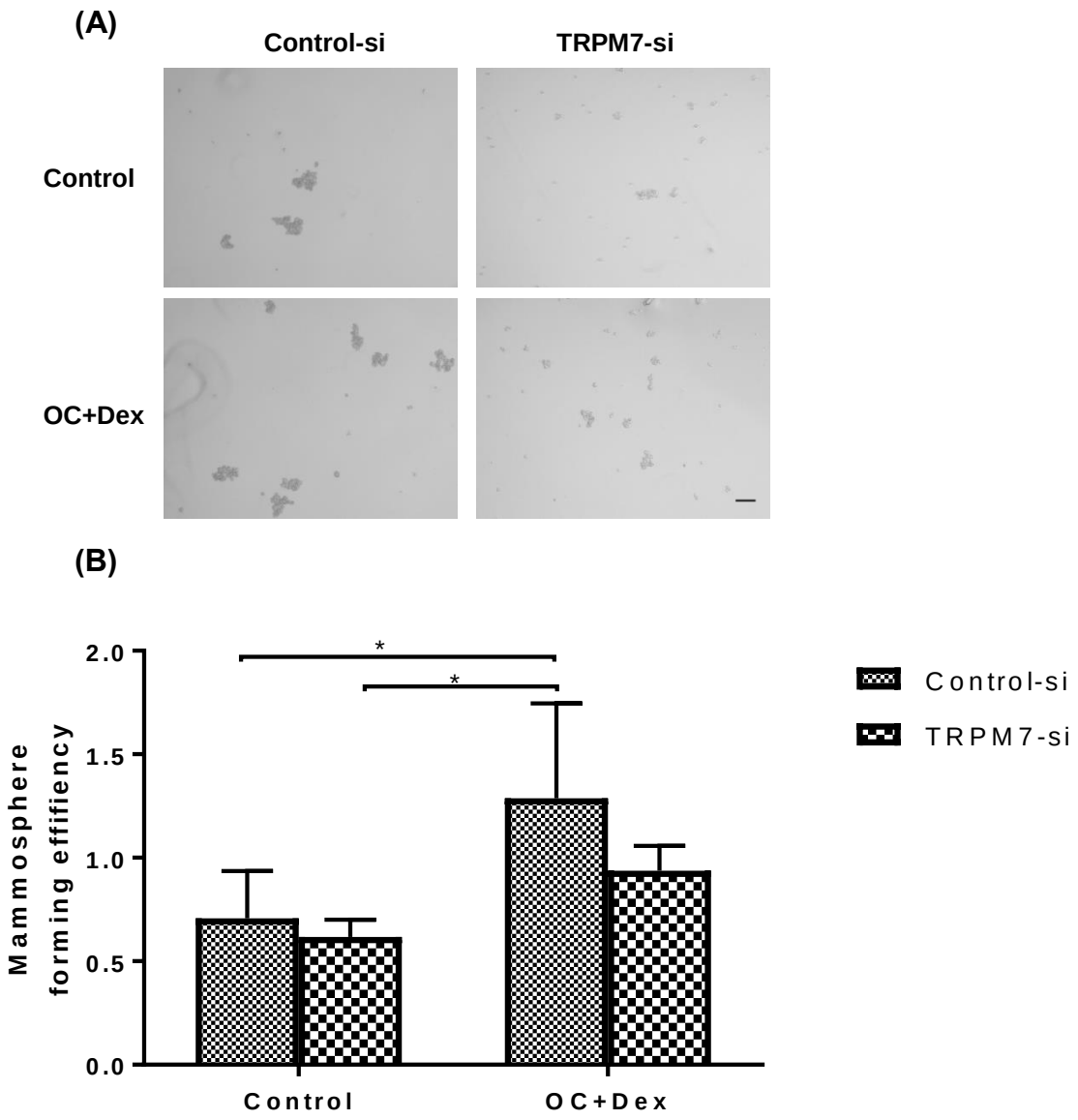

Figure 5.18 Effect of TRPM7 siRNA knockdown on formation of MDA-MB-231 tumourspheres. MDA-MB-231 cells cultured in control or OC+Dex media in were assessed for tumoursphere formation after 7 days. Cells were transfected with a TRPM7 targeting siRNA or a negative control siRNA 72 hours prior to plating in tumoursphere assays. Representative images shown at 10X magnification (A). OC+Dex media induced significant increases in sphere formation which were partially blocked by TRPM7 knockdown (B). Each point represents mean + SD. (N=3). All statistical significance was analysed by two-way ANOVA. *P<0.05. Scale bar represents 50 µm.

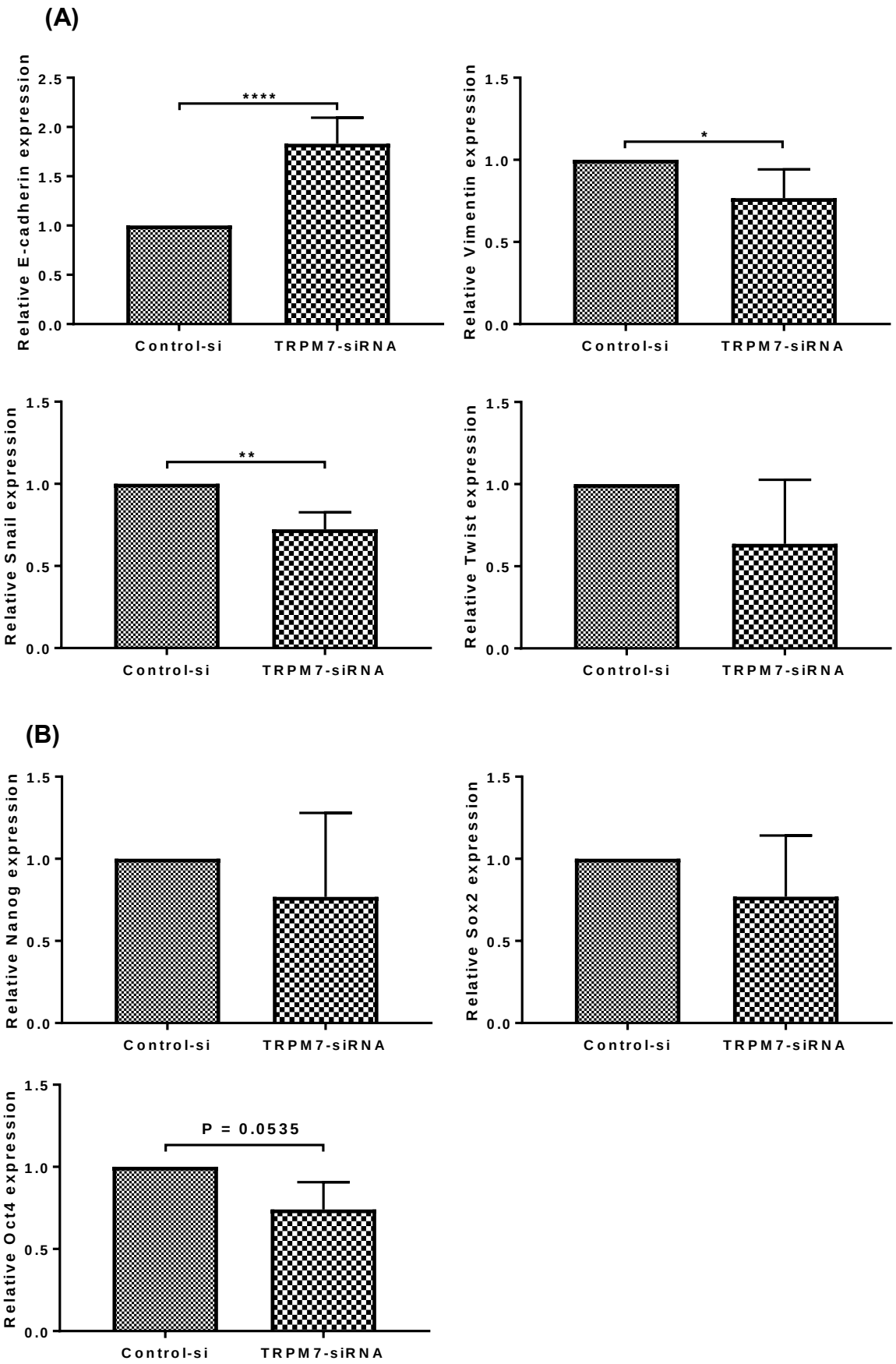

Figure 5.19 Effect of TRPM7 knockdown on expression of EMT and cancer stemness markers in MDA-MB-231 cells. Expression of markers of EMT (A) and cancer stemness (B) in MDA-MB-231 cells was analysed 72-hours post transfection with a control or TRPM7 targeting siRNA. Each point represents mean + SD. (N=3). All statistical significance was analysed by student t-test. *P<0.05.

5.2.5 In vivo mineralisation of MDA-MB-231 cells

Previous studies from our lab using the 4T1 and 4T1.2 murine cell lines confirmed that these cells could successfully produce mineralisations in an *in vivo* setting. To ensure that the MDA-MB-231 cell line utilised for the majority of experiments in this thesis displayed similar *in vivo* mineralisation ability, we acquired tissue samples from a xenograft model, using the same MDA-MB-231 cell line. *In vivo* samples were generated and kindly provided by Dr. Will Brackenbury (University of York, U.K.). 1×10^6 MDA-MB-231-GFP cells were suspended in Matrigel and injected into the inguinal mammary fat pads of *Rag2*$^{-/-}$ *Il2rg*$^{-/-}$ mice. Mice were euthanized when primary tumours reached 10% of starting body weight, or at the first sign of discomfort from metastasis. Tumours were fixed in paraformaldehyde and frozen before cryosections were cut and transferred to glass slides. Sections were stained by Alizarin Red S.

Upon staining with Alizarin Red S, significant levels of mineralisation were readily observed in the tumour tissue (Fig. 5.20). The fact that the MDA-MB-231 cell line forms mineralisation in an *in vivo* setting, without any of the exogenous reagents utilised in *in vitro* assays help to confirm the suitability of the cell line for our *in vitro* studies and demonstrate that any positive mineralisation are not an experimental artefact generated through artificial manipulation of the cell line.

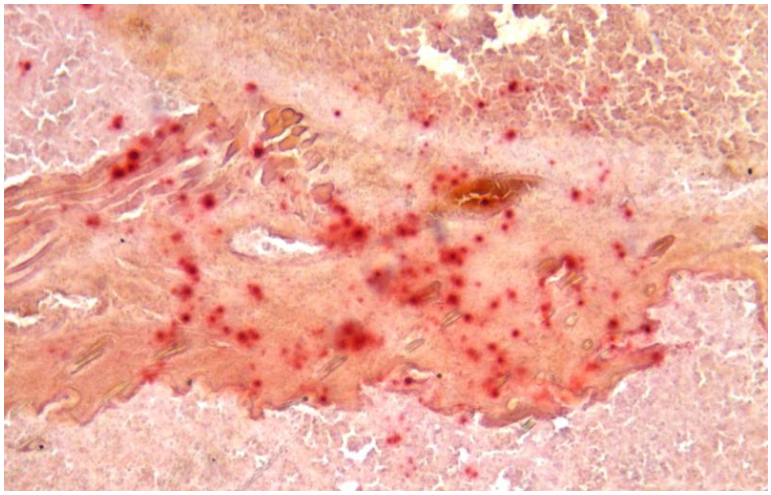

Figure 5.20 *In vivo* mineralisation of the MDA-MB-231 cell line. Alizarin Red S stained section of breast tumour tissue generated by injection of MDA-MB-231 cells into the inguinal mammary fat pads of *Rag2*$^{-/-}$ *Il2rg*$^{-/-}$ mice. Tumours were fixed in paraformaldehyde, frozen before cryosections were cut and transferred to glass slides. Sections were stained by Alizarin Red S as previously described.

5.2.6 Raman analysis of *in vitro* microcalcification samples

Raman spectroscopy has been shown in several studies to be an effective analysis technique for the study of breast microcalcifications (Barman et al., 2013, Haka et al., 2002, Saha et al., 2011) and offers the potential to discriminate type I (calcium oxalate) from type II (hydroxyapatite) calcifications. This is clinically relevant as hydroxyapatite calcifications are significantly more likely to be associated with malignancy (Frappart et al., 1984). To ensure that the calcifications produced in our model were representative of malignancy associated calcifications, we elected to examine the chemical composition of *in vitro* generated samples of microcalcifications. We also wished to analyse if the experimental technique used to induce mineralisation had any effect on the chemical composition of any subsequent calcifications. During the course of this thesis, we have induced mineralisation in breast cancer cells both through the organic Pi source β-glycerophosphate and the direct addition of inorganic sodium phosphate. We therefore tested cells cultured with 10 mM of β-glycerophosphate or sodium phosphate. Apart from the source of Pi, all other media components (ascorbic acid, dexamethasone) were identical between the treatment groups.

In order to provide optimum conditions for Raman analysis, cells were cultured on "windows" of calcium fluoride (CaF_2), which provides transmission of a wide range of wavelengths with minimal interference. We first examined if MDA-MB-231 cells would adhere to CaF_2 windows and mineralise in a similar manner to cells grown on standard tissue culture plates. CaF_2 windows were placed inside 6-well tissue culture plates and incubated in DMEM media for 1 hour prior to being seeded with MDA-MB-231 cells. 24 hours later, after confirming successful adherence of the cells to CaF_2 windows, each plate was switched to control media or either of our two formulations of mineralisation media and cultured for up to 14 days (Fig. 5.21 A), with replicates taken off at days 3, 7, 11 and 14.

Although we could not directly stain the CaF_2 windows with Alizarin Red S or von Kossa (which would interfere with Raman analysis) to verify successful mineralisation, a set of plates were grown in parallel to monitor development of calcifications. Alizarin Red S staining revealed initial mineralisation in cells cultured in Pi+Dex media at day 3, gradually increasing in intensity over the remainder of the time course (Fig. 5.21 B). Mineralisation was slower to initiate in OC+Dex wells, with positive staining first observed at day 11. No positive staining was seen in Control

wells at any stage. Although we did observe a significant level of cell death in cells cultured on CaF_2 windows with inorganic Pi, this did not seem to interfere with generation of a Raman spectra from these plates. Representative image of a single replicate are shown below (Fig. 5.22 A).

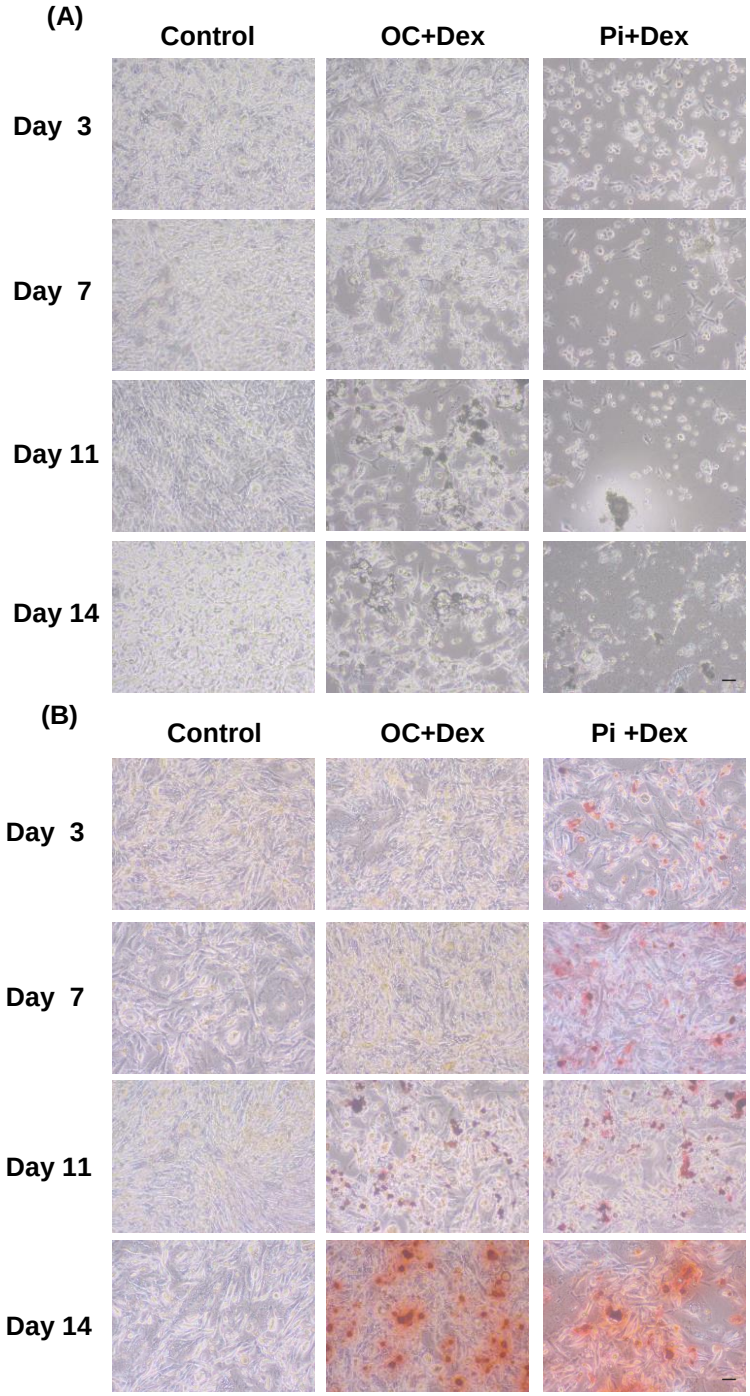

Figure 5.21 Mineralisation of MDA-MB-231 cells grown on CaF_2 windows. Representative images (10X magnification) of MDA-MB-231 cells grown on CaF_2 windows for up to 14 days in control media, or media supplemented with 50 µg/mL ascorbic acid, 100 nM dexamethasone and 10 mM of either β-glycerophosphate (OC+Dex) or sodium phosphate (Pi+Dex) (A). A parallel set of plates were stained with Alizarin Red S to monitor development of calcifications (B). Scale bar represents 50 µm.

All samples were fixed in 10% formalin for 30 minutes and shipped to University of Exeter for analysis by Pascaline Bouzy (Prof. Nick Stone lab). An average of 40 spectra per sample were captured using a 100 mW infrared (830 nm) excitation beam. Averaged results from one replicate are shown below.

(A)

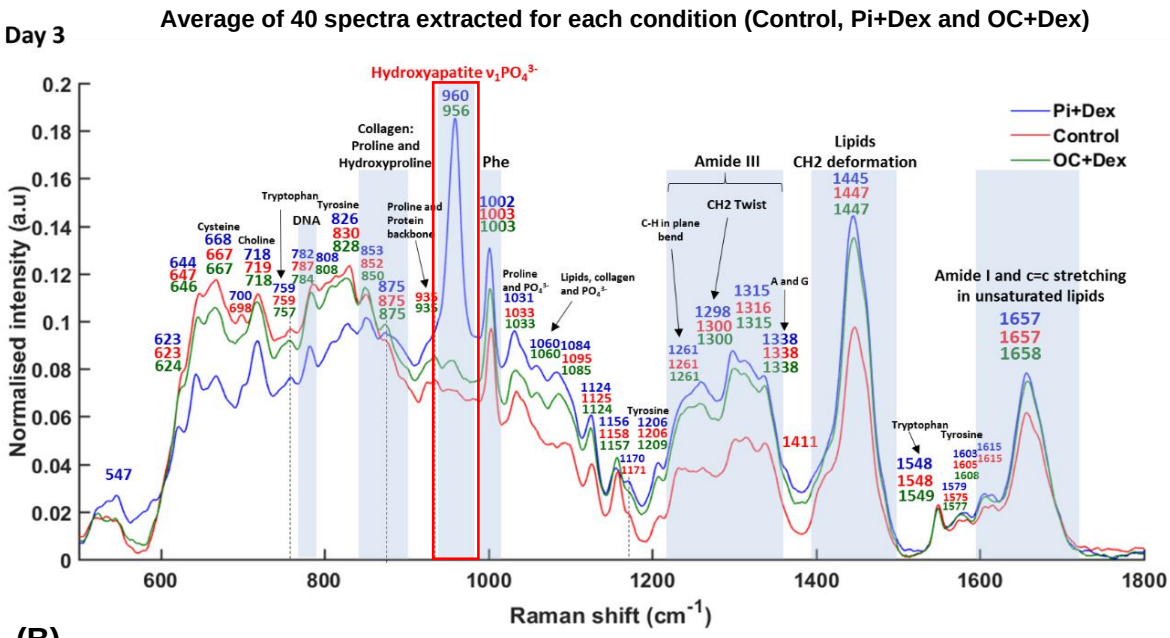

(B)

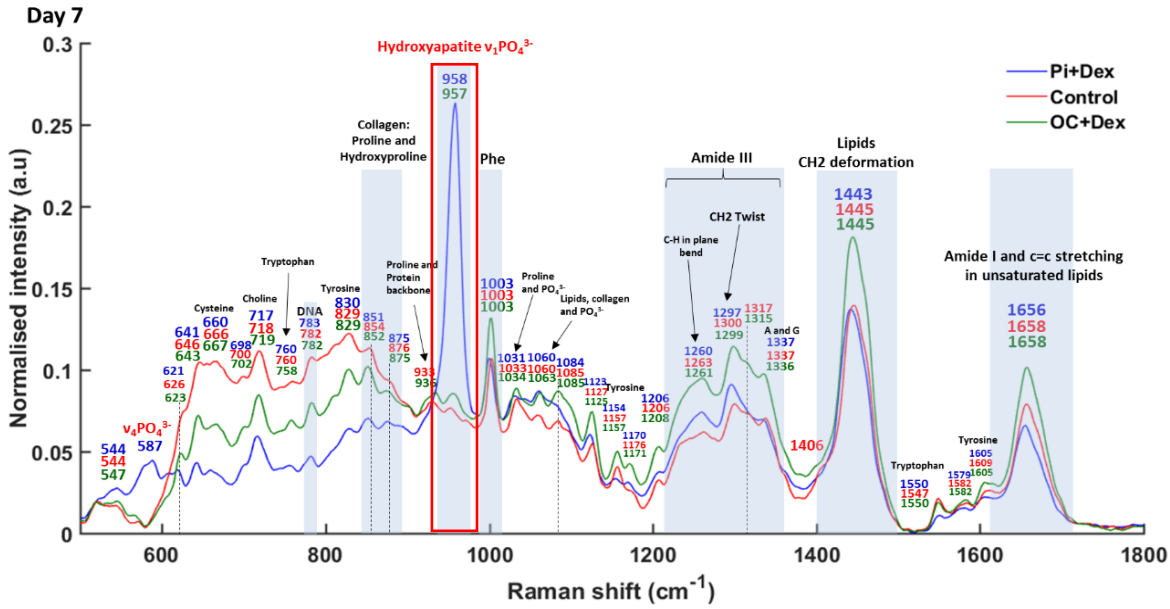

Figure continued below

Figure continued

(C)

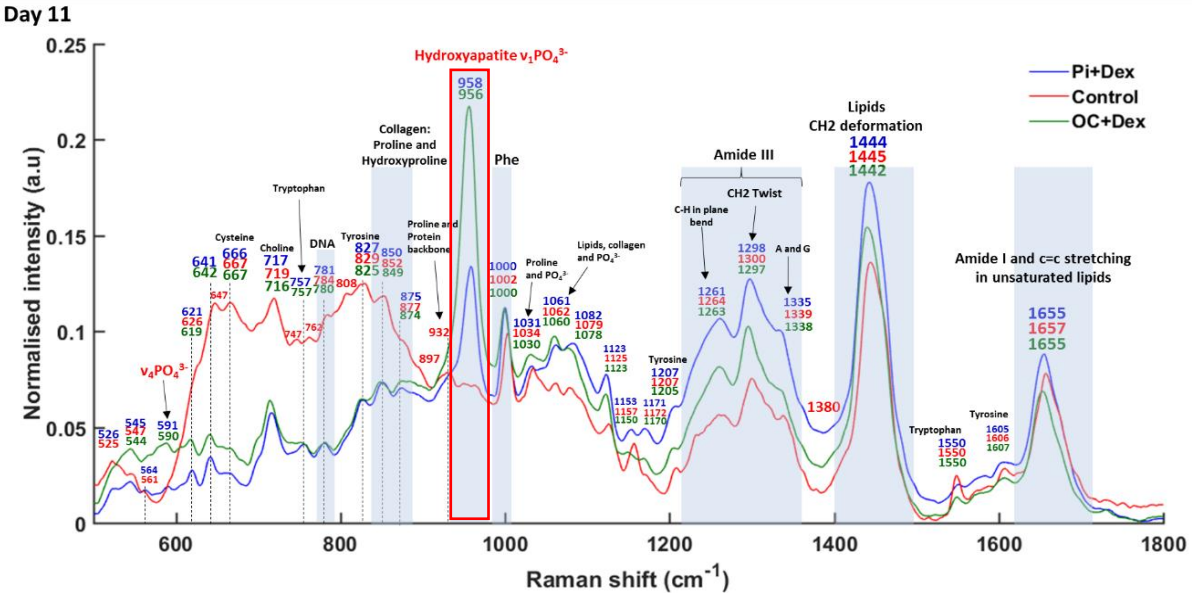

(D)

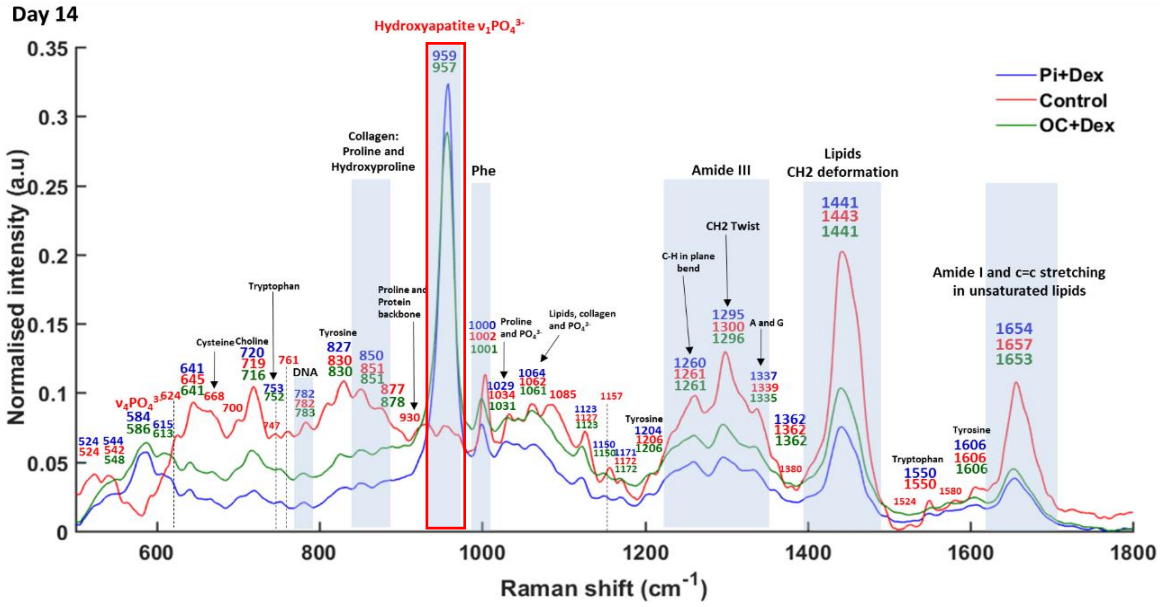

Figure 5.22 Raman analysis of mineralising MDA-MB-231 cells. Raman spectra gathered from MDA-MB-231 cells cultured on CaF_2 windows for up to 14 days in control media, or media supplemented with 50 µg/mL ascorbic acid, 100 nM dexamethasone and 10 mM of either β-glycerophosphate (OC+Dex) or sodium phosphate (Pi+Dex). Graphs represent samples taken at days 3 (A), 7 (B), 11 (C) and 14 (D). Each graph represents the averaged values of 40 spectra gathered for each samples. The presence of hydroxyapatite was detected by a spectral peak at 960 cm-1, highlighted in red.

The presence of hydroxyapatite was detected by a spectral peak at 960 cm^{-1}. This peak was detected in all samples taken from cells cultured in inorganic Pi, even at the earliest time point of day 3 (Fig. 5.22 A). In contrast, no hydroxyapatite peak was detected in the OC+Dex group until day 11 (Fig. 5.22 C). This peak began at a lower amplitude than the peak detected for inorganic Pi at the same time point, indicating a weaker hydroxyapatite signal. However, by day 14 similar peaks were detected in both groups. No hydroxyapatite peak was detected in control samples at any time point. The time points at which hydroxyapatite was detected in each sample corresponded to the point at which positive Alizarin Red S staining was first observed in a set of parallel plates (Fig. 5.21 B).

These results were further analysed using principal component analysis (PCA) to plot samples based on the two greatest sources of variation (Fig. 5.23). Control and OC+Dex samples were observed to cluster together separate from Pi+Dex samples at days 3 and 7, showing no significant differences in their spectral characteristics. In contrast, by days 11 and 14 when the peak of hydroxyapatite was observed in both mineralising samples, PCA analysis showed OC+Dex and Pi+Dex clustering away from control samples.

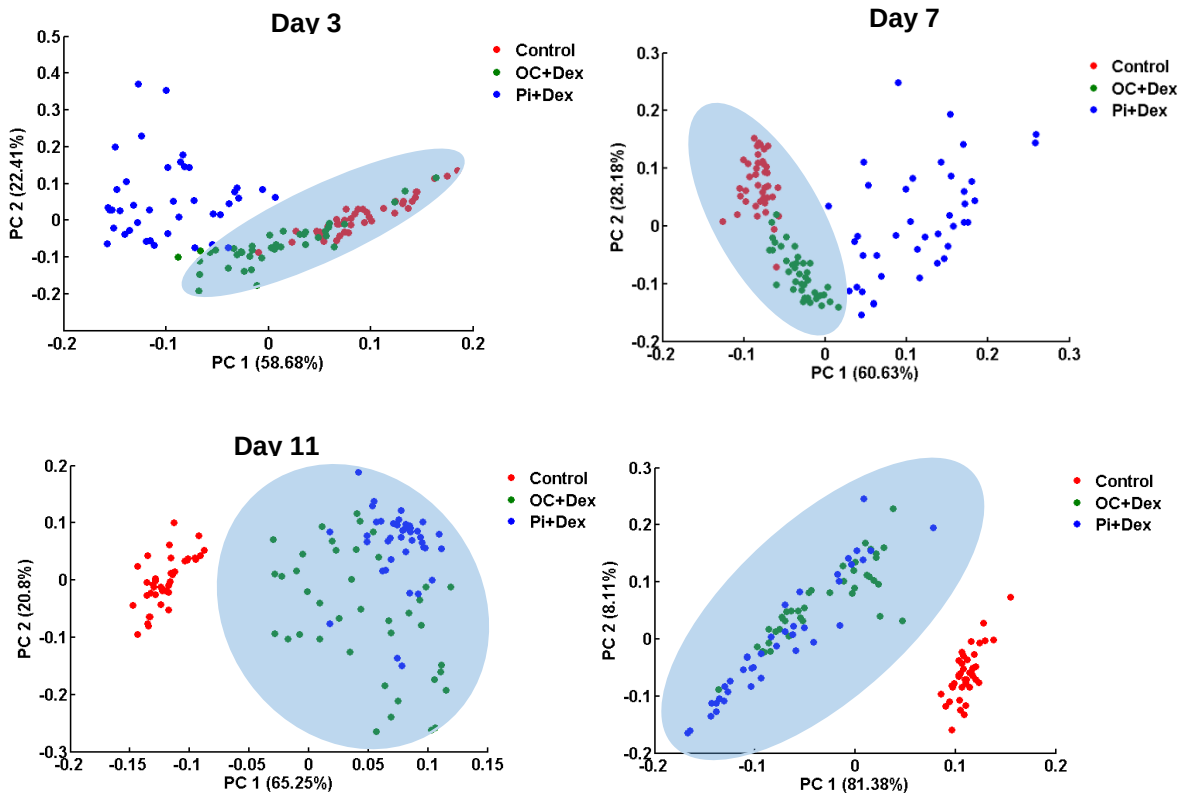

Figure 5.23 PCA of Raman spectra of mineralising MDA-MB-231 cells. PCA was used to plot spectra from 40 spectra from control, OC+Dex and Pi+Dex samples at 4 different time points. Clustering of OC+Dex and Pi+Dex samples at days 11 and 14 highlight their distinction from control samples.

5.3 Discussion

Our aim for this chapter was to examine any correlations between the presence of microcalcifications within the breast, as well as their underlying mechanisms of formation, to any potentially tumour-promoting effects. A possible mechanism behind the increased tumour aggressiveness often observed in calcification associated breast tumours is a direct stimulation effect of calcium phosphate crystals on both the breast tumour itself and associated tissue, including stroma and immune cells. HA stimulation of breast cancer cells has previously been shown to upregulate several inflammatory markers, including COX2, prostaglandins, matrix metalloproteinases and IL-1β (Cooke et al., 2003, Morgan et al., 2001). In addition, the presence of calcium phosphate crystals within other tissues has been linked to induction of an inflammatory state, and disease progression. For example, the formation of calcium phosphate crystals within the synovial joint in patients with osteoarthritis triggers upregulation of IL-1β and metalloprotease activity, leading to destruction of cartilage tissue (Ea et al., 2013). However, the number of characterised contributors to this inflammatory state in breast cancer cells to this date is low.

We elected to focus much of our studies on IL-6 due its significant association in the literature with both breast cancer (Dethlefsen et al., 2013, Knupfer and Preiss, 2007) and mineralisation (Nasi et al., 2016, Yang et al., 2007). Serum IL-6 levels are highly elevated in breast cancer patients (Hussein et al., 2004) and increased levels have been associated with decreased survival (Ahmed et al., 2006, Bachelot et al., 2003, Noman et al., 2017) and increased number of metastatic lesions (Salgado et al., 2003). Studies on the effect of IL-6 on proliferation in breast cancer have been highly inconsistent, with studies finding both increases (Sasser et al., 2007, Casneuf et al., 2016) and decreases (Selander et al., 2004, Badache and Hynes, 2001). IL-6 is also a potent inducer of aromatase activity, triggering increased production of estrogen and stimulation of ER+ breast tumours (Purohit et al., 2002). ER+ cell lines produce little IL-6, and depend on paracrine sources of the cytokine (Chiu et al., 1996). The primary source of this paracrine IL-6 within a breast tumour is likely to be cancer associated fibroblasts (CAFs), which produce up to 100 times more IL-6 than normal fibroblasts (Hugo et al., 2012).

In contrast, ER negative breast cancer cells lines typically display a high level of IL-6 expression (Chavey et al., 2007). The MDA-MB-231 cell line utilised for the majority of experiments in this thesis has previously been shown to express high levels of IL-6 (Casneuf et al., 2016) and we found IL-6 was easily detectable at both an mRNA and protein level in this cell line (Fig. 5.2). IL-6 secretion was significantly increased by 24 hour stimulation with HA nanoparticles. Increased IL-6 secretion following stimulation with HA has previously been demonstrated in other cell types (Liu and Sun, 2014, Zhao et al., 2013, Ea et al., 2013, Nasi et al., 2016) but this is the first report of an increase in IL-6 expression associated with HA stimulated breast cancer cells.

Upregulation of IL-6 was found to be dependent on Ca^{2+} influx, as inhibition of intracellular Ca^{2+} accumulation by BAPTA-AM completely blocked increases in IL-6 (Fig. 5.3). We did not find any previous reports on a relationship between intracellular Ca^{2+} and IL-6 secretion in breast cancer although constitutive activity of calcium sensing receptor (CaSR) promotes basal secretion of IL-6 whilst increased extracellular Ca^{2+} acts in the opposite manner to suppress IL-6 expression (Hernández-Bedolla et al., 2016). Although we did not examine the signalling pathways involved in HA-induced IL-6 expression in breast cancer, Nasi et al. found a dose dependent increase in IL-6 expression in HA stimulated chondrocytes (Nasi et al., 2016). This increase could be attenuated by inhibition of IL-6 signalling factors PI3K, Jak2 and STAT3, suggesting an autocrine loop. Similar autocrine IL-6 loops have been described in triple-negative breast cancer (Hartman et al., 2013). Serum IL-6 concentration is correlated with tumoural pSTAT3 levels (Casneuf et al., 2016) and MDA-MB-231 cells display constitutive STAT3 activation (Selander et al., 2004).

We did not observe any increase in mineralisation in MDA-MB-231 cells treated with IL-6 (Fig. 5.5). In addition, no increase in STAT3 phosphorylation was detected (Fig. 5.5). Other studies have also found no increase in pSTAT3 in MDA-MB-231 cells following IL-6 stimulation (Casneuf et al., 2016). These results would indicate that MDA-MB-231 are largely unresponsive to exogenous IL-6, possible indicating a lack of IL-6R expression. Co-stimulation of IL-6 with sIL-6R did increase STAT3 phosphorylation in MDA-MB-231, indicating activation of the IL-6 trans-signalling pathway.

The dependence of MDA-MB-231 cells on exogenous sources of sIL-6R was further shown by PCR analysis. We observed by PCR that although MDA-MB-231 possess significant expression of the ubiquitous gp130 signalling subunit, no detectable expression of either membrane-bound or soluble IL-6R was detected in MDA-MB-231 cells (Fig. 5.7). sIL-6R can be produced either via alternative splicing of IL-6R mRNA, or by proteolytic cleavage of membrane bound IL-6R (Kallen, 2002). Therefore the lack of sIL-6R detected by PCR analysis in MDA-MB-231 does not completely exclude its production by this cell line, although any amounts produced would likely be small, as evidenced by the lack of membrane-bound IL-6R expression detected. Although the MDA-MB-231 cell line does not produce sIL-6R, addition of exogenous sIL-6R to OC+Dex media resulted in a significant enhancement of calcium deposition (Fig. 5.5). As MDA-MB-231 cells produce high amounts of IL-6, sIL-6R could be binding to the endogenous IL-6 present within the media and promoting activation of signalling pathways. Similar results have been shown in a study of collagenase 3 expression in rat osteoblasts, with significant increases in expression observed in cells stimulated with sIL-6R alone (Franchimont et al., 1997).

Interestingly, no increase was observed when MDA-MB-231 cells were cultured in OC+Dex media with a combination of IL-6 and sIL-6R. It is unclear why the pro-mineralisation effect exerted by sIL-6R would seem to be inhibited when used together with exogenous IL-6, although this combination would result in greater levels of signalling than sIL-6R alone, suggesting that there may be an optimal level of IL-6 signalling that is conducive to mineralisation. Testing both IL-6 and sIL-6R at a range of concentrations could potentially address this question. Another possibility is activation of a signalling mechanism independent of IL-6 as several studies have suggested that sIL-6R can function independently of IL-6 (Knupfer and Preiss, 2007). sIL-6R increases pSTAT3 levels in hematopoietic cells in both *IL-6*$^{+/+}$ and *IL-6*$^{-/-}$ mice (Cho et al., 2013).

Although many studies have looked at the effect of IL-6 signaling on mineralisation, results are conflicting. Addition of IL-6 and sIL-6R to calcifying adipose-derived mesenchymal stem cells results in enhanced expression of RUNX2 and increased calcium deposition (Fukuyo et al., 2014).

This effect was found to be dependent on activation of STAT3 and signaling through the noncanonical wingless-type (Wnt) pathway via receptor tyrosine kinase-like orphan receptor 2 (ROR2). Other studies have found IL-6 to promote osteoblastic differentiation of periodontal ligament cells (Iwasaki et al., 2008) human osteoblastic cells (Nishimura et al., 1998) adipose-derived stromal cells (Huh and Lee, 2013), illustrating the potent ability of this cytokine to promote mineralisation in a variety of cell types. However, other studies have shown opposite effects. Secretion of IL-6 by Saos 2 osteosarcoma cells inhibited the osteogenic differentiation of mesenchymal stem cells (Bian et al., 2010). In addition, a recent study utilising a mouse model of osteoporosis found that osteoporotic bone marrow stem cells displayed both highly increased levels of IL-6 and phosphorylated STAT3 and impaired osteogenesis: this effect was reversed either through administration of IL-6 neutralizing antibodies or IL-6 knockdown (Li et al., 2016). Kaneshiro et al recently reported that stimulation of the osteoblast cell line MC3T3-E1 with IL-6 activated three signaling pathways (Kaneshiro et al., 2014). Whilst STAT3 appeared to promote osteoblastic differentiation, in agreement with other studies highlighting an important role for STAT3 in calcification (Huh and Lee, 2013, Lin et al., 2016, Parhami et al., 2002), activation of dual specificity mitogen-activated protein kinase kinase 2 (MEK2) and PI3K pathways lead to an inhibitory effect. Thus, the somewhat conflicting data on the effect of IL-6 signaling on osteoblast activity may be partly explained by which pathways are activated. Another possible reason for the inconsistent results may lie with Wnt signaling pathways. Whilst Fukuyo et al observed a pro-calcifying effect of IL-6 through activation of the non-cannonical Wnt pathway via ROR2 (Fukuyo et al., 2014) Li et al observed inhibition of β-catenin and the canonical Wnt pathway, speculating that the differing Wnt pathways active in their respective studies could explain the conflicting results (Li et al., 2016).

We also observed IL-6 and sIL-6R to promote mineralsation in MDA-MB-231 cells cultured in OC media without dexamethasone. This was the first time we observed dexamethasone-independent mineralisation of the MDA-MB-231 (excluding exogenous ALP or Pi). The fact that IL-6+sIL-6R seemed to be capable of substituting for dexamethasone in MDA-MB-231 mineralisation lead us to theorise that they could be acting on similar pahways. Interactions between the glucocorticoid receptor and STAT3 signalling have previously been demonstrated (Petta et al., 2016).

Both cell lines we identified as capable of producing mineralisations (MDA-MB-231 and SKBR3) display constitutive STAT3 phosphorylation (Selander et al., 2004). STAT3 is constitutively active in approximately 40% of breast tumours and contributes to tumour progression via deregulation of numerous downstream genes including Bcl-2, survivin, cyclin D1, c-Myc, HIF-1α, VEGF, vimentin, TWIST, and MMP-9 (Banerjee and Resat, 2016). Although we did not observe any change in pSTAT3 levels in MDA-MB-231 cells cultured in OC+Dex, phosphorylation of STAT3 was significantly increased in SKBR3 cells following incubation with OC+Dex (Fig. 5.8).

To further examine the effect of STAT3 phosphorylation in calcification, we utilised the small molecule inhibitor JSI-124, and observed significant reductions in both calcium deposition and ALP activity (Fig. 5.9). However, an examination of pSTAT3 levels in JSI-124 treated MDA-MB-231 cells did not detect any significant changes. We used JSI-124 at a concentration of 100 nM, which has been shown to effectively reduce pSTAT3 in multiple cell types (Huh and Lee, 2013, Zhang et al., 2015, Cucuzza et al., 2008). In contrast, many studies in breast cancer using JSI-124 have utilised the inhibitor at concentrations of up to 10 µM (Jiang et al., 2010, Lieblein et al., 2008). We observed a high degree of toxicity in MDA-MB-231 when JSI-124 was used at concentrations higher than 100 nM (data not shown), which prevented us from utilising a concentration more likely to effectively demonstrate suppression of pSTAT3. Other studies utilisng JSI-124 at high concentrations have been releatively short term studies (4-72 hours), in comparision to our long term mineralisation assays where a significiant loss of cell viabiltiy is far more detrimental.

It remains unclear as to why JSI-124 inhbited mineralisation in our studies but did not exert any detectable effect on pSTAT3. Although JSI-124 has been reported to have high selectivity (Blaskovich et al., 2003), off-target effects have been described, including activation of NF-κB (McFarland et al., 2013) and JNK (c-Jun N-terminal kinase) pathways (Ishdorj et al., 2011). Other STAT3 targeting agents are available and an analysis of their effect on mineralisation of breast cancer cell lines could help explain the discrepancy between the anti-mineralisation effect of JSI-124 in the absence of any detectable change on pSTAT3 levels.

In addition to examining the response of breast cancer cells to HA, we also explored the effect that increased expression of inflammatory markers could have on other cell types. Tumour associated macrophages (TAMS) are derived from circulating monocytes which are recruited to tumours by the activity of chemokine factors such as CCL2 where they differentiate to macrophages (Soria and Ben-Baruch, 2008). Macrophages are highly diverse and capable of differentiating to a range of functional phenotypes, with TAMs generally observed to display a "wound-healing" M2 type (Laoui et al., 2011). TAMs are powerful drivers of tumour progression and their levels within a tumour is predictive of patient prognosis (Medrek et al., 2012). TAMs and breast cancer cells exert a significant level of control over each others patterns of gene expression and the three inflammatory markers we examined (IL-1β, IL-6 and COX2) have been shown to be closely linked in previous studies of TAMs in breast cancer. Secretion of IL-1β from THP-1 cells has previously been shown to promote expression of COX2 in associated breast cancer cells (Hou et al., 2011) whilst upregulation of COX2 in TAMs promotes IL-6 secretion (Gan et al., 2016).

In an examination of the effect of direct stimualltion of HA nanoparticles on THP-1 cells, we observed a 6-fold upregulation of IL-1β (Fig. 5.4). HA has previously been shown to increase IL-1β secretion through activation of the NLRP3 inflammasome (Pazar et al., 2011). We also examined an indirect interaction between HA crystals and TAMs, wherein HA stimulated MDA-MB-231 were used to create conditioned media with increased inflammatory cytokine content, which was subsequently used to stimulate THP-1 cells. Although none of these were found to be significant, there was a clear trend towards increased upregulation following stimulation with conditioned media taken from HA-stimualted MDA-MB-231 cells (Fig. 5.4). If further replicates were to confirm this trend, it would demonstrate a previously unknown role for microcalcifications in promoting breast tumour growth as the markers we examined are all known contributors to the pro-tuomourigenic effect of TAMs in breast cancer. Conditioned media from MDA-MB-231 cells was previously shown to enhance IL-6 expression in macropahges via macrophage colony-stimulating factor (M-CSF) (Sousa et al., 2015) and IL-6 secretion by TAMs has been shown to contribute to invasion (Wolfe et al., 2016).

COX2 expression in TAMs promotes EMT and secetion of metalloproteinase from breast cancer cells (Gan et al., 2016), whilst IL-1β secretion from TAMs is essential for initiation of angiogenic signalling (Carmi et al., 2009). In conclusion, although this work will require validation, the potential link between increased expresson of inflammatory cytokines in HA stimulated breast cancer cells and activation of TAMs could be a significant contributor to tumour aggressiveness.

Breast epithelial cells have previously been shown to be capable of transitioning to a mesenchymal phenotype with stem cell like properties through an EMT process (Battula et al., 2010). Acquisition of a stem-like phenotype may allow for subsequent conversion to an osteogenic phenotype and could promote the formation of microcalcifications. In an examination of the stem-like properties of breast cancer cells in mineralising conditions, we observed a significant increase in the number of tumourspheres in both MDA-MB-231 (Fig. 5.12) and SKBR3 cells (Fig. 5.13) cultured in OC+Dex media. MDA-MB-231 cells cultured as tumourspheres have been shown to have increased tumourigenicity compared to adherent cell cultures (Wang et al., 2014).The rate of tumoursphere formation we observed in MDA-MB-231 cells was slightly lower in cells than reported in previous studies. Although we initially expected the highly aggressive MDA-MB-231 to effectively form tumourspheres, the ability to form tumourspheres is not necessarily linked to the aggressiveness of a cell line as several studies have found the highly tumourigenic MDA-MB-231 cell line to less efficiently form spheres than the non-tumourigenic MCF-7 cell line (Wang et al., 2014, Calvet et al., 2014, Morata-Tarifa et al., 2016). This may be related to high expression of E-cadherin in MCF-7 cells, as knockdown of E-cadherin decreases MCF-7 sphere forming ability whist overexpression in the SKBR3 cell line significantly enhances formation of tumourspheres (Manuel Iglesias et al., 2013). As MDA-MB-231 are a mesenchymal cell line with no E-cadherin expression (Chao et al., 2010)., this may explain their lower rate of tumoursphere formation. RUNX2, which we have previously shown to be upregulated in mineralising MDA-MB-231 (Fig. 4.9) has been found to promote formation of tumourspheres, in part by increasing proteolytic processing of the N-terminus of E-cadherin resulting in the release of a soluble fragment with oncogenic properties (Brusgard et al., 2015).

Out of the three reagents comprising the OC+Dex mix (β-glycerophosphate, ascorbic acid and dexamethasone), it is likely that dexamethasone is responsible for this increase in sphere forming ability. Dexamethasone signals through the glucocorticoid receptor (GR), a ligand activated transcription factor that upon binding dexamethasone (or endogenous glucocorticoids like cortisol) translocates to the nucleus and binds to response elements in the promoter region of target genes (Nicolaides et al., 2010). GR expression appears to act as a prognostic factor in breast cancer albeit in an opposing fashion depending on ER status, as high GR expression is associated with decreased RFS in ER- patients and increased RFS in patients with ER+ tumours (Pan et al., 2011). Several studies have suggested a link between GR signalling and cell stemness. Goodman et al. reported an increase in a basal-like CK5+/CD44+ subpopulation in MCF-7 cells stimulated with dexamethasone (Goodman et al., 2015). This subpopulation was associated with increased drug resistance and colony formation in soft agar. The glucocorticoid receptor antagonist Mifepristone was also recently shown to suppress tumoursphere formation in triple-negative breast cancer cells (Liu et al., 2016). Finally, a recent study by Sorrentino found that stimulation of GR by the synthetic glucocorticoid betamethasone resulted in activation of the Hippo signalling yes-associated protein (YAP) and a two-fold increase in tumoursphere formation in betamethasone stimulated MDA-MB-231 cells (Sorrentino et al., 2017). They also observed significant upregulation of the transcription factor Slug.

This was in contrast to some of our findings, as although we did not examine expresson of Slug, we did observe decreased expression in several other transcription factors known to regulate cell stemness, such as Sox2 and Oct4 (Fig. 5.15). Possible reasons for the different results could be the length and nature of the stimulation used to activate GR signalling. The authors treated cells with 1 µM betamethasone for 24 hours prior to analysis, whilst we used a lower concentration but longer time frame (100 nM dexamethasone for 72 hours). Investigating expression at different time points could shed light on any time dependent regualtion of expression of stem markers. In addition, the stem markers we tested are just a few of the wide number of reported influencers of cell stemness.

In addition, both vimentin and E-cadherin have been shown to contribute to formation of tumourspheres in breast cancer cells (Borgna et al., 2012, Manuel Iglesias et al., 2013), indicating a degree of flexibility in which pathways are active during formation of tumourspheres. Analysis of other markers such as CD44 or analysis of surface proteins by flow cytometry would give a more complete picture of any changes in the stem-like properties of cells cultured with OC+Dex.

Although we observed a significant increase the tumoursphere formation of both MDA-MB-231 and SKBR3 cells cultured in OC+Dex media, we did not find any evidence of positive mineralisation in these spheres. However, the lack of positive mineralisation in OC+Dex cultured tumourspheres is unsurprising, as calcium was analysed after only 7 days, when mineralisation typically first becomes apparent around day 11. Longer incubation time periods of tumoursphere culture were not analysed as these longer periods would likely result in poor viability of the spheres. In addition, due to the small number of cells present in each well any calcifications potentially formed would likely be extremely small and low in quantity, and below the detection capability of Alizarin staining. A more sensitive detection technique (e.g., the Raman spectroscopy analysis already used in this thesis to detect and analyse calcifications) could be used to examine this theory.

Although the morphology of our tumourspheres closely resembles the morphologies of MDA-MB-231 spheres published in other studies (Prud'homme et al., 2010, Shaw et al., 2012, Louie et al., 2010, Borgna et al., 2012), it is worth noting that some disagreement does exist within the literature on the tumoursphere forming ability of the MDA-MB-231 cell line, as they tend not to form compact spheres. Some studies have argued that the looser morphology of MDA-MB-231 tumourspheres are not representative of true tumourspheres (Manuel Iglesias et al., 2013). However, MDA-MB-231 cells cultured as spheres have been shown to possess enhanced tumour formation relative to adherent cells (Wang et al., 2014, Stivarou et al., 2016), indicating that despite not forming spherical structures, the culturing of MDA-MB-231 cells as non-adherent cultures does appear to selecting for cells with stem-like properties.

We also investigated several markers of EMT as Scimeca et al. recently noted increased levels of the mesenchymal protein vimentin in breast tumours with associated microcalcifications (Scimeca et al., 2014).

Similar to cell stemness, activation of GR signalling has also been suggested as a regulator of EMT. A chromatin immunoprecipitation with sequencing (ChIP-seq) analysis of dexamethasone stimulated MCF10A-Myc cells identified significant activation of the EMT pathway indicating an association between activation of GR signalling and shift towards a mesenchymal phenotype (Pan et al., 2011). Although we did not conduct a thorough analysis into a potential role for the EMT process in the formation of calcifications, we examined expression of several markers following 72 hours incubation in mineralisation promoting media and observed a decrease in the mesenchymal marker vimentin as well as the EMT associated transcription factor Twist. Interestingly, we also observed a decrease in the epithelial marker e-cadherin, indicating that cells are not undergoing a total transition to an epithelial phenotype, supported by the fact that cells retain approximately 60% of their vimentin expression. Although we initially expected an increase in mesenchymal markers in OC+Dex stimulated MDA-MB-231, our findings of decreased expression are in agreement with some previous studies. Ferrand et al. found decreased expression of vimentin and the EMT promoting transcription factor zinc finger E-box-binding homeobox 1 (Zeb1) in dexamethasone stimulated MDA-MB-231 cells (Ferrand et al., 2012). Dexamethasone stimulation of MDA-MB-231 cells was also previously shown to promote an increase in focal adhesion complexes and shift to a “cobblestone” like morphology, characteristic of an epithelial phenotype (Leo et al., 2004). Dexamethasone has also been shown to suppress EMT in other cell types (Yang et al., 2017, Kim et al., 2015b) and activation of GR seems to be important in E-cadherin function in breast cancer. Fluorescence microscopy of the MDA-MB-231 with forced over-expression of E-cadherin showed E-cadherin to be mostly cytoplasmic and non-functional. Administration of dexamethasone alongside the histone deacetylase (HDAC) inhibitor largazole restored the localisation of E-cadherin to junctions (Law et al., 2012). Thus the effect of GR signalling appears to be highly dependent on the cellular context, with different cell types responding in divergent manners.

A key attribute of stem cells is a multi-lineage differentiation capability and the ability to differentiate down an osteogenic pathway may be a key promoter of the development of microcalcifications (Scimeca et al., 2014). If true, the increased tumoursphere forming capability in OC+Dex cultured MDA-MB-231 cells may reflect an increased stemness and osteogenic differentiation ability.

Although we were unable to explore this idea in significant detail, several other groups have examined the multi-lineage differentiation capability of stem-like cells derived from breast epithelium. Human mammary epithelial cells (HMECs) overexpressing the EMT promoting transcription factors Snail and Twist display similar levels of CD44 and CD24 as mesenchymal stem cells (Battula et al., 2010). Furthermore, these EMT derived mammary cells were capable of differentiation towards osteoblast, adipocyte or chondrocyte lineages. Similar results were seen in MCF-7 cells treated with the matricellular protein periostin (Wang et al., 2013) or conditioned media from senescent fibroblasts (Ortiz-Montero et al., 2017). As such, an increase in the stemness of our cell lines could enhance their *in vitro* mineralisation capability. Tumourspheres can be cultured for several generations by enzymatically dissociating spheres and using the resulting single cell suspension to seed fresh plates (Manuel Iglesias et al., 2013). Serial passaging of tumoursphere cultures can promote enrichment of cells with stem-like properties. Subsequent examination of the mineralisation potential of this “stem-enriched” population could shed light on any potential involvement for cancer stem cells in the formation of microcalcifications.

Our findings of a significant alteration in expression of epithelial and mesenchymal markers in TRPM7-siRNA treated cells is also in agreement with previous studies. Breast carcinomas with associated calcifications express high levels of both TRPM7 (Mandavilli et al., 2013) and mesenchymal markers (Scimeca et al., 2014), suggesting the two factors could possibly be linked. Indeed, inhibition of TRPM7 by the small molecule inhibitor NS8593 or siRNA blocks EGF induced EMT in MDA-MB-468 breast cancer cells (Davis et al., 2014). Our investigation into a potential role for the channel in promotion of stemness was less clear. Cells treated with NS8593 or a TRPM7 targeting siRNA did not undergo as large of an increase in tumoursphere formation by OC+Dex media and direct comparison between the control-siRNA and TRPM7-siRNA in either control or OC+Dex media showed a trend towards decreased formation, although neither reached statistical significance. TRPM7 activity has been shown to promote formation of cancer stem cells in glioma (Liu et al., 2014) as well as maintain expression of progenitor cell-like feature in neuroblastoma (Middelbeek et al., 2015).

Based on this role in promoting stemness in other forms of cancer and the trend towards decreased sphere formation we observed in MDA-MB-231 with decreased TRPM7 function, we believe that the channel may play a similar role in breast cancer although a significant amount of further work will be required to establish such a role.

Our finding of mineralisations formed in a xenograft model is in agreement with other studies demonstrating an *in vivo* mineralisation capability for the MDA-MB-231 cell line (Felix et al., 2015, Wilson et al., 2014). The fact that these cell can form *in vivo* microcalcifications without further intervention is noteworthy and suggests that findings from our *in vitro* studies are likely to be applicable to the *in vivo* setting. As well as the MDA-MB-231 cell line, other groups have also successfully demonstrated the *in vivo* formation of calcifications using other breast cancer cell lines. *In vivo* calcification has been observed in BMP2-transfected R3230 rat tumour cells (Liu et al., 2008, Liu et al., 2010) and MCF-7 cells (Clement et al., 2005). In contrast to these studies, we observed mineralisation in implanted MDA-MB-231 cells with no further intervention and no source of exogenous BMP2 required. Similarly, previous findings from our lab showed successful mineralisation of the 4T1 and 4T1.2 cell lines in xenograft experiments (Cox et al., 2012a). When considered alongside the fact that we did not observe any positive mineralisation in the MCF-7 cell line even when treated with exogenous BMP2 (Fig. 4.4), the ability of a cell line to mineralise may not be a binary option, but may represent a spectrum of the “readiness” of a cell to mineralise under the right conditions with our *in vitro* assay selecting for the most “mineralisation-capable” cell lines (as evidenced by their ability to mineralise *in vivo* without exogenous BMP2). Further work will be necessary but the demonstration of an *in vivo* mineralisation capability in several breast cancer cell lines may point to the next stage in the study of formation of microcalcifications.

In the final part of this chapter, we sought to characterise the chemical composition of the calcifications produced within our *in vitro* model utilising Raman spectroscopy. Although Raman has previously been used to identify the chemical identity of *in vitro* generated samples of breast calcifications (Cox et al., 2012a), a thorough analysis of the their chemical properties and how they develop over a time-course has never been performed.

We identified a significant peak in the Raman spectrum characteristic of hydroxyapatite (960 cm^{-1}) which was observed for cells cultured in Pi+Dex from the earliest detected time point (day 3), but did not become evident until day 11 for OC+Dex samples. This was backed up by PCA analysis that showed clustering of control and OC+Dex samples at days 3 and 7, before OC+Dex began to cluster with Pi+Dex at days 11 and 14, indicating a change in spectral characteristics. The significant time difference in first detection of hydroxyapatite between the two different formulations of osteogenic media is unsurprising and can be explained by the different source of Pi within the medias. The β-glycerophosphate contained in OC+Dex acts as an organic Pi donor that require degradation by ALP whilst Pi+Dex media contained inorganic sodium phosphate that was available immediately for mineralisation without requiring any ALP degradation. Despite the longer incubation time required before onset of mineralisation, the organic Pi formulation of media appeared to be more suited to culturing cells on the Raman-compatible CaF_2 windows as we observed a significant amount of cell death in cells cultured with Pi+Dex at all tested time points.

Interestingly, because the CaF_2 windows were smaller than the wells of a 6-well plate, some cells adhered to the areas of the plate not covered by the CaF_2 windows. This allowed us to observe cells mineralising on two different surfaces within the same well. Significant cell death was observed in cells grown on CaF_2 windows in inorganic Pi group, but not on cells grown in the same well but on the surface of the tissue culture plate itself. In addition, no noticeable cell death was seen in cells grown on CaF_2 windows with control media. Therefore, the combination of growing on CaF_2 windows in the presence of mineralisation media appeared to be adversely affecting the viability of cells in this experiment. Nevertheless, Raman spectra were successfully derived from all replicates.

Unfortunately, although we were able to confirm the presence of hydroxyapatite within *in vitro* calcification samples, a full examination of the spectra was still ongoing by our collaborators group at the time of writing. A detailed examination of our Raman spectra may allow us to assess how closely the *in vitro* samples match previous findings from patient studies. Baker et al. found notable differences in the chemical composition of calcifications from benign and malignancy associated calcifications (Baker et al., 2010).

The carbonate content of calcifications is closely associated with malignancy, as demonstrated by the gradual decrease in carbonate content as tumours progress from benign (2.085% carbonate) to *in situ* lesions (1.83%) to invasive tumours (1.41%). Carbonate was also observed to significantly decrease going from low to high-grade lesions. Although this analysis was carried out using the related technique mid-Fourier transform infrared (FTIR) spectroscopy, analysis of carbonate content by Raman spectroscopy is also possible (Kerssens et al., 2010) as carbonate content of hydroxyapatite calcifications can be estimated from the width of the 960 cm^{-1} band, with increased carbonate substitution in the crystal lattice resulting in a loss of long-range order and broadening of the peak (Sathyavathi et al., 2015). Other features of malignant calcifications detectable by Raman spectroscopy include increased mineral:matrix ratio (Baker et al., 2010), the presence of magnesium whitlockite (Scott et al., 2016), increased levels of actin (Sathyavathi et al., 2015). If the calcifications produced in our *in vitro* assay are found to closely match the crystal structure and chemical composition of malignancy associated calcifications, it would further highlight the suitability of our assay to study the *in vivo* formation of mammary calcifications.

Although this analysis is ongoing, the data generated here are a significant resource and can be utilised in several ways to contribute to our understanding of mammary calcification. For instance, Raman analysis was also used in previous studies from our lab to confirm the presence of hydroxyapatite within *in vitro* mineralisations produced from multiple cell lines (Cox et al., 2012a). Interestingly, although mineralisations from different cell lines were all found to consist of hydroxyapatite, significant differences were observed in the carbonate content of calcification samples from different cell lines with the human Hs578Ts(i)8 producing calcifications of low carbonate content and therefore more representative of calcifications found within invasive tumours (Baker et al., 2010). Expanding the number of breast cancer cells with characterised *in vitro* calcification samples may allow for selection of a cell line with the most clinically relevant form of produced calcification. We have also examined mineralisations produced from both organic and inorganic sources of Pi. As the source of Pi used within *in vitro* mineralisation experiments has been shown to impact the properties of subsequent mineralisations (Schäck et al., 2013), careful selection of appropriate mineralisation media should

allow us to determine the ideal conditions required for the formation of hydroxyapatite mineralisations as similar as possible to clinical samples.

Finally, the fact that we collected samples from four different time points for all samples raises the potential of utilising the Raman spectra generated in this chapter to shed light on the early events in the formation of microcalcifications. During physiological mineralisation, hydroxyapatite is not formed directly but is believed to be initially deposited as an amorphous calcium phosphate before conversion to hydroxyapatite through a number of intermediaries (Tertuliano and Greer, 2016). Smith et al. recently utilised Raman spectroscopy to examine the early osteogenic changes in murine calvarial osteoblasts and used deconvolution of spectral peaks in the region of hydroxyapatites characteristic 960 cm^{-1} peak to successfully track the formation of several of these intermediaries (Smith et al., 2017). A similar analysis of the time course data presented here would represent the first time that the initiation, growth and development of mammary calcifications had been tracked from start to finish and would significantly enhance our understanding of the formation process of these vital diagnostic clues.

5.4 Summary and conclusions

In conclusion, the main findings from this chapter are as follows;

- Hydroxyapatite increases expression of a range of inflammatory markers in breast cancer cells and may indirectly promote the pro-tumourigenic effect of TAMs.
- sIL-6R promotes development of MDA-MB-231 mineralisations and when used in combination with IL-6, allows for dexamethasone independent mineralisation.
- Breast cancer cells in OC+Dex media have significantly enhance tumoursphere forming ability, although conversely, tend to have decreased expression of certain stemness markers.
- The MDA-MB-231 cell line is capable of generating *in vivo* mineralisation in the absence of any exogenous factors
- Generation of a time-course Raman spectroscopy data-set will allow for the first characterisation of initial microcalcification development.

Chapter 6.0

Concluding discussion

6.1 Summary of key findings

Although the clinical significance of breast microcalcifications has long been recognised, our understanding of the mechanism by which they form is incomplete. Previous work from our lab established the first *in vitro* model of mammary calcification and provided the first evidence in favour of an active, cell-regulated process with many similarities to physiological, osteoblast mediated mineralisation (Cox et al., 2012a, Cox et al., 2012b). The primary aims of this thesis were to expand on previous findings, which were carried out predominantly on murine cell lines, and improve the translational relevance by focusing on human breast cancer cell lines.

In Chapter 3, we screened a panel of human breast cancer cell lines representative of all major molecular subtypes, and observed positive mineralisation in the HER2+ SKBR3 and the triple-negative MDA-MB-231 cell lines. In total, we examined three cell lines with HER2 overexpression but observed positive mineralisation in only one. This was a significant finding, as the presence of microcalcifications is strongly linked to HER2 status in patients (Cen et al., 2017a). Our results indicate that although HER2 may be contributing to the promotion of calcification, its expression is not sufficient by itself. This is, in fact, consistent with the literature as, although the mammographic detection of microcalcifications is widely accepted as suggestive of HER2 amplification, it is by no means a universal feature of these tumours (Cen et al., 2017a, Killelea et al., 2013a, Ling et al., 2013). Analysis of the ALP activity of two mineralising cell lines (MDA-MB-231 and SKBR3) revealed significantly higher levels compared to the non-mineralising MCF-7 cell line. The critical role of ALP activity was demonstrated by the lack of mineralisation seen in cells cultured with the ALP inhibitor levamisole and by the development of mineralisation in the previously non-mineralising MCF-7 cell line when cultured with exogenous ALP, further highlighting the involvement of a cellular-dependent process in the formation of microcalcifications.

In Chapter 4, we explored the hypothesis that microcalcifications form as a result of an imbalance between pro- and anti-mineralisation factors. Similar models have been shown for many forms of pathological calcification but have never been explored in mammary calcification. Dysregulated expression of many of the key players in physiological mineralisation, including BMP2, osteonectin, osteopontin, and bone sialoprotein has been observed in close proximity to breast microcalcifications in clinical tissue samples (Bellahcène and Castronovo, 1995,

Bellahcène et al., 1994, Scimeca et al., 2014, Oyama et al., 2002), suggesting a potential for their involvement in the mineralisation process. In choosing potential genes for examination, we focused on those that with previously demonstrated roles in both breast cancer and pathological calcification, in an effort to examine if development of breast calcifications follows similar mechanisms to other, more well-studied forms of soft-tissue calcification.

In an analysis of the function of known physiological mediators of mineralisation we observed that addition of exogenous BMP2 significantly enhanced mineralisation whilst siRNA knockdown of the osteogenic transcription factor RUNX2 resulted in a decrease, demonstrating the involvement of physiological promoters of mineralisation in the development of breast calcifications. Conversely, we identified PPi and Mg^{2+} as important inhibitory regulators of mineralisation. The role of PPi was further demonstrated by a significant decrease in expression of ENPP1, a key enzyme involved in the creation of PPi. Results from both this thesis and previous studies from our lab have demonstrated a pathway of Pi processing and transport involving ENPP1, ALP and the Pi channel Pit1. However, the involvement of Ca^{2+} transport pathways has never been studied in an *in vitro* setting. We primarily focused on the cation channel TRPM7, which was previously shown to be highly expressed in breast tumours with associated calcifications(Mandavilli et al., 2013). In addition to showing a significant increase in TRPM7 expression in mineralising cells, we also observed significantly decreased mineralisation in studies using two separate TRPM7 inhibitors and a siRNA knockdown, demonstrating a functional role for the channel in promoting formation of microcalcifications for the first time. We also found a decrease in mineralisation following siRNA knockdown of the Ca^{2+} efflux pump PMCA2, further establishing a vital role for Ca^{2+} transport pathways.

Finally, in Chapter 5 we examined potential ways in which the deposition of calcium in the tumour microenvironment could affect both breast cancer cells themselves, and associated macrophages, by potentially promoting inflammation and a stem cell-like phenotype. Although the inflammatory cytokines IL-1β and TNF-α were found to inhibit mineralisation, IL-6 when used in combination with a soluble version of its receptor (sIL-6R) induced a dexamethasone independent form of mineralisation. sIL-6R also increased mineralisation in MDA-MB-231 cells cultured in OC+Dex.

Activation of the STAT3 pathway may be involved in formation of calcifications as both cell lines identified as capable of mineralising *in vitro* have constitutive STAT3 activation. Although the STAT3 inhibitor JSI-124 significantly inhibited both calcium deposition and ALP activity in MDA-MB-231 cells, we were unable to detect any changes in STAT3 phosphorylation. We also examined potential links between calcifications and the stem-like properties of breast cancer cells and observed a significant increase in tumoursphere formation of MDA-MB-231 and SKBR3 cells when cultured in OC+Dex media. This was accompanied by a decrease in expression of classical stemness markers, although analysis of other markers and time points may be merited. We also demonstrated preliminary evidence for a role of the TRPM7 channel in regulating tumoursphere formation. Our observation of *in vivo* mineralisation in the MDA-MB-231 cell line highlights the suitability of the cell line for these studies and supports the relevance of our *in vitro* findings to the *in vivo* setting. Finally, the chemical nature of *in vitro* calcification samples was confirmed as hydroxyapatite, the form of calcification most commonly associated with malignancy. Ongoing analysis of our Raman spectroscopy dataset has the potential to significantly enhance our understanding of the early events of calcium deposition and formation of mature hydroxyapatite crystals.

6.2 Future recommendations

Results from this thesis significantly enhance our current understanding of the molecular processes underlying the development of mammary calcifications. However, there are a number of avenues of research that due to time-constraints we were unable to fully explore. Further investigation of the following points may be warranted.

Although the MDA-MB-231 cell line utilised for the majority of our studies displayed a dependence on dexamethasone, we did observe dexamethasone-independent mineralisation following stimulation with a combination of IL-6 and sIL-6R. These results indicate that particular cytokines can substitute for glucocorticoid signalling and initiate osteogenic changes in breast cancer cells. An examination of other cytokines, in particular those likely to be upregulated within the breast tumour and associated tissue, would improve understanding of the link between microcalcifications and tumour microenvironment.

As we have observed upregulation of several tumourigenic cytokines following stimulation by hydroxyapatite, the possibility of a feed-back loop, wherein breast cancer cells deposit hydroxyapatite, triggering increased cytokine secretion and subsequent alteration of osteogenic pathways.

We have demonstrated the involvement of two Ca^{2+} transporters, TRPM7 and PMCA2 in the *in vitro* formation of microcalcifications. However, Ca^{2+} homeostasis is regulated by a large group of channels, transporters and other associated proteins, many of which are dysregulated in breast cancer and have been shown to contribute to tumourigenesis. The vast majority of these Ca^{2+} handling proteins have not been investigated for any potential influence on mammary calcification. Of particular interest, the TRPC1 channel, which we found to be upregulated in our studies has previously been shown to be highly expressed (alongside TRPM7) in calcification associated tumours. Functional characterisation of the effect of TRPC1 and other Ca^{2+} transport proteins including annexins could provide further evidence for the role of Ca^{2+} transport pathways. In addition, as our data indicate a role for both Ca^{2+} influx (TRPM7) and efflux (PMCA2) channels, an examination of changes in intracellular Ca^{2+} during the mineralisation process (for example, utilising fluorescence microscopy with the Fura-2 calcium indicator) would shed light on the role of intracellular Ca^{2+} levels.

The data from this thesis, when combined with previous results from our group and others, has identified a significant number of mediators of calcification in an *in vitro* setting. Previously, immunohistochemistry has been used to demonstrate the presence of several mineralisation associated proteins in the vicinity of microcalcifications. However, the number of analysed proteins is relatively low. Future studies of a selection of the genes highlighted by these studies would help bridge the gap between *in vitro* and *in vivo* studies. Based on our data, we believe the first targets to be analysed should be ALP, PMCA2, RUNX2 and MGP. In addition, demonstration of an *in vivo* mineralisation capability for the MDA-MB-231 cell line now raises the possibility of utilising an *in vivo* model for future studies. An example of proposed studies would involve xenograft transplantation of breast cancer cells with altered expression (generated by transfection with plasmids containing cDNA or shRNA sequences) of candidate genes, and monitoring for development of microcalcifications.

The increased rate of tumoursphere formation observed in cells cultured in OC+Dex media hints at the involvement of cell stemness in formation of microcalcifications. Considering that culturing breast cancer cells as tumourspheres has been shown to enhance their tumourigenicity, the question of whether a similar process could alter their ability to form microcalcifications would be an interesting avenue to explore. Further analysis of EMT and stemness markers at alternative time points and a functional study of how these two pathways interact could clarify the relationship between the these two pro-tumourigenic pathways and the development of microcalcifications.

6.3 Conclusion

Despite their central role in the clinical detection of a significant number of breast cancer cases every year, the formation of microcalcifications has not been extensively studied. In this thesis, we have expanded the number of mineralisation-capable human breast cancer cell lines and identified functional roles for several genes associated with physiological mineralisation. Many of the genes we identified as potential contributors to formation of microcalcifications have previously been shown to influence breast tumour behaviour, potentially linking the formation of microcalcifications to increased tumour aggressiveness. This work builds on our previous findings and further demonstrates the role of a cell-mediated process in the formation of mammary calcifications.

Chapter 7.0

References

ABD EL-REHIM, D. M., PINDER, S. E., PAISH, C. E., BELL, J., BLAMEY, R. W., ROBERTSON, J. F. R., NICHOLSON, R. I. & ELLIS, I. O. 2004. Expression of luminal and basal cytokeratins in human breast carcinoma. *The Journal of Pathology,* 203**,** 661-671.

ABDELGAWAD, I. A., EL-MOUSLY, R. H., SABER, M. M., MANSOUR, O. A. & SHOUMAN, S. A. 2015. Significance of serum levels of vitamin D and some related minerals in breast cancer patients. *Int J Clin Exp Pathol,* 8**,** 4074-82.

ABRAMSON, V. G., LEHMANN, B. D., BALLINGER, T. J. & PIETENPOL, J. A. 2015. Subtyping of triple-negative breast cancer: implications for therapy. *Cancer,* 121**,** 8-16.

ABRAMSON, V. G. & MAYER, I. A. 2014. Molecular Heterogeneity of Triple Negative Breast Cancer. *Current breast cancer reports,* 6**,** 154-158.

ADDISON, W. N., AZARI, F., SØRENSEN, E. S., KAARTINEN, M. T. & MCKEE, M. D. 2007. Pyrophosphate Inhibits Mineralization of Osteoblast Cultures by Binding to Mineral, Up-regulating Osteopontin, and Inhibiting Alkaline Phosphatase Activity. *Journal of Biological Chemistry,* 282**,** 15872-15883.

ADES, F., ZARDAVAS, D., BOZOVIC-SPASOJEVIC, I., PUGLIANO, L., FUMAGALLI, D., DE AZAMBUJA, E., VIALE, G., SOTIRIOU, C. & PICCART, M. 2014. Luminal B Breast Cancer: Molecular Characterization, Clinical Management, and Future Perspectives. *Journal of Clinical Oncology,* 32**,** 2794-2803.

ADEVA-ANDANY, M. M., FERNÁNDEZ-FERNÁNDEZ, C., SÁNCHEZ-BELLO, R., DONAPETRY-GARCÍA, C. & MARTÍNEZ-RODRÍGUEZ, J. 2015. The role of carbonic anhydrase in the pathogenesis of vascular calcification in humans. *Atherosclerosis,* 241**,** 183-191.

AHMED, O. I., ADEL, A. M., DIAB, D. R. & GOBRAN, N. S. 2006. Prognostic value of serum level of interleukin-6 and interleukin-8 in metastatic breast cancer patients. *Egypt J Immunol,* 13**,** 61-8.

ALARMO, E.-L. & KALLIONIEMI, A. 2010. Bone morphogenetic proteins in breast cancer: dual role in tumourigenesis? *Endocrine-Related Cancer,* 17**,** R123-R139.

ANDERSON, H. C. 2003. Matrix vesicles and calcification. *Current Rheumatology Reports,* 5**,** 222-226.

APOSTOLOU, P., TOLOUDI, M., CHATZIIOANNOU, M., IOANNOU, E. & PAPASOTIRIOU, I. 2012. Cancer stem cells stemness transcription factors expression correlates with breast cancer disease stage. *Curr Stem Cell Res Ther,* 7**,** 415-9.

ARANCIBIA HERNÁNDEZ, P. L., TAUB ESTRADA, T., LÓPEZ PIZARRO, A., DÍAZ CISTERNAS, M. L. & SÁEZ TAPIA, C. 2016. Breast calcifications: Description and classification according to BI-RADS 5th edition. *Revista chilena de radiología,* 22**,** 80-91.

ARNOLD, S. F., TIMS, E. & MCGRATH, B. E. 1999. Identification of bone morphogenetic proteins and their receptors in human breast cancer cell lines: importance of BMP2. *Cytokine,* 11**,** 1031-7.

ARNOULD, L., GELLY, M., PENAULT-LLORCA, F., BENOIT, L., BONNETAIN, F., MIGEON, C., CABARET, V., FERMEAUX, V., BERTHEAU, P., GARNIER, J., JEANNIN, J. F. & COUDERT, B. 2006. Trastuzumab-based treatment of HER2-positive breast cancer: an antibody-dependent cellular cytotoxicity mechanism? *Br J Cancer,* 94**,** 259-267.

AUTIER, P., BONIOL, M., KOECHLIN, A., PIZOT, C. & BONIOL, M. 2017. Effectiveness of and overdiagnosis from mammography screening in the Netherlands: population based study. *BMJ,* 359.

AWOLARAN, O., BROOKS, S. A. & LAVENDER, V. 2016. Breast cancer osteomimicry and its role in bone specific metastasis; an integrative, systematic review of preclinical evidence. *The Breast,* 30**,** 156-171.

AZZOPARDI, P. V., O'YOUNG, J., LAJOIE, G., KARTTUNEN, M., GOLDBERG, H. A. & HUNTER, G. K. 2010. Roles of Electrostatics and Conformation in Protein-Crystal Interactions. *PLoS ONE,* 5**,** e9330.

BACHELOT, T., RAY-COQUARD, I., MENETRIER-CAUX, C., RASTKHA, M., DUC, A. & BLAY, J. Y. 2003. Prognostic value of serum levels of interleukin 6 and of serum and plasma levels of vascular

endothelial growth factor in hormone-refractory metastatic breast cancer patients. *British Journal of Cancer,* 88**,** 1721-1726.

BADACHE, A. & HYNES, N. E. 2001. Interleukin 6 Inhibits Proliferation and, in Cooperation with an Epidermal Growth Factor Receptor Autocrine Loop, Increases Migration of T47D Breast Cancer Cells. *Cancer Research,* 61**,** 383.

BADVE, S., DABBS, D. J., SCHNITT, S. J., BAEHNER, F. L., DECKER, T., EUSEBI, V., FOX, S. B., ICHIHARA, S., JACQUEMIER, J., LAKHANI, S. R., PALACIOS, J., RAKHA, E. A., RICHARDSON, A. L., SCHMITT, F. C., TAN, P. H., TSE, G. M., WEIGELT, B., ELLIS, I. O. & REIS-FILHO, J. S. 2011. Basal-like and triple-negative breast cancers: a critical review with an emphasis on the implications for pathologists and oncologists. *Mod Pathol,* 24.

BAE, M. S., MOON, W. K., CHANG, J. M., CHO, N., PARK, S. Y., WON, J. K., JEON, Y. K., MOON, H. G., HAN, W. & PARK, I. A. 2013. Mammographic features of calcifications in DCIS: correlation with oestrogen receptor and human epidermal growth factor receptor 2 status. *Eur Radiol,* 23**,** 2072-8.

BAI, Y., ZHANG, J., XU, J., CUI, L., ZHANG, H., ZHANG, S. & FENG, X. 2015. Magnesium prevents β-glycerophosphate-induced calcification in rat aortic vascular smooth muscle cells. *Biomedical Reports,* 3**,** 593-597.

BAKER, R., ROGERS, K. D., SHEPHERD, N. & STONE, N. 2010. New relationships between breast microcalcifications and cancer. *Br J Cancer,* 103**,** 1034-1039.

BALINT, E., SZABO, P., MARSHALL, C. F. & SPRAGUE, S. M. 2001. Glucose-induced inhibition of in vitro bone mineralization. *Bone,* 28**,** 21-8.

BANERJEE, K. & RESAT, H. 2016. Constitutive activation of STAT3 in breast cancer cells: A review. *Int J Cancer,* 138**,** 2570-8.

BANERJEE, S., REIS-FILHO, J. S., ASHLEY, S., STEELE, D., ASHWORTH, A., LAKHANI, S. R. & SMITH, I. E. 2006. Basal-like breast carcinomas: clinical outcome and response to chemotherapy. *Journal of Clinical Pathology,* 59**,** 729-735.

BARMAN, I., DINGARI, N. C., SAHA, A., MCGEE, S., GALINDO, L. H., LIU, W., PLECHA, D., KLEIN, N., DASARI, R. R. & FITZMAURICE, M. 2013. Application of Raman spectroscopy to identify microcalcifications and underlying breast lesions at stereotactic core needle biopsy. *Cancer research,* 73**,** 3206-3215.

BARNES, G. L., HEBERT, K. E., KAMAL, M., JAVED, A., EINHORN, T. A., LIAN, J. B., STEIN, G. S. & GERSTENFELD, L. C. 2004. Fidelity of Runx2 Activity in Breast Cancer Cells Is Required for the Generation of Metastases-Associated Osteolytic Disease. *Cancer Research,* 64**,** 4506.

BARREAU, B., DE MASCAREL, I., FEUGA, C., MACGROGAN, G., DILHUYDY, M. H., PICOT, V., DILHUYDY, J. M., DE LARA, C. T., BUSSIERES, E. & SCHREER, I. 2005. Mammography of ductal carcinoma in situ of the breast: review of 909 cases with radiographic-pathologic correlations. *Eur J Radiol,* 54**,** 55-61.

BARTOSOVA, M., PARKKILA, S., POHLODEK, K., KARTTUNEN, T. J., GALBAVY, S., MUCHA, V., HARRIS, A. L., PASTOREK, J. & PASTOREKOVA, S. 2002. Expression of carbonic anhydrase IX in breast is associated with malignant tissues and is related to overexpression of c-erbB2. *J Pathol,* 197**,** 314-21.

BASELGA, J., BRADBURY, I., EIDTMANN, H., DI COSIMO, S., DE AZAMBUJA, E., AURA, C., GÓMEZ, H., DINH, P., FAURIA, K., VAN DOOREN, V., AKTAN, G., GOLDHIRSCH, A., CHANG, T.-W., HORVÁTH, Z., COCCIA-PORTUGAL, M., DOMONT, J., TSENG, L.-M., KUNZ, G., SOHN, J. H., SEMIGLAZOV, V., LERZO, G., PALACOVA, M., PROBACHAI, V., PUSZTAI, L., UNTCH, M., GELBER, R. D. & PICCART-GEBHART, M. 2012. Lapatinib with trastuzumab for HER2-positive early breast cancer (NeoALTTO): a randomised, open-label, multicentre, phase 3 trial. *Lancet (London, England),* 379**,** 633-640.

BASHARI, M. H., FAN, F., VALLET, S., SATTLER, M., ARN, M., LUCKNER-MINDEN, C., SCHULZE-BERGKAMEN, H., ZÖRNIG, I., MARME, F., SCHNEEWEISS, A., CARDONE, M. H., OPFERMAN, J. T., JÄGER, D. & PODAR, K. 2016. Mcl-1 confers protection of Her2-positive breast cancer cells to hypoxia: therapeutic implications. *Breast Cancer Research : BCR,* 18**,** 26.

BATTULA, V. L., EVANS, K. W., HOLLIER, B. G., SHI, Y., MARINI, F. C., AYYANAN, A., WANG, R.-Y., BRISKEN, C., GUERRA, R., ANDREEFF, M. & MANI, S. A. 2010. Epithelial-mesenchymal transition-derived cells exhibit multi-lineage differentiation potential similar to mesenchymal stem cells. *Stem cells (Dayton, Ohio),* 28**,** 1435-1445.

BECK, G. R., ZERLER, B. & MORAN, E. 2000. Phosphate is a specific signal for induction of osteopontin gene expression. *Proceedings of the National Academy of Sciences,* 97**,** 8352-8357.

BELLAHCÈNE, A. & CASTRONOVO, V. 1995. Increased expression of osteonectin and osteopontin, two bone matrix proteins, in human breast cancer. *Am J Pathol,* 146**,** 95-100.

BELLAHCÈNE, A., MERVILLE, M.-P. & CASTRONOVO, V. 1994. Expression of Bone Sialoprotein, a Bone Matrix Protein, in Human Breast Cancer. *Cancer Research,* 54**,** 2823-2826.

BEN-AHARON, I., VIDAL, L., RIZEL, S., YERUSHALMI, R., SHPILBERG, O., SULKES, A. & STEMMER, S. M. 2013. Bisphosphonates in the Adjuvant Setting of Breast Cancer Therapy—Effect on Survival: A Systematic Review and Meta-Analysis. *PLoS ONE,* 8**,** e70044.

BENNETT, R. L., EVANS, A. J., KUTT, E., RECORD, C., BOBROW, L. G., ELLIS, I. O., HANBY, A. & MOSS, S. M. 2011. Pathological and mammographic prognostic factors for screen detected cancers in a multi-centre randomised, controlled trial of mammographic screening in women from age 40 to 48 years. *Breast,* 20**,** 525-8.

BENT, C. K., BASSETT, L. W., D'ORSI, C. J. & SAYRE, J. W. 2010. The Positive Predictive Value of BI-RADS Microcalcification Descriptors and Final Assessment Categories. *American Journal of Roentgenology,* 194**,** 1378-1383.

BERTUCCI, F., FINETTI, P., CERVERA, N., ESTERNI, B., HERMITTE, F., VIENS, P. & BIRNBAUM, D. 2008. How basal are triple-negative breast cancers? *International Journal of Cancer,* 123**,** 236-240.

BHARTI, R., DEY, G., BANERJEE, I., DEY, K. K., PARIDA, S., KUMAR, B. N. P., DAS, C. K., PAL, I., MUKHERJEE, M., MISRA, M., PRADHAN, A. K., EMDAD, L., DAS, S. K., FISHER, P. B. & MANDAL, M. 2017. Somatostatin receptor targeted liposomes with Diacerein inhibit IL-6 for breast cancer therapy. *Cancer Letters,* 388**,** 292-302.

BHARTI, R., DEY, G., OJHA, P. K., RAJPUT, S., JAGANATHAN, S. K., SEN, R. & MANDAL, M. 2015. Diacerein-mediated inhibition of IL-6/IL-6R signaling induces apoptotic effects on breast cancer. *Oncogene,* 35**,** 3965.

BHUSHAN, K. R., MISRA, P., LIU, F., MATHUR, S., LENKINSKI, R. E. & FRANGIONI, J. V. 2008. Detection of breast cancer microcalcifications using a dual-modality SPECT/NIR fluorescent probe. *Journal of the American Chemical Society,* 130**,** 17648-17649.

BIAN, Z. Y., FAN, Q. M., LI, G., XU, W. T. & TANG, T. T. 2010. Human mesenchymal stem cells promote growth of osteosarcoma: involvement of interleukin-6 in the interaction between human mesenchymal stem cells and Saos-2. *Cancer Sci,* 101**,** 2554-60.

BILAL, M., BILAL, M., TABASSUM, S., SALEEM, M., MAHMOOD, H., SARWAR, U., BANGUSH, H., MUNIR, F., ASLAM ZIA, M., AHMED, M., SHAHZADA, S. & ULLAH KHAN, E. 2016. Optical Screening of Female Breast Cancer from Whole Blood Using Raman Spectroscopy. *Applied Spectroscopy,* 71**,** 1004-1013.

BIRMINGHAM, E., NIEBUR, G. L., MCHUGH, P. E., SHAW, G., BARRY, F. P. & MCNAMARA, L. M. 2012. Osteogenic differentiation of mesenchymal stem cells is regulated by osteocyte and osteoblast cells in a simplified bone niche. *Eur Cell Mater,* 23**,** 13-27.

BLASKOVICH, M. A., SUN, J., CANTOR, A., TURKSON, J., JOVE, R. & SEBTI, S. M. 2003. Discovery of JSI-124 (Cucurbitacin I), a Selective Janus Kinase/Signal Transducer and Activator of Transcription 3 Signaling Pathway Inhibitor with Potent Antitumor Activity against Human and Murine Cancer Cells in Mice. *Cancer Research,* 63**,** 1270.

BLEYER, A., BAINES, C. & MILLER, A. B. 2016. Impact of screening mammography on breast cancer mortality. *Int J Cancer,* 138**,** 2003-12.

BOCCA, C., IEVOLELLA, M., AUTELLI, R., MOTTA, M., MOSSO, L., TORCHIO, B., BOZZO, F., CANNITO, S., PATERNOSTRO, C., COLOMBATTO, S., PAROLA, M. & MIGLIETTA, A. 2014. Expression of

Cox-2 in human breast cancer cells as a critical determinant of epithelial-to-mesenchymal transition and invasiveness. *Expert Opinion on Therapeutic Targets,* 18**,** 121-135.

BOONRUNGSIMAN, S., GENTLEMAN, E., CARZANIGA, R., EVANS, N. D., MCCOMB, D. W., PORTER, A. E. & STEVENS, M. M. 2012. The role of intracellular calcium phosphate in osteoblast-mediated bone apatite formation. *Proceedings of the National Academy of Sciences,* 109**,** 14170-14175.

BORAH, A., RAVEENDRAN, S., ROCHANI, A., MAEKAWA, T. & KUMAR, D. S. 2015. Targeting self-renewal pathways in cancer stem cells: clinical implications for cancer therapy. *Oncogenesis,* 4**,** e177.

BORGNA, S., ARMELLIN, M., DI GENNARO, A., MAESTRO, R. & SANTAROSA, M. 2012. Mesenchymal traits are selected along with stem features in breast cancer cells grown as mammospheres. *Cell Cycle,* 11**,** 4242-4251.

BOSKEY, A. L., GUIDON, P., DOTY, S. B., STINER, D., LEBOY, P. & BINDERMAN, I. 1996. The mechanism of β-glycerophosphate action in mineralizing chick limb-bud mesenchymal cell cultures. *Journal of Bone and Mineral Research,* 11**,** 1694-1702.

BOSKEY, A. L. & ROY, R. 2008. Cell Culture Systems for Studies of Bone and Tooth Mineralization. *Chemical Reviews,* 108**,** 4716-4733.

BREASTCHECK. 2017. *Programme Report: 2015-2016* [Online]. Available: https://www.breastcheck.ie/sites/default/files/bcheck/documents/bc_programme_report_2015-2016.pdf [Accessed].

BRUDERER, M., RICHARDS, R. G., ALINI, M. & STODDART, M. J. 2014. Role and regulation of RUNX2 in osteogenesis. *Eur Cell Mater,* 28**,** 269-86.

BRUSGARD, J. L., CHOE, M., CHUMSRI, S., RENOUD, K., MACKERELL, A. D., SUDOL, M. & PASSANITI, A. 2015. RUNX2 and TAZ-dependent signaling pathways regulate soluble E-Cadherin levels and tumorsphere formation in breast cancer cells. *Oncotarget,* 6**,** 28132-28150.

BURNSIDE, E. S., OCHSNER, J. E., FOWLER, K. J., FINE, J. P., SALKOWSKI, L. R., RUBIN, D. L. & SISNEY, G. A. 2007. Use of microcalcification descriptors in BI-RADS 4th edition to stratify risk of malignancy. *Radiology,* 242**,** 388-95.

BYON, C. H., JAVED, A., DAI, Q., KAPPES, J. C., CLEMENS, T. L., DARLEY-USMAR, V. M., MCDONALD, J. M. & CHEN, Y. 2008. Oxidative Stress Induces Vascular Calcification through Modulation of the Osteogenic Transcription Factor Runx2 by AKT Signaling. *The Journal of Biological Chemistry,* 283**,** 15319-15327.

BYON, C. H., SUN, Y., CHEN, J., YUAN, K., MAO, X., HEATH, J. M., ANDERSON, P. G., TINTUT, Y., DEMER, L. L., WANG, D. & CHEN, Y. 2011. Runx2-Upregulated Receptor Activator of Nuclear Factor κB Ligand in Calcifying Smooth Muscle Cells Promotes Migration and Osteoclastic Differentiation of Macrophages. *Arteriosclerosis, Thrombosis, and Vascular Biology,* 31**,** 1387-1396.

CALVET, C. Y., ANDRÉ, F. M. & MIR, L. M. 2014. The Culture of Cancer Cell Lines as Tumorspheres Does Not Systematically Result in Cancer Stem Cell Enrichment. *PLoS ONE,* 9**,** e89644.

CAREY, L. A., DEES, E. C., SAWYER, L., GATTI, L., MOORE, D. T., COLLICHIO, F., OLLILA, D. W., SARTOR, C. I., GRAHAM, M. L. & PEROU, C. M. 2007. The Triple Negative Paradox: Primary Tumor Chemosensitivity of Breast Cancer Subtypes. *Clinical Cancer Research,* 13**,** 2329-2334.

CARMI, Y., VORONOV, E., DOTAN, S., LAHAT, N., RAHAT, M. A., FOGEL, M., HUSZAR, M., WHITE, M. R., DINARELLO, C. A. & APTE, R. N. 2009. The Role of Macrophage-Derived IL-1 in Induction and Maintenance of Angiogenesis. *The Journal of Immunology,* 183**,** 4705.

CARRARO, DIRCE M., ELIAS, ELIANA V. & ANDRADE, VICTOR P. 2014. Ductal carcinoma in situ of the breast: morphological and molecular features implicated in progression. *Bioscience Reports,* 34.

CASNEUF, T., AXEL, A. E., KING, P., ALVAREZ, J. D., WERBECK, J. L., VERHULST, T., VERSTRAETEN, K., HALL, B. M. & SASSER, A. K. 2016. Interleukin-6 is a potential therapeutic target in interleukin-6 dependent, estrogen receptor-α-positive breast cancer. *Breast Cancer : Targets and Therapy,* 8**,** 13-27.

CASTRONOVO, V. & BELLAHCÈNE, A. 1998. Evidence that breast cancer associated microcalcifications are mineralized malignant cells. *Int J Oncol,* 12**,** 305-8.

CATSBURG, C., MILLER, A. B. & ROHAN, T. E. 2015. Active cigarette smoking and risk of breast cancer. *Int J Cancer,* 136**,** 2204-9.

CEN, D., XU, L., LI, N., CHEN, Z., WANG, L., ZHOU, S., XU, B., LIU, C. L., LIU, Z. & LUO, T. 2017a. BI-RADS 3–5 microcalcifications can preoperatively predict breast cancer HER2 and Luminal a molecular subtype. *Oncotarget,* 8**,** 13855-13862.

CEN, D., XU, L., ZHANG, S., ZHOU, S., HUANG, Y., CHEN, Z., LI, N., WANG, Y. & WANG, Q. 2017b. BI-RADS 3–5 microcalcifications: prediction of lymph node metastasis of breast cancer. *Oncotarget,* 8**,** 30190-30198.

CHAE, E. Y., MOON, W. K., KIM, H. H., KIM, W. H., CHA, J. H., SHIN, H. J., CHOI, W. J., HAN, W., NOH, D.-Y., LEE, S. B. & AHN, S. H. 2016. Association between Ultrasound Features and the 21-Gene Recurrence Score Assays in Patients with Oestrogen Receptor-Positive, HER2-Negative, Invasive Breast Cancer. *PLoS ONE,* 11**,** e0158461.

CHALYA, P. L., LEMA, M. K., MABULA, J. B., RAMBAU, P., MCHEMBE, M. D., MASALU, N., KASANGA, G. A., GIITI, G. & GILYOMA, J. M. 2013. Triple assessment as a preoperative diagnostic tool for breast cancer at Bugando Medical Centre in northwestern Tanzania. *Tanzan J Health Res,* 15**,** 223-9.

CHAN, D. S. M. & NORAT, T. 2015. Obesity and Breast Cancer: Not Only a Risk Factor of the Disease. *Current Treatment Options in Oncology,* 16**,** 22.

CHANG, C.-H., FAN, T.-C., YU, J.-C., LIAO, G.-S., LIN, Y.-C., SHIH, A. C.-C., LI, W.-H. & YU, A. L.-T. 2014. The prognostic significance of RUNX2 and miR-10a/10b and their inter-relationship in breast cancer. *Journal of Translational Medicine,* 12**,** 257.

CHANG, J. C. 2016. Cancer stem cells: Role in tumor growth, recurrence, metastasis, and treatment resistance. *Medicine,* 95**,** S20-S25.

CHAO, Y. L., SHEPARD, C. R. & WELLS, A. 2010. Breast carcinoma cells re-express E-cadherin during mesenchymal to epithelial reverting transition. *Molecular Cancer,* 9**,** 179-179.

CHAVEY, C., BIBEAU, F., GOURGOU-BOURGADE, S., BURLINCHON, S., BOISSIÈRE, F., LAUNE, D., ROQUES, S. & LAZENNEC, G. 2007. Oestrogen receptor negative breast cancers exhibit high cytokine content. *Breast Cancer Research,* 9**,** R15-R15.

CHEN, A., WANG, D., LIU, X., HE, S., YU, Z. & WANG, J. 2012. Inhibitory effect of BMP-2 on the proliferation of breast cancer cells. *Mol Med Rep,* 6**,** 615-20.

CHEN, B., DAI, D., TANG, H., CHEN, X., AI, X., HUANG, X., WEI, W. & XIE, X. 2016. Pre-treatment serum alkaline phosphatase and lactate dehydrogenase as prognostic factors in triple negative breast cancer. *Journal of Cancer,* 7**,** 2309-2316.

CHEN, N. X., DUAN, D., O'NEILL, K. D. & MOE, S. M. 2006a. High glucose increases the expression of Cbfa1 and BMP-2 and enhances the calcification of vascular smooth muscle cells. *Nephrol Dial Transplant,* 21**,** 3435-42.

CHEN, N. X., DUAN, D., O'NEILL, K. D., WOLISI, G. O., KOCZMAN, J. J., LACLAIR, R. & MOE, S. M. 2006b. The mechanisms of uremic serum-induced expression of bone matrix proteins in bovine vascular smooth muscle cells. *Kidney International,* 70**,** 1046-1053.

CHEN, S. & PARMIGIANI, G. 2007. Meta-Analysis of BRCA1 and BRCA2 Penetrance. *Journal of clinical oncology : official journal of the American Society of Clinical Oncology,* 25**,** 1329-1333.

CHEN, W. Y., ROSNER, B., HANKINSON, S. E., COLDITZ, G. A. & WILLETT, W. C. 2011. Moderate alcohol consumption during adult life, drinking patterns, and breast cancer risk. *Jama,* 306**,** 1884-1890.

CHEN, Y. F., CHEN, Y. T., CHIU, W. T. & SHEN, M. R. 2013. Remodeling of calcium signaling in tumor progression. *J Biomed Sci,* 20**,** 23.

CHEUNG, H. S., DEVINE, T. R. & HUBBARD, W. 1997. Calcium phosphate particle induction of metalloproteinase and mitogenesis: effect of particle sizes. *Osteoarthritis and Cartilage,* 5**,** 145-151.

CHIU, J. J., SGAGIAS, M. K. & COWAN, K. H. 1996. Interleukin 6 acts as a paracrine growth factor in human mammary carcinoma cell lines. *Clinical Cancer Research,* 2**,** 215.

CHIU, L.-H., LAI, W.-F. T., CHANG, S.-F., WONG, C.-C., FAN, C.-Y., FANG, C.-L. & TSAI, Y.-H. 2014. The effect of type II collagen on MSC osteogenic differentiation and bone defect repair. *Biomaterials,* 35**,** 2680-2691.

CHIU, L. H., YEH, T. S., HUANG, H. M., LEU, S. J., YANG, C. B. & TSAI, Y. H. 2012. Diverse effects of type II collagen on osteogenic and adipogenic differentiation of mesenchymal stem cells. *J Cell Physiol,* 227**,** 2412-20.

CHO, S. W., PIRIH, F. Q., KOH, A. J., MICHALSKI, M., EBER, M. R., RITCHIE, K., SINDER, B., OH, S., AL-DUJAILI, S. A., LEE, J., KOZLOFF, K., DANCIU, T., WRONSKI, T. J. & MCCAULEY, L. K. 2013. The Soluble Interleukin-6 Receptor Is a Mediator of Hematopoietic and Skeletal Actions of Parathyroid Hormone. *Journal of Biological Chemistry,* 288**,** 6814-6825.

CHOKSHI, R., FRUASAHA, P. & KOZAK, J. A. 2012. 2-Aminoethyl diphenyl borinate (2-APB) inhibits TRPM7 channels through an intracellular acidification mechanism. *Channels,* 6**,** 362-369.

CHUBANOV, V., MEDEROS Y SCHNITZLER, M., MEIßNER, M., SCHÄFER, S., ABSTIENS, K., HOFMANN, T. & GUDERMANN, T. 2012. Natural and synthetic modulators of SK (K(ca)2) potassium channels inhibit magnesium-dependent activity of the kinase-coupled cation channel TRPM7. *British Journal of Pharmacology,* 166**,** 1357-1376.

CLEMENT, J. H., RAIDA, M., SANGER, J., BICKNELL, R., LIU, J., NAUMANN, A., GEYER, A., WALDAU, A., HORTSCHANSKY, P., SCHMIDT, A., HOFFKEN, K., WOLFT, S. & HARRIS, A. L. 2005. Bone morphogenetic protein 2 (BMP-2) induces in vitro invasion and in vivo hormone independent growth of breast carcinoma cells. *Int J Oncol,* 27**,** 401-7.

COLLABORATIVE GROUP ON HORMONAL FACTORS IN BREAST, C. 2012. Menarche, menopause, and breast cancer risk: individual participant meta-analysis, including 118 964 women with breast cancer from 117 epidemiological studies. *The Lancet Oncology,* 13**,** 1141-1151.

CONLEY, S. J., BOSCO, E. E., TICE, D. A., HOLLINGSWORTH, R. E., HERBST, R. & XIAO, Z. 2016. HER2 drives Mucin-like 1 to control proliferation in breast cancer cells. *Oncogene,* 35**,** 4225-4234.

COOKE, M., MCCARTHY, G., SALLIS, J. & MORGAN, M. 2003. Phosphocitrate Inhibits Calcium Hydroxyapatite Induced Mitogenesis and Upregulation of Matrix Metalloproteinase-1, Interleukin-1β and Cyclooxygenase-2 mRNA in Human Breast Cancer Cell Lines. *Breast Cancer Research and Treatment,* 79**,** 253-263.

COX, R. F., HERNANDEZ-SANTANA, A., RAMDASS, S., MCMAHON, G., HARMEY, J. H. & MORGAN, M. P. 2012a. Microcalcifications in breast cancer: novel insights into the molecular mechanism and functional consequence of mammary mineralisation. *Br J Cancer,* 106**,** 525-537.

COX, R. F., JENKINSON, A., POHL, K., O'BRIEN, F. J. & MORGAN, M. P. 2012b. Osteomimicry of Mammary Adenocarcinoma Cells In Vitro; Increased Expression of Bone Matrix Proteins and Proliferation within a 3D Collagen Environment. *PLoS ONE,* 7**,** e41679.

CROSS, B. M., BREITWIESER, G. E., REINHARDT, T. A. & RAO, R. 2014. Cellular calcium dynamics in lactation and breast cancer: from physiology to pathology. *Am J Physiol Cell Physiol,* 306**,** C515-26.

CROSS, B. M., HACK, A., REINHARDT, T. A. & RAO, R. 2013. SPCA2 Regulates Orai1 Trafficking and Store Independent Ca(2+) Entry in a Model of Lactation. *PLoS ONE,* 8**,** e67348.

CUCUZZA, L. S., MOTTA, M., MIRETTI, S., ACCORNERO, P. & BARATTA, M. 2008. Curcuminoid-phospholipid complex induces apoptosis in mammary epithelial cells by STAT-3 signaling. *Experimental & Molecular Medicine,* 40**,** 647-657.

CURTIS, C., SHAH, S. P., CHIN, S.-F., TURASHVILI, G., RUEDA, O. M., DUNNING, M. J., SPEED, D., LYNCH, A. G., SAMARAJIWA, S., YUAN, Y., GRÄF, S., HA, G., HAFFARI, G., BASHASHATI, A., RUSSELL, R., MCKINNEY, S., GROUP, M., LANGERØD, A., GREEN, A., PROVENZANO, E., WISHART, G., PINDER, S., WATSON, P., MARKOWETZ, F., MURPHY, L., ELLIS, I., PURUSHOTHAM, A., BØRRESEN-DALE, A.-L., BRENTON, J. D., TAVARÉ, S., CALDAS, C. & APARICIO, S. 2012. The genomic and transcriptomic architecture of 2,000 breast tumours reveals novel subgroups. *Nature,* 486**,** 346-352.

D'ORSI, C. J. 2013. Imaging for the Diagnosis and Management of Ductal Carcinoma In Situ. *Journal of the National Cancer Institute. Monographs,* 2010**,** 214-217.

DAI, X., LI, T., BAI, Z., YANG, Y., LIU, X., ZHAN, J. & SHI, B. 2015. Breast cancer intrinsic subtype classification, clinical use and future trends. *American Journal of Cancer Research,* 5**,** 2929-2943.

DANG, D., PRASAD, H. & RAO, R. 2017. Secretory pathway Ca2+ -ATPases promote in vitro microcalcifications in breast cancer cells. *Molecular Carcinogenesis,* 56**,** 2474–2485.

DAS, K., LEONG, D., GUPTA, A., SHEN, L., PUTTI, T., STEIN, G. S., VAN WIJNEN, A. J. & SALTO-TELLEZ, M. 2009. Positive Association between Nuclear Runx2 and Estrogen-Progesterone Receptor Gene Expression Characterizes a Biological Subtype of Breast Cancer. *European Journal of Cancer* 45**,** 2239-2248.

DAVIES, C., PAN, H., GODWIN, J., GRAY, R., ARRIAGADA, R., RAINA, V., ABRAHAM, M., ALENCAR, V. H. M., BADRAN, A., BONFILL, X., BRADBURY, J., CLARKE, M., COLLINS, R., DAVIS, S. R., DELMESTRI, A., FORBES, J. F., HADDAD, P., HOU, M.-F., INBAR, M., KHALED, H., KIELANOWSKA, J., KWAN, W.-H., MATHEW, B. S., MITTRA, I., MÜLLER, B., NICOLUCCI, A., PERALTA, O., PERNAS, F., PETRUZELKA, L., PIENKOWSKI, T., RADHIKA, R., RAJAN, B., RUBACH, M. T., TORT, S., URRÚTIA, G., VALENTINI, M., WANG, Y. & PETO, R. 2013. Long-term effects of continuing adjuvant tamoxifen to 10 years versus stopping at 5 years after diagnosis of oestrogen receptor-positive breast cancer: ATLAS, a randomised trial. *The Lancet,* 381**,** 805-816.

DAVIS, F. M., AZIMI, I., FAVILLE, R. A., PETERS, A. A., JALINK, K., PUTNEY, J. W., JR., GOODHILL, G. J., THOMPSON, E. W., ROBERTS-THOMSON, S. J. & MONTEITH, G. R. 2014. Induction of epithelial-mesenchymal transition (EMT) in breast cancer cells is calcium signal dependent. *Oncogene,* 33**,** 2307-16.

DELORD, J. P., ALLAL, C., CANAL, M., MERY, E., ROCHAIX, P., HENNEBELLE, I., PRADINES, A., CHATELUT, E., BUGAT, R., GUICHARD, S. & CANAL, P. 2005. Selective inhibition of HER2 inhibits AKT signal transduction and prolongs disease-free survival in a micrometastasis model of ovarian carcinoma. *Annals of Oncology,* 16**,** 1889-1897.

DETHLEFSEN, C., HOJFELDT, G. & HOJMAN, P. 2013. The role of intratumoral and systemic IL-6 in breast cancer. *Breast Cancer Res Treat,* 138**,** 657-64.

DHORE, C. R., CLEUTJENS, J. P. M., LUTGENS, E., CLEUTJENS, K. B. J. M., GEUSENS, P. P. M., KITSLAAR, P. J. E. H. M., TORDOIR, J. H. M., SPRONK, H. M. H., VERMEER, C. & DAEMEN, M. J. A. P. 2001. Differential Expression of Bone Matrix Regulatory Proteins in Human Atherosclerotic Plaques. *Arteriosclerosis, Thrombosis, and Vascular Biology,* 21**,** 1998.

DING, H., PAN, H., XU, X. & TANG, R. 2014. Toward a Detailed Understanding of Magnesium Ions on Hydroxyapatite Crystallization Inhibition. *Crystal Growth & Design,* 14**,** 763-769.

DOUGLAS, A. M., GOSS, G. A., SUTHERLAND, R. L., HILTON, D. J., BERNDT, M. C., NICOLA, N. A. & BEGLEY, C. G. 1997. Expression and function of members of the cytokine receptor superfamily on breast cancer cells. *Oncogene,* 14**,** 661-9.

DOWSETT, M., CUZICK, J., INGLE, J., COATES, A., FORBES, J., BLISS, J., BUYSE, M., BAUM, M., BUZDAR, A., COLLEONI, M., COOMBES, C., SNOWDON, C., GNANT, M., JAKESZ, R., KAUFMANN, M., BOCCARDO, F., GODWIN, J., DAVIES, C. & PETO, R. 2010. Meta-Analysis of Breast Cancer Outcomes in Adjuvant Trials of Aromatase Inhibitors Versus Tamoxifen. *Journal of Clinical Oncology,* 28**,** 509-518.

DU, W.-X., DUAN, S.-F., CHEN, J.-J., HUANG, J.-F., YIN, L.-M. & TONG, P.-J. 2014. Serum bone-specific alkaline phosphatase as a biomarker for osseous metastases in patients with malignant carcinomas: A systematic review and meta-analysis. *Journal of Cancer Research and Therapeutics,* 10**,** 140-143.

DUBOIS, C., VANDEN ABEELE, F. & PREVARSKAYA, N. 2013. Targeting apoptosis by the remodelling of calcium-transporting proteins in cancerogenesis. *Febs j,* 280**,** 5500-10.

DUNNWALD, L. K., ROSSING, M. A. & LI, C. I. 2007. Hormone receptor status, tumor characteristics, and prognosis: a prospective cohort of breast cancer patients. *Breast Cancer Research,* 9**,** R6-R6.

EA, H.-K., CHOBAZ, V., NGUYEN, C., NASI, S., VAN LENT, P., DAUDON, M., DESSOMBZ, A., BAZIN, D., MCCARTHY, G., JOLLES-HAEBERLI, B., IVES, A., VAN LINTHOUDT, D., SO, A., LIOTÉ, F. &

BUSSO, N. 2013. Pathogenic Role of Basic Calcium Phosphate Crystals in Destructive Arthropathies. *PLoS ONE,* 8**,** e57352.

EARLY BREAST CANCER TRIALISTS' COLLABORATIVE, G. 2011. Relevance of breast cancer hormone receptors and other factors to the efficacy of adjuvant tamoxifen: patient-level meta-analysis of randomised trials. *The Lancet,* 378**,** 771-784.

EBERL, M. M., FOX, C. H., EDGE, S. B., CARTER, C. A. & MAHONEY, M. C. 2006. BI-RADS Classification for Management of Abnormal Mammograms. *The Journal of the American Board of Family Medicine,* 19**,** 161-164.

EL-MAADAWY, S., KAARTINEN, M. T., SCHINKE, T., MURSHED, M., KARSENTY, G. & MCKEE, M. D. 2003. Cartilage formation and calcification in arteries of mice lacking matrix Gla protein. *Connect Tissue Res,* 44 Suppl 1**,** 272-8.

EL HIANI, Y., AHIDOUCH, A., LEHEN'KYI, V., HAGUE, F., GOUILLEUX, F., MENTAVERRI, R., KAMEL, S., LASSOUED, K., BRULE, G. & OUADID-AHIDOUCH, H. 2009a. Extracellular signal-regulated kinases 1 and 2 and TRPC1 channels are required for calcium-sensing receptor-stimulated MCF-7 breast cancer cell proliferation. *Cell Physiol Biochem,* 23**,** 335-46.

EL HIANI, Y., LEHEN'KYI, V., OUADID-AHIDOUCH, H. & AHIDOUCH, A. 2009b. Activation of the calcium-sensing receptor by high calcium induced breast cancer cell proliferation and TRPC1 cation channel over-expression potentially through EGFR pathways. *Archives of Biochemistry and Biophysics,* 486**,** 58-63.

ELIAS, S. G., ADAMS, A., WISNER, D. J., ESSERMAN, L. J., VAN'T VEER, L. J., MALI, W. P., GILHUIJS, K. G. & HYLTON, N. M. 2014. Imaging features of HER2 overexpression in breast cancer: a systematic review and meta-analysis. *Cancer Epidemiol Biomarkers Prev,* 23**,** 1464-83.

EROLES, P., BOSCH, A., ALEJANDRO PÉREZ-FIDALGO, J. & LLUCH, A. 2012. Molecular biology in breast cancer: Intrinsic subtypes and signaling pathways. *Cancer Treatment Reviews,* 38**,** 698-707.

ESTEVA, F. J., YU, D., HUNG, M. C. & HORTOBAGYI, G. N. 2010. Molecular predictors of response to trastuzumab and lapatinib in breast cancer. *Nat Rev Clin Oncol,* 7**,** 98-107.

ETIQUE, N., CHARDARD, D., CHESNEL, A., MERLIN, J. L., FLAMENT, S. & GRILLIER-VUISSOZ, I. 2004. Ethanol stimulates proliferation, ERalpha and aromatase expression in MCF-7 human breast cancer cells. *Int J Mol Med,* 13**,** 149-55.

EUCAN. 2017. *Estimated incidence, mortality & prevalence, 2012* [Online]. Available: http://eco.iarc.fr/EUCAN/CancerOne.aspx?Cancer=46&Gender=2 [Accessed].

EVANS, A. J., PINDER, S. E., JAMES, J. J., ELLIS, I. O. & CORNFORD, E. 2006. Is Mammographic Spiculation an Independent, Good Prognostic Factor in Screening-Detected Invasive Breast Cancer? *American Journal of Roentgenology,* 187**,** 1377-1380.

EWENCE, A. E., BOOTMAN, M., RODERICK, H. L., SKEPPER, J. N., MCCARTHY, G., EPPLE, M., NEUMANN, M., SHANAHAN, C. M. & PROUDFOOT, D. 2008. Calcium phosphate crystals induce cell death in human vascular smooth muscle cells: a potential mechanism in atherosclerotic plaque destabilization. *Circ Res,* 103**,** e28-34.

FEIG, S. A. 2014. Screening mammography benefit controversies: sorting the evidence. *Radiol Clin North Am,* 52**,** 455-80.

FELIPE LIMA, J., NOFECH-MOZES, S., BAYANI, J. & BARTLETT, J. M. S. 2016. EMT in Breast Carcinoma—A Review. *Journal of Clinical Medicine,* 5**,** 65.

FELIX, D. D., GORE, J. C., YANKEELOV, T. E., PETERSON, T. E., BARNES, S., WHISENANT, J., WEIS, J., SHOUKOUHI, S., VIROSTKO, J., NICKELS, M., MCINTYRE, J. O., SANDERS, M., ABRAMSON, V. & TANTAWY, M. N. 2015. Detection of breast cancer microcalcification using (99m)Tc-MDP SPECT or Osteosense 750EX FMT imaging. *Nuclear medicine and biology,* 42**,** 269-273.

FENG, M., GRICE, D. M., FADDY, H. M., NGUYEN, N., LEITCH, S., WANG, Y., MUEND, S., KENNY, P. A., SUKUMAR, S., ROBERTS-THOMSON, S. J., MONTEITH, G. R. & RAO, R. 2010. Store-independent activation of Orai1 by SPCA2 in mammary tumors. *Cell,* 143**,** 84-98.

FERRAND, N., STRAGIER, E., REDEUILH, G. & SABBAH, M. 2012. Glucocorticoids induce CCN5/WISP-2 expression and attenuate invasion in oestrogen receptor-negative human breast cancer cells. *Biochem J,* 447**,** 71-9.

FERRANTI, C., COOPMANS DE YOLDI, G., BIGANZOLI, E., BERGONZI, S., MARIANI, L., SCAPERROTTA, G. & MARCHESINI, M. 2000. Relationships between age, mammographic features and pathological tumour characteristics in non-palpable breast cancer. *Br J Radiol,* 73**,** 698-705.

FERREIRA, E., PORTER, R. M., WEHLING, N., O'SULLIVAN, R. P., LIU, F., BOSKEY, A., ESTOK, D. M., HARRIS, M. B., VRAHAS, M. S., EVANS, C. H. & WELLS, J. W. 2013. Inflammatory cytokines induce a unique mineralizing phenotype in mesenchymal stem cells derived from human bone marrow. *J Biol Chem,* 288**,** 29494-505.

FOULKES, W. D., BRUNET, J.-S., STEFANSSON, I. M., STRAUME, O., CHAPPUIS, P. O., BÉGIN, L. R., HAMEL, N., GOFFIN, J. R., WONG, N., TRUDEL, M., KAPUSTA, L., PORTER, P. & AKSLEN, L. A. 2004. The Prognostic Implication of the Basal-Like (Cyclin Ehigh/p27low/p53+/Glomeruloid-Microvascular-Proliferation+) Phenotype of BRCA1-Related Breast Cancer. *Cancer Research,* 64**,** 830-835.

FRANCESCHI, R. T., XIAO, G., JIANG, D., GOPALAKRISHNAN, R., YANG, S. & REITH, E. 2003. Multiple Signaling Pathways Converge on the Cbfa1/Runx2 Transcription Factor to Regulate Osteoblast Differentiation. *Connective tissue research,* 44**,** 109-116.

FRANCHIMONT, N., RYDZIEL, S., DELANY, A. M. & CANALIS, E. 1997. Interleukin-6 and Its Soluble Receptor Cause a Marked Induction of Collagenase 3 Expression in Rat Osteoblast Cultures. *Journal of Biological Chemistry,* 272**,** 12144-12150.

FRAPPART, L., BOUDEULLE, M., BOUMENDIL, J., LIN, H. C., MARTINON, I., PALAYER, C., MALLET-GUY, Y., RAUDRANT, D., BREMOND, A. & ROCHET, Y. 1984. Structure and composition of microcalcifications in benign and malignant lesions of the breast: study by light microscopy, transmission and scanning electron microscopy, microprobe analysis, and X-ray diffraction. *Human pathology,* 15**,** 880-889.

FRASER, D. M., SULLIVAN, F. M., THOMPSON, A. M. & MCCOWAN, C. 2014. Aspirin use and survival after the diagnosis of breast cancer: a population-based cohort study. *British Journal Of Cancer,* 111**,** 623.

FUKUYO, S., YAMAOKA, K., SONOMOTO, K., OSHITA, K., OKADA, Y., SAITO, K., YOSHIDA, Y., KANAZAWA, T., MINAMI, Y. & TANAKA, Y. 2014. IL-6-accelerated calcification by induction of ROR2 in human adipose tissue-derived mesenchymal stem cells is STAT3 dependent. *Rheumatology,* 53**,** 1282-1290.

GAJDOS, C., TARTTER, P. I., BLEIWEISS, I. J., HERMANN, G., DE CSEPEL, J., ESTABROOK, A. & RADEMAKER, A. W. 2002. Mammographic appearance of nonpalpable breast cancer reflects pathologic characteristics. *Annals of surgery,* 235**,** 246-251.

GAJRIA, D. & CHANDARLAPATY, S. 2011. HER2-amplified breast cancer: mechanisms of trastuzumab resistance and novel targeted therapies. *Expert Rev Anticancer Ther,* 11**,** 263-75.

GAN, L., QIU, Z., HUANG, J., LI, Y., HUANG, H., XIANG, T., WAN, J., HUI, T., LIN, Y., LI, H. & REN, G. 2016. Cyclooxygenase-2 in tumor-associated macrophages promotes metastatic potential of breast cancer cells through Akt pathway. *International Journal of Biological Sciences,* 12**,** 1533-1543.

GARCIA-HERNANDEZ, A., ARZATE, H., GIL-CHAVARRIA, I., ROJO, R. & MORENO-FIERROS, L. 2012. High glucose concentrations alter the biomineralization process in human osteoblastic cells. *Bone,* 50**,** 276-88.

GARCIA, R., BOWMAN, T. L., NIU, G., YU, H., MINTON, S., MURO-CACHO, C. A., COX, C. E., FALCONE, R., FAIRCLOUGH, R., PARSONS, S., LAUDANO, A., GAZIT, A., LEVITZKI, A., KRAKER, A. & JOVE, R. 2001. Constitutive activation of Stat3 by the Src and JAK tyrosine kinases participates in growth regulation of human breast carcinoma cells. *Oncogene,* 20**,** 2499.

GAUDET, M. M., GAPSTUR, S. M., SUN, J., DIVER, W. R., HANNAN, L. M. & THUN, M. J. 2013. Active Smoking and Breast Cancer Risk: Original Cohort Data and Meta-Analysis. *JNCI: Journal of the National Cancer Institute,* 105**,** 515-525.

GENIN, M., CLEMENT, F., FATTACCIOLI, A., RAES, M. & MICHIELS, C. 2015. M1 and M2 macrophages derived from THP-1 cells differentially modulate the response of cancer cells to etoposide. *BMC Cancer,* 15**,** 577.

GHEORGHE, S. R. & CRACIUN, A. M. 2016. Matrix Gla protein in tumoral pathology. *Clujul Medical,* 89**,** 319-321.

GHITA, A., MATOUSEK, P. & STONE, N. 2017. High sensitivity non-invasive detection of calcifications deep inside biological tissue using Transmission Raman Spectroscopy. *Journal of Biophotonics,* 11.

GHOSH-CHOUDHURY, N., GHOSH-CHOUDHURY, G., CELESTE, A., GHOSH, P. M., MOYER, M., ABBOUD, S. L. & KREISBERG, J. 2000a. Bone morphogenetic protein-2 induces cyclin kinase inhibitor p21 and hypophosphorylation of retinoblastoma protein in estradiol-treated MCF-7 human breast cancer cells. *Biochim Biophys Acta,* 1497**,** 186-96.

GHOSH-CHOUDHURY, N., WOODRUFF, K., QI, W., CELESTE, A., ABBOUD, S. L. & GHOSH CHOUDHURY, G. 2000b. Bone morphogenetic protein-2 blocks MDA MB 231 human breast cancer cell proliferation by inhibiting cyclin-dependent kinase-mediated retinoblastoma protein phosphorylation. *Biochem Biophys Res Commun,* 272**,** 705-11.

GIALELI, C., THEOCHARIS, A. D. & KARAMANOS, N. K. 2011. Roles of matrix metalloproteinases in cancer progression and their pharmacological targeting. *FEBS Journal,* 278**,** 16-27.

GILBERT, E. S. 2009. Ionizing Radiation and Cancer Risks: What Have We Learned From Epidemiology? *International journal of radiation biology,* 85**,** 467-482.

GOODMAN, C. R., SATO, T., PECK, A. R., GIRONDO, M. A., YANG, N., LIU, C., YANAC, A. F., KOVATICH, A. J., HOOKE, J. A., SHRIVER, C. D., MITCHELL, E. P., HYSLOP, T. & RUI, H. 2015. Steroid induction of therapy-resistant cytokeratin-5-positive cells in estrogen receptor-positive breast cancer through a BCL6-dependent mechanism. *Oncogene,* 35**,** 1373.

GORDON, J. A. R., TYE, C. E., SAMPAIO, A. V., UNDERHILL, T. M., HUNTER, G. K. & GOLDBERG, H. A. 2007. Bone sialoprotein expression enhances osteoblast differentiation and matrix mineralization in vitro. *Bone,* 41**,** 462-473.

GORRINGE, K. L. & FOX, S. B. 2017. Ductal Carcinoma In Situ Biology, Biomarkers, and Diagnosis. *Frontiers in Oncology,* 7.

GØTZSCHE, P. C. & JØRGENSEN, K. J. 2013. Screening for breast cancer with mammography. *The Cochrane database of systematic reviews,* 6.

GRAY, J. M., RASANAYAGAM, S., ENGEL, C. & RIZZO, J. 2017. State of the evidence 2017: an update on the connection between breast cancer and the environment. *Environmental Health,* 16**,** 94.

GREGORY, L. S., CHOI, W., BURKE, L. & CLEMENTS, J. A. 2013. Breast Cancer Cells Induce Osteolytic Bone Lesions In vivo through a Reduction in Osteoblast Activity in Mice. *PLOS ONE,* 8**,** e68103.

GRINIATSOS, J., VASSILOPOULOS, P. P., KELESSIS, N., AGELATOU, R. & APOSTOLIKAS, N. 1995. The prognostic significance of breast tumour microcalcifications. *European Journal of Surgical Oncology,* 21**,** 601-603.

GUILBERT, A., GAUTIER, M., DHENNIN-DUTHILLE, I., HAREN, N., SEVESTRE, H. & OUADID-AHIDOUCH, H. 2009. Evidence that TRPM7 is required for breast cancer cell proliferation. *American Journal of Physiology - Cell Physiology,* 297**,** C493.

GÜLSÜN, M., DEMIRKAZıK, F. B. & ARıYÜREK, M. 2003. Evaluation of breast microcalcifications according to breast imaging reporting and data system criteria and Le Gal's classification. *European Journal of Radiology,* 47**,** 227-231.

HAJJAWI, M. O. R., MACRAE, V. E., HUESA, C., BOYDE, A., MILLÁN, J. L., ARNETT, T. R. & ORRISS, I. R. 2014. Mineralisation of collagen rich soft tissues and osteocyte lacunae in Enpp1(−/−) mice. *Bone,* 69**,** 139-147.

HAKA, A. S., SHAFER-PELTIER, K. E., FITZMAURICE, M., CROWE, J., DASARI, R. R. & FELD, M. S. 2002. Identifying Microcalcifications in Benign and Malignant Breast Lesions by Probing Differences in Their Chemical Composition Using Raman Spectroscopy. *Cancer Research,* 62**,** 5375-5380.

HAKA, A. S., SHAFER-PELTIER, K. E., FITZMAURICE, M., CROWE, J., DASARI, R. R. & FELD, M. S. 2005. Diagnosing breast cancer by using Raman spectroscopy. *Proceedings of the National Academy of Sciences of the United States of America,* 102**,** 12371-12376.

HALVERSON, P. B., GREENE, A. & CHEUNG, H. S. 1998. Intracellular calcium responses to basic calcium phosphate crystals in fibroblasts. *Osteoarthritis and Cartilage,* 6**,** 324-329.

HAMILTON, L. J., EVANS, A. J., WILSON, A. R., SCOTT, N., CORNFORD, E. J., PINDER, S. E., KHAN, H. N. & MACMILLAN, R. D. 2004. Breast imaging findings in women with BRCA1- and BRCA2-associated breast carcinoma. *Clin Radiol,* 59**,** 895-902.

HANAHAN, D. & WEINBERG, R. A. 2000. The hallmarks of cancer. *Cell,* 100**,** 57-70.

HANLEY, J. A., HANNIGAN, A. & O'BRIEN, K. M. 2017. Mortality reductions due to mammography screening: Contemporary population-based data. *PLoS One,* 12**,** e0188947.

HARMEY, D., HESSLE, L., NARISAWA, S., JOHNSON, K. A., TERKELTAUB, R. & MILLÁN, J. L. 2004. Concerted Regulation of Inorganic Pyrophosphate and Osteopontin by Akp2, Enpp1, and Ank : An Integrated Model of the Pathogenesis of Mineralization Disorders. *The American Journal of Pathology,* 164**,** 1199-1209.

HARRO, C. M. & MONTEIRO, A. N. A. 2017. Dissecting genetic risk factors in breast cancer. *Oncotarget,* 8**,** 12540-12541.

HARTMAN, Z. C., POAGE, G. M., DEN HOLLANDER, P., TSIMELZON, A., HILL, J., PANUPINTHU, N., ZHANG, Y., MAZUMDAR, A., HILSENBECK, S. G., MILLS, G. B. & BROWN, P. H. 2013. Growth of triple-negative breast cancer cells relies upon coordinate autocrine expression of the pro-inflammatory cytokines IL-6 and IL-8. *Cancer research,* 73**,** 10.1158/0008-5472.CAN-12-4524-T.

HASHIMOTO, S., OCHS, R. L., ROSEN, F., QUACH, J., MCCABE, G., SOLAN, J., SEEGMILLER, J. E., TERKELTAUB, R. & LOTZ, M. 1998. Chondrocyte-derived apoptotic bodies and calcification of articular cartilage. *Proceedings of the National Academy of Sciences,* 95**,** 3094-3099.

HERNÁNDEZ-BEDOLLA, M. A., GONZÁLEZ-DOMÍNGUEZ, E., ZAVALA-BARRERA, C., GUTIÉRREZ-LÓPEZ, T. Y., HIDALGO-MOYLE, J. J., VÁZQUEZ-PRADO, J., SÁNCHEZ-TORRES, C. & REYES-CRUZ, G. 2016. Calcium-sensing-receptor (CaSR) controls IL-6 secretion in metastatic breast cancer MDA-MB-231 cells by a dual mechanism revealed by agonist and inverse-agonist modulators. *Molecular and Cellular Endocrinology,* 436**,** 159-168.

HERSCHKOWITZ, J., SIMIN, K., WEIGMAN, V., MIKAELIAN, I., USARY, J., HU, Z., RASMUSSEN, K., JONES, L., ASSEFNIA, S., CHANDRASEKHARAN, S., BACKLUND, M., YIN, Y., KHRAMTSOV, A., BASTEIN, R., QUACKENBUSH, J., GLAZER, R., BROWN, P., GREEN, J., KOPELOVICH, L., FURTH, P., PALAZZO, J., OLOPADE, O., BERNARD, P., CHURCHILL, G., VAN DYKE, T. & PEROU, C. 2007. Identification of conserved gene expression features between murine mammary carcinoma models and human breast tumors. *Genome Biology,* 8.

HESSLE, L., JOHNSON, K. A., ANDERSON, H. C., NARISAWA, S., SALI, A., GODING, J. W., TERKELTAUB, R. & MILLÁN, J. L. 2002. Tissue-nonspecific alkaline phosphatase and plasma cell membrane glycoprotein-1 are central antagonistic regulators of bone mineralization. *Proceedings of the National Academy of Sciences,* 99**,** 9445-9449.

HIDAYAT, K., CHEN, G. C., ZHANG, R., DU, X., ZOU, S. Y., SHI, B. M. & QIN, L. Q. 2016. Calcium intake and breast cancer risk: meta-analysis of prospective cohort studies. *Br J Nutr,* 116**,** 158-66.

HOEMANN, C. D., EL-GABALAWY, H. & MCKEE, M. D. 2009. In vitro osteogenesis assays: Influence of the primary cell source on alkaline phosphatase activity and mineralization. *Pathologie Biologie,* 57**,** 318-323.

HOFVIND, S., IVERSEN, B. F., ERIKSEN, L., STYR, B. M., KJELLEVOLD, K. & KURZ, K. D. 2011. Mammographic morphology and distribution of calcifications in ductal carcinoma in situ diagnosed in organized screening. *Acta Radiologica,* 52**,** 481-487.

HOLLIDAY, D. L. & SPEIRS, V. 2011. Choosing the right cell line for breast cancer research. *Breast Cancer Research,* 13**,** 215.

HOLMBERG, L., WONG, Y. N. S., TABAR, L., RINGBERG, A., KARLSSON, P., ARNESSON, L. G., SANDELIN, K., ANDERSON, H., GARMO, H. & EMDIN, S. 2013. Mammography casting-type calcification and risk of local recurrence in DCIS: analyses from a randomised study. *British journal of cancer,* 108**,** 812-819.

HONRADO, E., BENÍTEZ, J. & PALACIOS, J. 2004. The Pathology of Hereditary Breast Cancer. *Hereditary Cancer in Clinical Practice,* 2**,** 131.

HOU, Z., FALCONE, D. J., SUBBARAMAIAH, K. & DANNENBERG, A. J. 2011. Macrophages induce COX-2 expression in breast cancer cells: role of IL-1beta autoamplification. *Carcinogenesis,* 32**,** 695-702.

HRUBY, A., O'DONNELL, C. J., JACQUES, P. F., MEIGS, J. B., HOFFMANN, U. & MCKEOWN, N. M. 2014. Magnesium Intake Is Inversely Associated With Coronary Artery Calcification: The Framingham Heart Study. *JACC. Cardiovascular imaging,* 7**,** 59-69.

HRUSKA, K. A., SAAB, G., MATHEW, S. & LUND, R. 2007. PHOSPHORUS METABOLISM AND MANAGEMENT IN CHRONIC KIDNEY DISEASE: Renal Osteodystrophy, Phosphate Homeostasis, and Vascular Calcification. *Seminars in Dialysis,* 20**,** 309-315.

HU, H.-Z., GU, Q., WANG, C., COLTON, C. K., TANG, J., KINOSHITA-KAWADA, M., LEE, L.-Y., WOOD, J. D. & ZHU, M. X. 2004. 2-Aminoethoxydiphenyl Borate Is a Common Activator of TRPV1, TRPV2, and TRPV3. *Journal of Biological Chemistry,* 279**,** 35741-35748.

HU, Z., FAN, C., OH, D., MARRON, J. S., HE, X., QAQISH, B., LIVASY, C., CAREY, L., REYNOLDS, E., DRESSLER, L., NOBEL, A., PARKER, J., EWEND, M., SAWYER, L., WU, J., LIU, Y., NANDA, R., TRETIAKOVA, M., ORRICO, A., DREHER, D., PALAZZO, J., PERREARD, L., NELSON, E., MONE, M., HANSEN, H., MULLINS, M., QUACKENBUSH, J., ELLIS, M., OLOPADE, O., BERNARD, P. & PEROU, C. 2006. The molecular portraits of breast tumors are conserved across microarray platforms. *BMC Genomics,* 7.

HUANG, H., ZHAO, N., XU, X., XU, Y., LI, S., ZHANG, J. & YANG, P. 2011. Dose-specific effects of tumor necrosis factor alpha on osteogenic differentiation of mesenchymal stem cells. *Cell Prolif,* 44**,** 420-7.

HUANG, P., CHEN, A., HE, W., LI, Z., ZHANG, G., LIU, Z., LIU, G., LIU, X., HE, S., XIAO, G., HUANG, F., STENVANG, J., BRÜNNER, N., HONG, A. & WANG, J. 2017. BMP-2 induces EMT and breast cancer stemness through Rb and CD44. *Cell Death Discovery,* 3**,** 17039.

HUGHES, L., MALONE, C., CHUMSRI, S., BURGER, A. M. & MCDONNELL, S. 2008. Characterisation of breast cancer cell lines and establishment of a novel isogenic subclone to study migration, invasion and tumourigenicity. *Clin Exp Metastasis,* 25**,** 549-57.

HUGO, H. J., LEBRET, S., TOMASKOVIC-CROOK, E., AHMED, N., BLICK, T., NEWGREEN, D. F., THOMPSON, E. W. & ACKLAND, M. L. 2012. Contribution of Fibroblast and Mast Cell (Afferent) and Tumor (Efferent) IL-6 Effects within the Tumor Microenvironment. *Cancer Microenviron,* 5**,** 83-93.

HUH, J.-E. & LEE, S. Y. 2013. IL-6 is produced by adipose-derived stromal cells and promotes osteogenesis. *Biochimica et Biophysica Acta (BBA) - Molecular Cell Research,* 1833**,** 2608-2616.

HUNTER, G. K. 2013. Role of osteopontin in modulation of hydroxyapatite formation. *Calcified Tissue International,* 93**,** 348-54.

HUNTER, G. K., KYLE, C. L. & GOLDBERG, H. A. 1994. Modulation of crystal formation by bone phosphoproteins: structural specificity of the osteopontin-mediated inhibition of hydroxyapatite formation. *Biochemical Journal,* 300**,** 723-728.

HUSSEIN, M. Z., AL FIKKY, A., ABDEL BAR, I. & ATTIA, O. 2004. Serum IL-6 and IL-12 levels in breast cancer patients. *Egypt J Immunol,* 11**,** 165-70.

INAGAKI, Y., YOSHIDA, K., OHBA, H., SETO, H., KIDO, J., HANEJI, T. & NAGATA, T. 2010. High glucose levels increase osteopontin production and pathologic calcification in rat dental pulp tissues. *J Endod,* 36**,** 1014-20.

INOUE, K., LIU, F., HOPPIN, J., LUNSFORD, E. P., LACKAS, C., HESTERMAN, J., LENKINSKI, R. E., FUJII, H. & FRANGIONI, J. V. 2011. High-Resolution CT Imaging of Single Breast Cancer Microcalcifications In Vivo. *Molecular imaging,* 10**,** 295-304.

ISHDORJ, G., JOHNSTON, J. B. & GIBSON, S. B. 2011. Cucurbitacin-I (JSI-124) activates the JNK/c-Jun signaling pathway independent of apoptosis and cell cycle arrest in B Leukemic Cells. *BMC Cancer,* 11**,** 268.

ISHIMURA, E., OKUNO, S., KITATANI, K., TSUCHIDA, T., YAMAKAWA, T., SHIOI, A., INABA, M. & NISHIZAWA, Y. 2007. Significant association between the presence of peripheral vascular calcification and lower serum magnesium in hemodialysis patients. *Clin Nephrol,* 68**,** 222-7.

IWASAKI, K., KOMAKI, M., MIMORI, K., LEON, E., IZUMI, Y. & ISHIKAWA, I. 2008. IL-6 induces osteoblastic differentiation of periodontal ligament cells. *J Dent Res,* 87**,** 937-42.

JAHNEN-DECHENT, W., HEISS, A., SCHÄFER, C. & KETTELER, M. 2011. Fetuin-A Regulation of Calcified Matrix Metabolism. *Circulation Research,* 108**,** 1494.

JAHNEN-DECHENT, W. & KETTELER, M. 2012. Magnesium basics. *Clinical Kidney Journal,* 5**,** i3-i14.

JAMES, J. J., EVANS, A. J., PINDER, S. E., MACMILLAN, R. D., WILSON, A. R. M. & ELLIS, I. O. 2003. Is the Presence of Mammographic Comedo Calcification Really a Prognostic Factor for Small Screen-detected Invasive Breast Cancers? *Clinical Radiology,* 58**,** 54-62.

JAMES, P., BERTRAND, K. A., HART, J. E., SCHERNHAMMER, E. S., TAMIMI, R. M. & LADEN, F. 2017. Outdoor Light at Night and Breast Cancer Incidence in the Nurses' Health Study II. *Environ Health Perspect,* 125**,** 087010.

JANG, H. L., JIN, K., LEE, J., KIM, Y., NAHM, S. H., HONG, K. S. & NAM, K. T. 2014. Revisiting Whitlockite, the Second Most Abundant Biomineral in Bone: Nanocrystal Synthesis in Physiologically Relevant Conditions and Biocompatibility Evaluation. *ACS Nano,* 8**,** 634-641.

JEONG, J., VANHOUTEN, J. N., DANN, P., KIM, W., SULLIVAN, C., YU, H., LIOTTA, L., ESPINA, V., STERN, D. F., FRIEDMAN, P. A. & WYSOLMERSKI, J. J. 2016. PMCA2 regulates HER2 protein kinase localization and signaling and promotes HER2-mediated breast cancer. *Proceedings of the National Academy of Sciences of the United States of America,* 113**,** E282-E290.

JÉZÉQUEL, P., FRÉNEL, J.-S., CAMPION, L., GUÉRIN-CHARBONNEL, C., GOURAUD, W., RICOLLEAU, G. & CAMPONE, M. 2013. bc-GenExMiner 3.0: new mining module computes breast cancer gene expression correlation analyses. *Database: The Journal of Biological Databases and Curation,* 2013**,** bas060.

JIANG, L., MA, T., MORAN, M. S., KONG, X., LI, X., HAFFTY, B. G. & YANG, Q. 2011. Mammographic features are associated with clinicopathological characteristics in invasive breast cancer. *Anticancer Res,* 31**,** 2327-34.

JIANG, S., ZHANG, H.-W., LU, M.-H., HE, X.-H., LI, Y., GU, H., LIU, M.-F. & WANG, E.-D. 2010. MicroRNA-155 Functions as an OncomiR in Breast Cancer by Targeting the Suppressor of Cytokine Signaling 1 Gene. *Cancer Research,* 70**,** 3119.

JIMÉNEZ, M. J. G., BALBÍN, M., LÓPEZ, J. M., ALVAREZ, J., KOMORI, T. & LÓPEZ-OTÍN, C. 1999. Collagenase 3 Is a Target of Cbfa1, a Transcription Factor of the runt Gene Family Involved in Bone Formation. *Molecular and Cellular Biology,* 19**,** 4431-4442.

JIN, C., FRAYSSINET, P., PELKER, R., CWIRKA, D., HU, B., VIGNERY, A., EISENBARTH, S. C. & FLAVELL, R. A. 2011. NLRP3 inflammasome plays a critical role in the pathogenesis of hydroxyapatite-associated arthropathy. *Proceedings of the National Academy of Sciences of the United States of America,* 108**,** 14867-14872.

JOHNS, N. & DIXON, J. M. 2016. Should patients with early breast cancer still be offered the choice of breast conserving surgery or mastectomy? *European Journal of Surgical Oncology (EJSO),* 42**,** 1636-1641.

JONO, S., PEINADO, C. & GIACHELLI, C. M. 2000. Phosphorylation of Osteopontin Is Required for Inhibition of Vascular Smooth Muscle Cell Calcification. *Journal of Biological Chemistry,* 275**,** 20197-20203.

JOSHI, S., DIALANI, V., MAROTTI, J., MEHTA, T. S. & SLANETZ, P. J. 2013. Breast disease in the pregnant and lactating patient: radiological-pathological correlation. *Insights into Imaging,* 4**,** 527-538.

KAKHKI, V. R., ANVARI, K., SADEGHI, R., MAHMOUDIAN, A. S. & TORABIAN-KAKHKI, M. 2013. Pattern and distribution of bone metastases in common malignant tumors. *Nucl Med Rev Cent East Eur,* 16**,** 66-9.

KALIMUTHO, M., PARSONS, K., MITTAL, D., LÓPEZ, J. A., SRIHARI, S. & KHANNA, K. K. 2015. Targeted Therapies for Triple-Negative Breast Cancer: Combating a Stubborn Disease. *Trends in Pharmacological Sciences,* 36**,** 822-846.

KALLEN, K.-J. 2002. The role of transsignalling via the agonistic soluble IL-6 receptor in human diseases. *Biochimica et Biophysica Acta (BBA) - Molecular Cell Research,* 1592**,** 323-343.

KANESHIRO, S., EBINA, K., SHI, K., HIGUCHI, C., HIRAO, M., OKAMOTO, M., KOIZUMI, K., MORIMOTO, T., YOSHIKAWA, H. & HASHIMOTO, J. 2014. IL-6 negatively regulates osteoblast differentiation through the SHP2/MEK2 and SHP2/Akt2 pathways in vitro. *J Bone Miner Metab,* 32**,** 378-92.

KAPUSTIN, A. N., DAVIES, J. D., REYNOLDS, J. L., MCNAIR, R., JONES, G. T., SIDIBE, A., SCHURGERS, L. J., SKEPPER, J. N., PROUDFOOT, D., MAYR, M. & SHANAHAN, C. M. 2011. Calcium regulates key components of vascular smooth muscle cell-derived matrix vesicles to enhance mineralization. *Circ Res,* 109**,** e1-12.

KARAMOUZIS, M. V., LIKAKI-KARATZA, E., RAVAZOULA, P., BADRA, F. A., KOUKOURAS, D., TZORAKOLEFTHERAKIS, E., PAPAVASSILIOU, A. G. & KALOFONOS, H. P. 2002. Non-palpable breast carcinomas: Correlation of mammographically detected malignant-appearing microcalcifications and molecular prognostic factors. *International Journal of Cancer,* 102**,** 86-90.

KATO, Y., LAMBERT, C. A., COLIGE, A. C., MINEUR, P., NOËL, A., FRANKENNE, F., FOIDART, J. M., BABA, M., HATA, R. I. & MIYAZAKI, K. 2005. Acidic extracellular pH induces matrix metalloproteinase-9 expression in mouse metastatic melanoma cells through the phospholipase D-mitogen-activated protein kinase signaling. *J Biol Chem,* 280.

KENNECKE, H., YERUSHALMI, R., WOODS, R., CHEANG, M. C. U., VODUC, D., SPEERS, C. H., NIELSEN, T. O. & GELMON, K. 2010. Metastatic Behavior of Breast Cancer Subtypes. *Journal of Clinical Oncology,* 28**,** 3271-3277.

KERSSENS, M. M., MATOUSEK, P., ROGERS, K. & STONE, N. 2010. Towards a safe non-invasive method for evaluating the carbonate substitution levels of hydroxyapatite (HAP) in micro-calcifications found in breast tissue. *Analyst,* 135**,** 3156-61.

KESHAVIAH, A., DELLAPASQUA, S., ROTMENSZ, N., LINDTNER, J., CRIVELLARI, D., COLLINS, J., COLLEONI, M., THÜRLIMANN, B., MENDIOLA, C., AEBI, S., PRICE, K. N., PAGANI, O., SIMONCINI, E., CASTIGLIONE GERTSCH, M., GELBER, R. D., COATES, A. S. & GOLDHIRSCH, A. 2007. CA15-3 and alkaline phosphatase as predictors for breast cancer recurrence: a combined analysis of seven International Breast Cancer Study Group trials. *Annals of Oncology,* 18**,** 701-708.

KESSENBROCK, K., PLAKS, V. & WERB, Z. 2010. Matrix Metalloproteinases: Regulators of the Tumor Microenvironment. *Cell,* 141**,** 52-67.

KHARKWAL, S., SAMEER & MUKHERJEE, A. 2014. Triple Test in Carcinoma Breast. *Journal of Clinical and Diagnostic Research : JCDR,* 8**,** NC09-NC11.

KILLELEA, B., CHAGPAR, A., BISHOP, J., HOROWITZ, N., CHRISTY, C., TSANGARIS, T., RAGHU, M. & LANNIN, D. 2013a. Is There a Correlation Between Breast Cancer Molecular Subtype Using Receptors as Surrogates and Mammographic Appearance? *Annals of Surgical Oncology,* 20**,** 3247-3253.

KILLELEA, B. K., CHAGPAR, A. B., BISHOP, J., HOROWITZ, N. R., CHRISTY, C., TSANGARIS, T., RAGHU, M. & LANNIN, D. R. 2013b. Is there a correlation between breast cancer molecular subtype using receptors as surrogates and mammographic appearance? *Ann Surg Oncol,* 20**,** 3247-53.

KIM, H. D., JANG, H. L., AHN, H.-Y., LEE, H. K., PARK, J., LEE, E.-S., LEE, E. A., JEONG, Y.-H., KIM, D.-G., NAM, K. T. & HWANG, N. S. 2017. Biomimetic whitlockite inorganic nanoparticles-mediated in situ remodeling and rapid bone regeneration. *Biomaterials,* 112**,** 31-43.

KIM, J.-H., LEE, H.-K., CHO, J.-H., PARK, H.-K. & YANG, H.-J. 2015a. Correlations between female breast density and biochemical markers. *Journal of Physical Therapy Science,* 27**,** 2097-2100.

KIM, J. H., HWANG, Y.-J., HAN, S. H., LEE, Y. E., KIM, S., KIM, Y. J., CHO, J. H., KWON, K. A., KIM, J. H. & KIM, S.-H. 2015b. Dexamethasone inhibits hypoxia-induced epithelial-mesenchymal transition in colon cancer. *World Journal of Gastroenterology : WJG,* 21**,** 9887-9899.

KIM, S.-Y., KIM, H. Y., KIM, E.-K., KIM, M. J., MOON, H. J. & YOON, J. H. 2015c. Evaluation of Malignancy Risk Stratification of Microcalcifications Detected on Mammography: A Study Based on the 5th Edition of BI-RADS. *Annals of Surgical Oncology,* 22**,** 2895-2901.

KIM, S. H., SEO, B. K., LEE, J., KIM, S. J., CHO, K. R., LEE, K. Y., JE, B. K., KIM, H. Y., KIM, Y. S. & LEE, J. H. 2008. Correlation of ultrasound findings with histology, tumor grade, and biological markers in breast cancer. *Acta Oncol,* 47**,** 1531-8.

KINDER, M., CHISLOCK, E., BUSSARD, K. M., SHUMAN, L. & MASTRO, A. M. 2008. Metastatic breast cancer induces an osteoblast inflammatory response. *Experimental Cell Research,* 314**,** 173-183.

KIRSCH, T. 2006. Determinants of pathological mineralization. *Current Opinion in Rheumatology,* 18**,** 174-180.

KLEVESATH, M. B., PANTEL, K., AGBAJE, O., PROVENZANO, E., WISHART, G. C., GOUGH, P., PINDER, S. E., DUFFY, S. & PURUSHOTHAM, A. D. 2013. Patterns of metastatic spread in early breast cancer. *The Breast,* 22**,** 449-454.

KNUPFER, H. & PREISS, R. 2007. Significance of interleukin-6 (IL-6) in breast cancer (review). *Breast Cancer Res Treat,* 102**,** 129-35.

KOMORI, T. 2009. Regulation of bone development and extracellular matrix protein genes by RUNX2. *Cell and Tissue Research,* 339**,** 189.

KOO, K. C., PARK, S. U., KIM, K. H., RHA, K. H., HONG, S. J., YANG, S. C. & CHUNG, B. H. 2015. Predictors of survival in prostate cancer patients with bone metastasis and extremely high prostate-specific antigen levels. *Prostate International,* 3**,** 10-15.

KOUTRAS, A. K. & EVANS, T. R. J. 2008. The epidermal growth factor receptor family in breast cancer. *OncoTargets and therapy,* 1**,** 5-19.

KRONENBERG, H. M. 2003. Developmental regulation of the growth plate. *Nature,* 423**,** 332-336.

LANDIS, W. J. & JACQUET, R. 2013. Association of Calcium and Phosphate Ions with Collagen in the Mineralization of Vertebrate Tissues. *Calcified Tissue International,* 93**,** 329-337.

LANGENBACH, F. & HANDSCHEL, J. 2013. Effects of dexamethasone, ascorbic acid and β-glycerophosphate on the osteogenic differentiation of stem cells in vitro. *Stem Cell Research & Therapy,* 4**,** 117.

LAOUI, D., MOVAHEDI, K., VAN OVERMEIRE, E., VAN DEN BOSSCHE, J., SCHOUPPE, E., MOMMER, C., NIKOLAOU, A., MORIAS, Y., DE BAETSELIER, P. & VAN GINDERACHTER, J. A. 2011. Tumor-associated macrophages in breast cancer: distinct subsets, distinct functions. *Int J Dev Biol,* 55**,** 861-7.

LAU, W. L., FESTING, M. H. & GIACHELLI, C. M. 2010. Phosphate and Vascular Calcification: Emerging Role of the Sodium-Dependent Phosphate Cotransporter PiT-1. *Thrombosis and haemostasis,* 104**,** 464-470.

LAU, W. M., DOUCET, M., STADEL, R., HUANG, D., WEBER, K. L. & KOMINSKY, S. L. 2013. Enpp1: A Potential Facilitator of Breast Cancer Bone Metastasis. *PLOS ONE,* 8**,** e66752.

LAW, M. E., CORSINO, P. E., JAHN, S. C., DAVIS, B. J., CHEN, S., PATEL, B., PHAM, K., LU, J., SHEPPARD, B., NØRGAARD, P., HONG, J., HIGGINS, P., KIM, J. S., LUESCH, H. & LAW, B. K. 2012. Glucocorticoids and histone deacetylase inhibitors cooperate to block the invasiveness of basal-like breast cancer cells through novel mechanisms. *Oncogene,* 32**,** 1316.

LEBORGNE, R. 1951. Diagnosis of tumors of the breast by simple roentgenography; calcifications in carcinomas. *The American journal of roentgenology and radium therapy,* 65**,** 1-11.

LEE, C.-H., YU, C.-C., WANG, B.-Y. & CHANG, W.-W. 2016. Tumorsphere as an effective in vitro platform for screening anti-cancer stem cell drugs. *Oncotarget,* 7**,** 1215-1226.

LEE, K.-S., HAN, B.-H., CHUN, Y.-K., KIM, H.-S. & KIM, E. E. 1999. Correlation between mammographic manifestations and averaged histopathologic nuclear grade using prognosis-predict scoring system for the prognosis of ductal carcinoma in situ. *Clinical Imaging,* 23**,** 339-346.

LELEKAKIS, M., MOSELEY, J. M., MARTIN, T. J., HARDS, D., WILLIAMS, E., HO, P., LOWEN, D., JAVNI, J., MILLER, F. R., SLAVIN, J. & ANDERSON, R. L. 1999. A novel orthotopic model of breast cancer metastasis to bone. *Clinical & Experimental Metastasis,* 17**,** 163-170.

LENCEL, P., HARDOUIN, P. & MAGNE, D. 2010. Do cytokines induce vascular calcification by the mere stimulation of TNAP activity? *Medical Hypotheses,* 75**,** 517-521.

LEO, J. C. L., GUO, C., WOON, C. T., AW, S. E. & LIN, V. C. L. 2004. Glucocorticoid and Mineralocorticoid Cross-Talk with Progesterone Receptor to Induce Focal Adhesion and Growth Inhibition in Breast Cancer Cells. *Endocrinology,* 145**,** 1314-1321.

LEONG, D. T., LIM, J., GOH, X., PRATAP, J., PEREIRA, B. P., KWOK, H. S., NATHAN, S. S., DOBSON, J. R., LIAN, J. B., ITO, Y., VOORHOEVE, P. M., STEIN, G. S., SALTO-TELLEZ, M., COOL, S. M. & VAN WIJNEN, A. J. 2010. Cancer-related ectopic expression of the bone-related transcription factor RUNX2 in non-osseous metastatic tumor cells is linked to cell proliferation and motility. *Breast Cancer Res,* 12.

LI, B., NI CHONGHAILE, T., FAN, Y., MADDEN, S. F., KLINGER, R., CONNOR, A. E., WALSH, L., HURLEY, G., MALLYA UDUPI, G., JOSEPH, J., TARRANT, F., CONROY, E., GABER, A., CHIN, S.-F., BARDWELL, H. A., PROVENZANO, E., CROWN, J., DUBOIS, T., LINN, S., JIRSTROM, K., CALDAS, C., CONNOR, D. P. & GALLAGHER, W. M. 2017. Therapeutic Rationale to Target Highly Expressed CDK7 Conferring Poor Outcomes in Triple-Negative Breast Cancer. *Cancer Research,* 77**,** 3834.

LI, J.-J., CHEN, C., GU, Y., DI, G., WU, J., LIU, G. & SHAO, Z. 2014a. The Role of Mammographic Calcification in the Neoadjuvant Therapy of Breast Cancer Imaging Evaluation. *PLoS ONE,* 9**,** e88853.

LI, M., JIANG, J. & YUE, L. 2006. Functional Characterization of Homo- and Heteromeric Channel Kinases TRPM6 and TRPM7. *The Journal of General Physiology,* 127**,** 525-537.

LI, Q., PRATT, C. H., DIONNE, L. A., FAIRFIELD, H., KARST, S. Y., SUNDBERG, J. P. & UITTO, J. 2014b. Spontaneous asj-2J Mutant Mouse as a Model for Generalized Arterial Calcification of Infancy: A Large Deletion/Insertion Mutation in the Enpp1 Gene. *PLoS ONE,* 9**,** e113542.

LI, X., ZHOU, Z.-Y., ZHANG, Y.-Y. & YANG, H.-L. 2016. IL-6 Contributes to the Defective Osteogenesis of Bone Marrow Stromal Cells from the Vertebral Body of the Glucocorticoid-Induced Osteoporotic Mouse. *PLOS ONE,* 11**,** e0154677.

LI, Y.-M., SCHILLING, T., BENISCH, P., ZECK, S., MEISSNER-WEIGL, J., SCHNEIDER, D., LIMBERT, C., SEUFERT, J., KASSEM, M., SCHÜTZE, N., JAKOB, F. & EBERT, R. 2007. Effects of high glucose on mesenchymal stem cell proliferation and differentiation. *Biochemical and Biophysical Research Communications,* 363**,** 209-215.

LIEBLEIN, J. C., BALL, S., HUTZEN, B., SASSER, A. K., LIN, H.-J., HUANG, T. H. M., HALL, B. M. & LIN, J. 2008. STAT3 can be activated through paracrine signaling in breast epithelial cells. *BMC Cancer,* 8**,** 302.

LIN, L., HE, Y., XI, B.-L., ZHENG, H.-C., CHEN, Q., LI, J., HU, Y., YE, M.-H., CHEN, P. & QU, Y. 2016. miR-135a Suppresses Calcification in Senescent VSMCs by Regulating KLF4/STAT3 Pathway. *Current Vascular Pharmacology,* 14**,** 211-218.

LIN, M. E., CHEN, T., LEAF, E. M., SPEER, M. Y. & GIACHELLI, C. M. 2015. Runx2 Expression in Smooth Muscle Cells Is Required for Arterial Medial Calcification in Mice. *Am J Pathol,* 185**,** 1958-69.

LING, H., LIU, Z.-B., XU, L.-H., XU, X.-L., LIU, G.-Y. & SHAO, Z.-M. 2013. Malignant calcification is an important unfavorable prognostic factor in primary invasive breast cancer. *Asia-Pacific Journal of Clinical Oncology,* 9**,** 139-145.

LIU, F., BLOCH, N., BHUSHAN, K. R., DE GRAND, A. M., TANAKA, E., SOLAZZO, S., MERTYNA, P. M., GOLDBERG, N., FRANGIONI, J. V. & LENKINSKI, R. E. 2008. Humoral bone morphogenetic protein 2 is sufficient for inducing breast cancer microcalcification. *Mol Imaging,* 7**,** 175-86.

LIU, F., MISRA, P., LUNSFORD, E., VANNAH, J., LIU, Y., LENKINSKI, R. & FRANGIONI, J. 2010. A dose- and time-controllable syngeneic animal model of breast cancer microcalcification. *Breast Cancer Research and Treatment,* 122**,** 87-94.

LIU, M., INOUE, K., LENG, T., GUO, S. & XIONG, Z.-G. 2014. TRPM7 channels regulate glioma stem cell through STAT3 and Notch signaling pathways. *Cellular signalling,* 26**,** 2773-2781.

LIU, R., SHI, P., NIE, Z., LIANG, H., ZHOU, Z., CHEN, W., CHEN, H., DONG, C., YANG, R., LIU, S. & CHEN, C. 2016. Mifepristone Suppresses Basal Triple-Negative Breast Cancer Stem Cells by Down-regulating KLF5 Expression. *Theranostics,* 6**,** 533-544.

LIU, X. & SUN, J. 2014. Potential proinflammatory effects of hydroxyapatite nanoparticles on endothelial cells in a monocyte–endothelial cell coculture model. *International Journal of Nanomedicine,* 9**,** 1261-1273.

LOUIE, E., NIK, S., CHEN, J.-S., SCHMIDT, M., SONG, B., PACSON, C., CHEN, X. F., PARK, S., JU, J. & CHEN, E. I. 2010. Identification of a stem-like cell population by exposing metastatic breast cancer cell lines to repetitive cycles of hypoxia and reoxygenation. *Breast Cancer Research,* 12**,** R94.

LOUVET, L., BÜCHEL, J., STEPPAN, S., PASSLICK-DEETJEN, J. & MASSY, Z. A. 2013. Magnesium prevents phosphate-induced calcification in human aortic vascular smooth muscle cells. *Nephrology Dialysis Transplantation,* 28**,** 869-878.

LOWRY, M. C., GALLAGHER, W. M. & DRISCOLL, L. 2015. The Role of Exosomes in Breast Cancer. *Clinical Chemistry,* 61**,** 1457.

LUO, G., DUCY, P., MCKEE, M. D., PINERO, G. J., LOYER, E., BEHRINGER, R. R. & KARSENTY, G. 1997. Spontaneous calcification of arteries and cartilage in mice lacking matrix GLA protein. *Nature,* 386**,** 78-81.

LUO, T., YAN, H.-M., HE, P., LUO, Y., YANG, Y.-F. & ZHENG, H. 2012. Aspirin use and breast cancer risk: a meta-analysis. *Breast Cancer Research and Treatment,* 131**,** 581-587.

MACMILLAN, R. D., PURUSHOTHAM, A. D., CORDINER, C., DOBSON, H., MALLON, E. & GEORGE, W. D. 1995. Predicting local recurrence by correlating pre-operative mammographic findings with pathological risk factors in patients with breast cancer. *The British Journal of Radiology,* 68**,** 445-449.

MAHAMID, J., SHARIR, A., GUR, D., ZELZER, E., ADDADI, L. & WEINER, S. 2011. Bone mineralization proceeds through intracellular calcium phosphate loaded vesicles: A cryo-electron microscopy study. *Journal of Structural Biology,* 174**,** 527-535.

MALIK, H. Z., WILKINSON, L., GEORGE, W. D. & PURUSHOTHAM, A. D. 2000. Preoperative mammographic features predict clinicopathological risk factors for the development of local recurrence in breast cancer. *The Breast,* 9**,** 329-333.

MANDAVILLI, S., SINGH, B. B. & SAHMOUN, A. E. 2012. Serum calcium levels, TRPM7, TRPC1, microcalcifications, and breast cancer using breast imaging reporting and data system scores. *Breast Cancer (Dove Med Press),* 2013**,** 1-7.

MANDAVILLI, S., SINGH, B. B. & SAHMOUN, A. E. 2013. Serum calcium levels, TRPM7, TRPC1, microcalcifications, and breast cancer using breast imaging reporting and data system scores. *Breast Cancer : Targets and Therapy,* 5**,** 1-7.

MÅNSSON, E., BERGKVIST, L., CHRISTENSON, G., PERSSON, C. & WÄRNBERG, F. 2009. Mammographic casting-type calcifications is not a prognostic factor in unifocal small invasive breast cancer: A population-based retrospective cohort study. *Journal of Surgical Oncology,* 100**,** 670-674.

MANUEL IGLESIAS, J., BELOQUI, I., GARCIA-GARCIA, F., LEIS, O., VAZQUEZ-MARTIN, A., EGUIARA, A., CUFI, S., PAVON, A., MENENDEZ, J. A., DOPAZO, J. & MARTIN, A. G. 2013. Mammosphere Formation in Breast Carcinoma Cell Lines Depends upon Expression of E-cadherin. *PLOS ONE,* 8**,** e77281.

MARMOT, M. G., ALTMAN, D. G., CAMERON, D. A., DEWAR, J. A., THOMPSON, S. G. & WILCOX, M. 2013. The benefits and harms of breast cancer screening: an independent review. *Br J Cancer,* 108**,** 2205-2240.

MASTRO, A. M., GAY, C. V., WELCH, D. R., DONAHUE, H. J., JEWELL, J., MERCER, R., DIGIROLAMO, D., CHISLOCK, E. M. & GUTTRIDGE, K. 2004. Breast cancer cells induce osteoblast apoptosis: a possible contributor to bone degradation. *J Cell Biochem,* 91**,** 265-76.

MATTHEWS, B. G., NAOT, D., CALLON, K. E., MUSSON, D. S., LOCKLIN, R., HULLEY, P. A., GREY, A. & CORNISH, J. 2014. Enhanced osteoblastogenesis in three-dimensional collagen gels. *BoneKEy Rep,* 3.

MAYER, I. A., ABRAMSON, V. G., LEHMANN, B. D. & PIETENPOL, J. A. 2014. NEW STRATEGIES FOR TRIPLE NEGATIVE BREAST CANCER – DECIPHERING THE HETEROGENEITY. *Clinical cancer research : an official journal of the American Association for Cancer Research,* 20**,** 782-790.

MCCARTHY, G. M., CHEUNG, H. S., ABEL, S. M. & RYAN, L. M. 1998. Basic calcium phosphate crystal-induced collagenase production: role of intracellular crystal dissolution. *Osteoarthritis Cartilage,* 6**,** 205-13.

MCCARTHY, G. M., MITCHELL, P. G., STRUVE, J. A. & CHEUNG, H. S. 1992. Basic calcium phosphate crystals cause coordinate induction and secretion of collagenase and stromelysin. *Journal of cellular physiology,* 153**,** 140-146.

MCCARTHY, G. M., WESTFALL, P. R., MASUDA, I., CHRISTOPHERSON, P. A., CHEUNG, H. S. & MITCHELL, P. G. 2001. Basic calcium phosphate crystals activate human osteoarthritic synovial fibroblasts and induce matrix metalloproteinase-13 (collagenase-3) in adult porcine articular chondrocytes. *Annals of the Rheumatic Diseases,* 60**,** 399-406.

MCDONALD, L., FERRARI, N., TERRY, A., BELL, M., MOHAMMED, Z. M., ORANGE, C., JENKINS, A., MULLER, W. J., GUSTERSON, B. A., NEIL, J. C., EDWARDS, J., MORRIS, J. S., CAMERON, E. R. & BLYTH, K. 2014. RUNX2 correlates with subtype-specific breast cancer in a human tissue microarray, and ectopic expression of Runx2 perturbs differentiation in the mouse mammary gland. *Dis Model Mech,* 7**,** 525-34.

MCFARLAND, B. C., GRAY, G. K., NOZELL, S. E., HONG, S. W. & BENVENISTE, E. N. 2013. Activation of the NF-κB pathway by the STAT3 inhibitor JSI-124 in human glioblastoma cells. *Molecular cancer research : MCR,* 11**,** 494-505.

MEDREK, C., PONTÉN, F., JIRSTRÖM, K. & LEANDERSSON, K. 2012. The presence of tumor associated macrophages in tumor stroma as a prognostic marker for breast cancer patients. *BMC Cancer,* 12**,** 306-306.

MENDOZA-VILLANUEVA, D., DENG, W., LOPEZ-CAMACHO, C. & SHORE, P. 2010. The Runx transcriptional co-activator, CBFβ, is essential for invasion of breast cancer cells. *Molecular Cancer,* 9**,** 171.

MENG, X., CAI, C., WU, J., CAI, S., YE, C., CHEN, H., YANG, Z., ZENG, H., SHEN, Q. & ZOU, F. 2013. TRPM7 mediates breast cancer cell migration and invasion through the MAPK pathway. *Cancer Letters,* 333**,** 96-102.

MIDDELBEEK, J., KUIPERS, A. J., HENNEMAN, L., VISSER, D., EIDHOF, I., VAN HORSSEN, R., WIERINGA, B., CANISIUS, S. V., ZWART, W., WESSELS, L. F., SWEEP, F. C. G. J., BULT, P., SPAN, P. N., VAN LEEUWEN, F. N. & JALINK, K. 2012. TRPM7 Is Required for Breast Tumor Cell Metastasis. *Cancer Research,* 72**,** 4250.

MIDDELBEEK, J., VISSER, D., HENNEMAN, L., KAMERMANS, A., KUIPERS, A. J., HOOGERBRUGGE, P. M., JALINK, K. & VAN LEEUWEN, F. N. 2015. TRPM7 maintains progenitor-like features of neuroblastoma cells: implications for metastasis formation. *Oncotarget,* 6**,** 8760-8776.

MIGLIETTA, A., TOSELLI, M., RAVARINO, N., VENCIA, W., CHIECCHIO, A., BOZZO, F., MOTTA, M., TORCHIO, B. & BOCCA, C. 2010. COX-2 expression in human breast carcinomas: correlation with clinicopathological features and prognostic molecular markers. *Expert Opinion on Therapeutic Targets,* 14**,** 655-664.

MIHARA, M., HASHIZUME, M., YOSHIDA, H., SUZUKI, M. & SHIINA, M. 2012. IL-6/IL-6 receptor system and its role in physiological and pathological conditions. *Clinical Science,* 122**,** 143.

MOJA, L., TAGLIABUE, L., BALDUZZI, S., PARMELLI, E., PISTOTTI, V., GUARNERI, V. & D'AMICO, R. 2012. Trastuzumab containing regimens for early breast cancer. *Cochrane Database of Systematic Reviews*.

MONTEILH-ZOLLER, M. K., HERMOSURA, M. C., NADLER, M. J. S., SCHARENBERG, A. M., PENNER, R. & FLEIG, A. 2003. TRPM7 Provides an Ion Channel Mechanism for Cellular Entry of Trace Metal Ions. *The Journal of General Physiology,* 121**,** 49-60.

MONTES DE OCA, A., GUERRERO, F., MARTINEZ-MORENO, J. M., MADUEÑO, J. A., HERENCIA, C., PERALTA, A., ALMADEN, Y., LOPEZ, I., AGUILERA-TEJERO, E., GUNDLACH, K., BÜCHEL, J., PETER, M. E., PASSLICK-DEETJEN, J., RODRIGUEZ, M. & MUÑOZ-CASTAÑEDA, J. R. 2014. Magnesium Inhibits Wnt/β-Catenin Activity and Reverses the Osteogenic Transformation of Vascular Smooth Muscle Cells. *PLOS ONE,* 9**,** e89525.

MONTEZANO, A. C., ZIMMERMAN, D., YUSUF, H., BURGER, D., CHIGNALIA, A. Z., WADHERA, V., VAN LEEUWEN, F. N. & TOUYZ, R. M. 2010. Vascular Smooth Muscle Cell Differentiation to an Osteogenic Phenotype Involves TRPM7 Modulation by Magnesium. *Hypertension,* 56**,** 453.

MORATA-TARIFA, C., JIMÉNEZ, G., GARCÍA, M. A., ENTRENA, J. M., GRIÑÁN-LISÓN, C., AGUILERA, M., PICON-RUIZ, M. & MARCHAL, J. A. 2016. Low adherent cancer cell subpopulations are enriched in tumorigenic and metastatic epithelial-to-mesenchymal transition-induced cancer stem-like cells. *Scientific Reports,* 6**,** 18772.

MORGAN, M. P., COOKE, M. M., CHRISTOPHERSON, P. A., WESTFALL, P. R. & MCCARTHY, G. M. 2001. Calcium hydroxyapatite promotes mitogenesis and matrix metalloproteinase expression in human breast cancer cell lines. *Molecular Carcinogenesis,* 32**,** 111-117.

MORGAN, M. P., WHELAN, L. C., SALLIS, J. D., MCCARTHY, C. J., FITZGERALD, D. J. & MCCARTHY, G. M. 2004. Basic calcium phosphate crystal–induced prostaglandin E2 production in human fibroblasts: Role of cyclooxygenase 1, cyclooxygenase 2, and interleukin-1β. *Arthritis & Rheumatism,* 50**,** 1642-1649.

MORIGUCHI, T., YANO, K., NAKAGAWA, S. & KAJI, F. 2003. Elucidation of adsorption mechanism of bone-staining agent alizarin red S on hydroxyapatite by FT-IR microspectroscopy. *J Colloid Interface Sci,* 260**,** 19-25.

MORRIS, K. T., POMMIER, R. F., MORRIS, A. & ET AL. 2001. Usefulness of the triple test score for palpable breast masses. *Archives of Surgery,* 136**,** 1008-1013.

MUNDY, G. R. 2002. Metastasis: Metastasis to bone: causes, consequences and therapeutic opportunities. *Nat Rev Cancer,* 2**,** 584-593.

NAHAR, N., MISSANA, L., GARIMELLA, R., TAGUE, S. & ANDERSON, H. C. 2008. Matrix vesicles are carriers of bone morphogenetic proteins (BMPs), vascular endothelial growth factor (VEGF), and noncollagenous matrix proteins. *Journal of Bone and Mineral Metabolism,* 26**,** 514-519.

NAHTA, R. & ESTEVA, F. J. 2006. HER2 therapy: Molecular mechanisms of trastuzumab resistance. *Breast Cancer Research,* 8**,** 215-215.

NAM, H. K., LIU, J., LI, Y., KRAGOR, A. & HATCH, N. E. 2011. Ectonucleotide Pyrophosphatase/Phosphodiesterase-1 (ENPP1) Protein Regulates Osteoblast Differentiation. *Journal of Biological Chemistry,* 286**,** 39059-39071.

NASEEM, M., MURRAY, J., HILTON, J. F., KARAMCHANDANI, J., MURADALI, D., FARAGALLA, H., POLENZ, C., HAN, D., BELL, D. C. & BREZDEN-MASLEY, C. 2015. Mammographic microcalcifications and breast cancer tumorigenesis: a radiologic-pathologic analysis. *BMC Cancer,* 15**,** 307.

NASI, S., SO, A., COMBES, C., DAUDON, M. & BUSSO, N. 2016. Interleukin-6 and chondrocyte mineralisation act in tandem to promote experimental osteoarthritis. *Annals of the Rheumatic Diseases,* 75**,** 1372.

NATHAN, M. R. & SCHMID, P. 2017. A Review of Fulvestrant in Breast Cancer. *Oncology and Therapy,* 5**,** 17-29.

NCRI. 2012. *Breast Cancer Incidence, Mortality, Treatment and Survival in Ireland: 1994-2009* [Online]. Available: https://www.ncri.ie/sites/ncri/files/pubs/BreastCancerIncidenceMortalityTreatmentandSurvivalinIreland1994-2009.pdf [Accessed].

NCRI. 2016. *Cancer Trends No 29. Breast cancer* [Online]. National Cancer Registry, Ireland. Available: https://www.ncri.ie/sites/ncri/files/pubs/bc_trends_21.pdf [Accessed].

NCRI. 2017. *Cancer in Ireland 1994-2015 with estimates for 2015-2017: Annual Report of the National Cancer Registry* [Online]. Available: https://www.ncri.ie/sites/ncri/files/pubs/NCRReport_2017_full%20report.pdf [Accessed].

NELSON, H. D., TYNE, K., NAIK, A., BOUGATSOS, C., CHAN, B. K. & HUMPHREY, L. 2009. Screening for Breast Cancer: An Update for the U.S. Preventive Services Task Force. *Annals of Internal Medicine,* 151**,** 727-737.

NGUYEN, C., LIEBERHERR, M., BORDAT, C., VELARD, F., CÔME, D., LIOTÉ, F. & EA, H. K. 2012. Intracellular calcium oscillations in articular chondrocytes induced by basic calcium

phosphate crystals lead to cartilage degradation. *Osteoarthritis and Cartilage,* 20**,** 1399-1408.

NICOLAIDES, N. C., GALATA, Z., KINO, T., CHROUSOS, G. P. & CHARMANDARI, E. 2010. The Human Glucocorticoid Receptor: Molecular Basis of Biologic Function. *Steroids,* 75**,** 1.

NISHIMURA, R., MORIYAMA, K., YASUKAWA, K., MUNDY, G. R. & YONEDA, T. 1998. Combination of interleukin-6 and soluble interleukin-6 receptors induces differentiation and activation of JAK-STAT and MAP kinase pathways in MG-63 human osteoblastic cells. *J Bone Miner Res,* 13**,** 777-85.

NOMAN, A. S., UDDIN, M., CHOWDHURY, A. A., NAYEEM, M. J., RAIHAN, Z., RASHID, M. I., AZAD, A. K., RAHMAN, M. L., BARUA, D., SULTANA, A., SHIRIN, A., FERDOUS, J., PARAG, R. R., RAHMAN, S. M., MAHMUD, M. R., JERIN, C. S., JAHAN, N., SIDDIQUA, A., ARA, T., SABUR, E. B., ALAM, S. S., BAIDYA, S., AKTHER, S., RAHMAN, M. Z., BANU, T., MURUGAN, A. K., SABRI, S., ISLAM, S. M. S., KARAKAS, B., ABOUSSEKHRA, A., YEGER, H., FARHAT, W. A. & ISLAM, S. S. 2017. Serum sonic hedgehog (SHH) and interleukin-(IL-6) as dual prognostic biomarkers in progressive metastatic breast cancer. *Scientific Reports,* 7**,** 1796.

NYANTE, S. J., LEE, S. S., BENEFIELD, T. S., HOOTS, T. N. & HENDERSON, L. M. 2017. The association between mammographic calcifications and breast cancer prognostic factors in a population-based registry cohort. *Cancer,* 123**,** 219-227.

O'NEILL, W. C. 2006. Pyrophosphate, Alkaline Phosphatase, and Vascular Calcification. *Circulation Research,* 99**,** e2.

OLIVERAS-FERRAROS, C., COROMINAS-FAJA, B., CUFI, S., VAZQUEZ-MARTIN, A., MARTIN-CASTILLO, B., IGLESIAS, J. M., LOPEZ-BONET, E., MARTIN, A. G. & MENENDEZ, J. A. 2012. Epithelial-to-mesenchymal transition (EMT) confers primary resistance to trastuzumab (Herceptin). *Cell Cycle,* 11**,** 4020-32.

ORTIZ-MONTERO, P., LONDOÑO-VALLEJO, A. & VERNOT, J.-P. 2017. Senescence-associated IL-6 and IL-8 cytokines induce a self- and cross-reinforced senescence/inflammatory milieu strengthening tumorigenic capabilities in the MCF-7 breast cancer cell line. *Cell Communication and Signaling,* 15**,** 17.

OUADID-AHIDOUCH, H., DHENNIN-DUTHILLE, I., GAUTIER, M., SEVESTRE, H. & AHIDOUCH, A. 2012. [TRP calcium channel and breast cancer: expression, role and correlation with clinical parameters]. *Bull Cancer,* 99**,** 655-64.

OYAMA, T., SANO, T., HIKINO, T., XUE, Q., IIJIMA, K., NAKAJIMA, T. & KOERNER, F. 2002. Microcalcifications of breast cancer and atypical cystic lobules associated with infiltration of foam cells expressing osteopontin. *Virchows Arch,* 440**,** 267-73.

PACE, L. E. & KEATING, N. L. 2014. A systematic assessment of benefits and risks to guide breast cancer screening decisions. *JAMA,* 311**,** 1327-1335.

PALKA, I., ORMANDI, K., GAAL, S., BODA, K. & KAHAN, Z. 2007. Casting-type calcifications on the mammogram suggest a higher probability of early relapse and death among high-risk breast cancer patients. *Acta Oncol,* 46**,** 1178-83.

PAN, D., KOCHERGINSKY, M. & CONZEN, S. D. 2011. Activation of the Glucocorticoid Receptor Is Associated with Poor Prognosis in Estrogen Receptor-Negative Breast Cancer. *Cancer Research,* 71**,** 6360.

PARHAMI, F., BASSERI, B., HWANG, J., TINTUT, Y. & DEMER, L. L. 2002. High-density lipoprotein regulates calcification of vascular cells. *Circ Res,* 91**,** 570-6.

PARKER, J. S., MULLINS, M., CHEANG, M. C. U., LEUNG, S., VODUC, D., VICKERY, T., DAVIES, S., FAURON, C., HE, X., HU, Z., QUACKENBUSH, J. F., STIJLEMAN, I. J., PALAZZO, J., MARRON, J. S., NOBEL, A. B., MARDIS, E., NIELSEN, T. O., ELLIS, M. J., PEROU, C. M. & BERNARD, P. S. 2009. Supervised Risk Predictor of Breast Cancer Based on Intrinsic Subtypes. *Journal of Clinical Oncology,* 27**,** 1160-1167.

PATHI, S. P., KOWALCZEWSKI, C., TADIPATRI, R. & FISCHBACH, C. 2010. A Novel 3-D Mineralized Tumor Model to Study Breast Cancer Bone Metastasis. *PLoS ONE,* 5.

PAZAR, B., EA, H. K., NARAYAN, S., KOLLY, L., BAGNOUD, N., CHOBAZ, V., ROGER, T., LIOTE, F., SO, A. & BUSSO, N. 2011. Basic calcium phosphate crystals induce monocyte/macrophage IL-1beta secretion through the NLRP3 inflammasome in vitro. *J Immunol,* 186**,** 2495-502.

PEACOCK, C., GIVEN-WILSON, R. M. & DUFFY, S. W. 2004. Mammographic casting-type calcification associated with small screen-detected invasive breast cancers: is this a reliable prognostic indicator? *Clinical Radiology,* 59**,** 165-170.

PEGRAM, M. D., FINN, R. S., ARZOO, K., BERYT, M., PIETRAS, R. J. & SLAMON, D. J. 1997. The effect of HER-2/neu overexpression on chemotherapeutic drug sensitivity in human breast and ovarian cancer cells. *Oncogene,* 15**,** 537-47.

PEREZ, A. A., ROCHA, R. M., BALABRAM, D., DA SILVA SOUZA, Á. & GOBBI, H. 2013. Immunohistochemical profile of high-grade ductal carcinoma in situ of the breast. *Clinics,* 68**,** 674-678.

PEROU, C. M., SORLIE, T., EISEN, M. B., VAN DE RIJN, M., JEFFREY, S. S., REES, C. A., POLLACK, J. R., ROSS, D. T., JOHNSEN, H., AKSLEN, L. A., FLUGE, O., PERGAMENSCHIKOV, A., WILLIAMS, C., ZHU, S. X., LONNING, P. E., BORRESEN-DALE, A.-L., BROWN, P. O. & BOTSTEIN, D. 2000. Molecular portraits of human breast tumours. *Nature,* 406**,** 747-752.

PETERS, A. A., MILEVSKIY, M. J. G., LEE, W. C., CURRY, M. C., SMART, C. E., SAUNUS, J. M., REID, L., DA SILVA, L., MARCIAL, D. L., DRAY, E., BROWN, M. A., LAKHANI, S. R., ROBERTS-THOMSON, S. J. & MONTEITH, G. R. 2016. The calcium pump plasma membrane Ca2+-ATPase 2 (PMCA2) regulates breast cancer cell proliferation and sensitivity to doxorubicin. *Scientific Reports,* 6**,** 25505.

PETTA, I., DEJAGER, L., BALLEGEER, M., LIEVENS, S., TAVERNIER, J., DE BOSSCHER, K. & LIBERT, C. 2016. The Interactome of the Glucocorticoid Receptor and Its Influence on the Actions of Glucocorticoids in Combatting Inflammatory and Infectious Diseases. *Microbiology and Molecular Biology Reviews,* 80**,** 495-522.

POSADAS-SANCHEZ, R., POSADAS-ROMERO, C., CARDOSO-SALDANA, G., VARGAS-ALARCON, G., VILLARREAL-MOLINA, M. T., PEREZ-HERNANDEZ, N., RODRIGUEZ-PEREZ, J. M., MEDINA-URRUTIA, A., JORGE-GALARZA, E., JUAREZ-ROJAS, J. G. & TORRES-TAMAYO, M. 2016. Serum magnesium is inversely associated with coronary artery calcification in the Genetics of Atherosclerotic Disease (GEA) study. *Nutr J,* 15**,** 22.

PRAT, A. & PEROU, C. M. 2011. Deconstructing the molecular portraits of breast cancer. *Molecular Oncology,* 5**,** 5-23.

PRATAP, J., JAVED, A., LANGUINO, L. R., VAN WIJNEN, A. J., STEIN, J. L., STEIN, G. S. & LIAN, J. B. 2005. The Runx2 osteogenic transcription factor regulates matrix metalloproteinase 9 in bone metastatic cancer cells and controls cell invasion. *Mol Cell Biol,* 25.

PROIA, A. D. & BRINN, N. T. 1985. Identification of calcium oxalate crystals using alizarin red S stain. *Arch Pathol Lab Med,* 109**,** 186-9.

PROUDFOOT, D. & SHANAHAN, C. M. 2006. Molecular mechanisms mediating vascular calcification: role of matrix Gla protein. *Nephrology (Carlton),* 11**,** 455-61.

PROUDFOOT, D., SKEPPER, J. N., HEGYI, L., BENNETT, M. R., SHANAHAN, C. M. & WEISSBERG, P. L. 2000. Apoptosis Regulates Human Vascular Calcification In Vitro: Evidence for Initiation of Vascular Calcification by Apoptotic Bodies. *Circulation Research,* 87**,** 1055-1062.

PRUD'HOMME, G. J., GLINKA, Y., TOULINA, A., ACE, O., SUBRAMANIAM, V. & JOTHY, S. 2010. Breast Cancer Stem-Like Cells Are Inhibited by a Non-Toxic Aryl Hydrocarbon Receptor Agonist. *PLoS ONE,* 5**,** e13831.

PULASKI, B. A. & OSTRAND-ROSENBERG, S. 2001. Mouse 4T1 Breast Tumor Model. *Current Protocols in Immunology.* John Wiley & Sons, Inc.

PUROHIT, A., NEWMAN, S. P. & REED, M. J. 2002. The role of cytokines in regulating estrogen synthesis: implications for the etiology of breast cancer. *Breast Cancer Research : BCR,* 4**,** 65-69.

QI, X., CHEN, A., ZHANG, P., ZHANG, W., CAO, X. & XIAO, C. 2017. Mammographic calcification can predict outcome in women with breast cancer treated with breast-conserving surgery. *Oncol Lett,* 14**,** 79-88.

QIU, X., MEI, J., YIN, J., WANG, H., WANG, J. & XIE, M. 2017. Correlation analysis between expression of PCNA, Ki-67 and COX-2 and X-ray features in mammography in breast cancer. *Oncology Letters,* 14**,** 2912-2918.

RADI, M. J. 1989. Calcium oxalate crystals in breast biopsies. An overlooked form of microcalcification associated with benign breast disease. *Archives of pathology & laboratory medicine,* 113**,** 1367-1369.

RAMASWAMY, G., RAO, V. R., KRISHNAMOORTHY, L., RAMESH, G., GOMATHY, R. & RENUKADEVI, D. 2000. Serum levels of bone alkaline phosphatase in breast and prostate cancers with bone metastasis. *Indian Journal of Clinical Biochemistry,* 15**,** 110-113.

RAO, A. A., FENEIS, J., LALONDE, C. & OJEDA-FOURNIER, H. 2016. A Pictorial Review of Changes in the BI-RADS Fifth Edition. *RadioGraphics,* 36**,** 623-639.

RAUCH, G. M., HOBBS, B. P., KUERER, H. M., SCOGGINS, M. E., BENVENISTE, A. P., PARK, Y. M., CAUDLE, A. S., FOX, P. S., SMITH, B. D., ADRADA, B. E., KRISHNAMURTHY, S. & YANG, W. T. 2016. Microcalcifications in 1657 Patients with Pure Ductal Carcinoma in Situ of the Breast: Correlation with Clinical, Histopathologic, Biologic Features, and Local Recurrence. *Ann Surg Oncol,* 23**,** 482-9.

RAYSON, D., LUTES, S., WALSH, G., SELLON, M., COLWELL, B., DORREEN, M., DRUCKER, A., JEYAKUMAR, A. & YOUNIS, T. 2014. Trastuzumab beyond progression for HER2 positive metastatic breast cancer: progression-free survival on first-line therapy predicts overall survival impact. *Breast J,* 20**,** 408-13.

REALE, M. G., SANTINI, D., MARCHEI, G. G., MANNA, A., DEL NERO, A., BIANCO, V., MARCHEI, P. & FRATI, L. 1995. Skeletal alkaline phosphatase as a serum marker of bone metastases in the follow-up of patients with breast cancer. *Int J Biol Markers,* 10**,** 42-6.

REINHARDT, T. A., LIPPOLIS, J. D., SHULL, G. E. & HORST, R. L. 2004. Null Mutation in the Gene Encoding Plasma Membrane Ca2+-ATPase Isoform 2 Impairs Calcium Transport into Milk. *Journal of Biological Chemistry,* 279**,** 42369-42373.

REUBEN, P. M., WENGER, L., CRUZ, M. & CHEUNG, H. S. 2001. Induction of matrix metalloproteinase-8 in human fibroblasts by basic calcium phosphate and calcium pyrophosphate dihydrate crystals: effect of phosphocitrate. *Connective tissue research,* 42**,** 1-12.

REXER, B. N. & ARTEAGA, C. L. 2012. Intrinsic and Acquired Resistance to HER2-Targeted Therapies in HER2 Gene-Amplified Breast Cancer: Mechanisms and Clinical Implications. *Critical Reviews in Oncogenesis,* 17**,** 1-16.

REYNOLDS, J. L., JOANNIDES, A. J., SKEPPER, J. N., MCNAIR, R., SCHURGERS, L. J., PROUDFOOT, D., JAHNEN-DECHENT, W., WEISSBERG, P. L. & SHANAHAN, C. M. 2004. Human Vascular Smooth Muscle Cells Undergo Vesicle-Mediated Calcification in Response to Changes in Extracellular Calcium and Phosphate Concentrations: A Potential Mechanism for Accelerated Vascular Calcification in ESRD. *Journal of the American Society of Nephrology,* 15**,** 2857-2867.

RODENBECK, S. D., ZARSE, C. A., MCKENNEY-DRAKE, M. L., BRUNING, R. S., STUREK, M., CHEN, N. X. & MOE, S. M. 2017. Intracellular calcium increases in vascular smooth muscle cells with progression of chronic kidney disease in a rat model. *Nephrology Dialysis Transplantation,* 32**,** 450-458.

RODGERS, K. M., UDESKY, J. O., RUDEL, R. A. & BRODY, J. G. 2018. Environmental chemicals and breast cancer: An updated review of epidemiological literature informed by biological mechanisms. *Environmental Research,* 160**,** 152-182.

ROMINGER, M., WISGICKL, C. & TIMMESFELD, N. 2012. Breast microcalcifications as type descriptors to stratify risk of malignancy: a systematic review and meta-analysis of 10665 cases with special focus on round/punctate microcalcifications. *RoFo : Fortschritte auf dem Gebiete der Rontgenstrahlen und der Nuklearmedizin,* 184**,** 1144-1152.

RUCCI, N. 2008. Molecular biology of bone remodelling. *Clinical Cases in Mineral and Bone Metabolism,* 5**,** 49-56.

RUNGBY, J., KASSEM, M., ERIKSEN, E. F. & DANSCHER, G. 1993. The von Kossa reaction for calcium deposits: silver lactate staining increases sensitivity and reduces background. *The Histochemical Journal,* 25**,** 446-451.

RYAZANOVA, L. V., RONDON, L. J., ZIERLER, S., HU, Z., GALLI, J., YAMAGUCHI, T. P., MAZUR, A., FLEIG, A. & RYAZANOV, A. G. 2010. TRPM7 is essential for Mg2+ homeostasis in mammals. 1**,** 109.

SAGE, A. P., LU, J., TINTUT, Y. & DEMER, L. L. 2011. Hyperphosphatemia-induced nanocrystals upregulate the expression of bone morphogenetic protein-2 and osteopontin genes in mouse smooth muscle cells in vitro. *Kidney international,* 79**,** 414-422.

SAHA, A., BARMAN, I., DINGARI, N. C., MCGEE, S., VOLYNSKAYA, Z., GALINDO, L. H., LIU, W., PLECHA, D., KLEIN, N., DASARI, R. R. & FITZMAURICE, M. 2011. Raman spectroscopy: a real-time tool for identifying microcalcifications during stereotactic breast core needle biopsies. *Biomedical Optics Express,* 2**,** 2792-2803.

SAK, M. A., LITTRUP, P. J., DURIC, N., MULLOOLY, M., SHERMAN, M. E. & GIERACH, G. L. 2015. Current and Future Methods for Measuring Breast Density: A Brief Comparative Review. *Breast cancer management,* 4**,** 209-221.

SALGADO, R., JUNIUS, S., BENOY, I., VAN DAM, P., VERMEULEN, P., VAN MARCK, E., HUGET, P. & DIRIX, L. Y. 2003. Circulating interleukin-6 predicts survival in patients with metastatic breast cancer. *International Journal of Cancer,* 103**,** 642-646.

SAPIR-KOREN, R. & LIVSHITS, G. 2011. Bone mineralization and regulation of phosphate homeostasis. *IBMS BoneKEy,* 8**,** 286-300.

SARTORI, S., NIELSEN, I., TASSINARI, D., MAZZOTTA, D., VECCHIATTI, G., SERO, A. & ABBASCIANO, V. 1992. Serum and erythrocyte magnesium concentrations in solid tumours: relationship with stage of malignancy. *Magnes Res,* 5**,** 189-92.

SASSER, A. K., SULLIVAN, N. J., STUDEBAKER, A. W., HENDEY, L. F., AXEL, A. E. & HALL, B. M. 2007. Interleukin-6 is a potent growth factor for ER-alpha-positive human breast cancer. *Faseb j,* 21**,** 3763-70.

SATHYAVATHI, R., SAHA, A., SOARES, J. S., SPEGAZZINI, N., MCGEE, S., RAO DASARI, R., FITZMAURICE, M. & BARMAN, I. 2015. Raman spectroscopic sensing of carbonate intercalation in breast microcalcifications at stereotactic biopsy. *Scientific Reports,* 5**,** 9907.

SCHÄCK, L. M., NOACK, S., WINKLER, R., WIßMANN, G., BEHRENS, P., WELLMANN, M., JAGODZINSKI, M., KRETTEK, C. & HOFFMANN, A. 2013. The Phosphate Source Influences Gene Expression and Quality of Mineralization during In Vitro Osteogenic Differentiation of Human Mesenchymal Stem Cells. *PLOS ONE,* 8**,** e65943.

SCHELLER, J., CHALARIS, A., SCHMIDT-ARRAS, D. & ROSE-JOHN, S. 2011. The pro- and anti-inflammatory properties of the cytokine interleukin-6. *Biochimica et Biophysica Acta (BBA) - Molecular Cell Research,* 1813**,** 878-888.

SCHURGERS, L. J., CRANENBURG, E. C. & VERMEER, C. 2008. Matrix Gla-protein: the calcification inhibitor in need of vitamin K. *Thromb Haemost,* 100**,** 593-603.

SCHURGERS, L. J., UITTO, J. & REUTELINGSPERGER, C. P. 2013. Vitamin K-dependent carboxylation of matrix Gla-protein: a crucial switch to control ectopic mineralization. *Trends in Molecular Medicine,* 19**,** 217-226.

SCIMECA, M., GIANNINI, E., ANTONACCI, C., PISTOLESE, C., SPAGNOLI, L. & BONANNO, E. 2014. Microcalcifications in breast cancer: an active phenomenon mediated by epithelial cells with mesenchymal characteristics. *BMC Cancer,* 14.

SCOTT, R., STONE, N., KENDALL, C., GERAKI, K. & ROGERS, K. 2016. Relationships between pathology and crystal structure in breast calcifications: an in situ X-ray diffraction study in histological sections. *Npj Breast Cancer,* 2**,** 16029.

SELANDER, K. S., LI, L., WATSON, L., MERRELL, M., DAHMEN, H., HEINRICH, P. C., MÜLLER-NEWEN, G. & HARRIS, K. W. 2004. Inhibition of gp130 Signaling in Breast Cancer Blocks Constitutive Activation of Stat3 and Inhibits In Vivo Malignancy. *Cancer Research,* 64**,** 6924.

SEO, B. K., PISANO, E. D., KUZIMAK, C. M., KOOMEN, M., PAVIC, D., LEE, Y., COLE, E. B. & LEE, J. 2006. Correlation of HER-2/neu Overexpression With Mammography and Age Distribution in Primary Breast Carcinomas. *Academic Radiology,* 13**,** 1211-1218.

SHAPIRO, I. M., LANDIS, W. J. & RISBUD, M. V. 2015. MATRIX VESICLES: ARE THEY ANCHORED EXOSOMES? *Bone,* 79**,** 29-36.

SHASTRY, M. & YARDLEY, D. A. 2013. Updates in the treatment of basal/triple-negative breast cancer. [Miscellaneous Article]. *Current Opinion in Obstetrics & Gynecology February 2013,* 25**,** 40-48.

SHAW, F. L., HARRISON, H., SPENCE, K., ABLETT, M. P., SIMÕES, B. M., FARNIE, G. & CLARKE, R. B. 2012. A Detailed Mammosphere Assay Protocol for the Quantification of Breast Stem Cell Activity. *Journal of Mammary Gland Biology and Neoplasia,* 17**,** 111-117.

SHIN, S. U., LEE, J., KIM, J. H., KIM, W. H., SONG, S. E., CHU, A., KIM, H. S., HAN, W., RYU, H. S. & MOON, W. K. 2017. Gene expression profiling of calcifications in breast cancer. *Scientific Reports,* 7**,** 11427.

SHOJI, K. 1993. [Alizarin red S staining of calcium compound crystals in synovial fluid]. *Nihon Seikeigeka Gakkai Zasshi,* 67**,** 201-10.

SINGH, A. K., PANDEY, A., TEWARI, M., KUMAR, R., SHARMA, A., SINGH, K. A., PANDEY, H. P. & SHUKLA, H. S. 2013. Advanced stage of breast cancer hoist alkaline phosphatase activity: risk factor for females in India. *3 Biotech,* 3**,** 517-520.

SKANDALIS, S. S., LABROPOULOU, V. T., RAVAZOULA, P., LIKAKI-KARATZA, E., DOBRA, K., KALOFONOS, H. P., KARAMANOS, N. K. & THEOCHARIS, A. D. 2011. Versican but not decorin accumulation is related to malignancy in mammographically detected high density and malignant-appearing microcalcifications in non-palpable breast carcinomas. *BMC Cancer,* 11**,** 314-314.

SMITH, S. J., EMERY, R., PITSILLIDES, A., CLARKIN, C. E. & MAHAJAN, S. 2017. Detection of early osteogenic commitment in primary cells using Raman spectroscopy. *Analyst,* 142**,** 1962-1973.

SODA, H., RAYMOND, E., SHARMA, S., LAWRENCE, R., CERNA, C., GOMEZ, L., TIMONY, G. A., VON HOFF, D. D. & IZBICKA, E. 1998. Antiproliferative effects of recombinant human bone morphogenetic protein-2 on human tumor colony-forming units. *Anticancer Drugs,* 9**,** 327-31.

SONOU, T., OHYA, M., YASHIRO, M., MASUMOTO, A., NAKASHIMA, Y., ITO, T., MIMA, T., NEGI, S., KIMURA-SUDA, H. & SHIGEMATSU, T. 2017. Magnesium prevents phosphate-induced vascular calcification via TRPM7 and Pit-1 in an aortic tissue culture model. *Hypertens Res,* 40**,** 562-567.

SONTROP, H. M., REINDERS, M. J. & MOERLAND, P. D. 2016. Breast cancer subtype predictors revisited: from consensus to concordance? *BMC Medical Genomics,* 9**,** 26.

SORIA, G. & BEN-BARUCH, A. 2008. The inflammatory chemokines CCL2 and CCL5 in breast cancer. *Cancer Lett,* 267**,** 271-85.

SORLIE, T., PEROU, C. M., TIBSHIRANI, R., AAS, T., GEISLER, S., JOHNSEN, H., HASTIE, T., EISEN, M. B., RIJN, M. V. A. N. D. E., JEFFREY, S. S., THORSEN, T., QUIST, H., MATESE, J. C., BROWN, P. O., BOTSTEIN, D., EYSTEIN LONNING, P. & BORRESEN-DALE, A. L. 2001. Gene expression patterns of breast carcinomas distinguish tumor subclasses with clinical implications. *Proc Natl Acad Sci USA,* 98.

SORRENTINO, G., RUGGERI, N., ZANNINI, A., INGALLINA, E., BERTOLIO, R., MAROTTA, C., NERI, C., CAPPUZZELLO, E., FORCATO, M., ROSATO, A., MANO, M., BICCIATO, S. & DEL SAL, G. 2017. Glucocorticoid receptor signalling activates YAP in breast cancer. *Nature Communications,* 8**,** 14073.

SOUSA, S., BRION, R., LINTUNEN, M., KRONQVIST, P., SANDHOLM, J., MÖNKKÖNEN, J., KELLOKUMPU-LEHTINEN, P.-L., LAUTTIA, S., TYNNINEN, O., JOENSUU, H., HEYMANN, D. & MÄÄTTÄ, J. A. 2015. Human breast cancer cells educate macrophages toward the M2 activation status. *Breast Cancer Research,* 17**,** 101.

SPAN, P. N., BUSSINK, J., MANDERS, P., BEEX, L. V. A. M. & SWEEP, C. G. J. 2003. Carbonic anhydrase-9 expression levels and prognosis in human breast cancer: association with treatment outcome. *British Journal of Cancer,* 89**,** 271-276.

SPEER, M. Y., MCKEE, M. D., GULDBERG, R. E., LIAW, L., YANG, H.-Y., TUNG, E., KARSENTY, G. & GIACHELLI, C. M. 2002. Inactivation of the Osteopontin Gene Enhances Vascular Calcification of Matrix Gla Protein–deficient Mice: Evidence for Osteopontin as an Inducible Inhibitor of Vascular Calcification In Vivo. *The Journal of Experimental Medicine,* 196**,** 1047-1055.

SREEKUMAR, A., ROARTY, K. & ROSEN, J. M. 2015. The mammary stem cell hierarchy: a looking glass into heterogeneous breast cancer landscapes. *Endocrine-Related Cancer,* 22**,** T161-T176.

STEITZ, S. A., SPEER, M. Y., MCKEE, M. D., LIAW, L., ALMEIDA, M., YANG, H. & GIACHELLI, C. M. 2002. Osteopontin inhibits mineral deposition and promotes regression of ectopic calcification. *Am J Pathol,* 161**,** 2035-46.

STEWART, T. A., YAPA, K. T. D. S. & MONTEITH, G. R. 2015. Altered calcium signaling in cancer cells. *Biochimica et Biophysica Acta (BBA) - Biomembranes,* 1848**,** 2502-2511.

STIVAROU, T., STELLAS, D., VARTZI, G., THOMAIDOU, D. & PATSAVOUDI, E. 2016. Targeting highly expressed extracellular HSP90 in breast cancer stem cells inhibits tumor growth in vitro and in vivo. *Cancer Biol Ther,* 17**,** 799-812.

STOMPER, P. C. & CONNOLLY, J. L. 1992. Mammographic features predicting an extensive intraductal component in early-stage infiltrating ductal carcinoma. *American Journal of Roentgenology,* 158**,** 269-272.

SUN, Y., BYON, C. H., YUAN, K., CHEN, J., MAO, X., HEATH, J. M., JAVED, A., ZHANG, K., ANDERSON, P. G. & CHEN, Y. 2012. Smooth Muscle Cell-Specific Runx2 Deficiency Inhibits Vascular Calcification. *Circulation research,* 111**,** 543-552.

SUZUKI, R., ORSINI, N., SAJI, S., KEY, T. J. & WOLK, A. 2009. Body weight and incidence of breast cancer defined by estrogen and progesterone receptor status--a meta-analysis. *Int J Cancer,* 124**,** 698-712.

TABÁR, L., CHEN, H.-H., DUFFY, S. W., YEN, M. F., CHIANG, C. F., DEAN, P. B. & SMITH, R. A. 2000. A novel method for prediction of long-term outcome of women with T1a, T1b, and 10–14 mm invasive breast cancers: a prospective study. *The Lancet,* 355**,** 429-433.

TABAR, L. & DEAN, P. B. 2008. Thirty years of experience with mammography screening: a new approach to the diagnosis and treatment of breast cancer. *Breast Cancer Research : BCR,* 10**,** S3-S3.

TABAR, L., TONY CHEN, H.-H., AMY YEN, M. F., TOT, T., TUNG, T.-H., CHEN, L.-S., CHIU, Y.-H., DUFFY, S. W. & SMITH, R. A. 2004. Mammographic tumor features can predict long-term outcomes reliably in women with 1–14-mm invasive breast carcinoma. *Cancer,* 101**,** 1745-1759.

TAKAHASHI, R.-U., MIYAZAKI, H., TAKESHITA, F., YAMAMOTO, Y., MINOURA, K., ONO, M., KODAIRA, M., TAMURA, K., MORI, M. & OCHIYA, T. 2015. Loss of microRNA-27b contributes to breast cancer stem cell generation by activating ENPP1. 6**,** 7318.

TAN, C.-C., LI, G.-X., TAN, L.-D., DU, X., LI, X.-Q., HE, R., WANG, Q.-S. & FENG, Y.-M. 2016. Breast cancer cells obtain an osteomimetic feature via epithelial-mesenchymal transition that have undergone BMP2/RUNX2 signaling pathway induction. *Oncotarget,* 7**,** 79688-79705.

TAO, M.-H., DAI, Q., MILLEN, A. E., NIE, J., EDGE, S. B., TREVISAN, M., SHIELDS, P. G. & FREUDENHEIM, J. L. 2016. Associations of intakes of magnesium and calcium and survival among women with breast cancer: results from Western New York Exposures and Breast Cancer (WEB) Study. *American Journal of Cancer Research,* 6**,** 105-113.

TAYLOR, S. E. B., SHAH, M. & ORRISS, I. R. 2014. Generation of rodent and human osteoblasts. *BoneKEy Rep,* 3.

TERKELTAUB, R. A. 2001. Inorganic pyrophosphate generation and disposition in pathophysiology. *American Journal of Physiology - Cell Physiology,* 281**,** C1-C11.

TERTULIANO, O. A. & GREER, J. R. 2016. The nanocomposite nature of bone drives its strength and damage resistance. *Nature Materials,* 15**,** 1195.

THE CANADIAN TASK FORCE ON PREVENTIVE HEALTH CARE 2011. Recommendations on screening for breast cancer in average-risk women aged 40–74 years. *Canadian Medical Association Journal,* 183**,** 1991-2001.

THURFJELL, E., THURFJELL, M. & LINDGREN, A. 2001. Mammographic finding as predictor of survival in 1–9mm invasive breast cancers. Worse prognosis for cases presenting as calcifications alone. *Breast Cancer Research and Treatment,* 67**,** 177-180.

TIAGO, D. M., CONCEICAO, N., CAIADO, H., LAIZE, V. & CANCELA, M. L. 2016. Matrix Gla protein repression by miR-155 promotes oncogenic signals in breast cancer MCF-7 cells. *FEBS Lett,* 590**,** 1234-41.

TIAN, H., ZHAO, J., BROCHMANN, E. J., WANG, J. C. & MURRAY, S. S. 2017. Bone morphogenetic protein-2 and tumor growth: Diverse effects and possibilities for therapy. *Cytokine & Growth Factor Reviews,* 34**,** 73-91.

TIEDEMANN, K., HUSSEIN, O., SADVAKASSOVA, G., GUO, Y., SIEGEL, P. M. & KOMAROVA, S. V. 2009. Breast Cancer-derived Factors Stimulate Osteoclastogenesis through the Ca2+/Protein Kinase C and Transforming Growth Factor-β/MAPK Signaling Pathways. *Journal of Biological Chemistry,* 284**,** 33662-33670.

TOGASHI, K., INADA, H. & TOMINAGA, M. 2008. Inhibition of the transient receptor potential cation channel TRPM2 by 2-aminoethoxydiphenyl borate (2-APB). *British Journal of Pharmacology,* 153**,** 1324-1330.

TOMOAIA, G. & PASCA, R.-D. 2015. On the Collagen Mineralization. A Review. *Clujul Medical,* 88**,** 15-22.

TOWLER, D. A. & DEMER, L. L. 2011. THEMATIC SERIES ON THE PATHOBIOLOGY OF VASCULAR CALCIFICATION: AN INTRODUCTION. *Circulation research,* 108**,** 1378-1380.

TSAU, H.-S., YEN, A. M.-F., FANN, J. C.-Y., WU, W. Y.-Y., YU, C.-P., CHEN, S. L.-S., CHIU, S. Y.-H., TABÁR, L., KUO, W.-H., CHEN, H.-H. & CHANG, K.-J. 2015. Mammographic tumour appearance and triple-negative breast cancer associated with long-term prognosis of breast cancer death: A Swedish Cohort Study. *Cancer Epidemiology,* 39**,** 200-208.

TSE, G. M., TAN, P. H., CHEUNG, H. S., CHU, W. C. & LAM, W. W. 2008. Intermediate to highly suspicious calcification in breast lesions: a radio-pathologic correlation. *Breast Cancer Res Treat,* 110**,** 1-7.

TUO, Y. L. & YE, Y. F. 2017. MGP is downregulated due to promoter methylation in chemoresistant ER+ breast cancer and high MGP expression predicts better survival outcomes. *Eur Rev Med Pharmacol Sci,* 21**,** 3871-3878.

VANDECAETSBEEK, I., VANGHELUWE, P., RAEYMAEKERS, L., WUYTACK, F. & VANOEVELEN, J. 2011. The Ca(2+) Pumps of the Endoplasmic Reticulum and Golgi Apparatus. *Cold Spring Harbor Perspectives in Biology,* 3**,** a004184.

VANHOUTEN, J. N., NEVILLE, M. C. & WYSOLMERSKI, J. J. 2007. The Calcium-Sensing Receptor Regulates Plasma Membrane Calcium Adenosine Triphosphatase Isoform 2 Activity in Mammary Epithelial Cells: A Mechanism for Calcium-Regulated Calcium Transport into Milk. *Endocrinology,* 148**,** 5943-5954.

VEIS, A. & DORVEE, J. R. 2013. Biomineralization Mechanisms: A new paradigm for crystal nucleation in organic matricies. *Calcified tissue international,* 93**,** 307-315.

VENKATESAN, A., CHU, P., KERLIKOWSKE, K., SICKLES, E. A. & SMITH-BINDMAN, R. 2009. Positive Predictive Value of Specific Mammographic Findings according to Reader and Patient Variables. *Radiology,* 250**,** 648-657.

VILLA-BELLOSTA, R. & EGIDO, J. 2017. Phosphate, pyrophosphate, and vascular calcification: a question of balance. *European Heart Journal,* 38**,** 1801-1804.

VILLA-BELLOSTA, R., MILLAN, A. & SORRIBAS, V. 2011. Role of calcium-phosphate deposition in vascular smooth muscle cell calcification. *American Journal of Physiology - Cell Physiology,* 300**,** C210.

VIMALRAJ, S., ARUMUGAM, B., MIRANDA, P. J. & SELVAMURUGAN, N. 2015. Runx2: Structure, function, and phosphorylation in osteoblast differentiation. *International Journal of Biological Macromolecules,* 78**,** 202-208.

VINOGRADOV, S., WARREN, G. & WEI, X. 2014. Macrophages associated with tumors as potential targets and therapeutic intermediates. *Nanomedicine (London, England),* 9**,** 695-707.

VISHAL, M., SWETHA, R., THEJASWINI, G., ARUMUGAM, B. & SELVAMURUGAN, N. 2017. Role of Runx2 in breast cancer-mediated bone metastasis. *International Journal of Biological Macromolecules,* 99**,** 608-614.

VISSER, D., MIDDELBEEK, J., VAN LEEUWEN, F. N. & JALINK, K. 2014. Function and regulation of the channel-kinase TRPM7 in health and disease. *European Journal of Cell Biology,* 93**,** 455-465.

VISVADER, J. E. 2009. Keeping abreast of the mammary epithelial hierarchy and breast tumorigenesis. *Genes & Development,* 23**,** 2563-2577.

VISVADER, J. E. & STINGL, J. 2014. Mammary stem cells and the differentiation hierarchy: current status and perspectives. *Genes & Development,* 28**,** 1143-1158.

VRBIC, S., PEJCIC, I., FILIPOVIC, S., KOCIC, B. & VRBIC, M. 2013. Current and future anti-HER2 therapy in breast cancer. *J buon,* 18**,** 4-16.

WANG, R., LV, Q., MENG, W., TAN, Q., ZHANG, S., MO, X. & YANG, X. 2014. Comparison of mammosphere formation from breast cancer cell lines and primary breast tumors. *Journal of Thoracic Disease,* 6**,** 829-837.

WANG, T. K., BOLLAND, M. J., VAN PELT, N. C., HORNE, A. M., MASON, B. H., AMES, R. W., GREY, A. B., RUYGROK, P. N., GAMBLE, G. D. & REID, I. R. 2010a. Relationships between vascular calcification, calcium metabolism, bone density, and fractures. *J Bone Miner Res,* 25**,** 2777-85.

WANG, X., CHAO, L., CHEN, L., TIAN, B., MA, G., ZANG, Y., HUA, M. & SUN, J. 2008. Correlation of Mammographic Calcifications with HER-2/neu Overexpression in Primary Breast Carcinomas. *Journal of Digital Imaging,* 21**,** 170-176.

WANG, X., CHAO, L., MA, G., CHEN, L., JIN, G., HUA, M., LIU, H., OUYANG, A. & ZHANG, X. 2010b. Primary breast carcinoma: association of mammographic calcifications with osteopontin expression. *Radiology,* 254**,** 69-78.

WANG, X., LIU, J., WANG, Z., HUANG, Y., LIU, W., ZHU, X., CAI, Y., FANG, X., LIN, S., YUAN, L. & OUYANG, G. 2013. Periostin Contributes to the Acquisition of Multipotent Stem Cell-Like Properties in Human Mammary Epithelial Cells and Breast Cancer Cells. *PLoS ONE,* 8**,** e72962.

WEEDON-FEKJÆR, H., ROMUNDSTAD, P. R. & VATTEN, L. J. 2014. *Modern mammography screening and breast cancer mortality: population study*.

WEIGELT, B., MACKAY, A., A'HERN, R., NATRAJAN, R., TAN, D. S. P., DOWSETT, M., ASHWORTH, A. & REIS-FILHO, J. S. 2010. Breast cancer molecular profiling with single sample predictors: a retrospective analysis. *The Lancet Oncology,* 11**,** 339-349.

WHO. 2017. *Breast Cancer Estimated Incidence, Mortality and Prevalence Worldwide in 2012* [Online]. Available: http://globocan.iarc.fr/Pages/fact_sheets_cancer.aspx [Accessed].

WILSON, G. H., GORE, J. C., YANKEELOV, T. E., BARNES, S., PETERSON, T. E., TRUE, J. M., SHOKOUHI, S., MCINTYRE, J. O., SANDERS, M., ABRAMSON, V., NGYUEN, T.-Q., MAHADEVAN-JANSEN, A. & TANTAWY, M. N. 2014. A novel approach to breast cancer diagnosis via PET imaging of microcalcifications using (18)F-NaF. *Journal of nuclear medicine : official publication, Society of Nuclear Medicine,* 55**,** 1138-1143.

WINSTON, J. S., YEH, I. T., EVERS, K. & FRIEDMAN, A. K. 1993. Calcium oxalate is associated with benign breast tissue. Can we avoid biopsy? *American journal of clinical pathology,* 100**,** 488-492.

WOLFE, A. R., TRENTON, N. J., DEBEB, B. G., LARSON, R., RUFFELL, B., CHU, K., HITTELMAN, W., DIEHL, M., REUBEN, J. M., UENO, N. T. & WOODWARD, W. A. 2016. Mesenchymal stem cells and macrophages interact through IL-6 to promote inflammatory breast cancer in pre-clinical models. *Oncotarget,* 7**,** 82482-82492.

WOODARD, G. A., RAY, K. M., JOE, B. N. & PRICE, E. R. 2017. Qualitative Radiogenomics: Association between Oncotype DX Test Recurrence Score and BI-RADS Mammographic and Breast MR Imaging Features. *Radiology,* 286**,** 60-70.

WU, C. Y., DU, S. L., ZHANG, J., LIANG, A. L. & LIU, Y. J. 2016. Exosomes and breast cancer: a comprehensive review of novel therapeutic strategies from diagnosis to treatment. *Cancer Gene Therapy,* 24**,** 6.

WYSOKINSKI, D., BLASIAK, J. & PAWLOWSKA, E. 2015. Role of RUNX2 in Breast Carcinogenesis. *International Journal of Molecular Sciences,* 16**,** 20969-20993.

XU, J., BAI, Y., JIN, J., ZHANG, J., ZHANG, S., CUI, L. & ZHANG, H. 2015a. Magnesium modulates the expression levels of calcification-associated factors to inhibit calcification in a time-dependent manner. *Exp Ther Med,* 9**,** 1028-1034.

XU, S.-Z., ZENG, F., BOULAY, G., GRIMM, C., HARTENECK, C. & BEECH, D. J. 2005. Block of TRPC5 channels by 2-aminoethoxydiphenyl borate: a differential, extracellular and voltage-dependent effect. *British Journal of Pharmacology,* 145**,** 405-414.

XU, Z., YANG, Y., ZHAO, W., WANG, Z., LANDIS, W. J., CUI, Q. & SAHAI, N. 2015b. Molecular mechanisms for intrafibrillar collagen mineralization in skeletal tissues. *Biomaterials,* 39**,** 59-66.

YADAV, B. S., SHARMA, S. C., CHANANA, P. & JHAMB, S. 2014. Systemic treatment strategies for triple-negative breast cancer. *World Journal of Clinical Oncology,* 5**,** 125-133.

YAMAMOTO, S., ORIMO, H., MATSUMOTO, T., IIJIMA, O., NARISAWA, S., MAEDA, T., MILLÁN, J. L. & SHIMADA, T. 2011. Prolonged Survival and Phenotypic Correction of Akp2(−/−) Hypophosphatasia Mice by Lentiviral Gene Therapy. *Journal of Bone and Mineral Research,* 26**,** 135-142.

YANG, H.-W., LEE, S.-A., SHIN, J.-M., PARK, I.-H. & LEE, H.-M. 2017. Glucocorticoids ameliorate TGF-β1-mediated epithelial-to-mesenchymal transition of airway epithelium through MAPK and Snail/Slug signaling pathways. *Scientific Reports,* 7**,** 3486.

YANG, H., CURINGA, G. & GIACHELLI, C. M. 2004. Elevated extracellular calcium levels induce smooth muscle cell matrix mineralization in vitro11See Editorial by Towler, p. 2467. *Kidney International,* 66**,** 2293-2299.

YANG, W.-T., DRYDEN, M., BROGLIO, K., GILCREASE, M., DAWOOD, S., DEMPSEY, P. J., VALERO, V., HORTOBAGYI, G., ATCHLEY, D. & ARUN, B. 2008. Mammographic features of triple receptor-negative primary breast cancers in young premenopausal women. *Breast Cancer Research and Treatment,* 111**,** 405-410.

YANG, X., RICCIARDI, B. F., HERNANDEZ-SORIA, A., SHI, Y., PLESHKO CAMACHO, N. & BOSTROM, M. P. G. 2007. Callus mineralization and maturation are delayed during fracture healing in interleukin-6 knockout mice. *Bone,* 41**,** 928-936.

YAO, H., HE, G., YAN, S., CHEN, C., SONG, L., ROSOL, T. J. & DENG, X. 2017. Triple-negative breast cancer: is there a treatment on the horizon? *Oncotarget,* 8**,** 1913-1924.

YE, S., PARK, B.-H., SONG, K.-J., KIM, J.-R., JANG, K.-Y., PARK, H.-S., BAE, J. S., BROCHMANN, E. J., WANG, J. C., MURRAY, S. S. & LEE, K.-B. 2013. In Vivo Inhibition of Bone Morphogenetic Protein-2 on Breast Cancer Cell Growth. *Spine,* 38**,** E143-E150.

YEPES, M. M., ROMILLY, A. P., COLLADO-MESA, F., NET, J. M., KISZONAS, R., ARHEART, K. L., YOUNG, D. & GLÜCK, S. 2014. Can mammographic and sonographic imaging features predict the Oncotype DX™ recurrence score in T1 and T2, hormone receptor positive, HER2 negative and axillary lymph node negative breast cancers? *Breast Cancer Research and Treatment,* 148**,** 117-123.

YERSAL, O. & BARUTCA, S. 2014. Biological subtypes of breast cancer: Prognostic and therapeutic implications. *World Journal of Clinical Oncology,* 5**,** 412-424.

YOO, T.-K., CHAE, B. J., KIM, S. J., LEE, J., YOON, T. I., LEE, S. J., PARK, H. Y., PARK, H. K., EOM, Y. H., KIM, H. S., KIM, C. J., SHIN, M. S., YOU, S. H. & SONG, B. J. 2017. Identifying long-term survivors among metastatic breast cancer patients undergoing primary tumor surgery. *Breast Cancer Research and Treatment,* 165**,** 109-118.

ZAJCHOWSKI, D. A., BARTHOLDI, M. F., GONG, Y., WEBSTER, L., LIU, H.-L., MUNISHKIN, A., BEAUHEIM, C., HARVEY, S., ETHIER, S. P. & JOHNSON, P. H. 2001. Identification of Gene Expression Profiles That Predict the Aggressive Behavior of Breast Cancer Cells. *Cancer Research,* 61**,** 5168.

ZEBBOUDJ, A. F., IMURA, M. & BOSTRÖM, K. 2002. Matrix GLA Protein, a Regulatory Protein for Bone Morphogenetic Protein-2. *Journal of Biological Chemistry,* 277**,** 4388-4394.

ZEISBERG, M. & NEILSON, E. G. 2009. Biomarkers for epithelial-mesenchymal transitions. *The Journal of Clinical Investigation,* 119**,** 1429-1437.

ZHANG, J.-H., WANG, J., TANG, J., BARNETT, B., DICKSON, J., HAHSIMOTO, N., WILLIAMS, P., MA, W., ZHENG, W., YONEDA, T., PAGEAU, S. & CHEN, J. 2004. Bone Sialoprotein Promotes Bone Metastasis of a Non-bone-seeking Clone of Human Breast Cancer Cells. *Anticancer Research,* 24**,** 1361-1368.

ZHANG, K., ZHANG, Y., FENG, W., CHEN, R., CHEN, J., TOUYZ, R. M., WANG, J. & HUANG, H. 2017. Interleukin-18 Enhances Vascular Calcification and Osteogenic Differentiation of Vascular Smooth Muscle Cells Through TRPM7 Activation. *Arteriosclerosis, Thrombosis, and Vascular Biology,* 37**,** 1933-1943.

ZHANG, N., DUAN, W. D., LENG, J. J., ZHOU, L., WANG, X., XU, Y. Z., WANG, X. D., ZHANG, A. Q. & DONG, J. H. 2015. STAT3 regulates the migration and invasion of a stemlike subpopulation through microRNA21 and multiple targets in hepatocellular carcinoma. *Oncol Rep,* 33**,** 1493-8.

ZHANG, Z., SCHWARTZ, S., WAGNER, L. & MILLER, W. 2000. A greedy algorithm for aligning DNA sequences. *J Comput Biol,* 7**,** 203-14.

ZHAO, X., NG, S., HENG, B. C., GUO, J., MA, L., TAN, T. T., NG, K. W. & LOO, S. C. 2013. Cytotoxicity of hydroxyapatite nanoparticles is shape and cell dependent. *Arch Toxicol,* 87**,** 1037-52.

ZHEN, D., CHEN, Y. & TANG, X. 2010. Metformin reverses the deleterious effects of high glucose on osteoblast function. *J Diabetes Complications,* 24**,** 334-44.

ZHENG, K., TAN, J. X., LI, F., WEI, Y. X., YIN, X. D., SU, X. L., LI, H. Y., LIU, Q. L., MA, B. L., OU, J. H., LI, H., YANG, S. S., JIANG, A. M., NI, Q., LIU, J. L., LIU, J. P., ZHENG, H., SONG, Z. J., WANG, L., HE, J. J., ZOU, T. N., JIANG, J. & REN, G. S. 2017. Relationship between mammographic calcifications and the clinicopathologic characteristics of breast cancer in Western China: a retrospective multi-center study of 7317 female patients. *Breast Cancer Res Treat,* 166**,** 569–582.

ZHENG, Y., XU, B., ZHAO, Y., GU, H., LI, C., WANG, Y. & CHANG, X. 2015. CA1 contributes to microcalcification and tumourigenesis in breast cancer. *BMC Cancer,* 15**,** 679.

ZHONG, H., DAVIS, A., OUZOUNOVA, M., CARRASCO, R. A., CHEN, C., BREEN, S., CHANG, Y. S., HUANG, J., LIU, Z., YAO, Y., HURT, E., MOISAN, J., FUNG, M., TICE, D. A., CLOUTHIER, S. G., XIAO, Z., WICHA, M. S., KORKAYA, H. & HOLLINGSWORTH, R. E. 2016. A Novel IL6 Antibody Sensitizes Multiple Tumor Types to Chemotherapy Including Trastuzumab-Resistant Tumors. *Cancer Research,* 76**,** 480.

ZHU, Z., LI, L., YE, Z., FU, T., DU, Y., SHI, A., WU, D., LI, K., ZHU, Y., WANG, C. & FAN, Z. 2017. Prognostic value of routine laboratory variables in prediction of breast cancer recurrence. *Scientific Reports,* 7**,** 8135.

Chapter 8.0

Appendix

8.1 Supporting information

Table 8.1 Key studies demonstrating association between mammographic calcifications and prognostic factors in breast cancer patients. Note, "fine-linear" and "casting" are used interchangeable depending on terminology used within each individual study.

References	Study Cohort	Key Findings
(Bae et al., 2013)	101 cases of pure DCIS	• Fine linear branching and segmental calcifications significantly associated with HER2 positivity. • Clustered calcifications more frequent in ER positive cancers.
(Barreau et al., 2005)	909 cases of DCIS	• Significant association between fine-linear branching calcifications and grade 3 DCIS with associated necrosis.
(Bennett et al., 2011)	232 screen-detected cases of invasive cancer	• 3-fold increased hazard-ratio for mortality in patients with comedo-type DCIS with associated calcification.
(Cen et al., 2017a)	485 patients with infiltrating ductal carcinoma with intermediate or high-risk calcifications	• Linear calcification range and diameter independently predictive of HER2 subtype
(Cen et al., 2017b)	419 cases of invasive ductal carcinoma with BI-RADS 3–5 calcifications	• Calcification density associated with lymph node status
(Chae et al., 2016)	267 patients with ER+, HER2- invasive breast cancer	• Presence of calcification within a mass associated with high recurrence risk on Oncotype assay
Dershaw (1993)	23 cases of male breast cancer	• Calcifications rarely observed in male breast cancer but are highly suspicious as calcifications considered benign in women may indicate cancer in men.
(Ferranti et al., 2000)	982 screen detected carcinomas	• Presence of microcalcifications associated with increased tumour grade and size and positive node status.
(Gajdos et al., 2002)	543 mammographically detected nonpalpable malignancies	• Calcifications associated with more extensive intraductal carcinoma and Her2 positivity, invasive cancers presenting as masses with calcifications associated with lymphatic invasion
(Hamilton et al., 2004)	Retrospective comparison of 28 BRCA mutation carriers versus 54 age-matched, sporadic breast carcinoma controls	• Calcifications observed in 73% of BRCA2 cases versus 12% of BRCA1 cases and 8% of control patients
(Hofvind et al., 2011)	217 cases of pure DCIS with no microinfiltration	• 84% of DCIS cases with associated fine linear and fine linear branching calcifications were high grade lesions.
(Holmberg et al., 2013)	Case-cohort study of 198 patients with DCIS	• 16-fold increased relative risk of ipsilateral, *in situ* recurrence in patients with casting-calcifications
(Karamouzis et al., 2002)	58 mammographically detected non-palpable breast carcinomas	• Increased rates of nuclear ER and PR positivity, HER-2 overexpression, Bax , Fas and DFF positivity in patients with suspicious microcalcifications.
(Killelea et al., 2013b)	985 cases of invasive breast cancer	• Calcifications associated with HER2 positivity and extensive intraductal component
(Kim et al., 2008)	Analysis of ultrasound findings in 435 invasive cancers and 23 cases of DCIS	• Presence of calcifications significantly associated with high grade and HER2 positivity in DCIS

Table continued on next page

Table continued

(Lee et al., 1999)	37 patients with mammographically detected DCIS	• High tumour grade in casting-calcification associated tumours
(Ling et al., 2013)	721 cases of confirmed invasive ductal carcinoma	• Increased tumour size and lymph node involvement, lower ER/PR expression and higher HER2 expression • Significantly decreased RFS and OS in patients with calcifications • Patients with casting-type calcifications suffer further decreases in survival compared to patients with other calcification morphology
(Macmillan et al., 1995)	231 cases of invasive breast cancer treated with breast conserving surgery.	• Residual microscopic disease associated with casting calcification • Both casting and non-casting calcifications linked to extensive intraductal component and residual disease after lumpectomy
(Malik et al., 2000)	357 cases of invasive breast cancer treated with breast conserving surgery.	• Casting calcification predictive of extensive *in situ* disease and tumour bed positivity after lumpectomy
(Naseem et al., 2015)	937 cases of breast cancer	• Calcifications more common in patients with HER2 over-expression, heterogeneous density and multifocal breast disease. Borderline significant (p = 0.057) with increased grade. • No significant association between calcifications and node status, tumour size or rate of recurrence.
(Nyante et al., 2017)	8472 invasive breast cancers	• Calcifications positively associated with high grade and tumours with an *in situ* component • Calcifications inversely associated with hormone receptor-negative status and size
(Peacock et al., 2004)	50 invasive tumours with size, histology and lymph node status matched controls	• 5 deaths in patients with casting calcifications, none in controls • Casting calcifications linked with higher grade , increased risk of recurrence and decreased survival
(Rauch et al., 2016)	1657 patients with DCIS and calcifications	• Casting calcifications associated with high tumour grade, increased risk of recurrence and comedonecrosis
(Seo et al., 2006)	543 primary breast carcinomas	• 56% of HER2 overexpressing cases associated with calcifications compared to 40% of those without HER2 overexpression. • Fine linear associated calcifications carries a 2.1 increased relative risk of HER2 overexpression versus other morphologies
(Stomper and Connolly, 1992)	304 breast carcinomas detected by mammographic calcifications	• Invasive foci more likely with calcification size of 11 mm and greater compared with 1–10 mm
(Tabár et al., 2000)	343 screen detected invasive cancers, 1-14 mm size	• 20 year survival of 55% for patients with casting calcifications versus 87% for patients without • Greater likelihood of high-grade tumours in patients with casting calcifications
(Tabar et al., 2004)	714 screen detected invasive cancers, 1-14 mm size	• Presence of casting calcifications associated with higher histological grade, positive lymph node status and decreased survival
(Thurfjell et al., 2001)	96 women with 1–9mm invasive breast cancers	• Significantly higher risk of death in patients with casting or pleomorphic calcifications
(Tsau et al., 2015)	498 patients diagnosed with invasive breast cancer	• Casting calcifications associated with 3.47-fold increased hazard ratio for mortality

Table continued on next page

Table continued

(Wang et al., 2008)	Retrospective study of preoperative mammograms in 152 breast carcinoma patients	• Higher rate of HER2 over-expression, TNM III stage and axillary lymph node metastasis in patients with calcifications.
(Qi et al., 2017)	409 patients with breast carcinoma treated with breast conserving surgery	• Calcifications associated with risk ratios of 2.46 for local recurrence, 2.24 for metastasis and 2.5 for mortality.

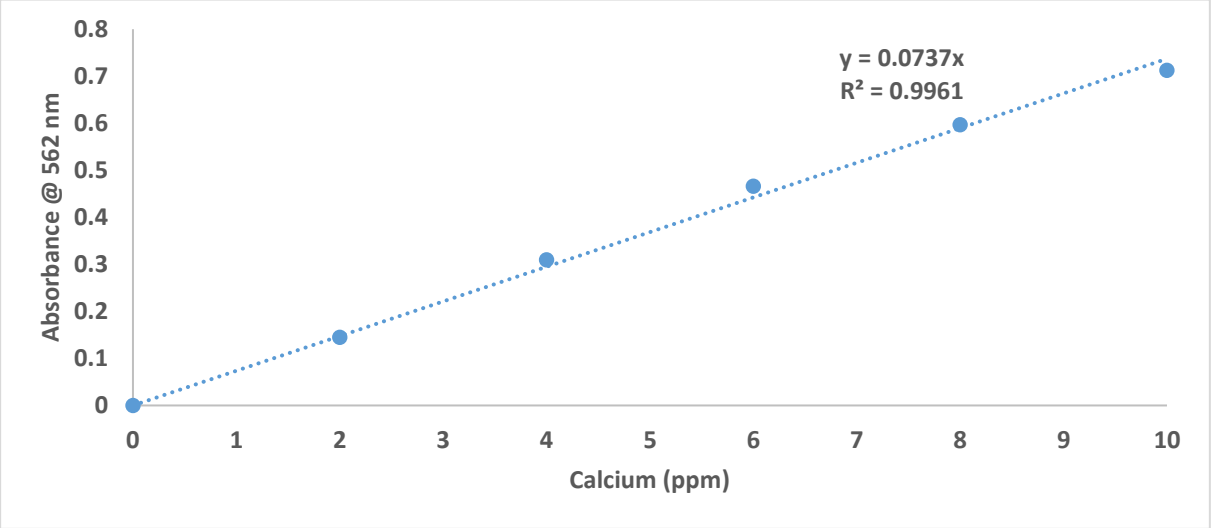

Figure 8.1 Representative standard curve for OCP calcium assay. A Ca^{2+} standard solution of known concentration was diluted in 1N nitric acid create a standard curve in the range of 2-10 ppm. 70 µL was added to each well of a 96-well plate along with 70 µL OCP and 170 µL AMP. Absorbance was read at 562 nm. Standards were analysed in triplicate for every assay performed.

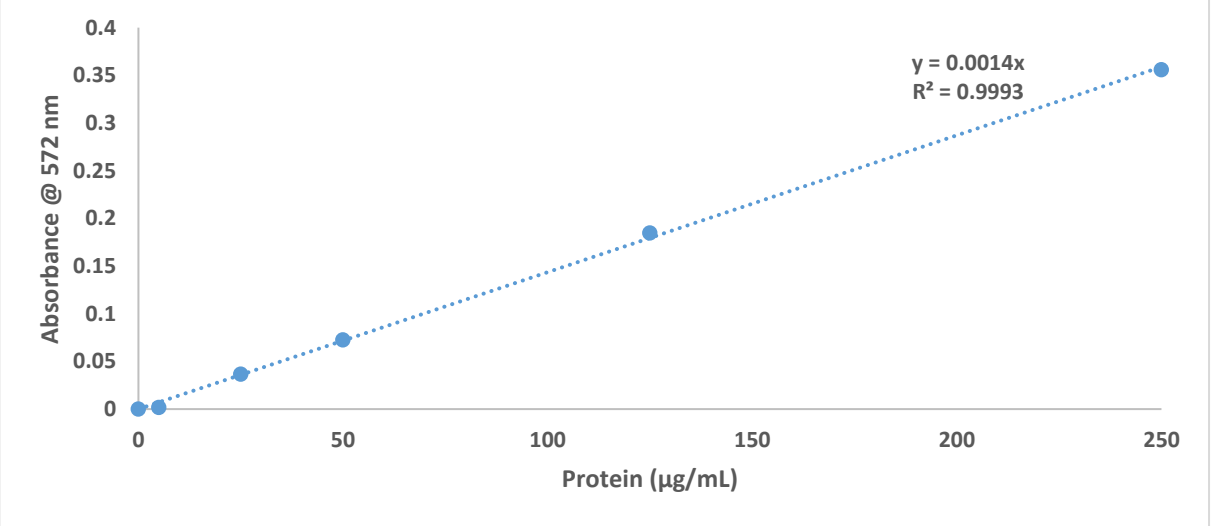

Figure 8.2 Representative standard curve for BCA protein assay. BSA was diluted in PBS to create a standard curve in the range of 5-250 µg/mL. 25 µL was added to each well of a 96-well plate along with 200 µL BCA working reagent and incubated at 37°C for 1 hour before absorbance was read at 562 nm. Standards were analysed in triplicate for every assay performed.

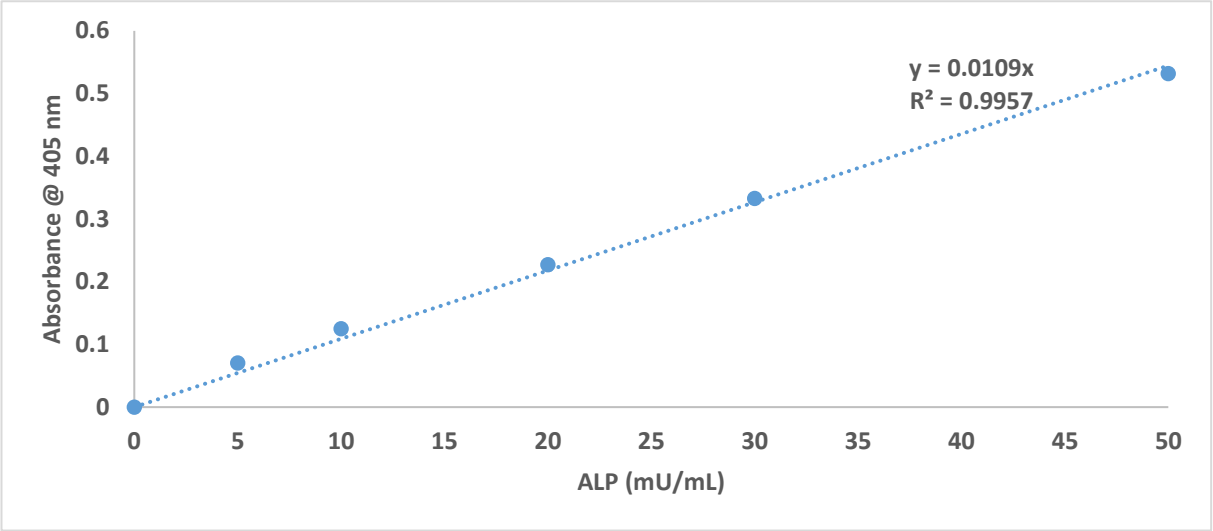

Figure 8.3 Representative standard curve of ALP activity assay. Bovine intestinal ALP was diluted in ALP assay buffer to create a standard curve of 5-50 mU/mL. 50 µL was added to each well of a 96-well plate along with 100 µL of pNPP substrate and incubated at 37ºC for 30 minutes. Absorbance was read at 405 nm. Standards were analysed in triplicate for every assay performed.

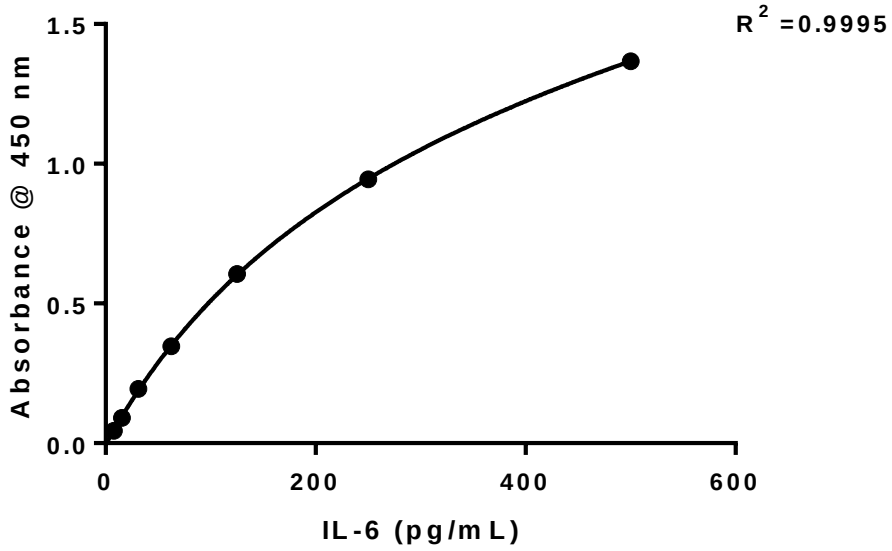

Figure 8.4 Representative standard curve of IL-6 ELISA. An IL-6 standard solution was diluted in PBS to create a standard curve in the range of 8 – 500 pg/ml. 100 µL was added to each well of a high-binding ELISA plate coated with IL-6 capture antibody (Immunotools) and incubated at room temperature for 2 hours. Plates were subsequently washed, incubated with detection antibody and finally analysed with TMB substrate, following manufacturer's instructions. Standards were analysed in triplicate for every assay performed.

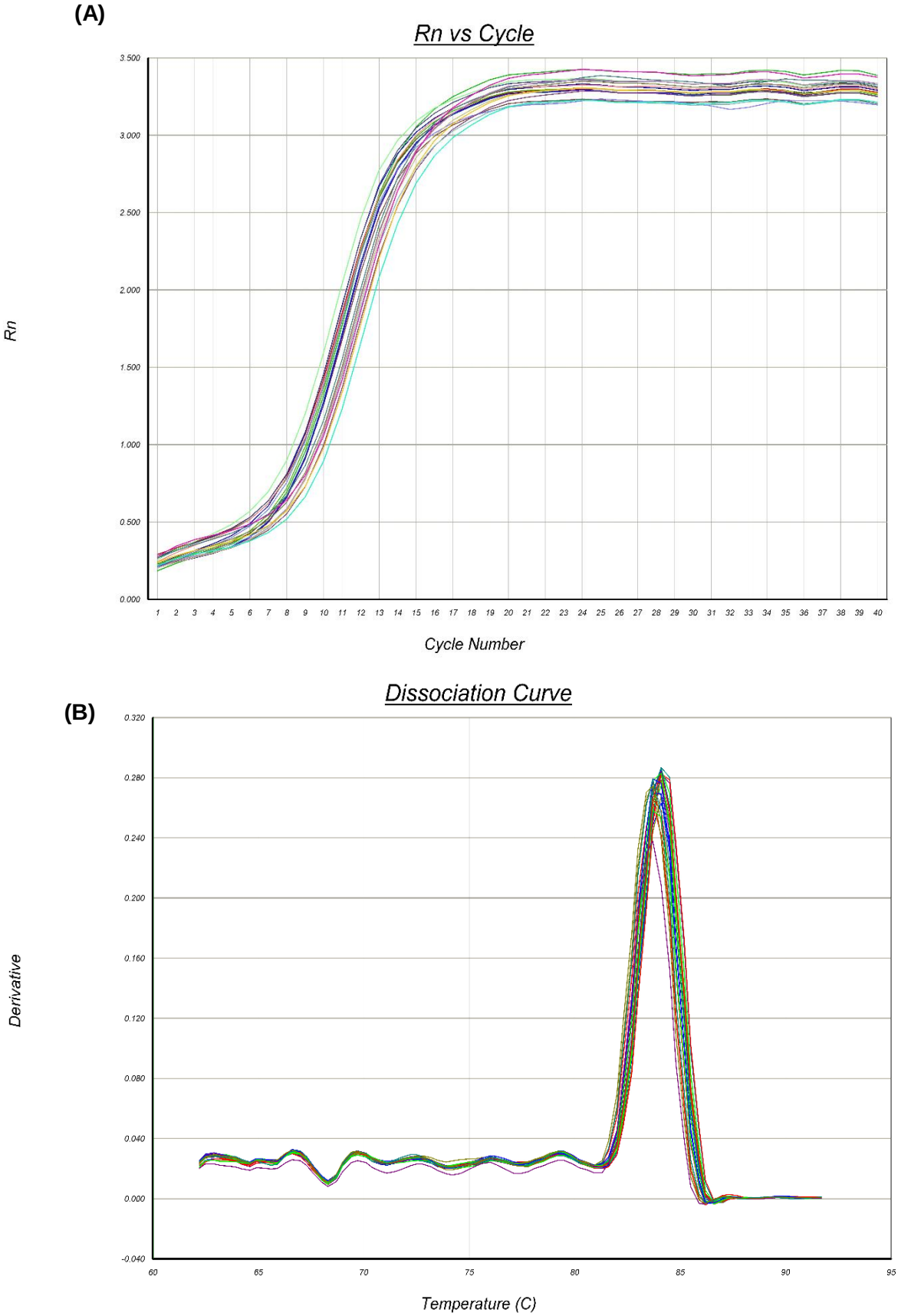

Figure 8.5 Representative amplification curve (A) and melting-curve analysis (B) of qPCR assay. 18S expression was analysed used specific primers in a qPCR assay, with fluorescence measured at the elongation stage of each cycle (A). Dissociation curve analysis was performed after every qPCR assay to confirm primer specificity (B).

Table 8.2 Formulation of buffers used

Buffer	Formulation
10X PBS	1.37 M NaCl, 27 mM KCl, 100 mM Na2HPO4, 18 mM KH2PO4
PBS	137 mM NaCl, 2.7 mM KCl, 10 mM Na2HPO4, 1.8 mM KH2PO4
10X TBS	500 mM Tris-HCl pH 7.5, 1.5 M NaCl
TBS	50 mM Tris-HCl pH 7.5, 150 mM NaCl
TBST	50 mM Tris-HCl pH 7.5, 150 mM NaCl, 0.1% Triton X-100
RIPA buffer	50 mM Tris-HCl pH 8.0, 150 mM NaCl, 1% NP-40, 0.5% sodium deoxycholate, 0.1% SDS
5X SDS loading buffer	250 mM Tris-HCl, pH 6.8, 10% SDS, 30% glycerol, 5% β-mercaptoethanol, 0.05% bromophenol blue
Resolving gel buffer	1.5 M Tris-HCl, pH 8.8
Stacking gel buffer	0.5 M Tris-HCl, pH 6.8
10X SDS running buffer	250 mM Tris, 1.92 M glycine, 1% SDS
SDS running buffer	25 mM Tris, 192 mM glycine, 0.1% SDS
10X Transfer buffer	250 mM Tris, 192 mM glycine
Transfer buffer	25 mM Tris, 1.92 M glycine, 10% methanol
Blocking buffer	TBS, 5% BSA
Antibody incubation buffer	TBS, 0.1% Tween-20, 5% BSA
ALP buffer	100 mM Tris-HCl pH 9.5, 100 mM NaCl, 5 mM MgCl, 1% Triton X-100
50X TAE	2 M Tris pH 8.3, 1 M acetic acid, 50 mM EDTA
TAE	40mM Tris pH 8.3, 20mM acetic acid, 1 mM EDTA
TE	10 mM Tris-HCl pH 8.0, 1 mM EDTA
ELISA diluent	PBS, 0.05% Tween-20, 1% BSA

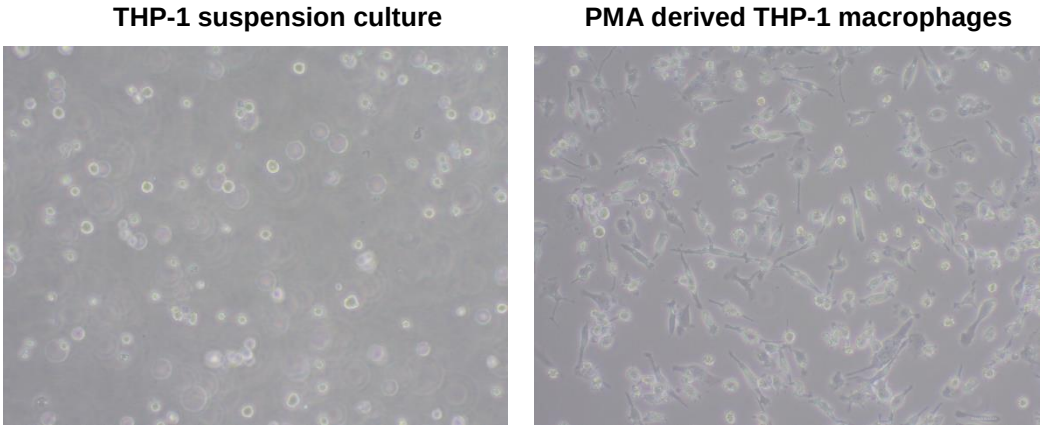

Figure 8.6 PMA promotes differentiation of THP-1 cells to a macrophage like phenotype. Representative images at 10X magnification of THP-1 monocyte cells grown as suspension culture or differentiated to an adherent macrophage phenotype by 24 hours incubation with 10 nM PMA.

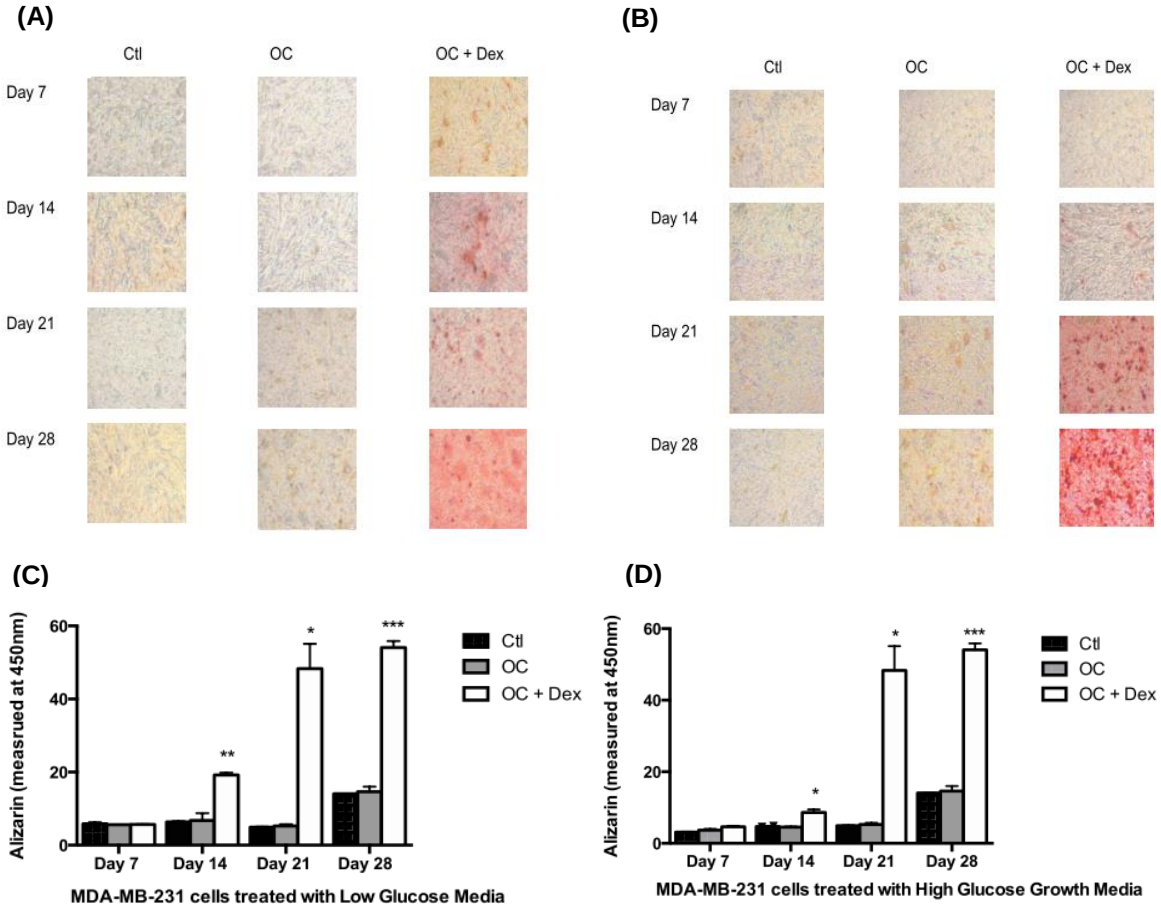

Figure 8.7 Glucose concentration influences mineralisation of MDA-MB-231 cells. Representative images were captured at 10X magnification of Alizarin Red S stained of cells grown in low (A) or high (B) glucose DMEM, supplemented with OC or OC+Dex, at the specified time points. Quantification of extracted Alizarin Red S dye from cell monolayers demonstrates positive mineralisation at days 14, 21 and 28 in both groups in cells cultured in OC+Dex media. Reproduced from “Investigating the role of breast cancer microcalcifications in driving inflammatory processes, and the potential consequences for tumour progression” (Amy Colin, 2013, M.Sc. thesis).

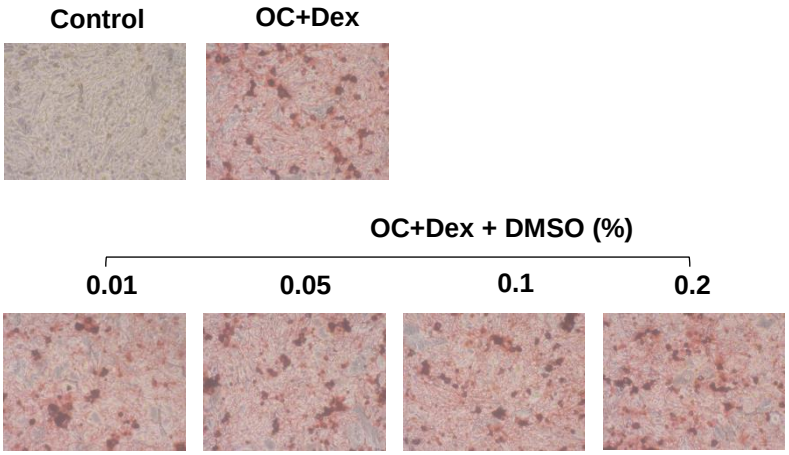

Figure 8.8 DMSO does not alter development of MDA-MB-231 mineralisations. MDA-MB-231 cells were cultured for 21 days in OC+Dex supplemented media, with the indicated concentraion of DMSO. Alizarin Red S staining revealed no significant inhbitory effects of DMSO on cell mineralisation, even at relatively high concentrations.

8.2 Presentations

Table 8.3 Oral and poster conference presentations

Oral/ Poster	Title	Authors	Conference
Poster	Microcalcifications in breast cancer: Novel insights into the molecular mechanism and functional consequences	S O'Grady, M P Morgan	RCSI Research Day (Feb, 2015)
Poster	Microcalcifications in breast cancer: Novel insights into the molecular mechanism and functional consequences	S O'Grady, M P Morgan	Irish Association of Cancer Research (Mar, 2015)
Poster	Development of an *in vitro* model of breast tumour microcalcification	S O'Grady, N Azizi, M P Morgan	Royal Academy of Biomedical Sciences (June, 2015)
Poster	Matrix metalloproteinase activity is required for microcalcification formation in an *in vitro* model	S O'Grady, M P Morgan	Irish Association of Cancer Research (Feb, 2016)
Poster	Exogenous magnesium reduces calcium deposition in an *in vitro* model of breast cancer microcalcification formation	S O'Grady, M P Morgan	RCSI Research Day (Feb, 2016)
Poster	Magnesium ions, TRPM7 transporters and the development of mammary calcifications	S O'Grady, M P Morgan	Early Career Physiologist Symposium (Jul, 2016)
Poster	Investigating the role of tumour-environmental factors on the formation of mammary microcalcification in an *in vitro* model	S O'Grady, M P Morgan	EACR: Goodbye Flat Biology (Oct, 2016)
Oral	Investigation of tumour-environmental factors on formation of mammary microcalcification using an *in vitro* model	S O'Grady, M P Morgan	Matrix Biology Ireland (Nov, 2016)
Poster	Protective effect of TRPM7 inhibition in a model of breast tumour calcification	S O'Grady, M P Morgan	Irish Association of Pharmacologists (Dec, 2016)
Poster	Tumour associated cytokines impact the formation and development of breast microcalcifications in an *in vitro* model	S O'Grady, M P Morgan	RCSI Research Day (Feb, 2017)
Poster	Functional role of BMP signalling pathway and inflammatory cytokines in an *in vitro* model of breast calcification.	S O'Grady, M P Morgan	Irish Association of Cancer Research (Feb, 2017)
Poster	Tumour micro-environmental factors and the development of mammary calcifications: Recent findings from an *in vitro* model	S O'Grady, M P Morgan	American Association of Cancer Research (Apr, 2017)
Oral	Deposition of calcium in a novel *in vitro* model of breast tumour calcification reveals functional role for ALP/ENPP1 balance and dysregulation of TRPM7 ion channel	S O'Grady, M P Morgan	Matrix Biology Ireland (Dec, 2017)

8.3 Students supervised

- Samar Atteih, Student Select Component (SSC) 2015: Helped with the early establishment of the MDA-MB-231 model.
- Naqeem Azizi, M.Sc. Translational Oncology (2015): Examined effect of hypoxia on formation of microcalcifications.
- Farrah Adamali Summer Research School (2015): Helped characterise mineralisation characteristics of several cell lines
- Fatemah Hassan, SSC (2016): Carried out western blot and MTT analysis of a novel anti-cancer agent. See publications (Section 8.4)
- Ahmed Alabdulkareem Summer Research School (2016): Investigated potential anti-mineralisation activity of MMP inhibitors.
- Ali Alsahlanee, SSC (2017): Generated mRNA time courses to examine expression of PMCA1 and PMCA2 in MDA-MB-231 cells.
- Nadine Copty Summer Research School (2017): Performed siRNA transfection targeting RUNX2 expression.

8.4 Publications

Kelly GJ, Kia AF, Hassan F, O'Grady S, Morgan MP, Creaven BS, McClean S, Harmey JH, Devocelle M. (2016). Polymeric prodrug combination to exploit the therapeutic potential of antimicrobial peptides against cancer cells. *Org Biomol Chem* 14(39):9278-9286.

O'Grady S, Morgan MP. Microcalcifications in breast cancer: From pathophysiology to diagnosis and prognosis. Biochim Biophys Acta. 2018;1869(2):310-20.

8.5 Science promotion and other academic activities

- Postgraduate Student Union. 1 year as Communications Officer, 1 year as President. Acted as student liaison and representative on several academic committees and boards.
- Organising committee for “2016 Postgraduate De-Stress Day” and “2017 Postgraduate Careers Fair”.
- Lab demonstrator for biomedical science practicals.
- Assisted in Leaving Certificate teaching demonstrations.
- Visits to a local primary school to carry out science demonstrations.
- Tour-guide during the inaugural “MCT Lab-Safari”, as part of Science Week.